AD NUMBER

AD861519

LIMITATION CHANGES

TO:

Approved for public release; distribution is unlimited.

FROM:

**Distribution authorized to U.S. Gov't. agencies and their contractors;
Administrative/Operational Use; APR 1969. Other requests shall be referred to Army Aviation Materiel Labs., Fort Eustis, VA.**

AUTHORITY

USAAVLABS ltr 30 Mar 1976

USAAVLABS TECHNICAL REPORT 68-38C

RADIAL OUTFLOW COMPRESSOR COMPONENT DEVELOPMENT

VOLUME III

PHASE III - MECHANICAL DESIGN AND EXPERIMENTAL INVESTIGATION USING MODIFIED ROTOR

By

John R. Erwin

August 1969

U. S. ARMY AVIATION MATERIEL LABORATORIES
FORT EUSTIS, VIRGINIA

CONTRACT DA 44-177-AMC-180(T)
GENERAL ELECTRIC COMPANY
CINCINNATI, OHIO

DISCLAIMERS

The findings in this report are not to be construed an an official Department of the Army position unless so designated by other authorized documents.

When Government drawings, specifications, or other data are used for any purpose other than in connection with a definitely related Government procurement operation, the United States Government thereby incurs no responsibility not any obligation whatsoever; and the fact that the Government may have formulated, furnished, or in any way supplied the said drawings, specifications, or other data is not to be regarded by implication or otherwise as in any manner licensing the holder or any other person or corporation, or conveying any rights or permission, to manufacture, use, or sell any patented invention that may in any way be related thereto.

DISPOSITION INSTRUCTIONS

Destroy this report when no longer needed. Do not return it to the originator.

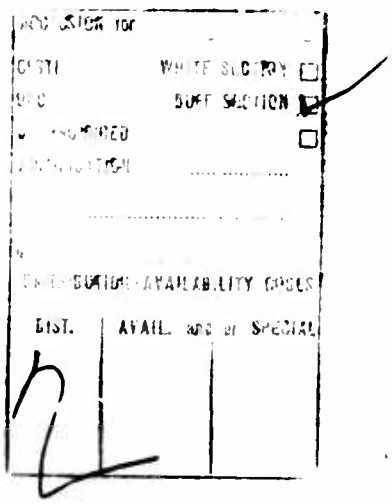

DEPARTMENT OF THE ARMY
U. S. ARMY AVIATION MATERIEL LABORATORIES
FORT EUSTIS, VIRGINIA 23604

The object of this contractual effort was to test the concept of the high-pressure-ratio radial outflow compressor and to determine its suitability for use in small gas turbine engines.

This report was prepared by General Electric Company under the terms of Contract DA 44-177-AMC-180(T). It describes the tests performed and the results of those tests.

The full potential of the radial outflow compressor concept was not achieved. However, useful performance of the compressor at reduced speed and pressure ratio was demonstrated.

This report has been reviewed by technical personnel of this Command, and the conclusions and recommendations contained herein are concurred in by this Command.

Task 1G121401D14413
Contract DA 44-177-AMC-180 (T)
USAAVLABS Technical Report 68-38C
August 1969

RADIAL OUTFLOW COMPRESSOR COMPONENT DEVELOPMENT

Volume III

Phase III - Mechanical Design and Experimental Investigation Using Modified Rotor

by

John R. Erwin

Prepared by

General Electric Company
Cincinnati, Ohio

for

U. S. ARMY AVIATION MATERIEL LABORATORIES
FT. EUSTIS, VIRGINIA

SUMMARY

The purposes of the Phase III investigation were to apply the information obtained from the experimental and analytical investigations of the first two phases to the design of an improved ROC and to demonstrate this improvement by tests of a complete compressor over the full speed range. Because of delays in completing the earlier phases and due to the inevitable time expenditure occurring in the design and procurement phases of obtaining new rotating parts, the selection of the Phase III rotor design was made prior to the time that all of the Phase II test results were available. In particular, the excellent rotor performance observed at 70 percent speed during the last testing sequence of the Phase II investigation, Buildup F, was not obtained until after the Phase III rotor design was committed to manufacture. A summary of information concerning each test run is presented in Appendix I.

The evidence from tests of Buildup F and from the low-speed investigation of the vaneless diffuser having one stationary porous wall and one rotating wall is that more severe effective static pressure gradients can be sustained by a rotating wall than the earlier Phase II results had indicated (uniform inlet conditions to the rotor are evidently critical to efficient rotor performance). In retrospect, more contraction of the rotating vaneless diffuser was probably incorporated into the Phase III rotor design than was necessary for best high-speed performance.

FOREWORD

Under United States Army Contract DA 44-177-AMC-180(T), the Flight Propulsion Division of the General Electric Company in Cincinnati, Ohio, is conducting a program to advance and demonstrate high-pressure-ratio compressor technology for small gas turbine engines. The investigation concerning the analysis, design, construction, and testing of a Radial Outflow Compressor (ROC) is presented in three volumes, each volume generally describing one of the three phases of the program. Volume I presents the ROC design philosophy, mechanical analysis and bench test results, inlet system and rotating wall vaneless diffuser studies using a low-speed compressor, the design and supersonic cascade tests of the rotor blade sections, and high-speed transonic and supersonic cascade tests of single-row and tandem-row stator vanes. The design of the high-speed compressor test vehicle used in the Phase II and III investigations was also presented in Volume I.

Volume II describes the Phase II investigation including the aerodynamic and mechanical design of the high-speed rotor and the stator system. The experiments conducted consisted of testing 6 major buildups (A through F) of the compressor. A number of aerodynamic, mechanical, and operational problems were encountered during testing of the new compressor using a new test vehicle. During Buildup F, encouraging rotor performance was obtained at 70 percent speed, with a maximum rotor efficiency of 92.1 percent recorded at a rotor exit total pressure ratio of 3.97, and a rotor exit static pressure ratio of 1.97. This performance was accomplished by elimination of the inlet guide vanes, the use of a circular inlet vane, the Phase III rotor blades, and the subsonic stators. Analysis of the rotating wall vaneless diffuser was described, and further low-speed compressor test results were presented. The rotating diffuser configuration selected for the Phase III rotor was also presented in Volume II.

Volume III describes the Phase III investigation of 3 major buildups (A through C) of the high-speed compressor. Buildup A was intended to provide direct comparison of the Phase III rotor performance with the best performance obtained with the Phase II rotor during Buildup F. The circular inlet vane was not used in Buildup A (Phase III) because the rotor inlet curvature was more gradual and it was hoped that the assembly, balancing and installation difficulties inherent with the circular inlet vane could be avoided. Operating problems with the bellmouth liner used to form the air path into the new rotor were encountered. Fracture of the liner occurred at low speed. Continued operation of the compressor was obtained by machining the liner back to eliminate interference with the rotor. Although an unsatisfactory rotor entrance condition existed, some aerodynamic and mechanical data were obtained. A satisfactory inlet was constructed by modifying the bellmouth with a liner composed of pyrolytic graphite and glass fibers bonded with phenolic resin.

For the final test phases, the circular inlet vane was used, the rotor strain gages and leads were removed, and the supersonic stator vanes were installed upstream of the subsonic stators. An improved seal was employed upstream of the rotor for Buildup B. Builcup C was similar to Buildup B except that reduced seal clearance was established, reduced rotor to casing offset (cold, nonrotating) was used, and greater capacity to remove flow from the forward cavity was provided. A systematic series of stator vane settings was tested during Buildup C at speeds up to 100 percent.

The manager of the Small Gas Turbine Engine Compressor Technology Program is J. R. Erwin, and the principal contributing engineers are N. G. Vitale, R. G. Giffin, E. L. Timperman, C. H. Gay, and R. E. Troeger. Volume I was compiled and edited by Mr. D. V. Robinett. The assistance and consultations provided by Dr. D. C. Prince, Jr., and Dr. L. H. Smith, both of the General Electric Company, are gratefully acknowledged, as are the services of Dr. G. F. Wislicenus of Pennsylvania State University, who served as consultant on the program. Mr. LeRoy H. Hubert is Project Engineer and Mr. John White is Assistant Project Engineer for this program on behalf of the U.S. Army.

TABLE OF CONTENTS

LIST OF ILLUSTRATIONS

LIST OF SYMBOLS

A	area, inches^2
$\bar{r}$	radius of centroid, inches
e	eccentricity, inches
$\bar{\omega}$	loss coefficient

EXPERIMENTAL INVESTIGATIONS

TEST CONFIGURATION FOR BUILDUP A

A partial assembly of the configuration tested as Buildup A of the Phase III investigation is presented in Figure 1. The new rotor disc shown in Figures 2, 3, 4, and 5 was employed. The Phase III rotor blades (Figure 6), which had been used in Buildup F of the Phase II investigation, were used in the assembly of the Phase III rotor. Figures 7 and 8 illustrate the new rotating shroud which was used with all buildups of the Phase III investigation. A close-up of the shroud (Figure 9) shows strain gages used in bench vibration testing. The new rotor disc and rotating shroud formed the contracted rotating diffuser passage contour previously described as Contour Number 5 (Reference 1) and shown in Figure 1.

One of the purposes of the Buildup A investigation was to permit direct comparison between the rotor performance measured during the Phase II, Buildup F testing and the modified rotating diffuser incorporated in the Phase III rotor. To permit detailed surveys of rotor exit flow conditions, the supersonic stators (Figure 10) were not used in Buildup A for the same reason they were not used in Buildup F. The subsonic stator vanes (Figure 11) were installed to provide diffusion of the airflow and to isolate the circumferential static pressure variations of the scroll from the rotor. This was also done in Buildup F. Although a circular inlet vane was used to good advantage in Buildup F, the entrance passage up to the rotor blades has a more gradual turn than the case of the Phase II rotor, and it was hoped that satisfactory flow into the rotor blades could be achieved with the Phase III rotor without the use of a circular inlet vane. Since the circular inlet vane complicates the assembly, balance, and installation of the rotor, the omission of the circular inlet vane would greatly simplify engine applications of the Radial Outflow Compressor (ROC). Therefore, the circular inlet vane was not installed for the Buildup A configuration of the Phase III investigation.

The bellmouth liner machined from an aluminum alloy forging used during the first run of the Buildup A, Phase III configuration is shown in Figure 12. The fairing pieces used on the centerbody with or without a circular inlet vane are shown in Figure 13. A Phase III rotor blade which carries leads from the shroud is shown in Figure 14. A close-up of the rotor blades, disc, and strain gage leads is presented in Figure 15. A detail of the special washers which were relieved to permit passage of the leads to the strain gages is shown in Figure 16. A partial assembly of the rotor is seen on Figure 17. In Figure 18, counterweights, the seal teeth, and the strain gage detail of the Phase III ROC rotor shroud are presented. The clearance between the rotor blades and the rotating shroud for the Buildup A assembly is illustrated in Figure 19. Upstream and side views of the Phase III rotor are presented in Figures 20 and 21, respectively. An overall view of the Phase III ROC installed in the test cell is presented in Figure 22, and a close-up of the inlet screen

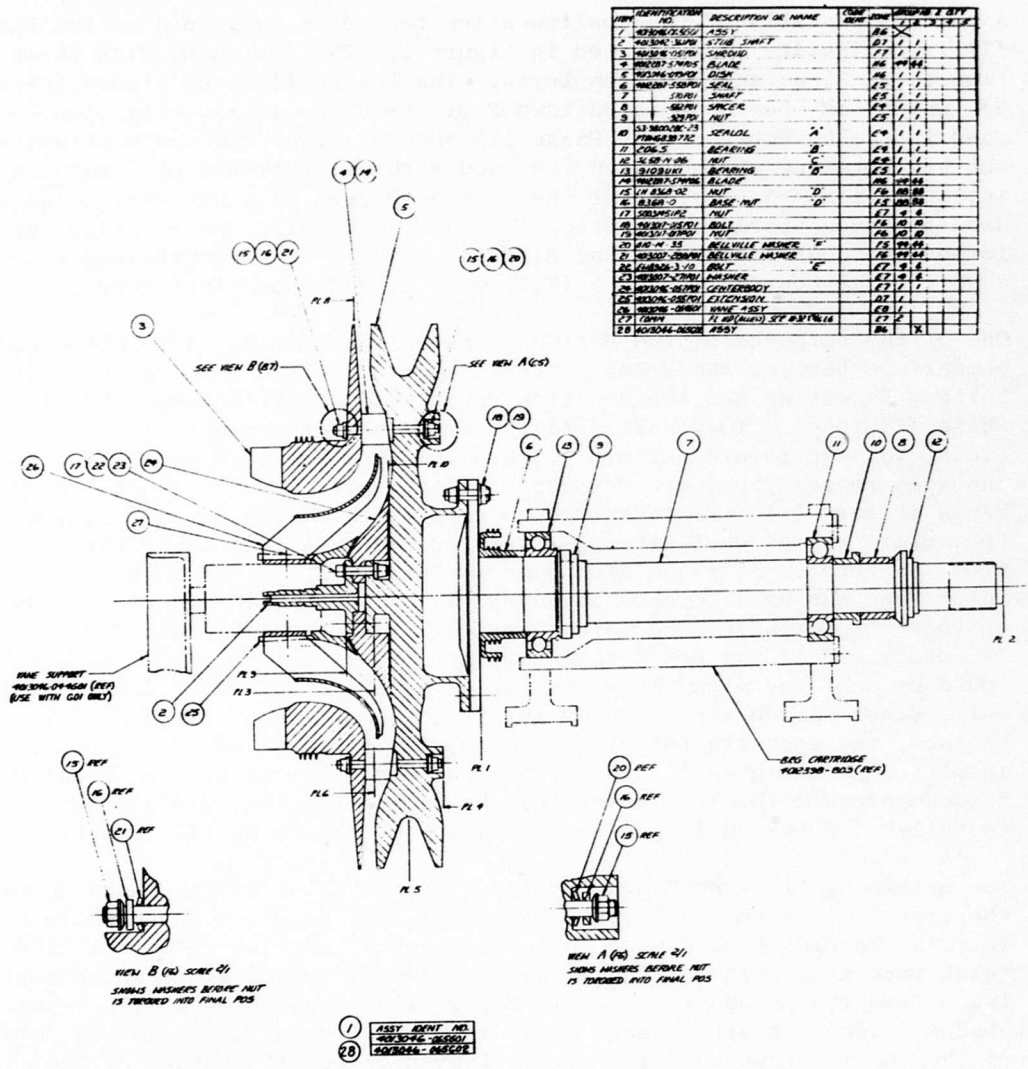

Figure 1. Assembly of the Phase III Rotor and Circular Inlet Vane.

Figure 2. Forward View of Phase III Rotor Disc.

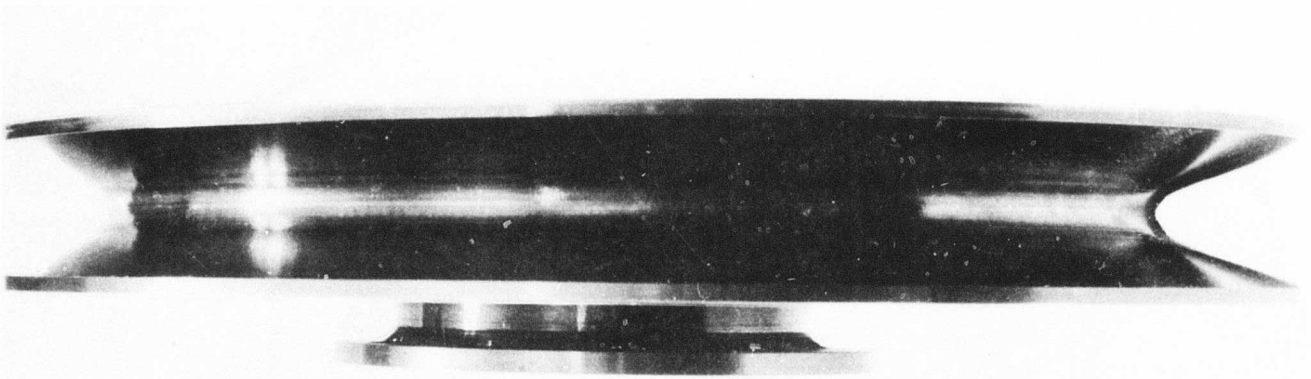

Figure 3. Side View of Phase III Rotor Disc.

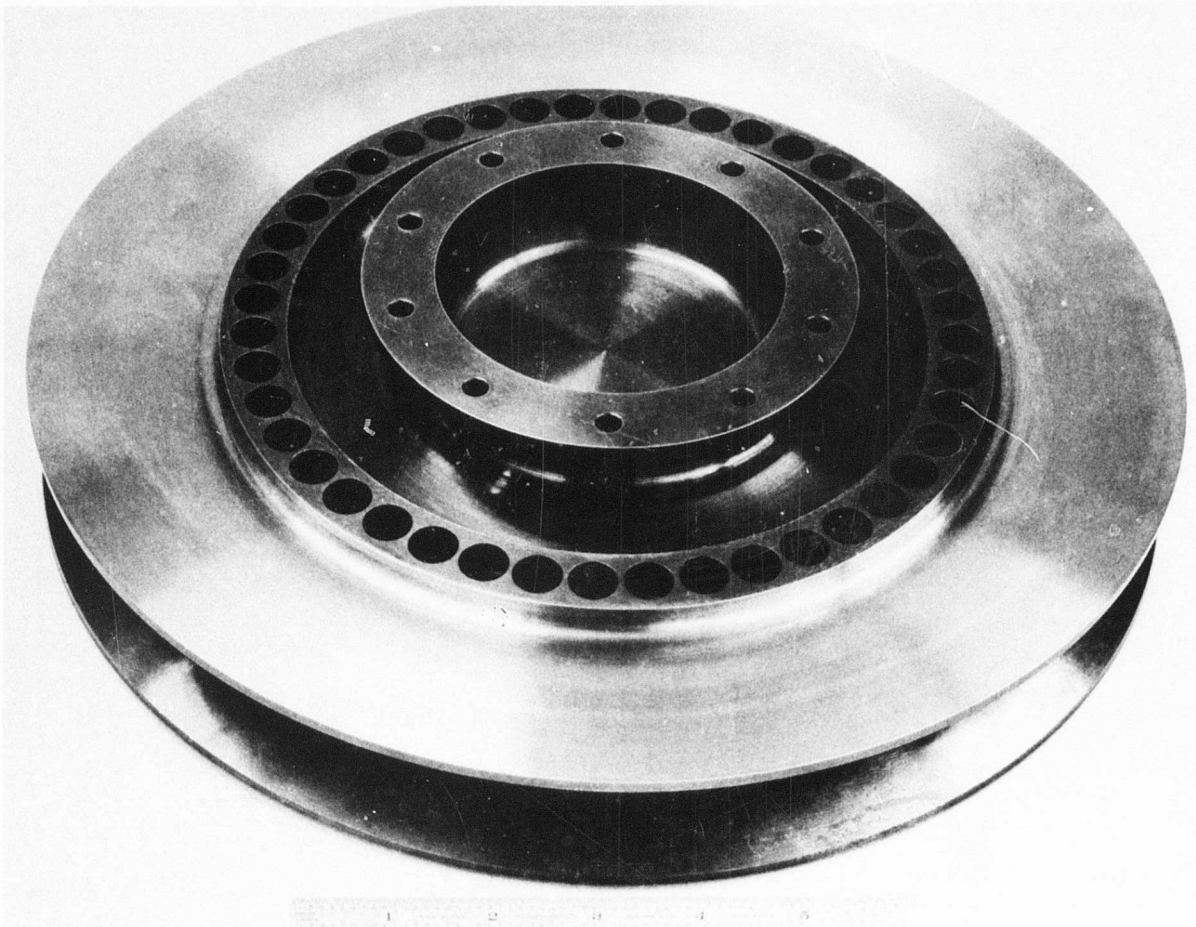

Figure 4. Aft View of Phase III Rotor Disc.

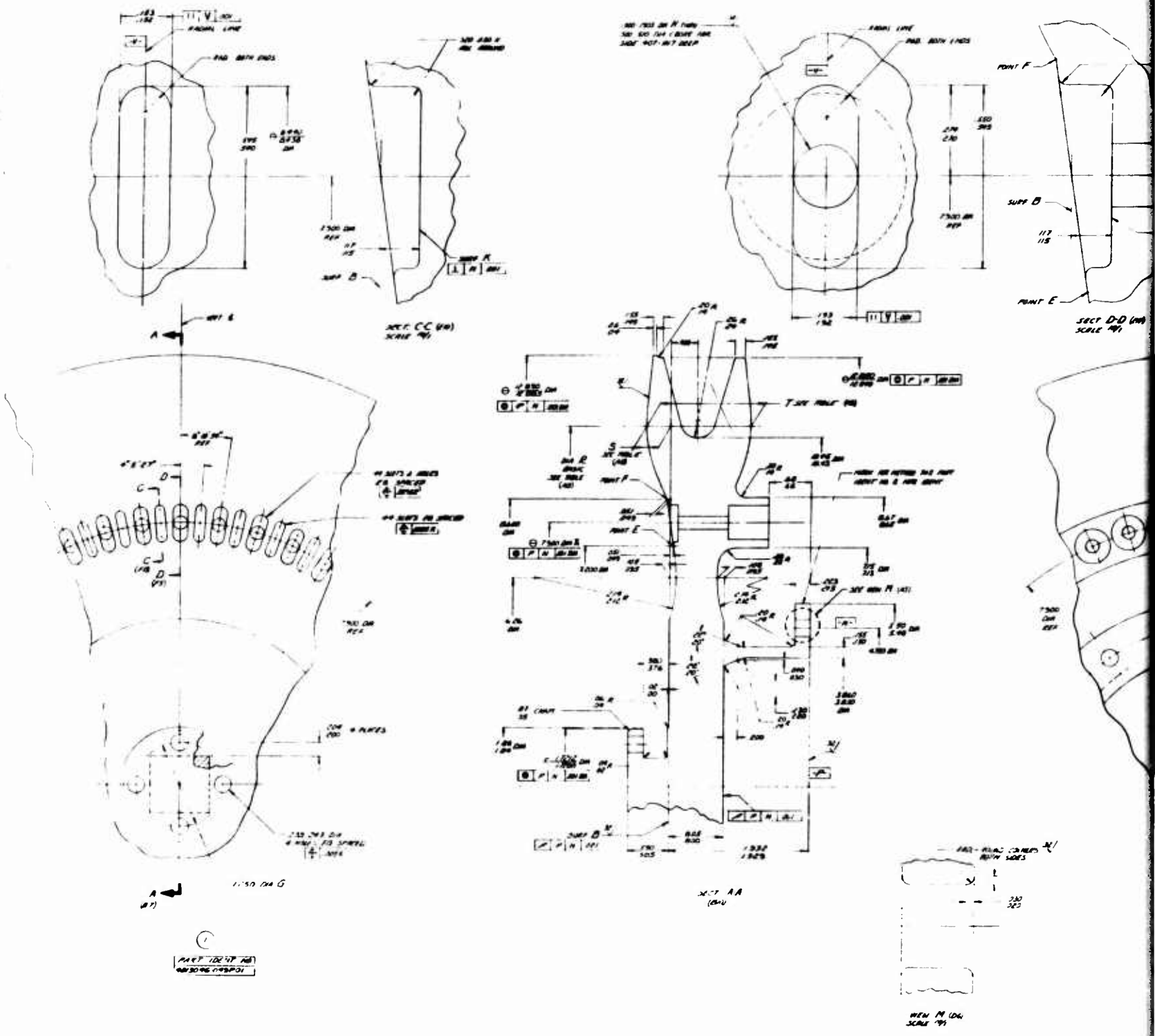

Figure 5. Drawing of Phase III Rotor Disc.

A

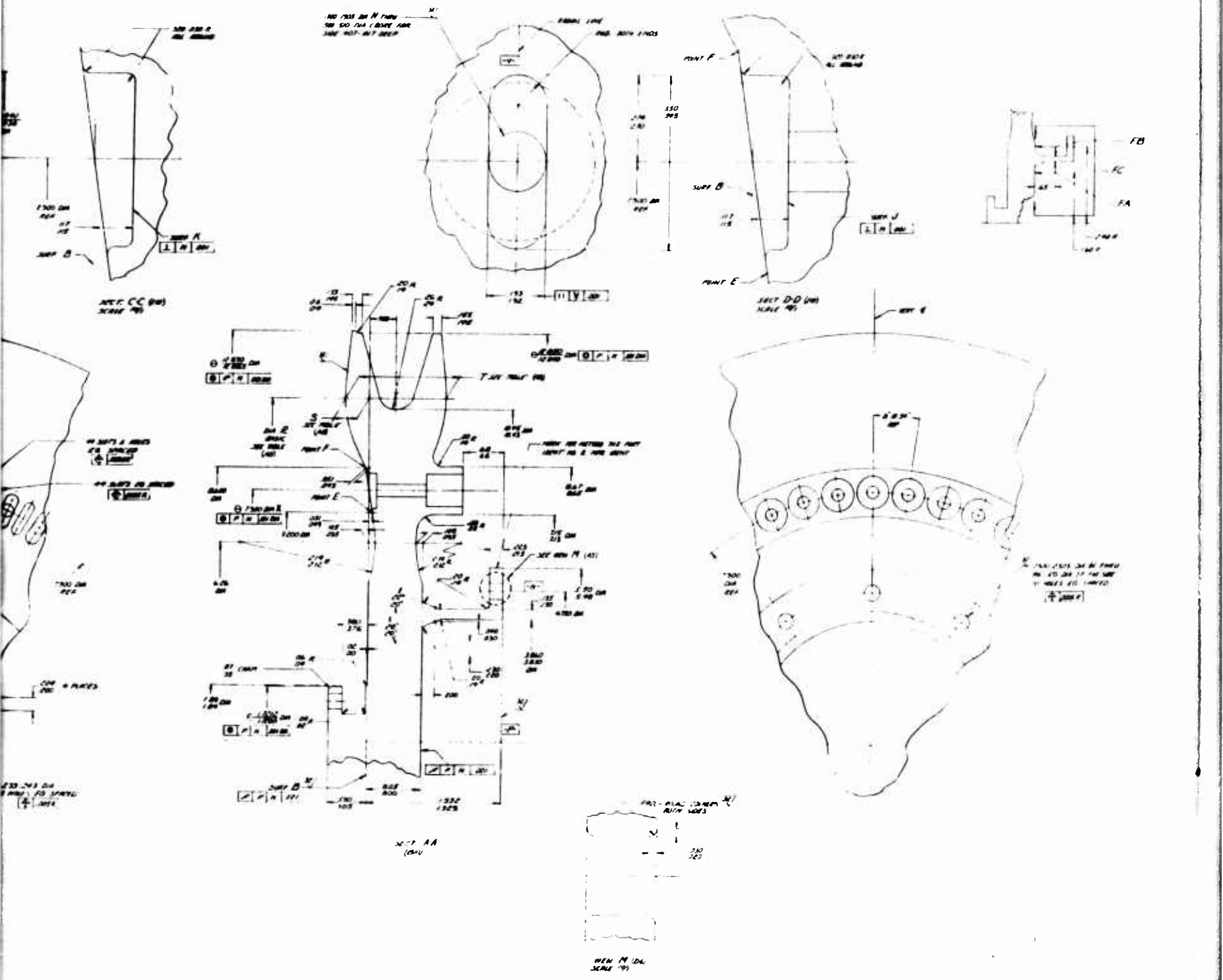

Drawing of Phase III Rotor Disc.

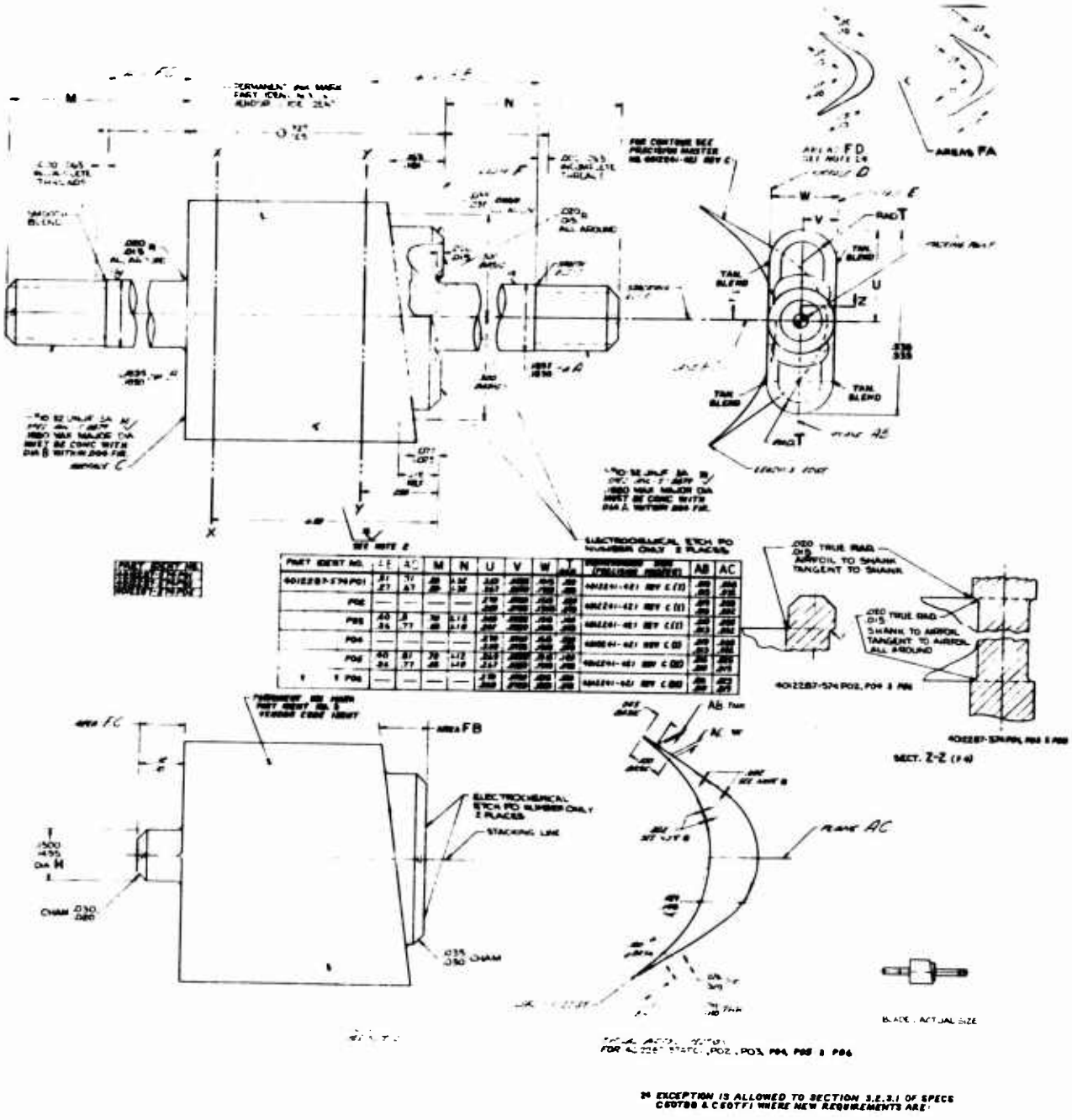

Figure 6. Drawing of Rotor Blade.

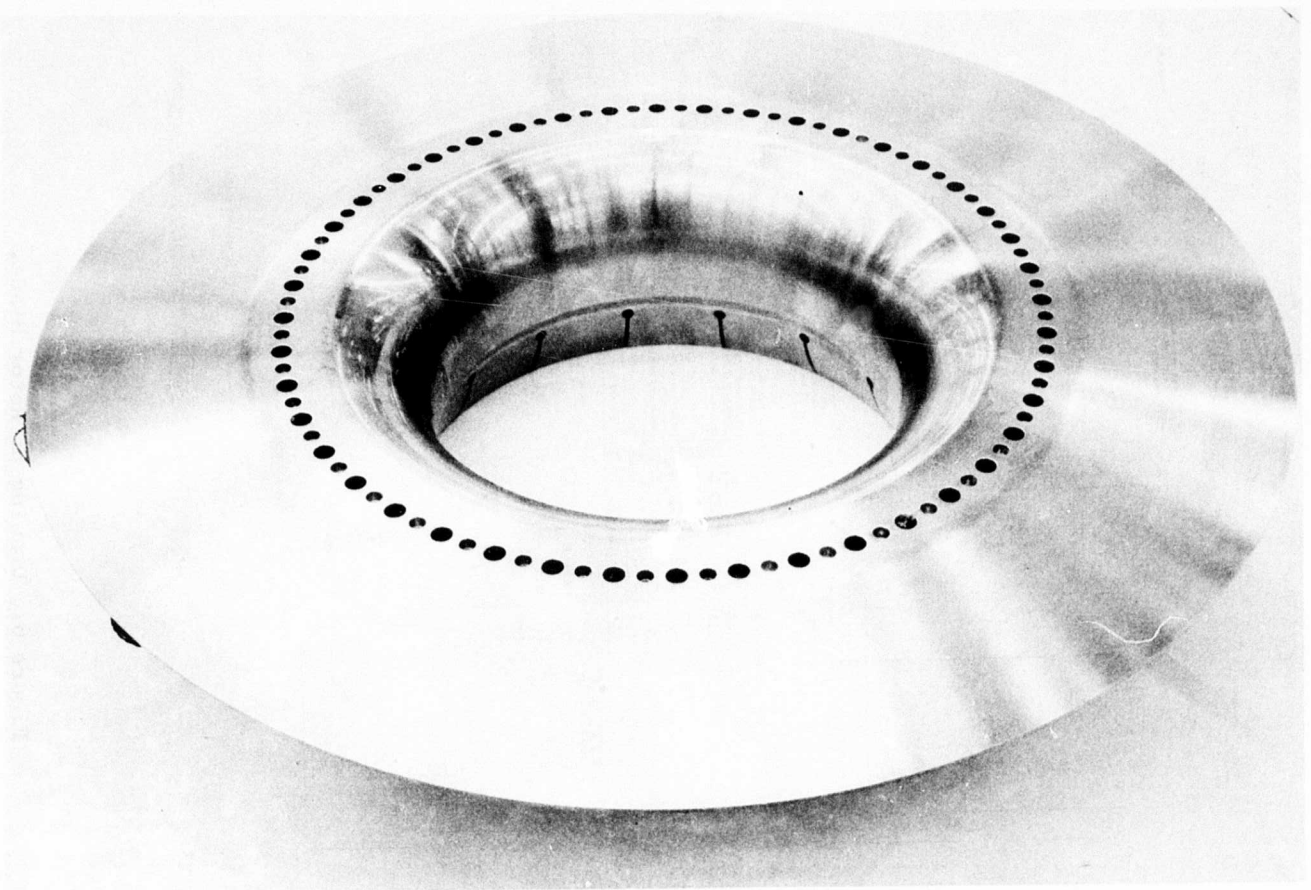

Figure 7. Aft View of Rotating Shroud for Phase III Rotor.

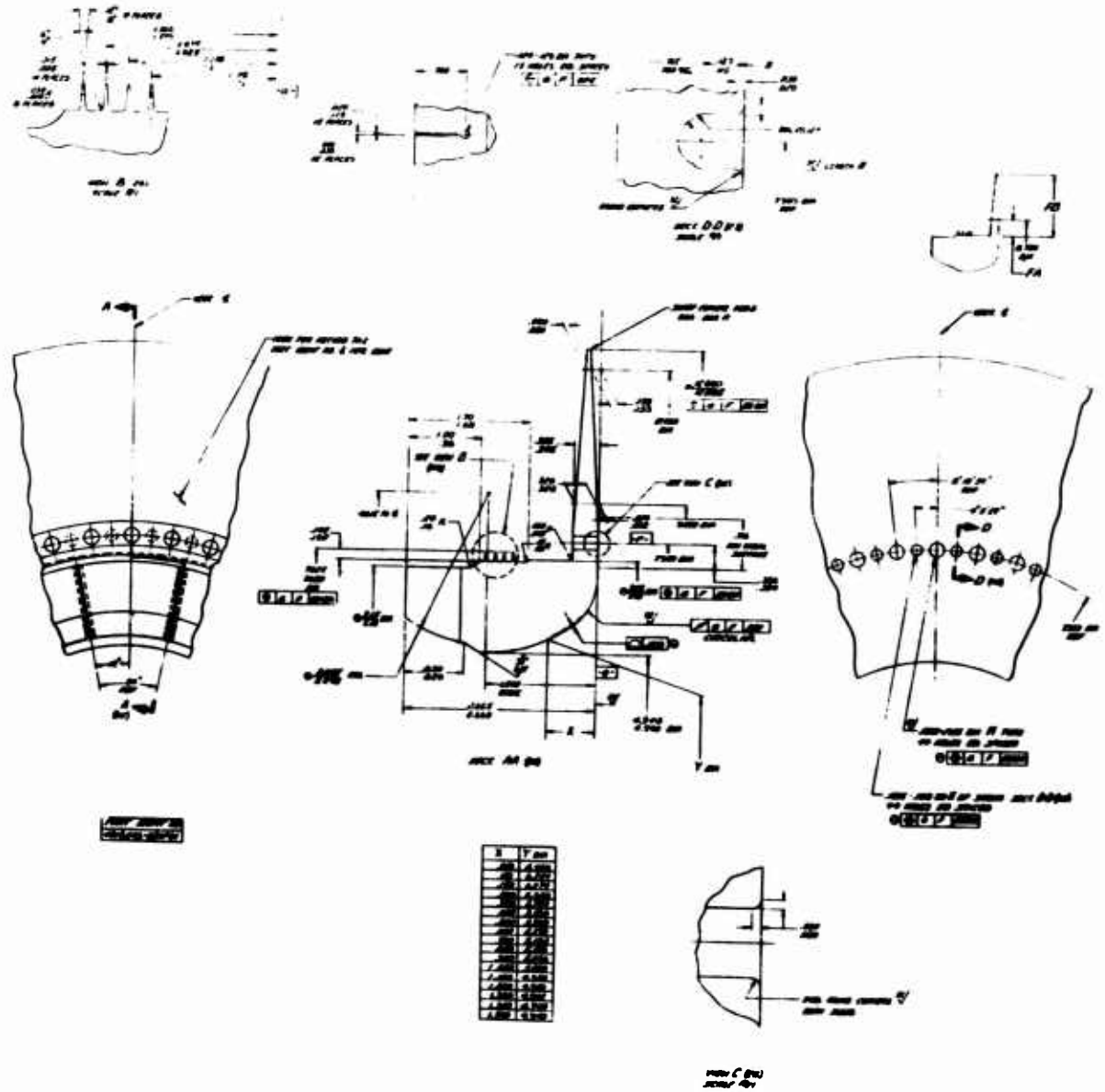

Figure 8. Drawing of Rotating Shroud.

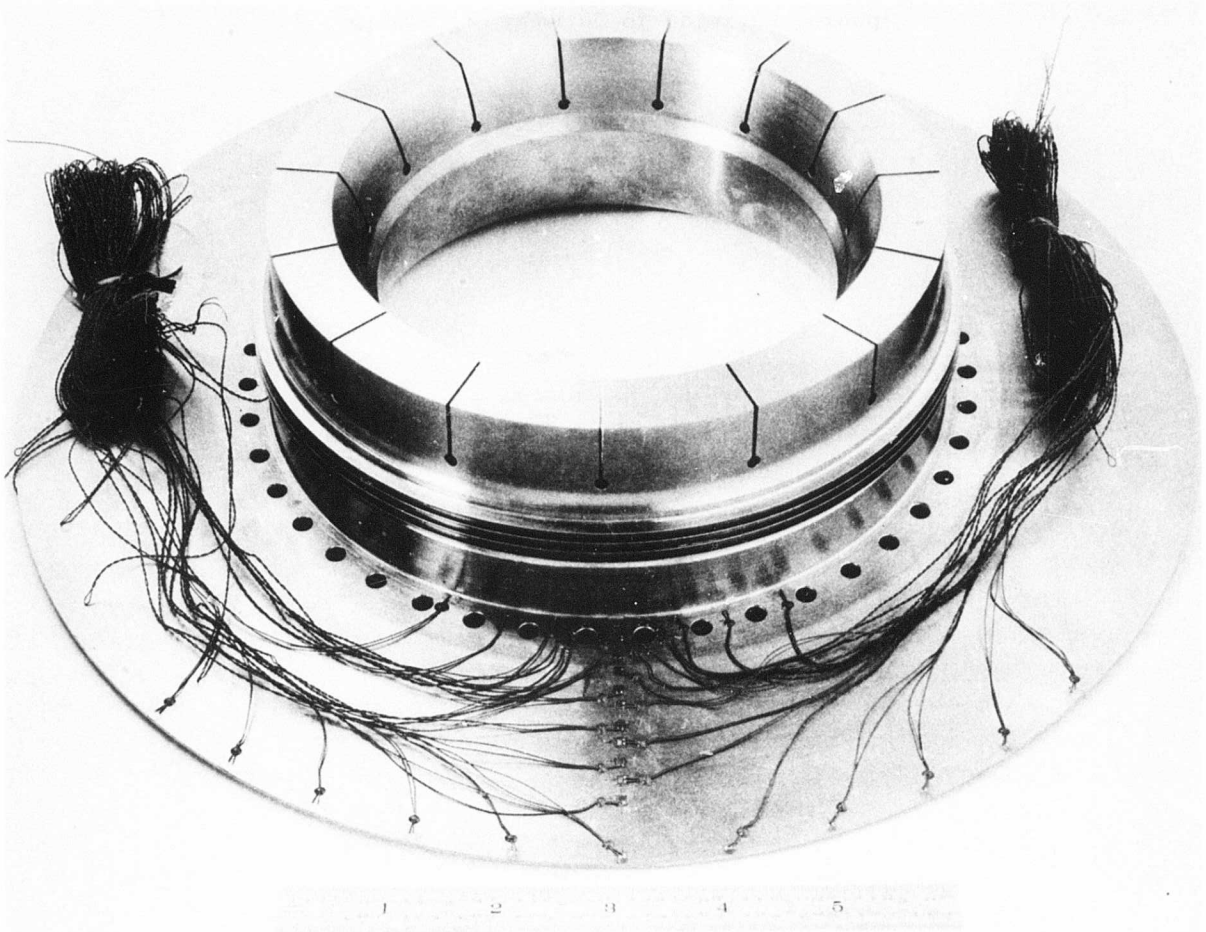

Figure 9. Rotating Shroud Showing Strain Gages Used During Bench Vibration.

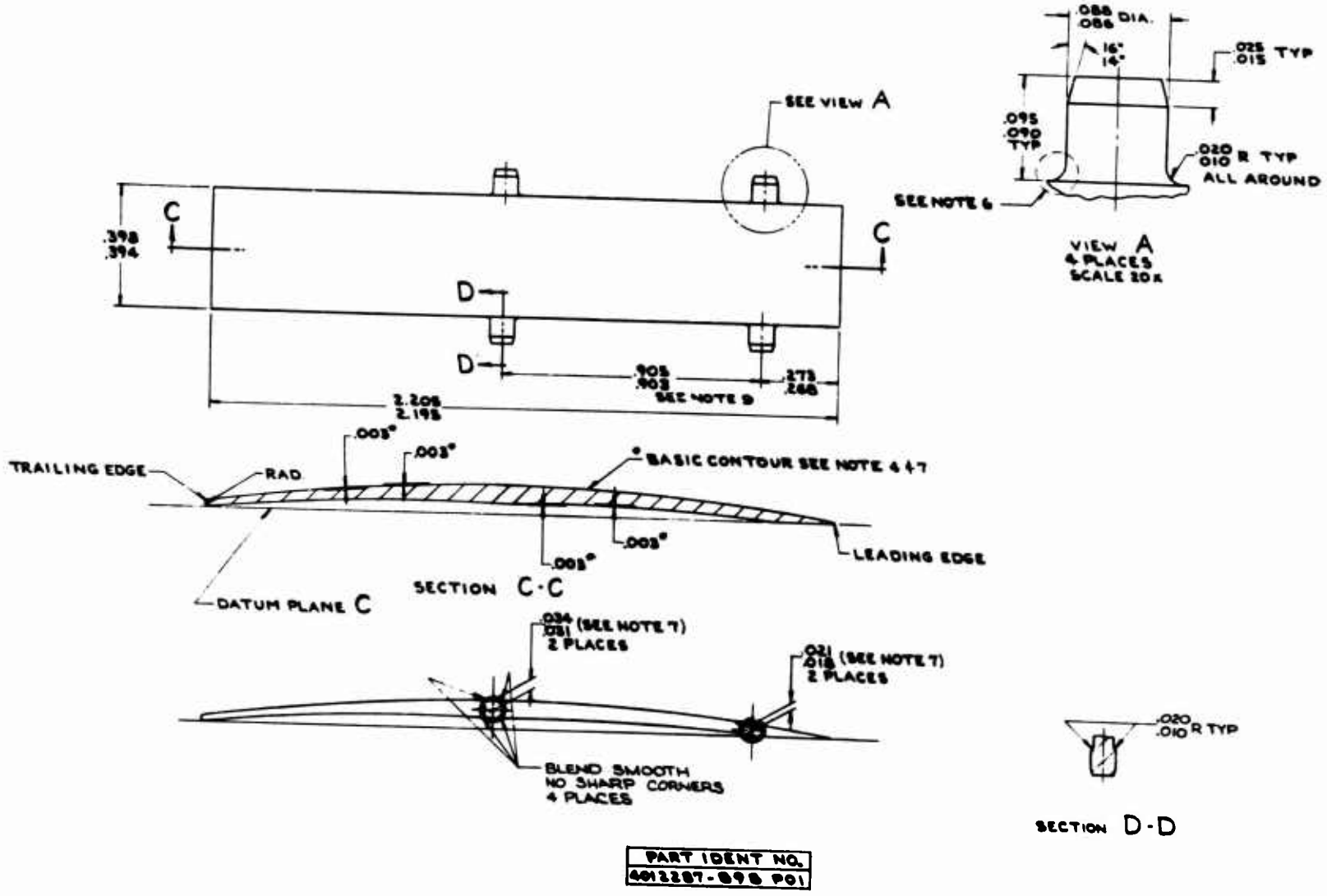

Figure 10. Drawing of Supersonic Stator Vane.

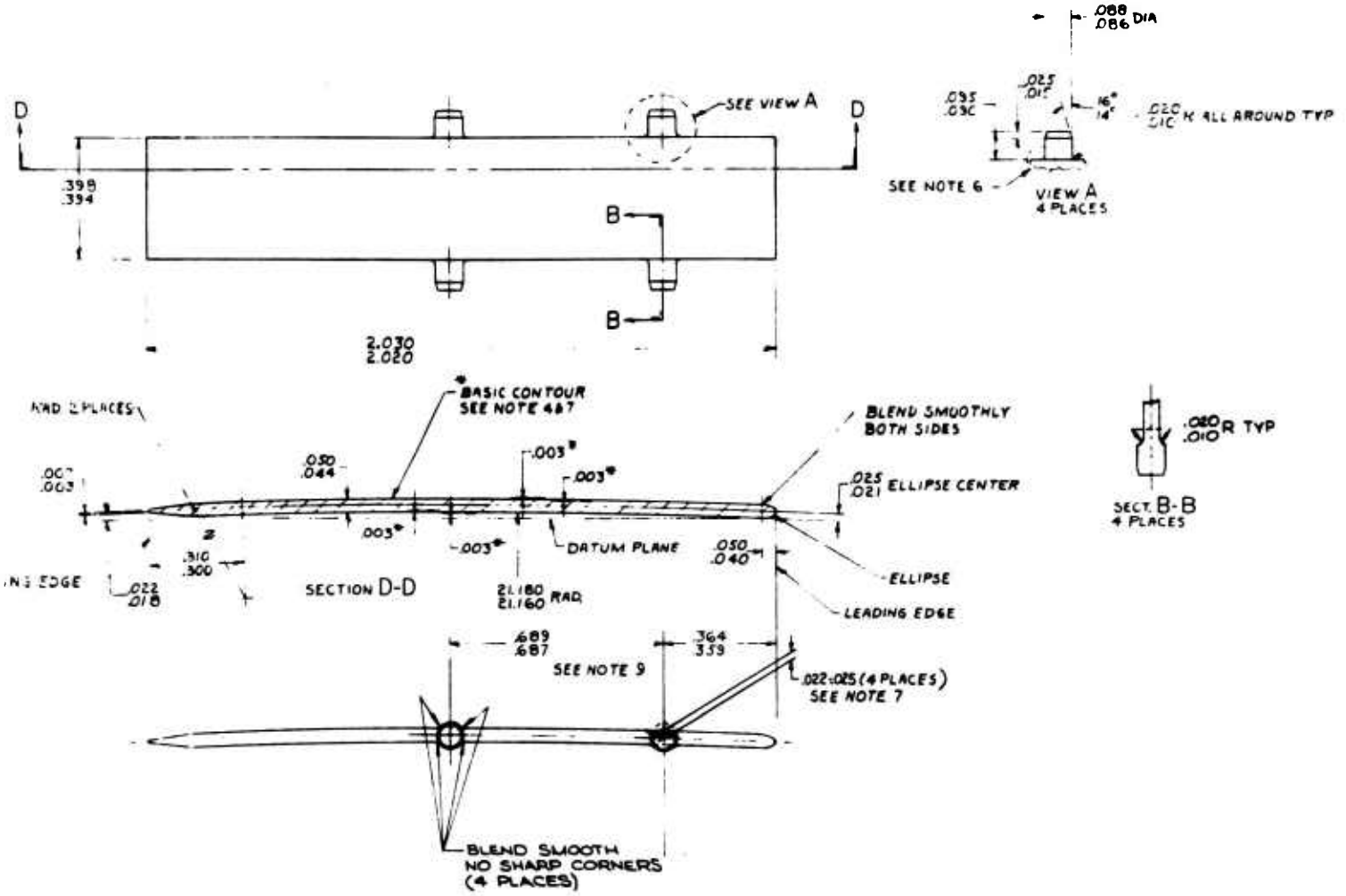

Figure 11. Drawing of Subsonic Stator Vane.

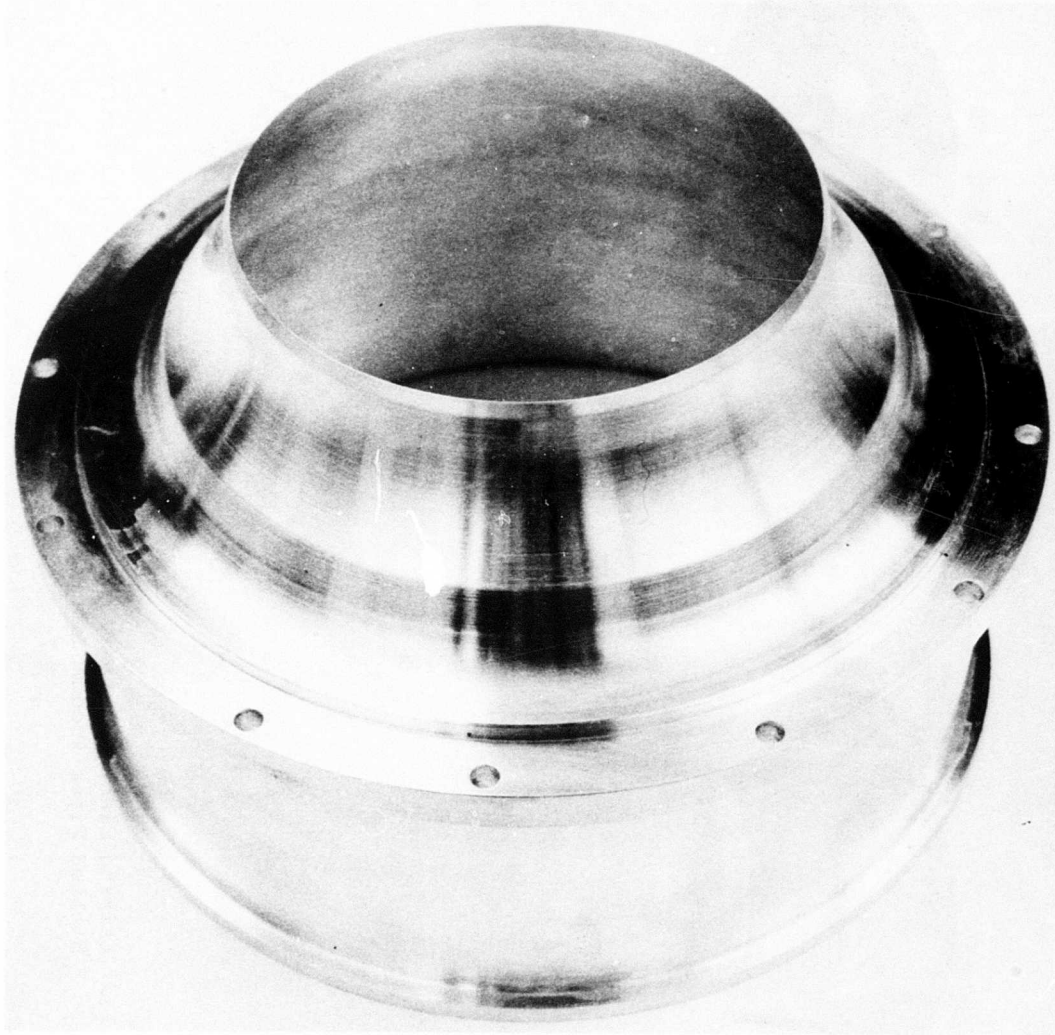

Figure 12. Bellmouth Liner for Inlet Casing Used With Buildup A, Phase III Investigation.

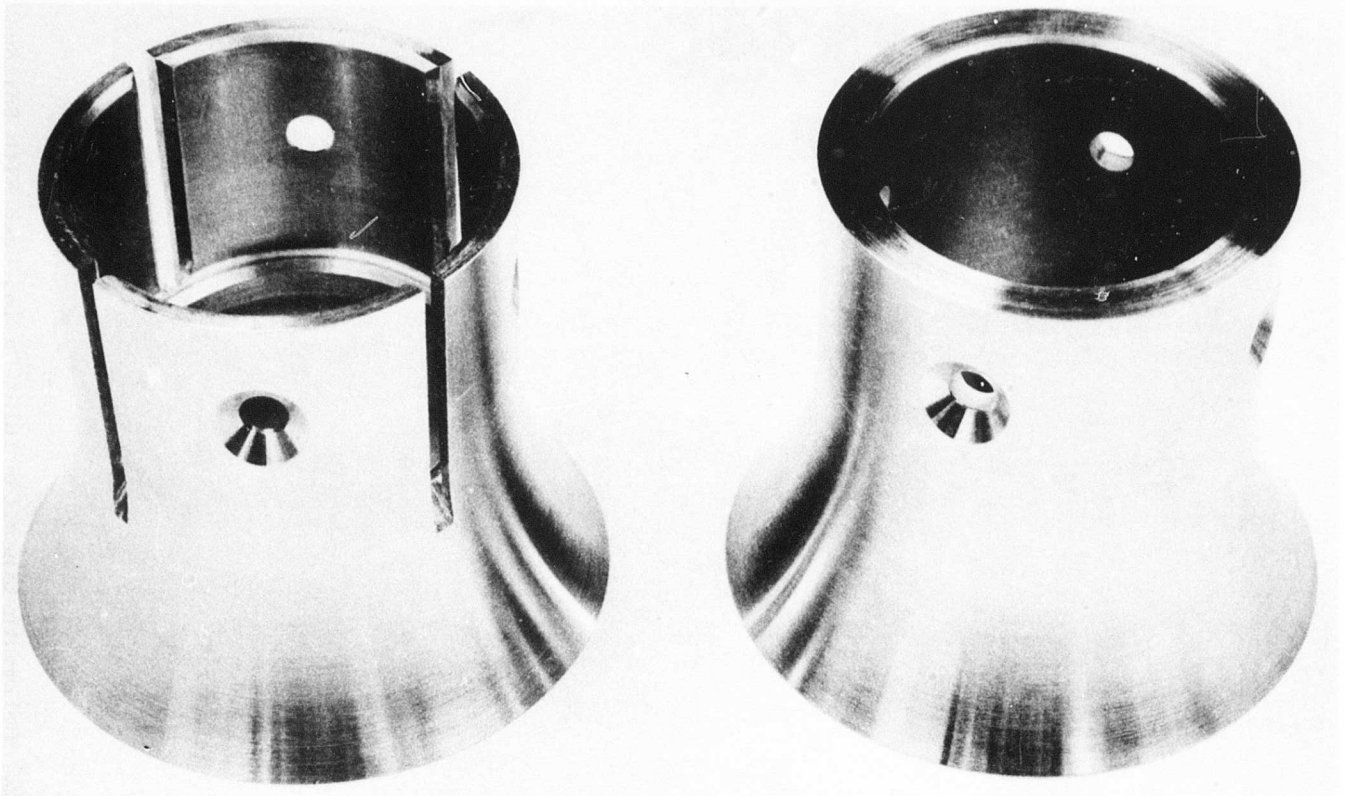

Figure 13. Fairing Pieces Used on Centerbody Adjacent to Phase III Rotor - Slotted Piece Accommodates a Circular Inlet Vane.

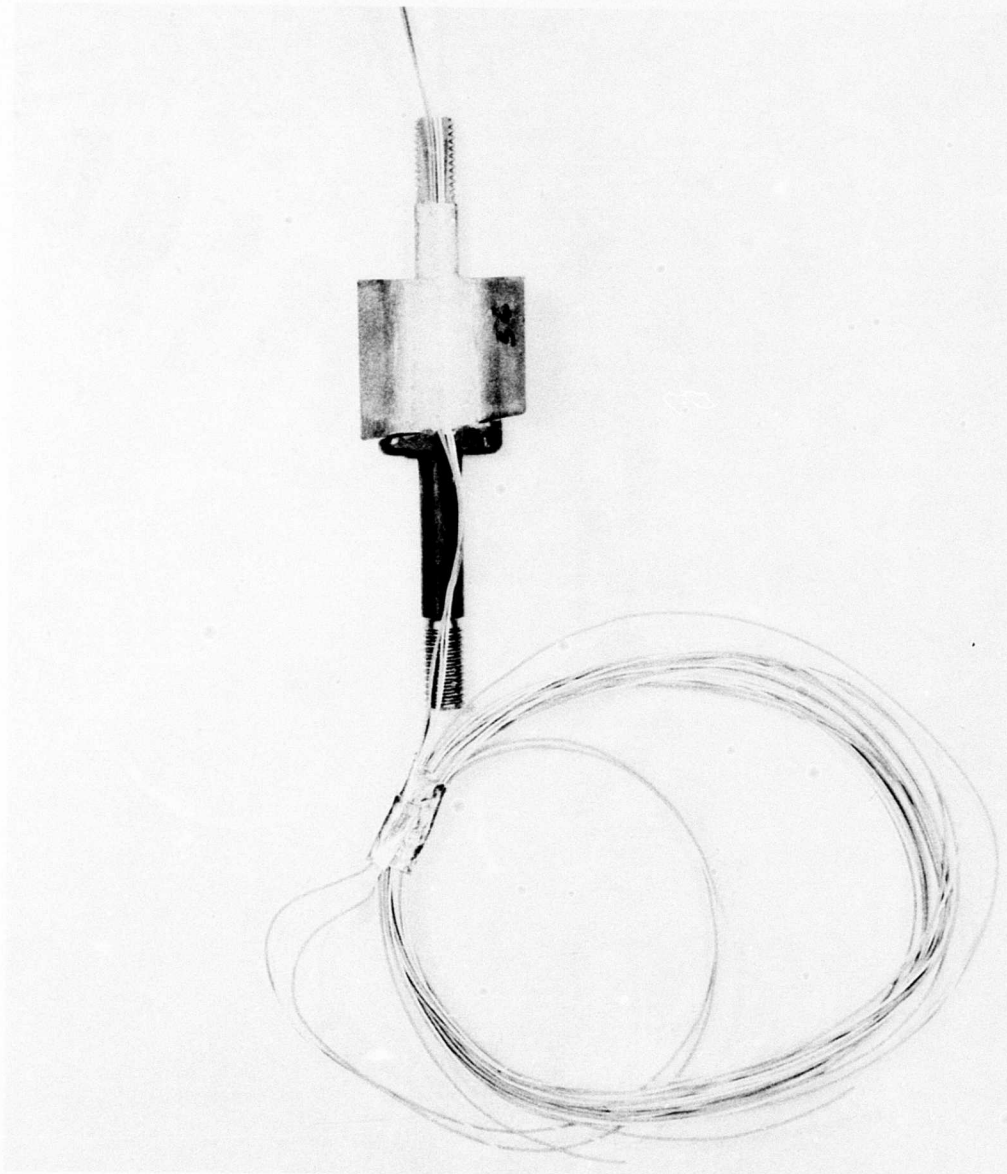

Figure 14. Phase III Rotor Blade and Strain Gage Leads.

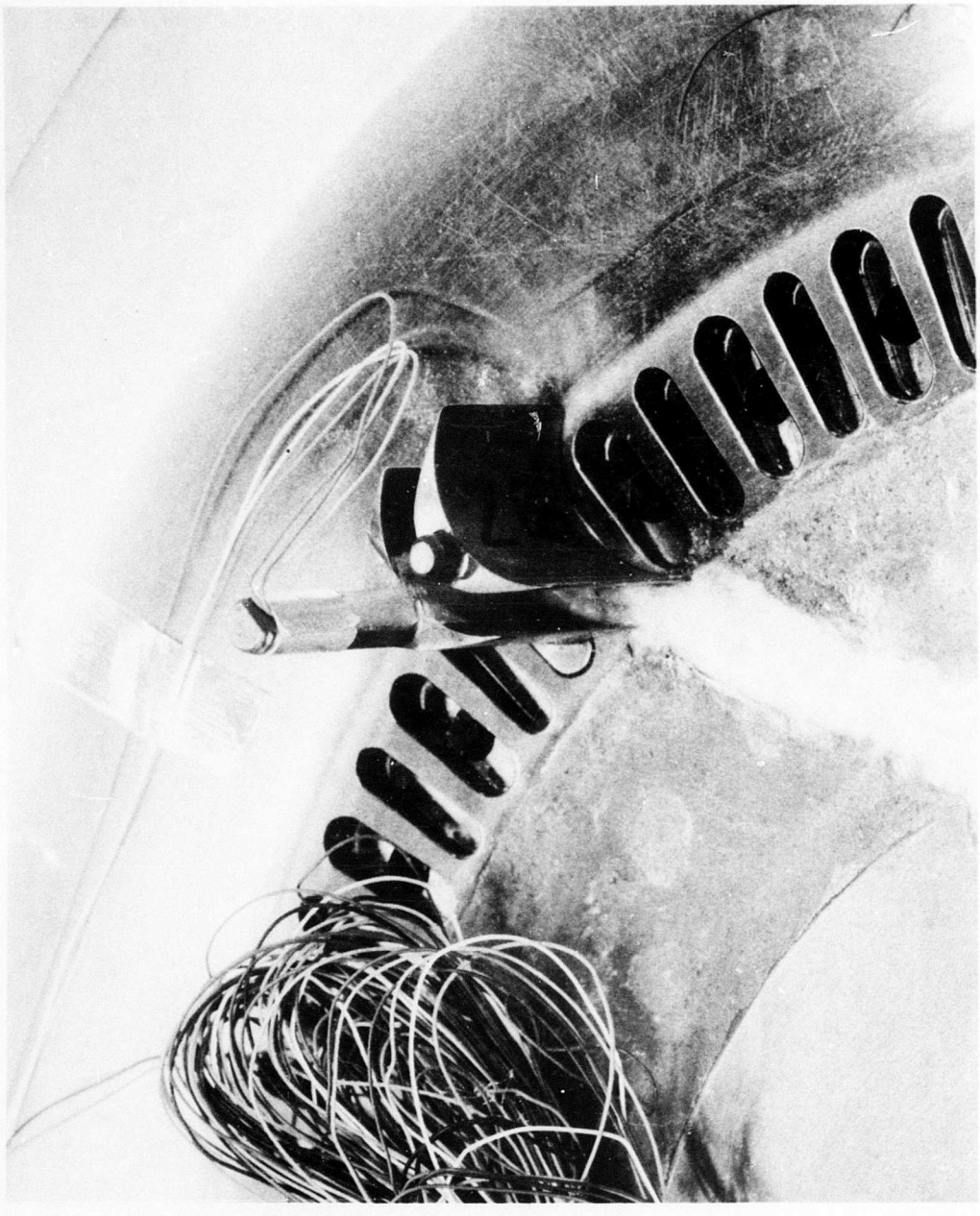

Figure 15. Close-up of Phase III Rotor Blades Showing Path of Strain Gage Leads.

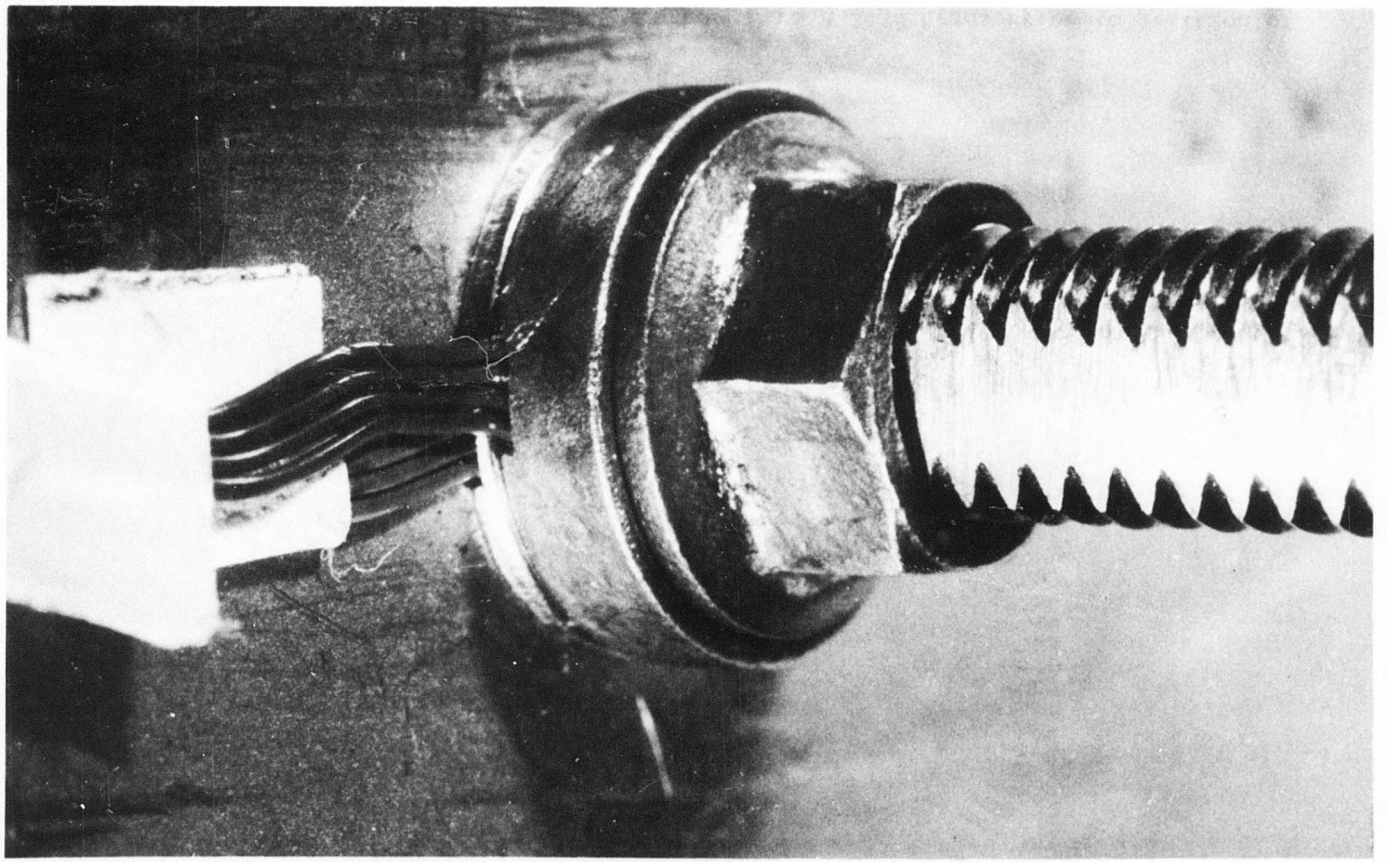

Figure 16. Close-up of Special Washers Grooved to Pass Leads to Strain Gages on Exterior of Rotating Shroud.

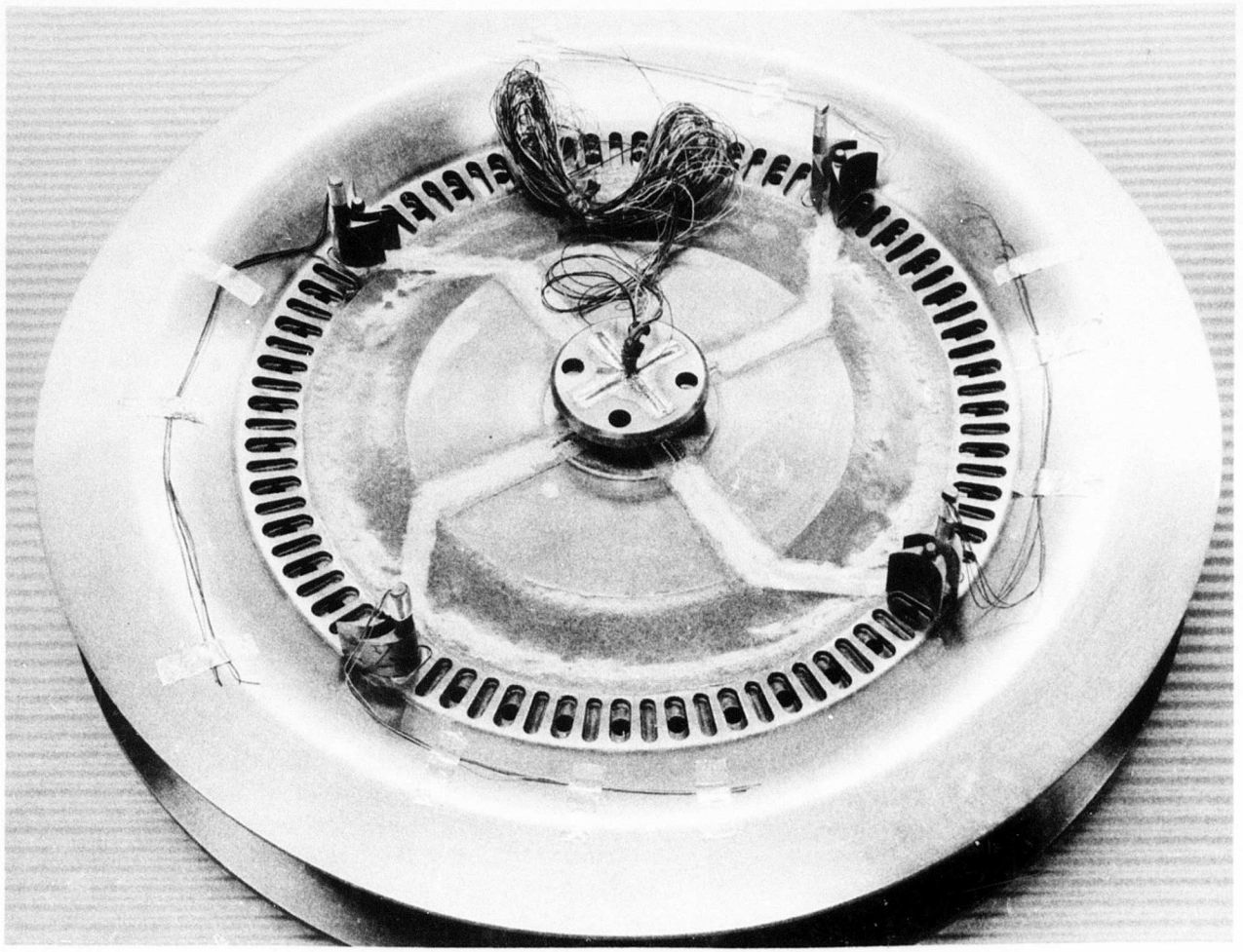

Figure 17. Assembly of Phase III Rotor Disc Showing Strain Gage Leads Prior to Addition of Rotating Centerbody.

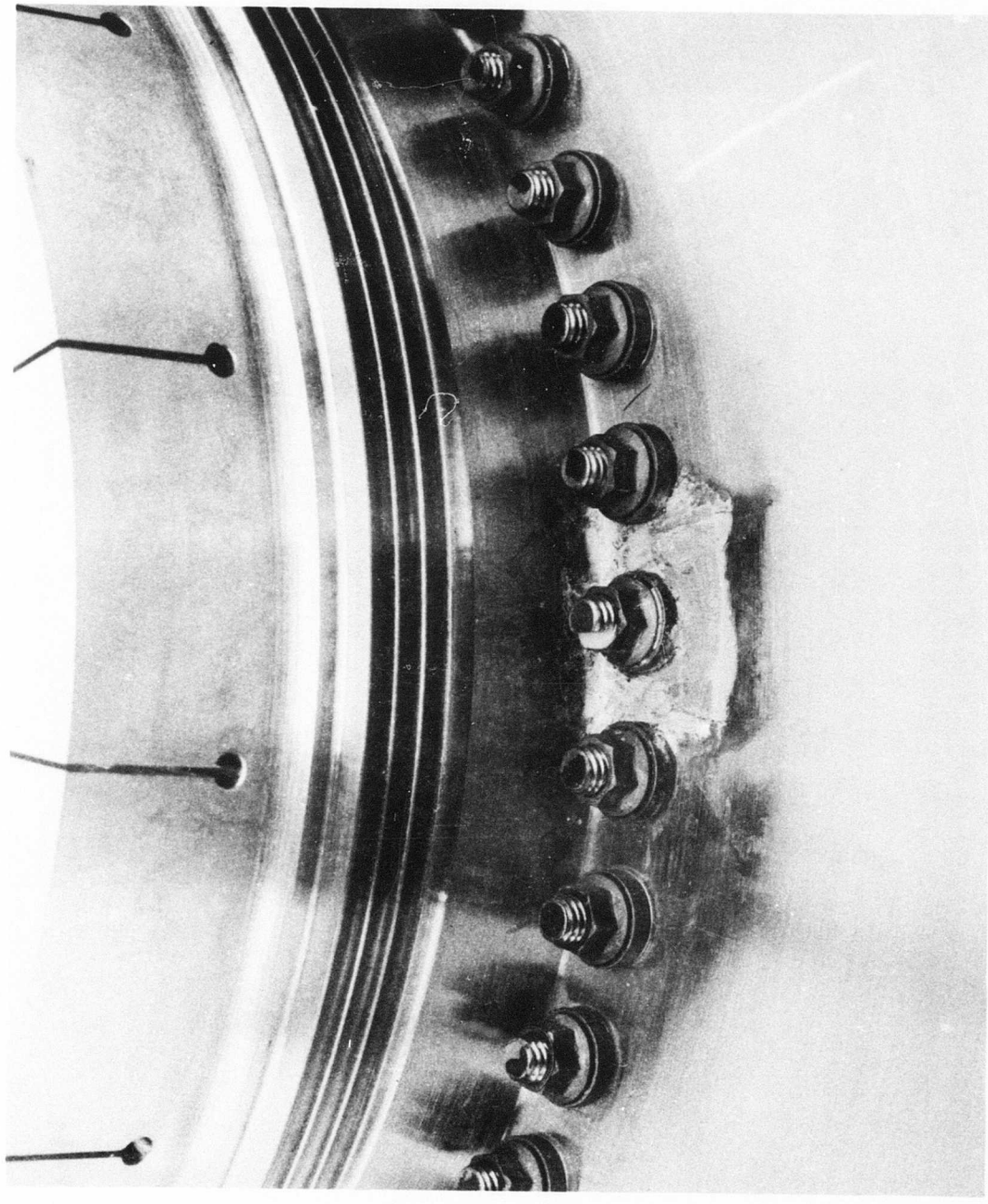

Figure 18. Rotating Shroud Seal Teeth and Strain Gage Application Prior to Run Number 19 of Buildup A.

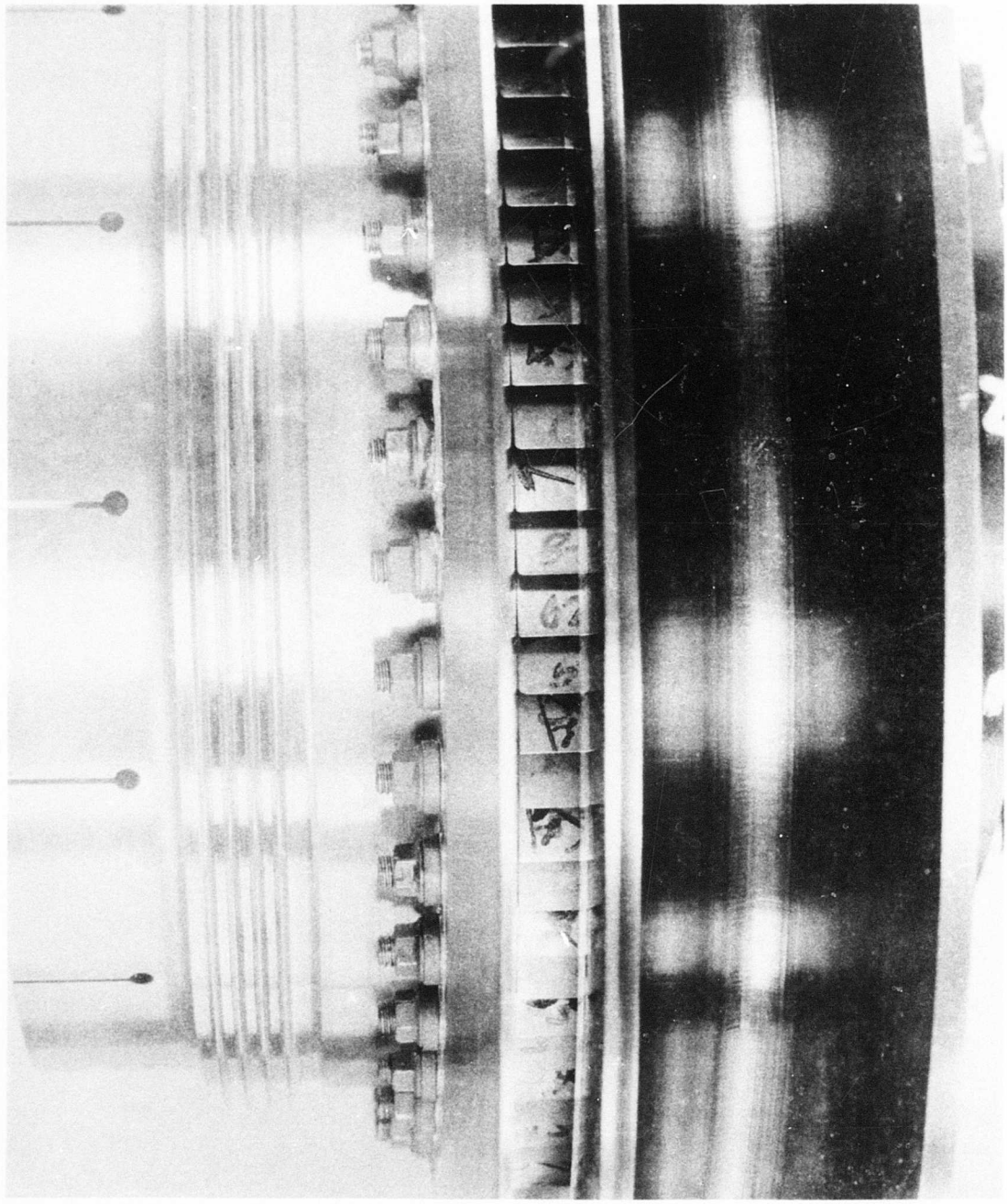

Figure 19. Close-up of Phase III Rotor Illustrating Clearance Between Rotor Blade Trailing Edges and the Rotating Shroud.

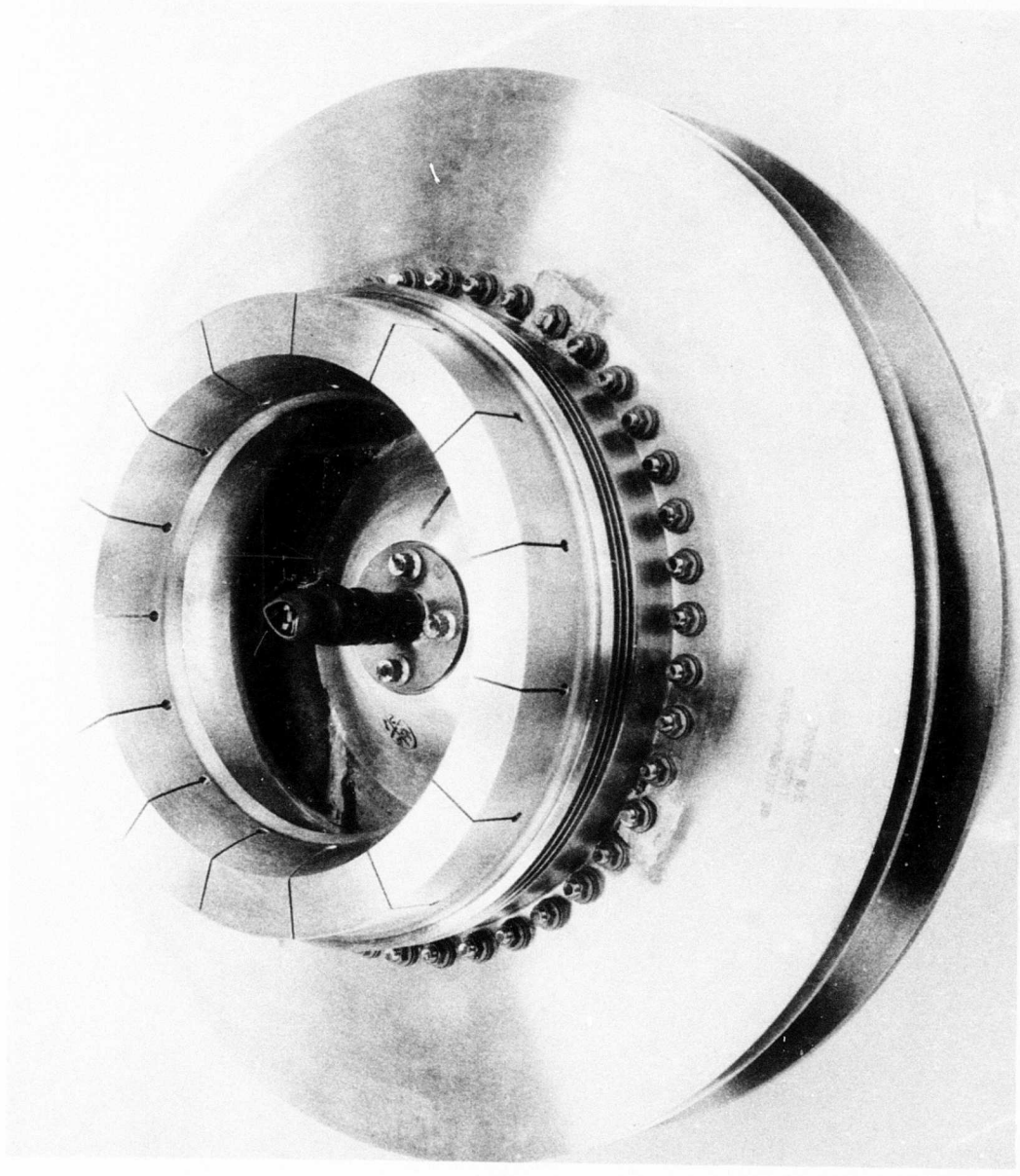

Figure 20. Upstream View of Phase III Rotor.

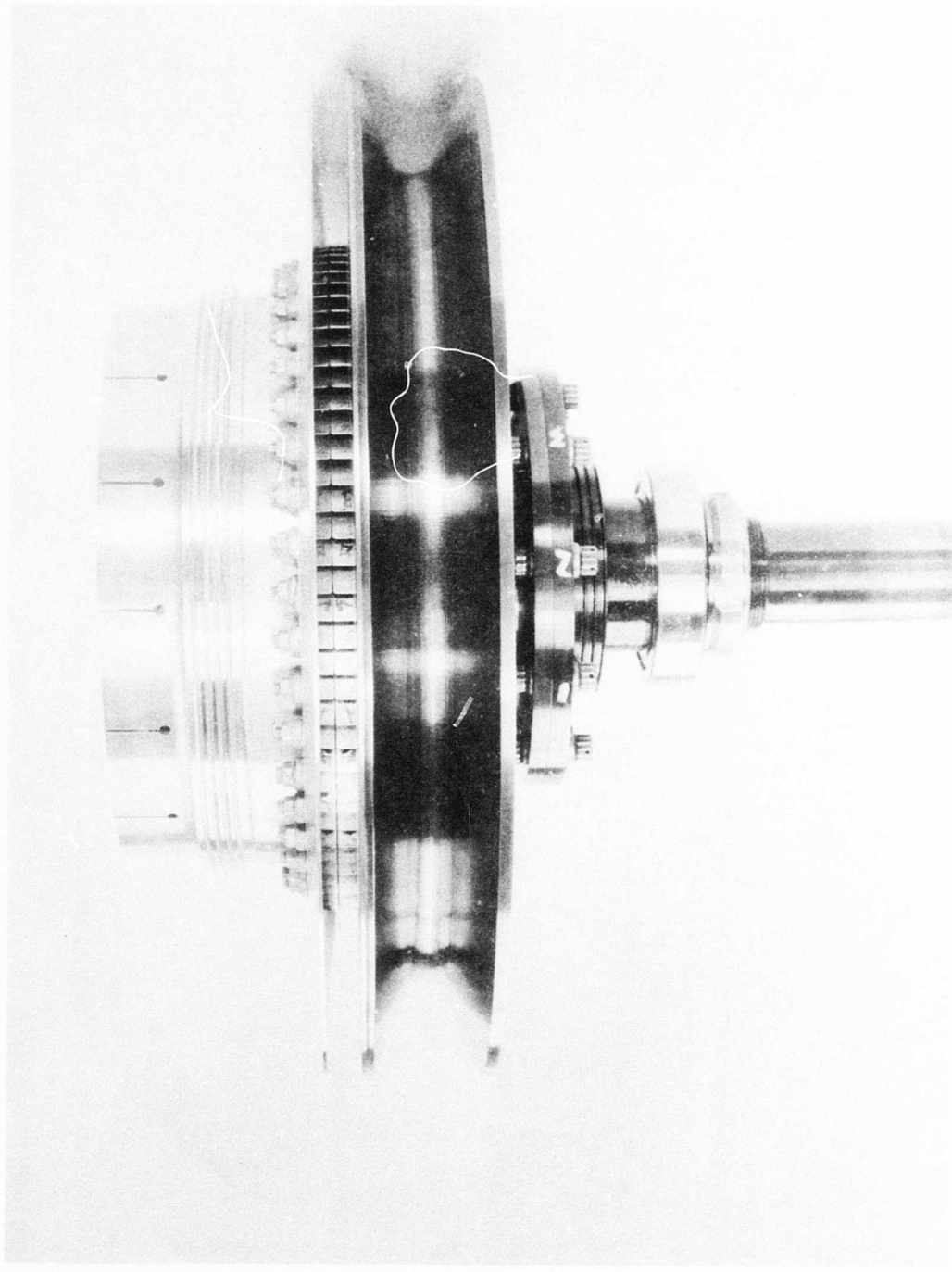

Figure 21. Side View of Phase III Rotor.

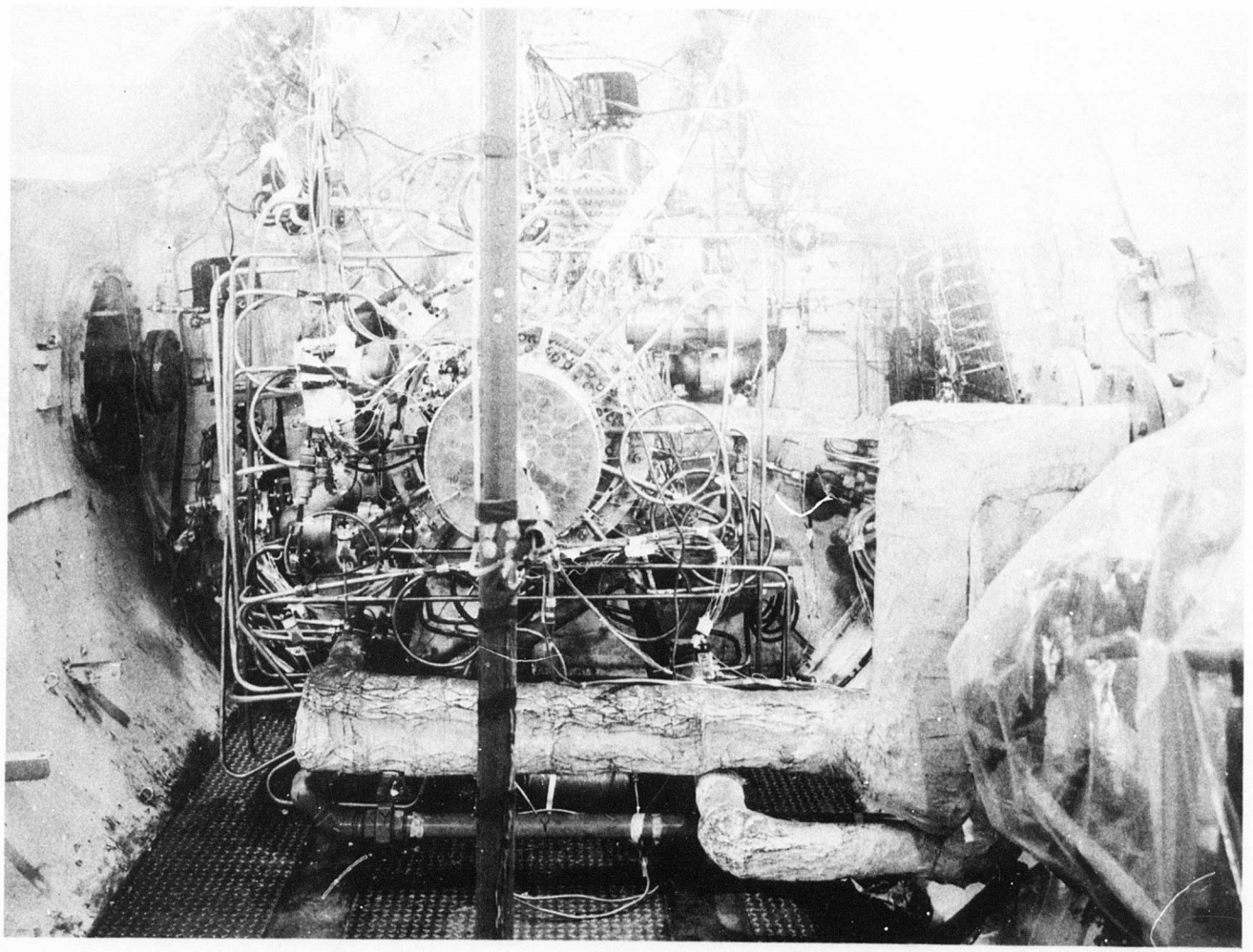

Figure 22. Phase III ROC Installed in Test Cell for Buildup A.

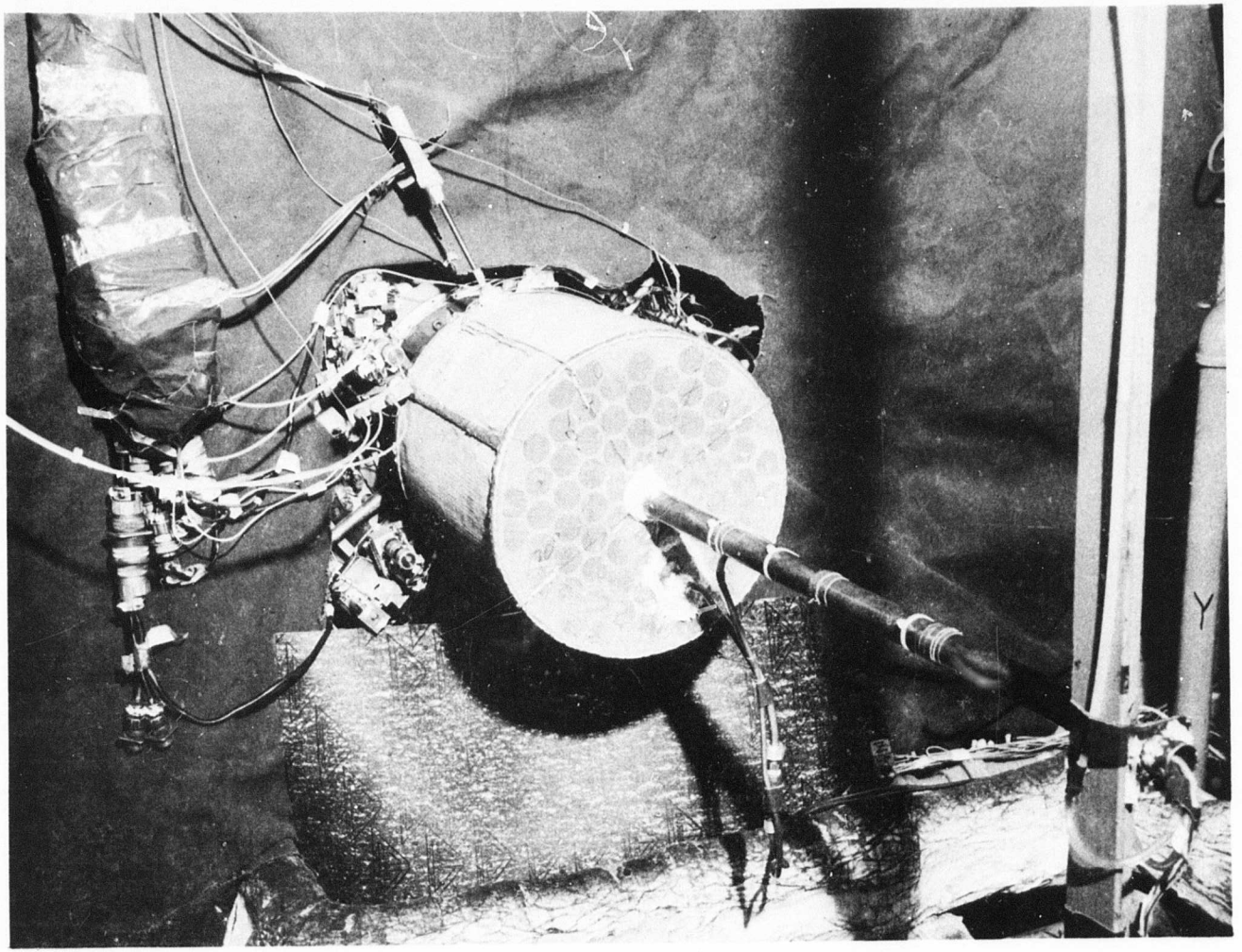

Figure 23. Close-up of Compressor Inlet Screen and Instrumentation Prior to Test of Buildup A, Phase III Investigation.

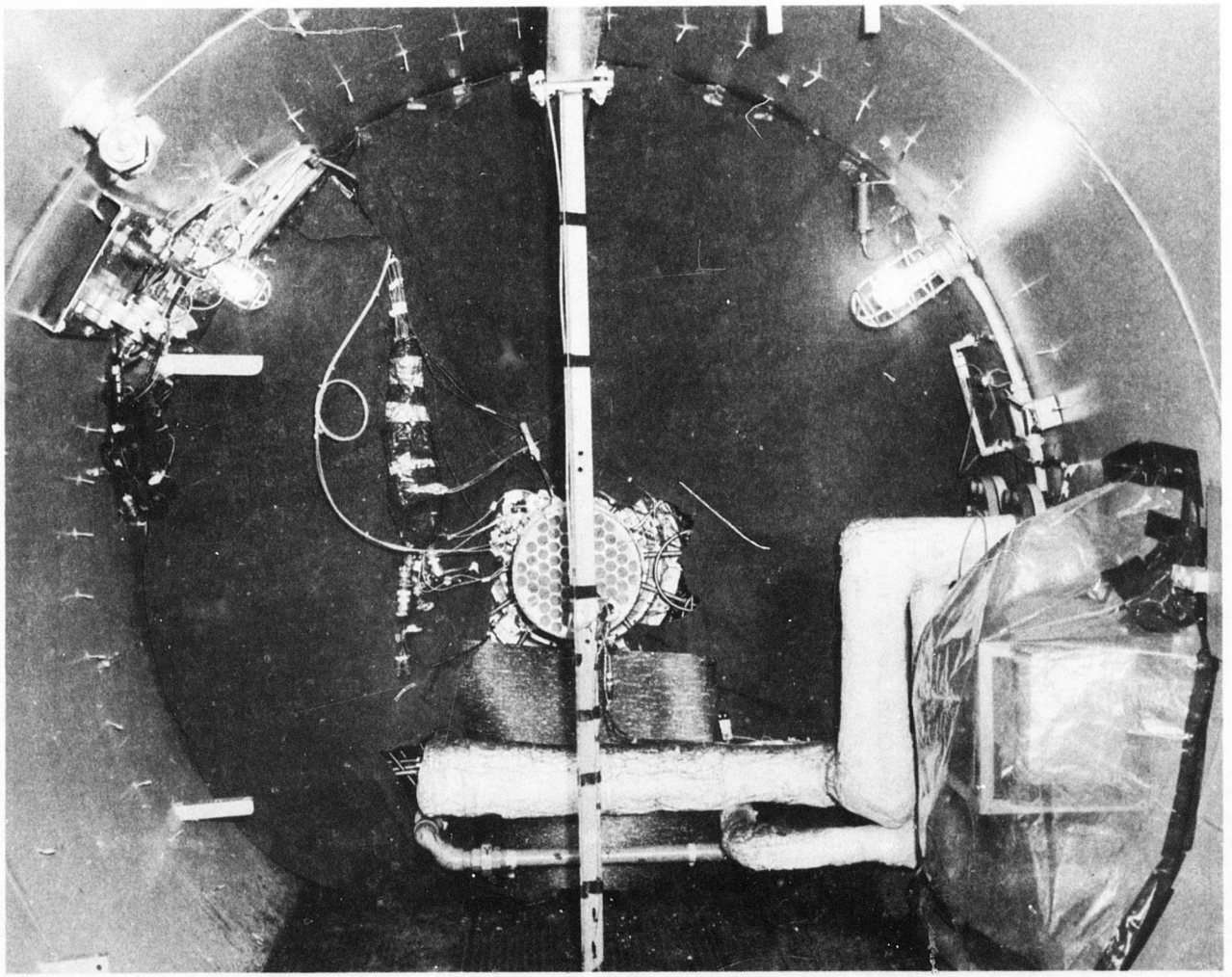

Figure 24. Overall View of ROC in Test Cell for Buildup A, Phase III Investigation.

and instrumentation is shown in Figure 23. An overall view of the test cell after the canvas screen has been installed is presented in Figure 24.

TESTS OF BUILDUP A

An attempt was made to run the compressor on February 7, 1968, and minor vibrations of the compressor bellmouth in the horizontal plane were observed at 3,000 rpm. Acceleration of the compressor to 5,000 rpm excited horizontal bellmouth vibrations exceeding 3 mils, resulting in an automatic tripout of the compressor drive system. Several attempts were made to accelerate beyond this speed. The drive system permits some test rotor acceleration after tripout has occurred. By this means, evidence was seen that slightly above 5,000 rpm the vibrations were reduced. With this evidence, it was felt that a safe acceleration could be made above 5,000 rpm with the tripout system inoperative. This can be done by disconnecting it at the control panel. This was done, and once the 5,000 rpm speed had been exceeded and the low vibration region reached, the tripout system was reconnected at the control panel, making it operative once again. Only minor vibrations were seen in the 5,000 to 10,000 rpm speed range. At slightly above 10,000 rpm, a rapid buildup in the vibration level to 8 mils was observed in the horizontal mode. Within a few seconds, vibrations were detected at other parts of the test vehicle and the tripout of the drive system occurred. Inspection of the compressor revealed that the extended lip of the bellmouth liner had seized to the rotor; about 1 inch of this liner was torn loose and became firmly attached to the rotor (Figure 25). Loose shreds of aluminum were found in the locations shown on Figures 26 and 27.

Subsequent removal of the screen, the bellmouth, and the bellmouth liner indicated no damage to the compressor other than shearing of the thin aluminum ring. Photographs of the various parts were taken before removal of the aluminum ring from the rotor was begun (Figures 28 through 30).

The rotor with the aluminum ring attached to it is shown in Figure 27. A view of the broken ring after it had been removed from the rotor (with some difficulty) is shown in Figure 28. The liner after the fracture is shown in Figures 29 and 30.

In spite of the fracture of the bellmouth liner and the generation of sizeable metal shreds, the rotor blades sustained no damage. Small particles of aluminum adhered to the rotor blade leading edges, but these were easily removed with emery paper.

Most of the aluminum ring was removed intact from the rotor, but several hours of sanding using a small hand-held power tool were required to remove all but a very thin layer. The shroud liner was then cut back to the groove seen on Figure 29 and refaired to provide an axial clearance of

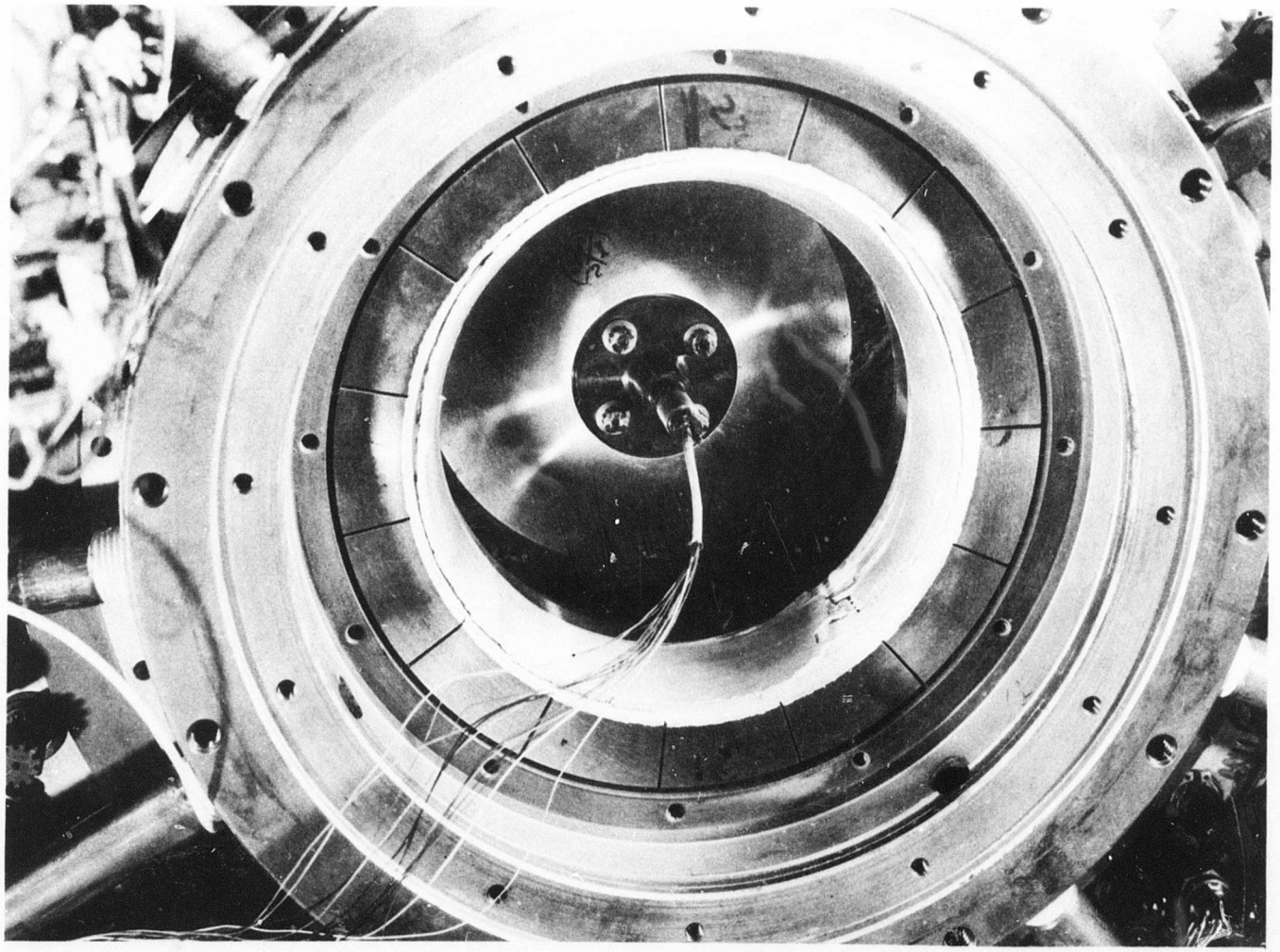

Figure 25. View of Fractured Aluminum Ring Attached to Counterweight Area of Rotating Shroud.

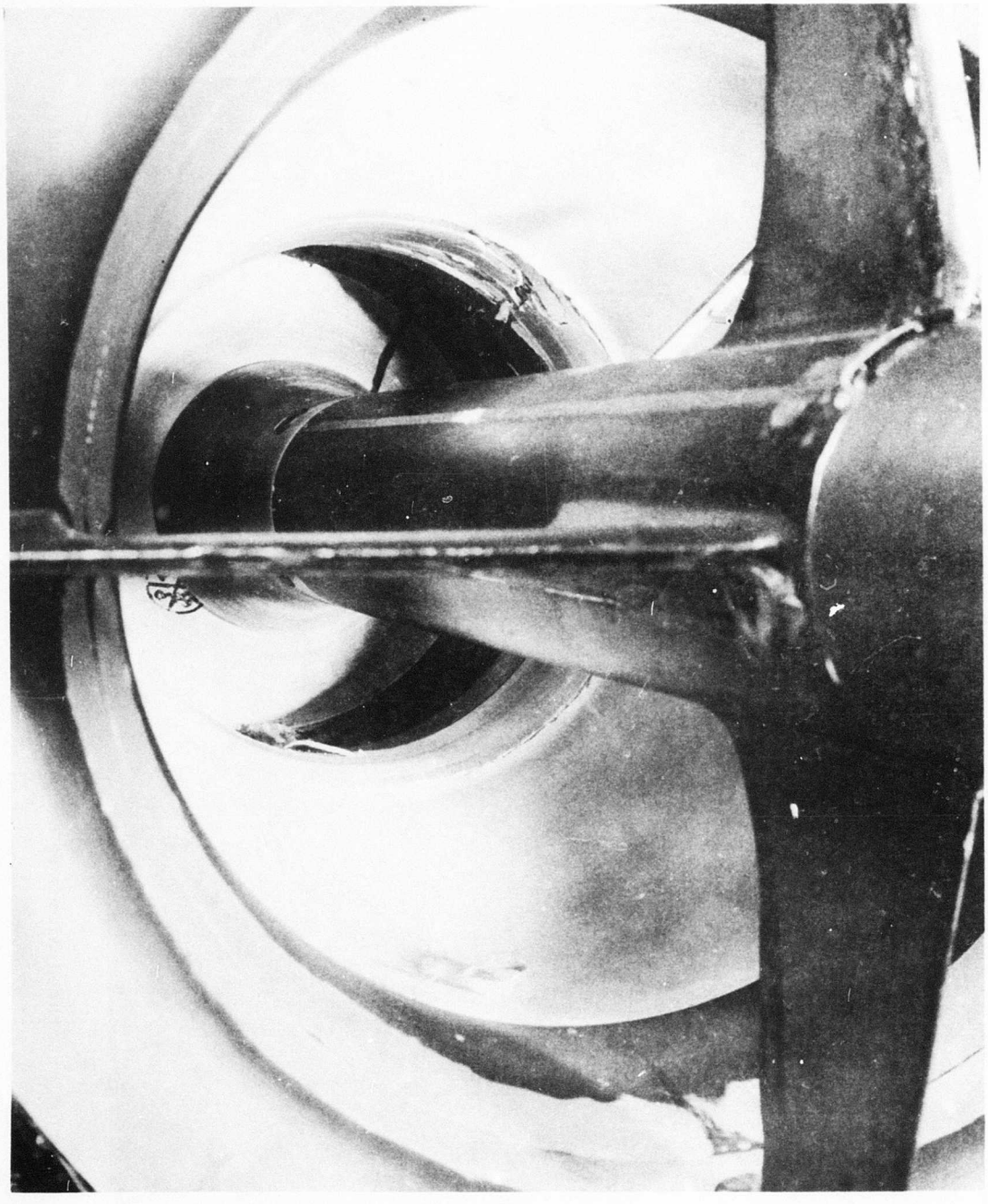

Figure 26. Fractures of Bellmouth Liner and Loose Chip Lying in Bellmouth Following Operation at 10,000 RPM During Buildup A, Phase III Investigation.

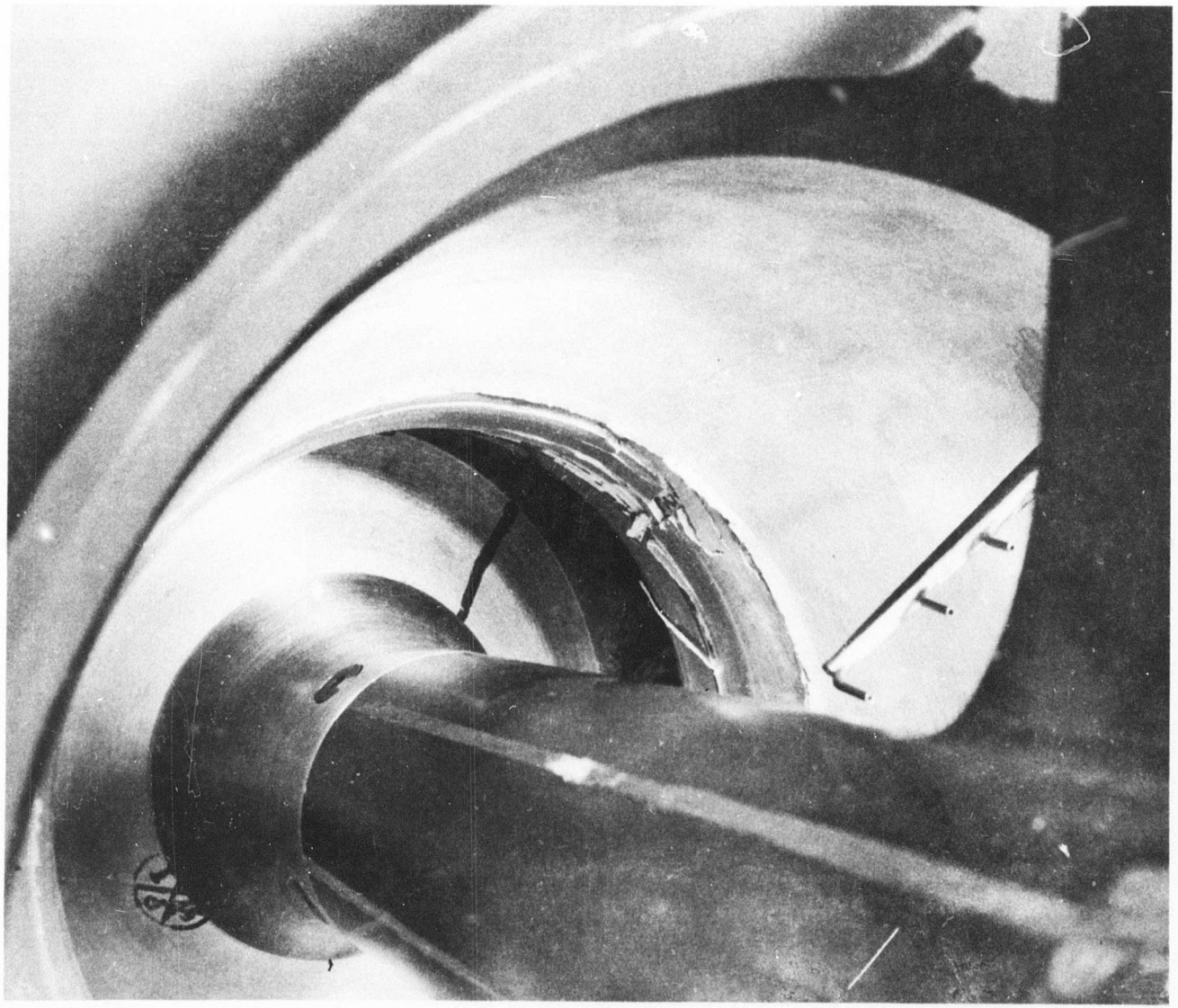

Figure 27. Close-up View of Fractured Ring and Metal Shred After First Run of Buildup A, Phase III Investigation.

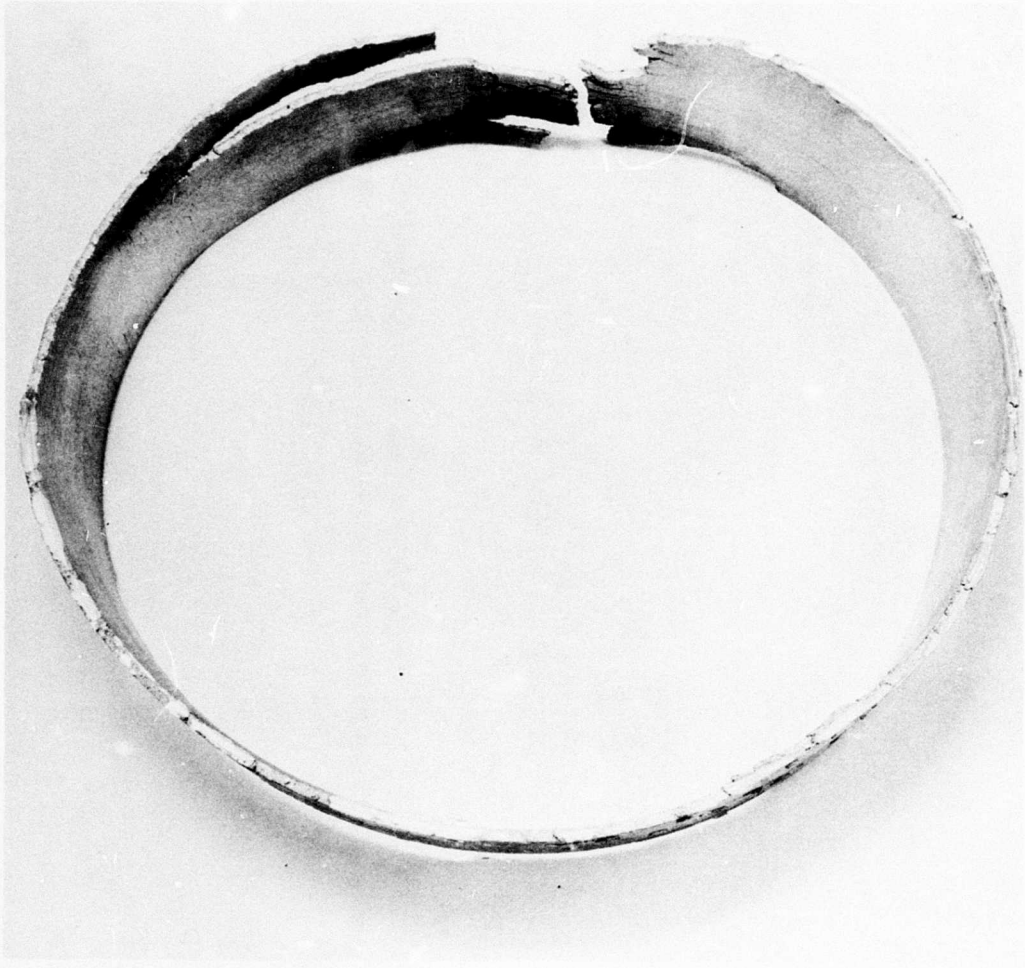

Figure 28. Fractured Ring From Bellmouth Liner After Removal From Counterweight Area of Rotating Shroud.

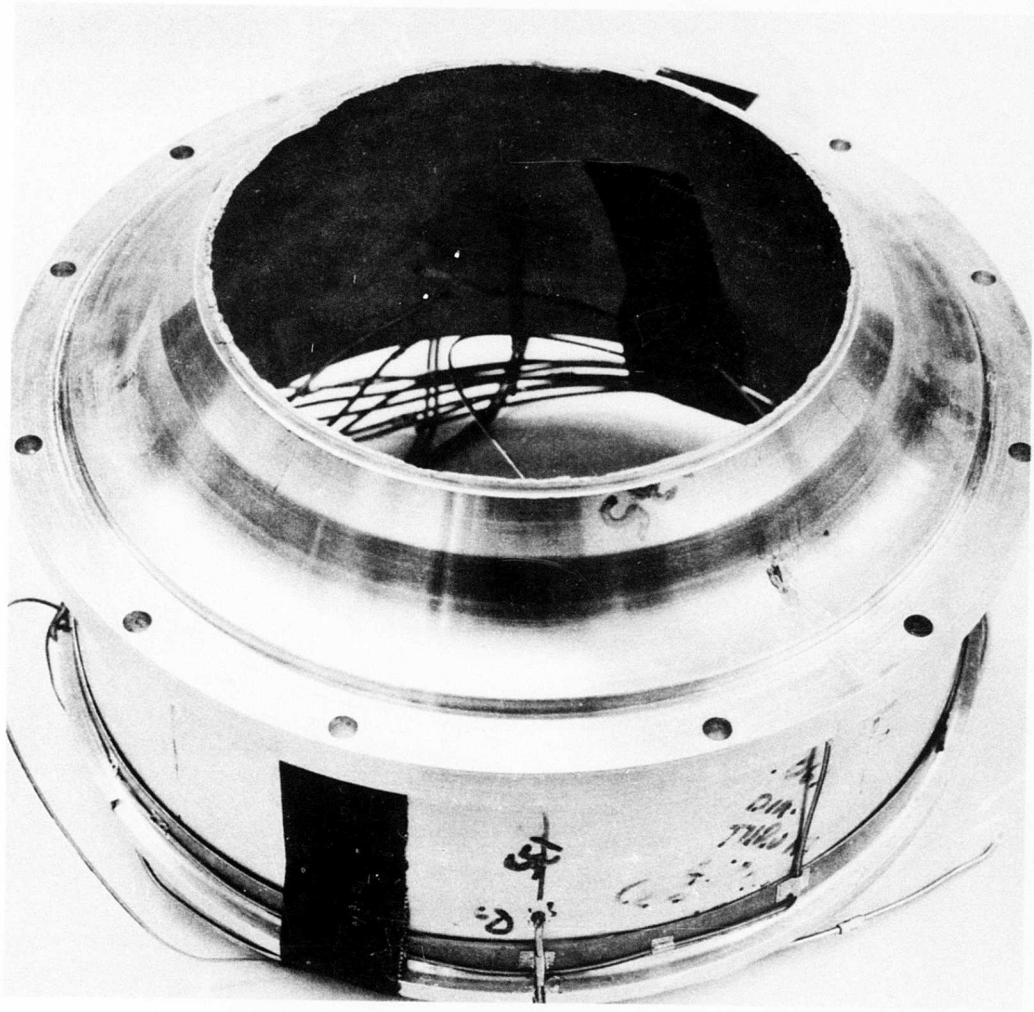

Figure 29. Bellmouth Liner Following Fracture.

Figure 30. Bellmouth Liner and Fractured Ring Following Run 19 of Buildup A, Phase III Investigation.

about 25 mils between the downstream edge of the liner and the upstream edge of the rotor. Cutting back the bellmouth liner exposed to the air stream the slots in the counterweight area of the shroud seen in Figure 9. An unsatisfactory air path resulted as the downstream lip of the modified liner was smaller in diameter by at least 50 mils from the forward edge of the shroud. A rather abrupt step in the airflow path was formed. Furthermore, the abrupt slope between the counterweights and the continuing surface of the shroud (Figure 9) was aerodynamically undesirable.

Run Number 19

In spite of these undesirable aerodynamic characteristics at the entrance to the rotor, it was decided to run the compressor to as high a speed as was mechanically feasible in order to obtain this important operating experience. Although minor rotor vibrations were observed at 80 percent and at 90 percent speed, no rotor nor test vehicle vibrations greater than 3 mils were seen at any speed. This statement must be qualified since proximeter readings showed a steady motion of the shroud rim of 8 mils for each revolution. However, mechanical measurement of the rotor after assembly had indicated a 6-mil runout of the shroud rim, and it is believed that the proximeter signals were due to this cause rather than to vibrations.

In spite of the unsatisfactory inlet conditions to the rotor shroud reasonably satisfactory performance was obtained at 30, 40, 50, and 60 percent speed. In fact, the highest rotor efficiency obtained in any configuration at 60 percent speed was observed with a corrected efficiency of 88.1 percent obtained during Run Number 19.

At speeds above 60 percent, the running was limited to a few minutes because of overheating of a bearing in the high-speed gearbox. For this reason, only a few points were taken at 70 percent speed, although efficiencies of 82.7 and 85.0 percent were obtained. There was reason to believe that with further vane closure and appropriate throttle adjustments, improved performance could be obtained. It was decided to continue the acceleration in order to achieve the mechanical objectives. The rotor exit flow angle and total pressure profiles were not uniform with flow angle approaching and exceeding 90 degrees near the shroud. Because of the bearing temperature problem, sufficient running time was not available to obtain complete aerodynamic data at 80 and 90 percent speed. As noted previously, rotor vibrations were not excessive, and there is reason to have confidence that operation at 100 percent speed can be accomplished. During attempted acceleration to full speed, all of the strain gage signals were lost and the run was discontinued.

Following Run Number 19 of the Buildup A configuration, Phase III investigation, the compressor was disassembled to repair instrumentation and to replace the bellmouth liner. The compressor rotor following

disassembly is shown in Figure 31. The discoloration of the disc shown on the left in the region between the aluminum centerbody and the rotor blades is a plastic material used in attempting to smooth the flame-sprayed surface. A discrete flow pattern is visible on the rotor disc external to the rotor blades, suggesting that the flow adhered to the disc surface; no separation was present. A similar situation was apparent on the surface of the rotating shroud shown on the right. A close-up of the disc and the rotor blade removed from the assembly is presented in Figure 32. The soot pattern on the concave surface of the rotor blades is relatively uniform. It is not clear what material formed the white deposit near the shroud on the aft portion of the rotor blade. The seal used during this buildup has a silver foam rubbing surface, but examination of this seal following the run showed very little wear. It seems more likely, therefore, that the deposit may be aluminum rubbed from the liner during the short run on February 7 during which fracture of the bellmouth liner occurred. The compressor was not disassembled between the run on February 7 and Run Number 19 on February 19. Due to the high camber and solidity of the rotor blades, only the forward portion of the rotor blades can be observed unless the compressor is disassembled, so the outer regions were not examined between these runs.

A close-up of the rotating shroud is shown in Figure 33. On the outer portion of the shroud, the expected flow pattern is seen left of center and right of center on the shroud surface. In the center of the outer portion of the shroud and to the left, an essentially radial line can be observed. Careful examination of the rotor disc (Figure 31) shows similar radial streaks adjacent to the rotor blades to which the strain gage leads are attached. At least 1 additional radial streak can be seen at 240 degrees measuring clockwise from the top. Rather surprisingly, 2 of the streaks originating from the zone of the strain gage leads appeared to have etched the surface of the disc. In other words, more than a soot pattern appears in these 2 zones, as a definite roughness of the surface could be felt. This does not appear to be so on the rotating shroud, and it is possible that the radial line center of Figure 33 is merely a soot pattern outboard of a rotor blade having strain gage leads. The presence of these 4 blades having leads could be detected in the pressure pattern produced by the high frequency response static pressure crystals mounted in the stator casing.

Run Number 20

The compressor was disassembled and 3 of the rotor shroud strain gages were returned to service. The special spindle holding the Number 4 crystal was ground to fit in place over the ring gear located on the rear of the main bearing housing. A relatively short Run Number 20 was conducted on February 24, 1968. Significant compressor vehicle vibrations were observed, and considerable difficulty was encountered when attempting to accelerate through the low-speed range to 30 percent speed.

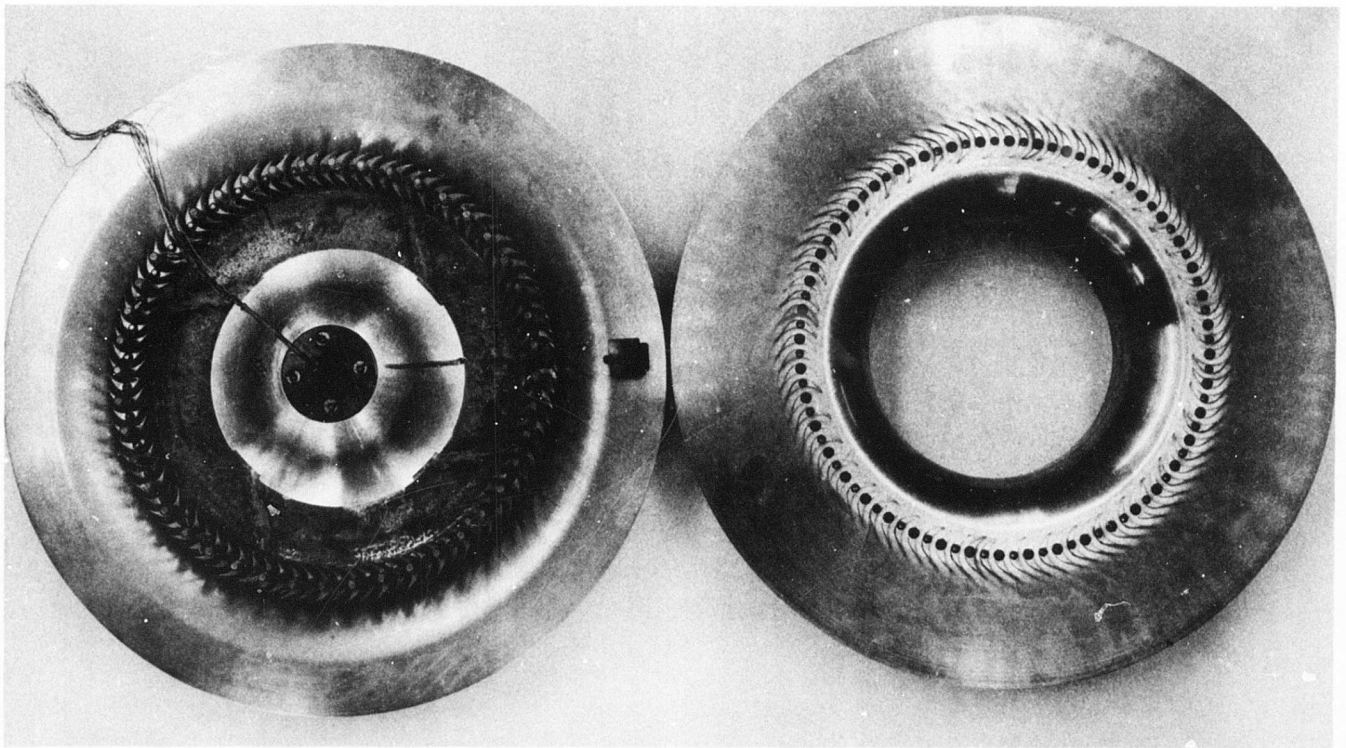

Figure 31. Soot Patterns on Rotor Disc and Rotating Shroud Following Run Number 19 of Buildup A, Phase III Investigation.

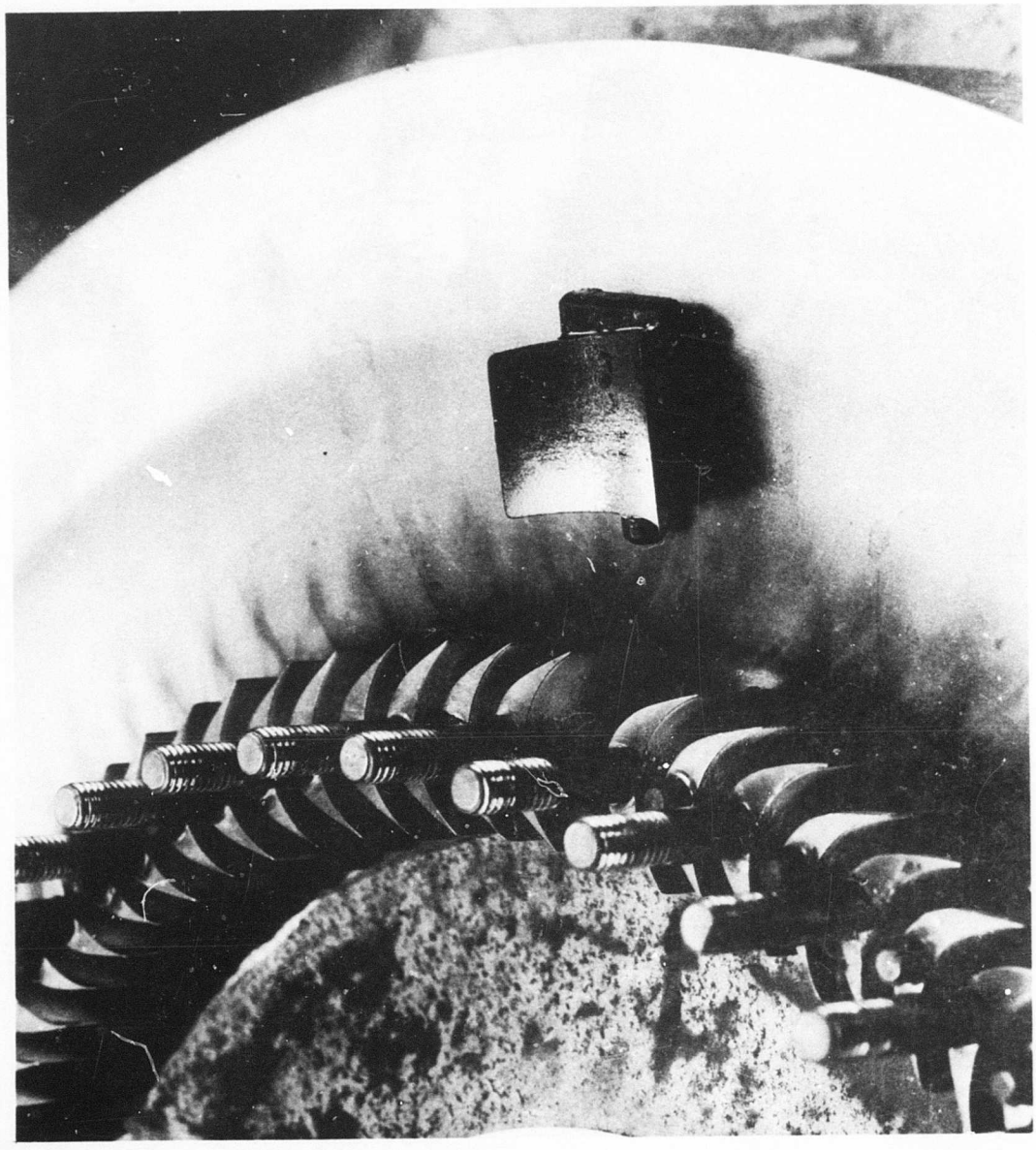

Figure 32. Soot Patterns on Rotor Blades and Disc Following Run Number 19 of Buildup A, Phase III Investigation.

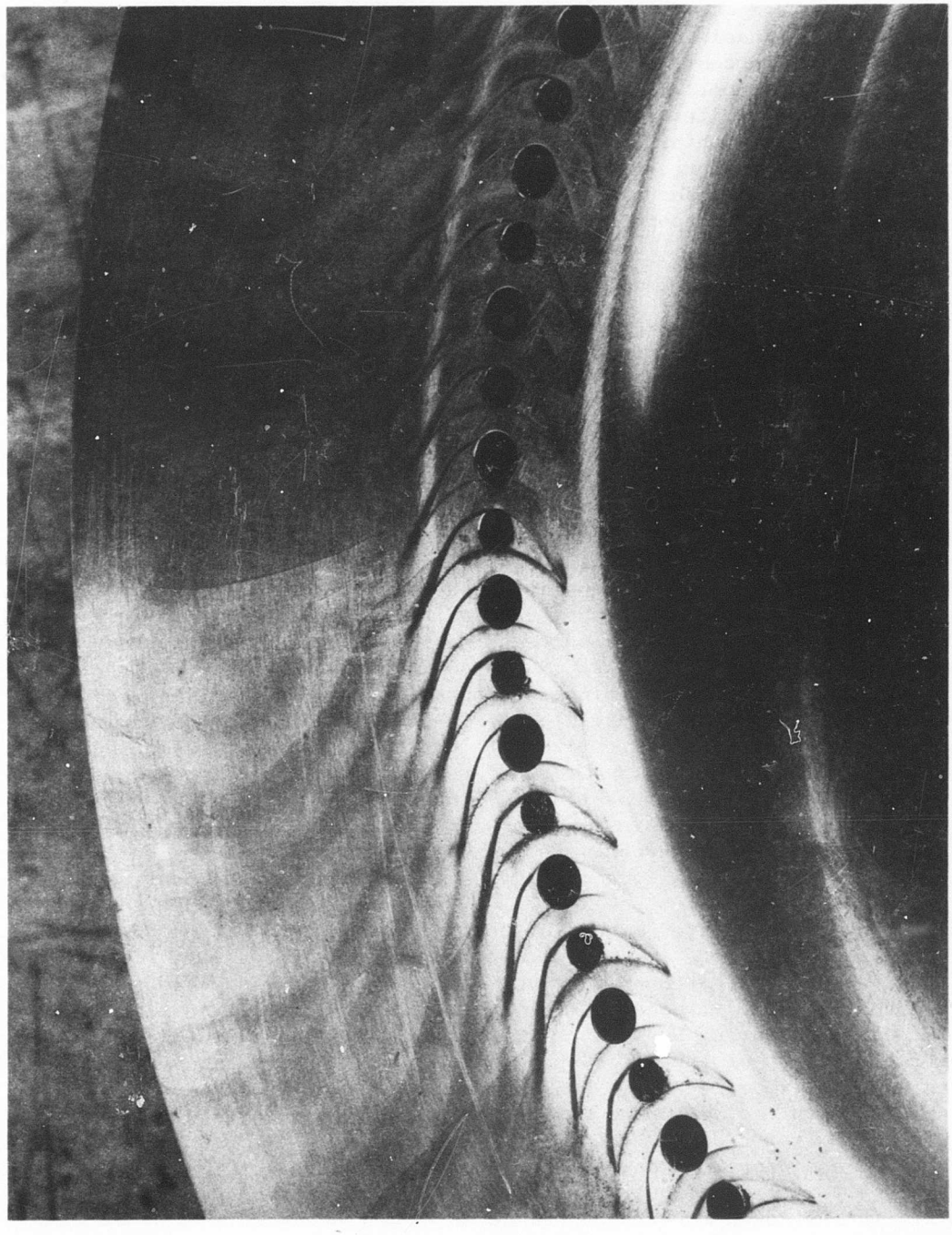

Figure 33. Close-up of Soot Patterns on Rotating Shroud Following Run Number 19 of Buildup A, Phase III Investigation.

The primary emphasis during the February 24 run was to get to high speed, hopefully 100 percent; therefore, no attempt was made to optimize aerodynamic performance. Data points were taken at speeds up to 60 percent, but due to the limited time and the vibration difficulties encountered, the maximum speed obtained was 70 percent. First operation of the ROC at reduced inlet pressure was accomplished during Run Number 20. Data taken at 50 percent speed for atmospheric inlet and for two-thirds atmospheric inlet pressure correspond satisfactorily.

Run Number 21

Before Run Number 21 was started about 40 pounds of 1/16-inch-diameter lead shot were poured into the spacing around the main bearing housing. The purposes of the lead shot were to stiffen the support of the main bearing housing and to provide friction dampening to reduce the horizontal vibrations. This approach was successful in reducing the horizontal vibrations. Again the prime purpose of the run was to obtain data at speeds in the 65 to 100 percent range. Although test data were taken at 30, 40, 50, 60, 65, 70, 76, and 80 percent speed, only 1 rotor strain gage was still functioning, so time was not taken to optimize settings for maximum aerodynamic performance. The test vehicle operated very satisfactorily at 80 percent speed at reduced inlet pressure, and several accelerations to 90 percent and slightly higher speed were made. However, immediate shutdown on reaching 90 percent speed happened automatically on 3 occasions. No reason for the tripouts at 90 percent speed could be determined since no vibration, insufficient oil, or water pressure nor overtemperature signal was observed or recorded during or after the tripouts. The test vehicle was brought back to atmospheric pressure for examination. A circumferential crack was discovered in the lip of the cast replacement liner (Figures 34 and 35). It is believed that a spurious electronic impulse was responsible for the tripouts of the compressor at 90 percent speed. Due to the crack in the bellmouth liner and impending failure of that part, the test was discontinued.

Although only a limited amount of test data was taken during Run Numbers 19, 20, and 21, there was ample evidence that the rotor exit flow adjacent to the shroud was not nearly as uniform as during Buildup F of the Phase II investigation. Traces of flow angle and total pressure taken at 50 percent speed during Run Number 20 (Figure 36) illustrate this trend. Over 60 percent of the rotor span adjacent to the disc, the flow angle varied only ± 1 degree from 74.5 degrees. The flow angle increased rapidly as the rotor shroud was approached, reaching a value of about 85 degrees from radial. The rotor exit total pressure was highest at the disc and decreased only slightly over 80 percent of the passage adjacent to the disc, but dropped rapidly as the shroud was approached. A similar but even more rapid change of conditions occurred in the traverse taken at 60 percent speed (Figure 37). Unfortunately, this point was of low efficiency, 71.6 percent. A point of better performance at 60 percent speed with an efficiency of 81.8 percent showed an angle variation of about ± 2 degrees over 80 percent of the rotor exit

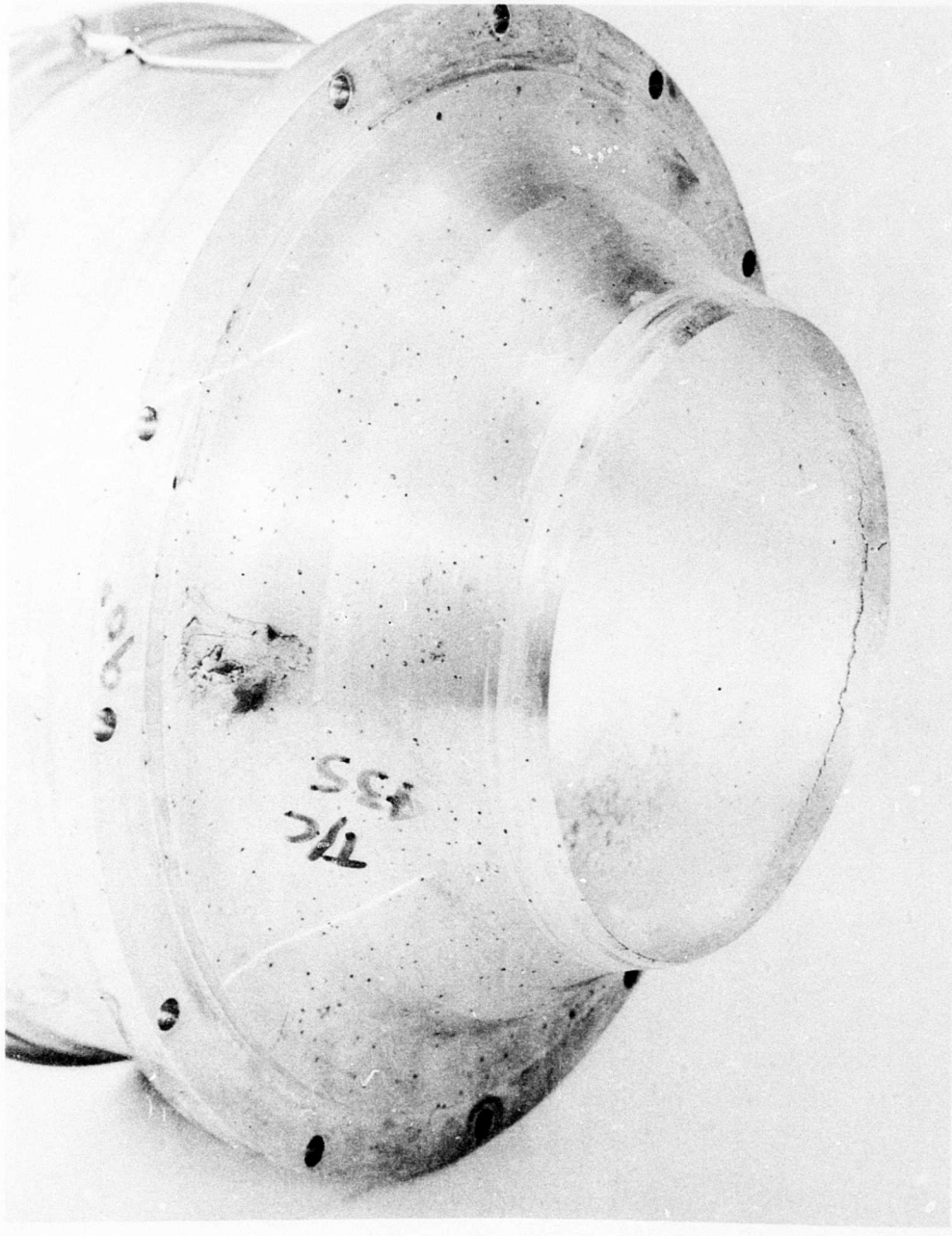

Figure 34. View of Crack in Cast Replacement Liner Following Run Numbers 20 and 21 of Buildup A, Phase III Investigation.

Figure 35. Close-up of Fracture in Cast Bellmouth Liner.

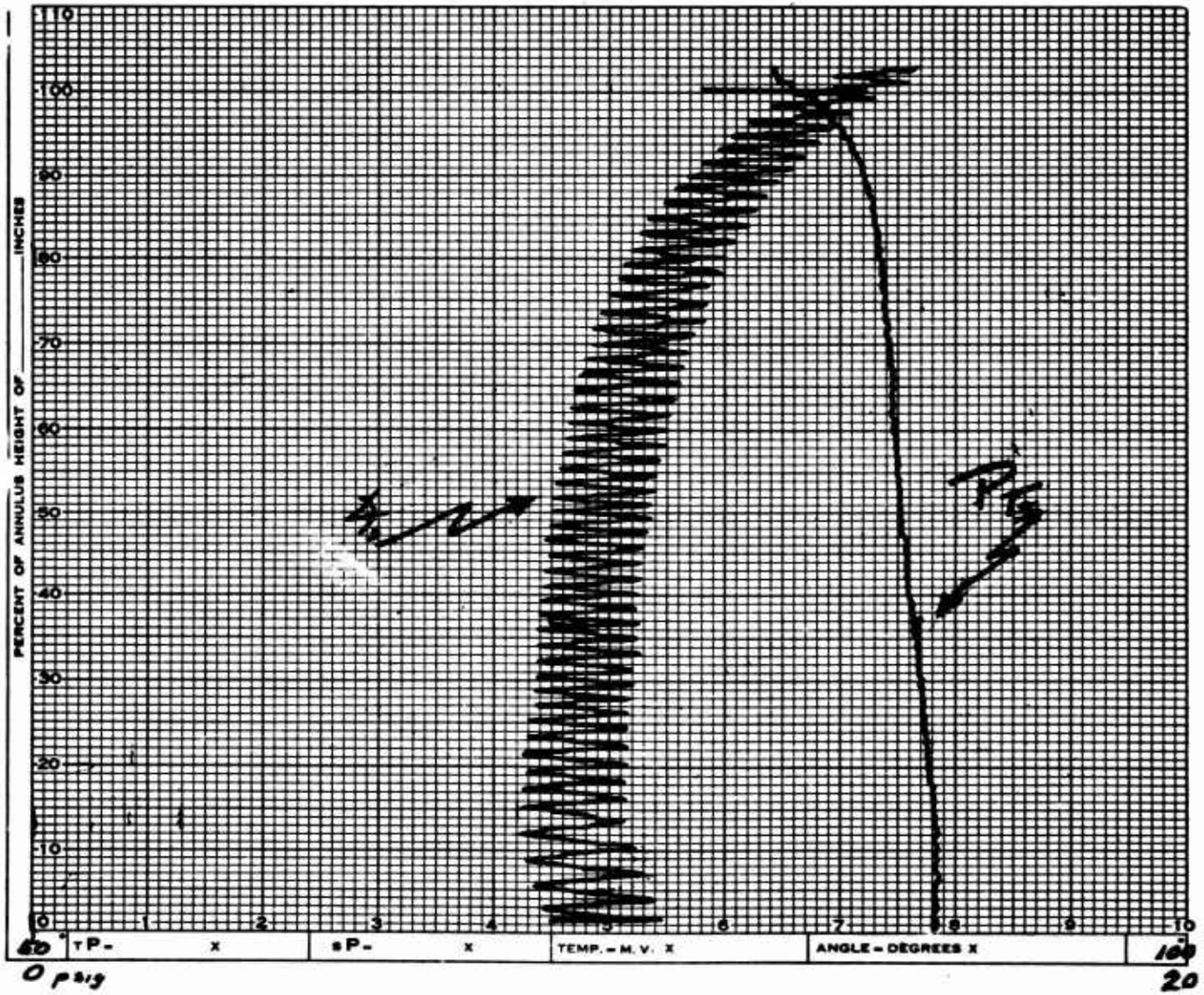

Figure 36. Traverse Plot of Flow Angle and Total Pressure at Rotor Exit for 50 Percent Speed Taken During Run Number 20.

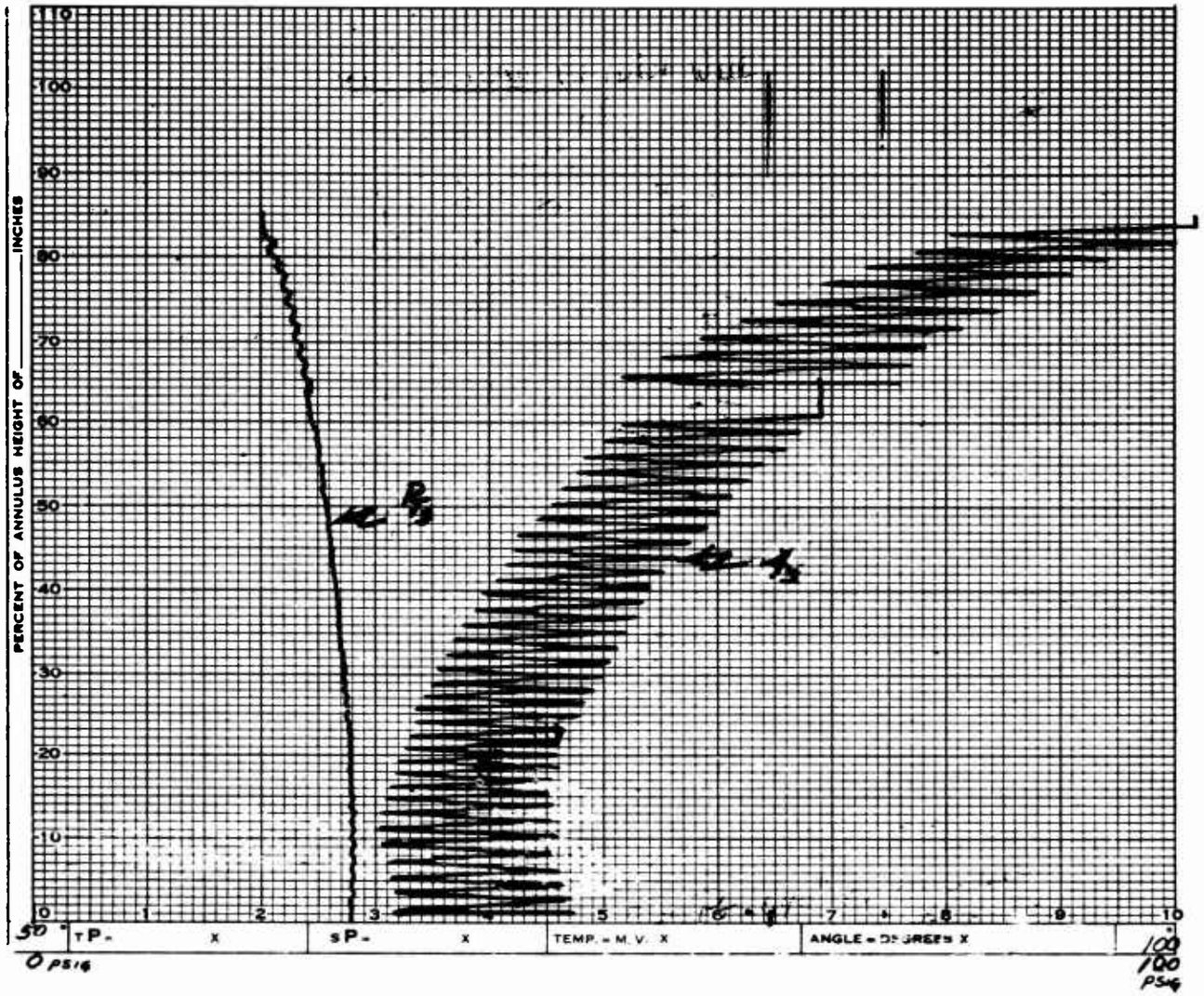

Figure 37. Traverse Plot of Flow Angle and Total Pressure at Rotor Exit for 60 Percent Speed Taken During Run Number 20.

width from the disc with an increase of about 8 degrees as the shroud was approached. There was ample evidence, therefore, that the use of a circular inlet vane should improve the performance of the Phase III rotor. It was therefore decided to employ a circular inlet vane for Buildup B of the Phase III investigation.

TEST CONFIGURATION FOR BUILDUP B

The compressor configuration tested as Buildup B, Phase III, is presented in Figure 38. The details of the circular inlet vane used with the Phase III rotor are presented in Figure 39. The bellmouth liner was modified by the application of an extension of pyrolytic graphite fibers that were covered with a fiber glass cloth and bonded with phenolic resin (Figure 40). The inlet total pressure rake and the static pressure leads are visible in this photograph. The graphite fibers are abradable and have a high modulus of elasticity. The material and resins used are capable of maintaining strength in the 400°F temperature range.

The Buildup B configuration consisting of the new circular inlet vane, the Phase III rotor blades, the supersonic stator vanes (Figure 10), and the subsonic stator vanes (Figure 11) was assembled. The stator system prior to adding the aft stator casing is shown in Figure 41. New strain gages were applied to the rotating shroud at 4 circumferential locations on the rotor blade centerline and also to 2 supersonic stators. Since the strain gages on the subsonic vanes were operating satisfactorily at the end of Run Number 21, Buildup A, it was not felt necessary to replace these gages. Three total pressure tubes were installed on each of 2 supersonic stators (Figure 42), and 2 flow angle measuring probes were installed on 2 supersonic stators (Figure 43). A small slot was cut in 6 subsonic stators to permit passage of the pressure tubes and strain gage leads from the supersonic stators. A 10-element wake rake was installed downstream of the subsonic stators (Figure 43). This rake can be traversed across the flow path at the stator exit. A 15-element total pressure rake also containing 14 thermocouples (Figure 44) was installed in the upper exit arm of the compressor (plane 8). This rake can be traversed completely across the exit duct at plane 8. Static pressure crystals were installed in the bellmouth, at 4 locations in the compressor casing (on the subsonic stator spindle centerline), and at 1 location in the lower compressor exit. A single total pressure tube and a single thermocouple were installed in the lower exit arm of the compressor in a location corresponding to the survey rake in the upper arm, so that both locations correspond to plane 8.

TEST RESULTS FROM BUILDUP B

Run Number 22

The first run of Buildup B, Run Number 22, was conducted on April 15, 1968. Because the test vehicle and all of its instrumentation had been

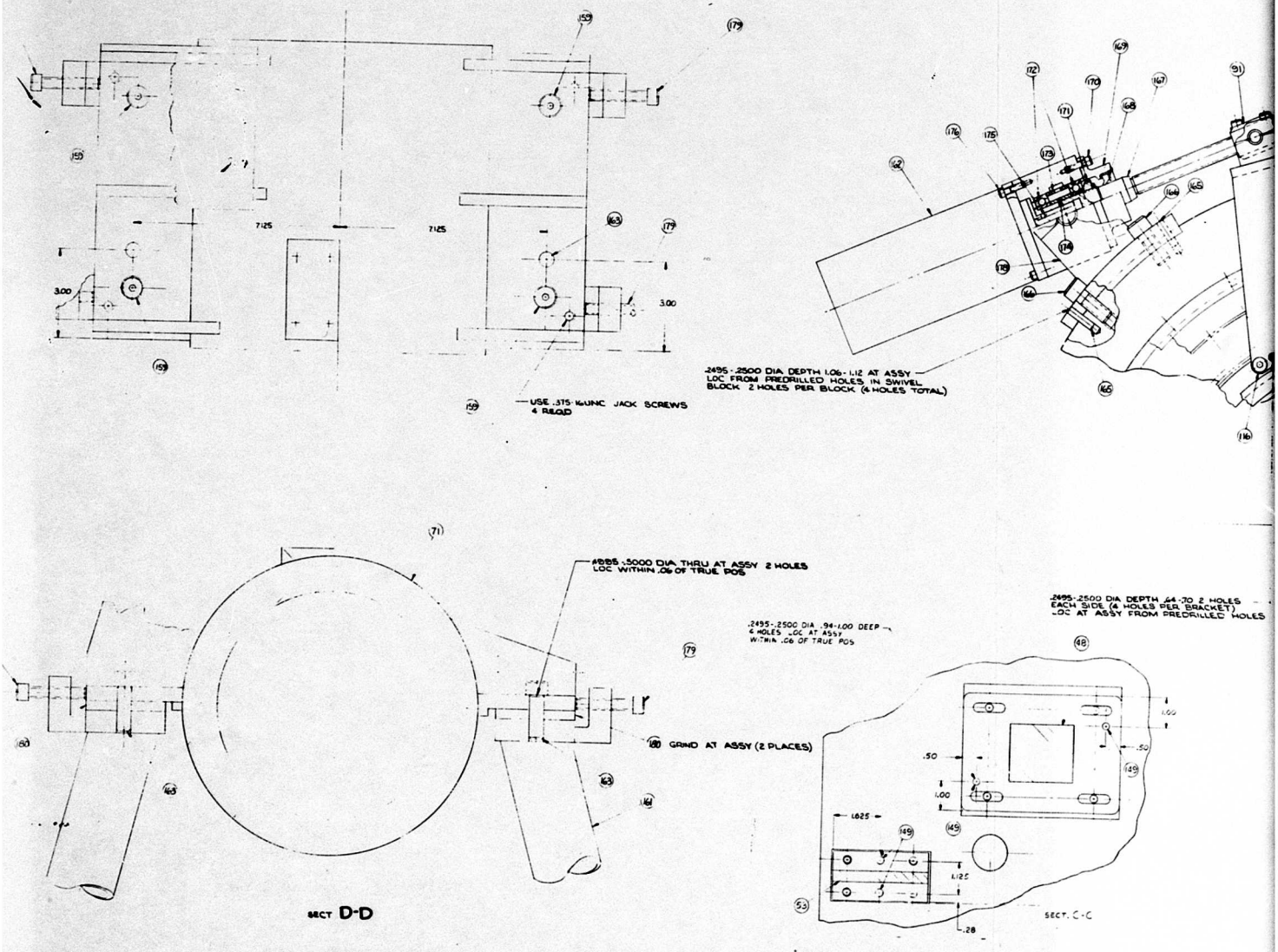

Figure 38. Assembly Drawing of ROC as Tested in Buildups B and C, Phase III Investigation.

A

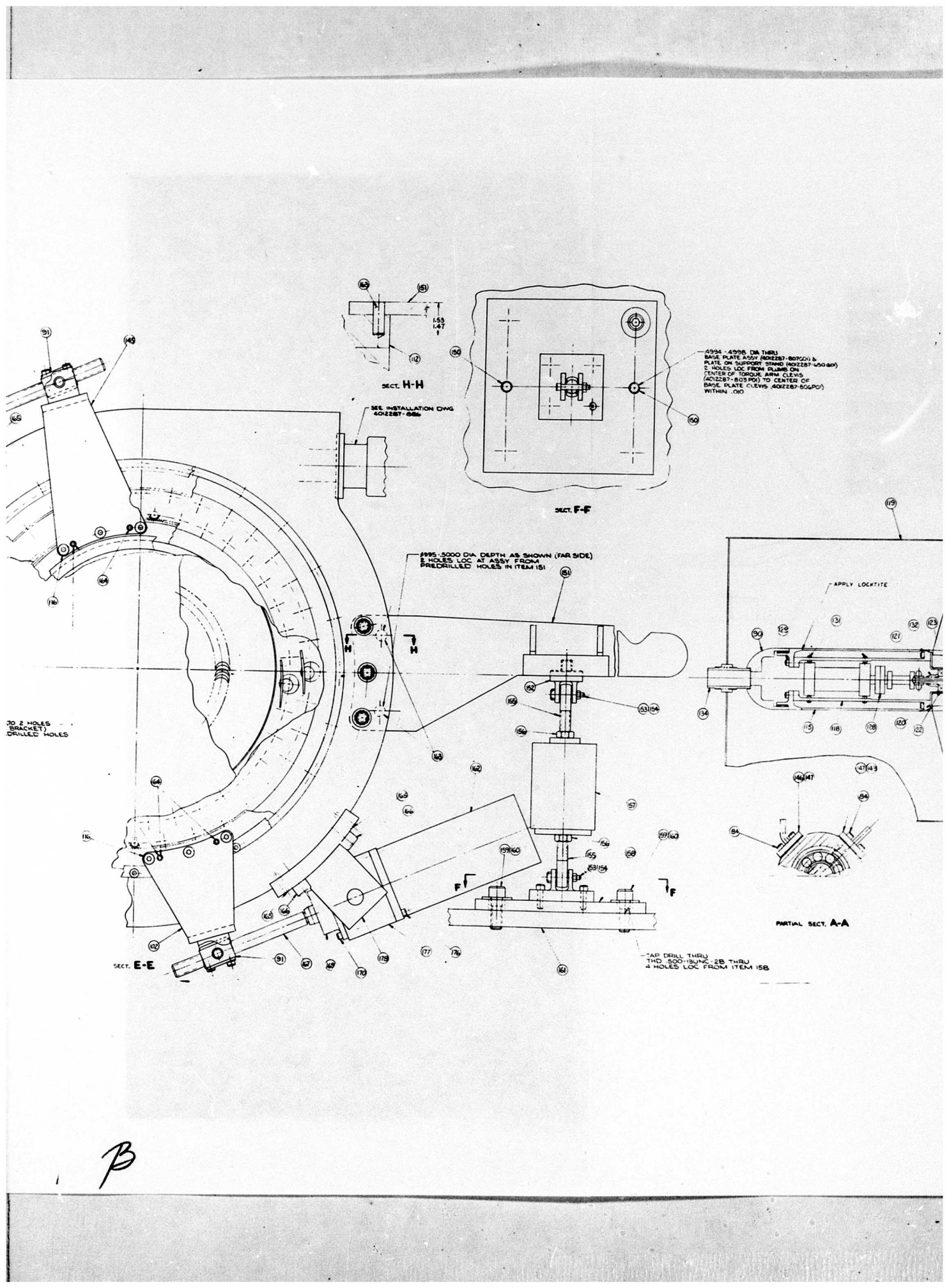
SECT. H-H
SEE INSTALLATION DWG 4012287-
.4994 - .4998 DIA THRU BASE PLATE ASSY (4012287-807 OR) & PLATE ON SUPPORT STAND (4012287-050 OR) 2 HOLES LOC FROM PLANE ON CENTER OF TORQUE ARM CLEVIS (4012287-803 POI) TO CENTER OF BASE PLATE CLEVIS (4012287-806 POI) WITHIN .010
SECT. F-F
.4995 - .5000 DIA DEPTH AS SHOWN (FAR SIDE) 2 HOLES LOC AT ASSY FROM PREDRILLED HOLES IN ITEM 151
APPLY LOCKTITE
70 2 HOLES (BRACKET) DRILLED HOLES
SECT. E-E
PARTIAL SECT. A-A
TAP DRILL THRU THD .500-13UNC-2B THRU 4 HOLES LOC FROM ITEM 158

B

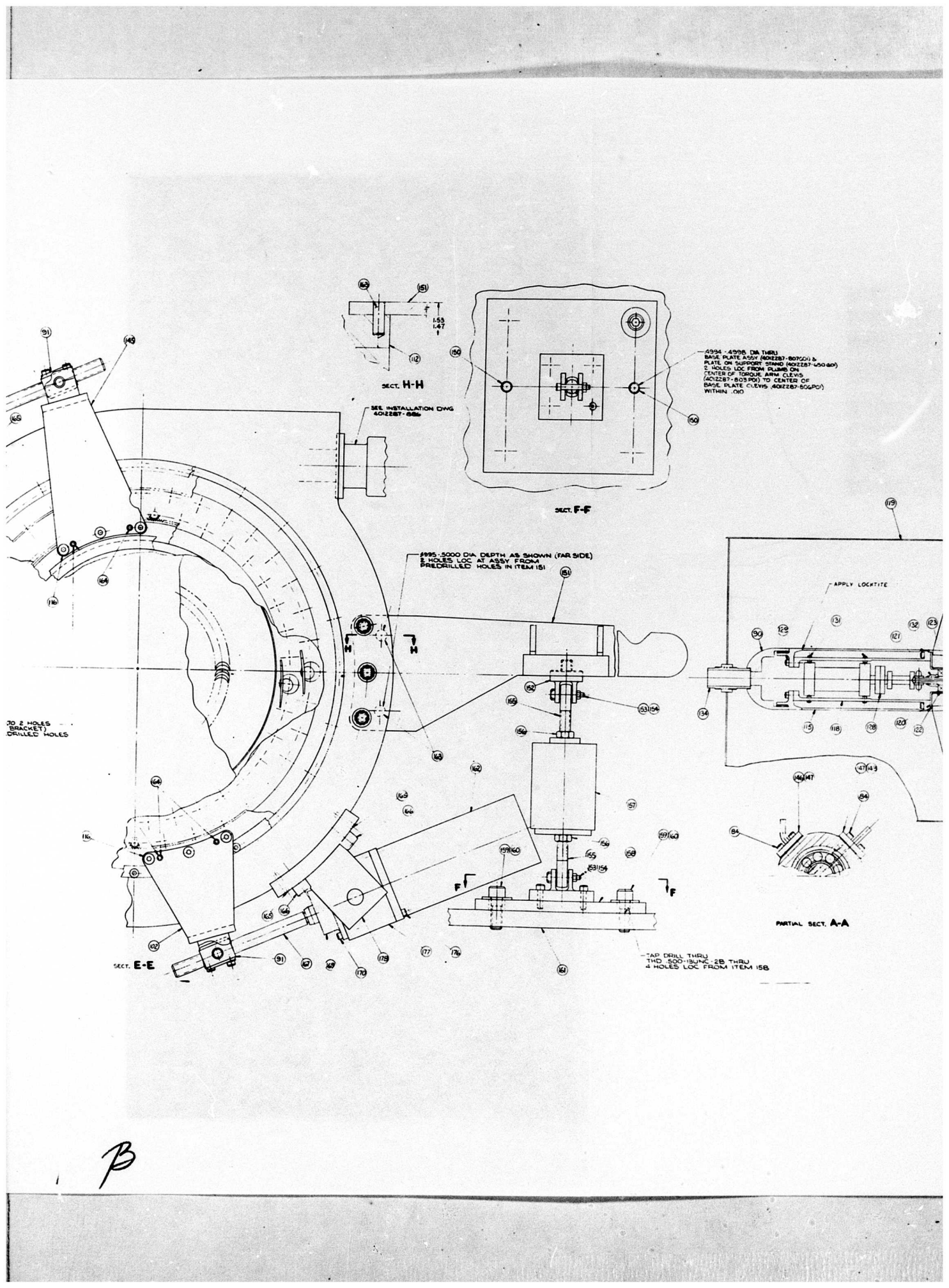
SECT. H-H
SEE INSTALLATION DWG 4012287-
.4994 - .4998 DIA THRU BASE PLATE ASSY (4012287-807 OR) & PLATE ON SUPPORT STAND (4012287-050 OR) 2 HOLES LOC FROM PLANE ON CENTER OF TORQUE ARM CLEVIS (4012287-803 POI) TO CENTER OF BASE PLATE CLEVIS (4012287-806 POI) WITHIN .010
SECT. F-F
.4995 - .5000 DIA DEPTH AS SHOWN (FAR SIDE) 2 HOLES LOC AT ASSY FROM PREDRILLED HOLES IN ITEM 151
APPLY LOCKTITE
70 2 HOLES (BRACKET) DRILLED HOLES
SECT. E-E
PARTIAL SECT. A-A
TAP DRILL THRU THD .500-13UNC-2B THRU 4 HOLES LOC FROM ITEM 158

B

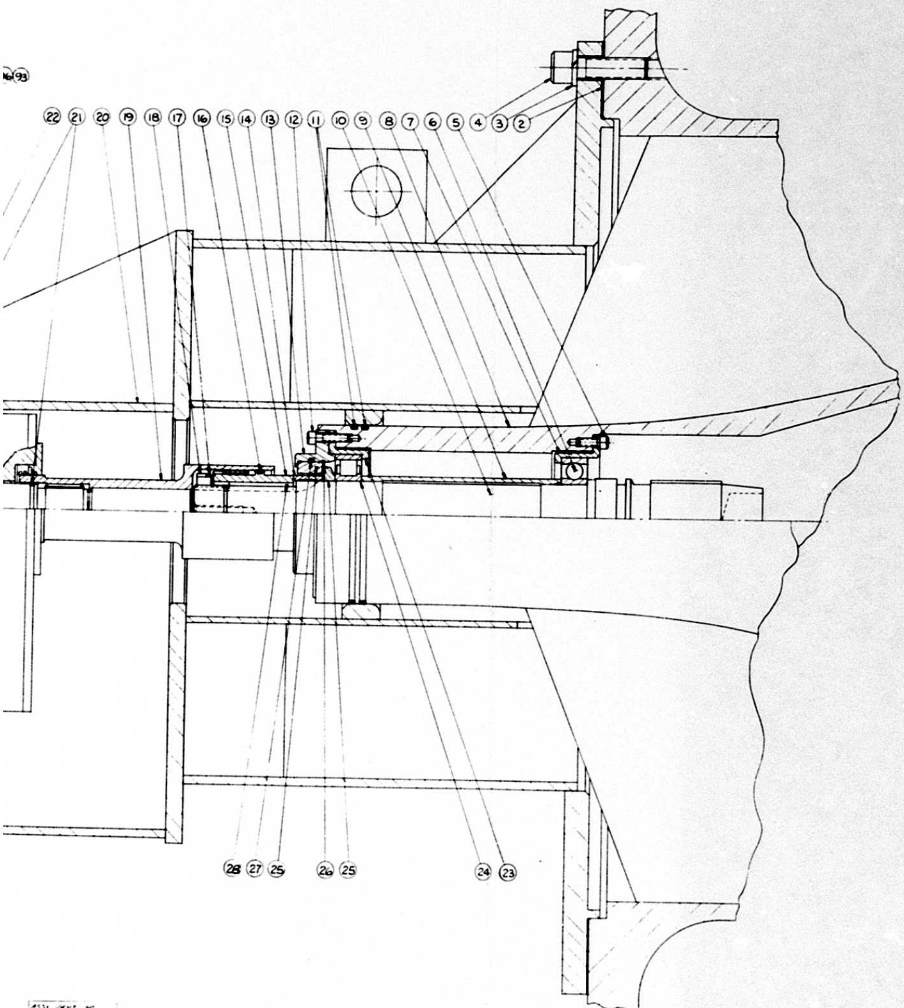

[illegible]	[illegible]	[illegible]	[illegible]	[illegible]	[illegible]	[illegible]	[illegible]
163	COML	DOWEL PIN 1/2 DIA x 1 1/2 LG	C25	2	2		
164	1/8 DIA x [illegible] LG	PULL DOWEL PIN (Y)	C[illegible]	6	6		
165	1/8 DIA x 1 LG	PULL DOWEL PIN (Y)	H27	4	4		
166	COML	SOC HD CAP SCR/NYLOK 1/2-13UNC x 1 1/4 LG	H27	8	8		
167	4012287-[illegible]	SHAFT	J27	2	2		
168	511219	SEAL (Z)	H27	2	2		
169	4012287-[illegible]P01	RETAINER	J27	2	2		
170	COML	SOC HD CAP SCR/NYLOK #10-24UNC x 5/8 LG	J27	6	6		
171	SL58-N-05	LOCKNUT (M)	[illegible]	2	2		
172	105 KRDU	BEARING (A)	J2[illegible]	4	4		
173	4012287-67[illegible]P01	SPACER	H[illegible]	2	2		
174	↓ -[illegible]	SPACER	H[illegible]	2	2		
175	COML	KEY 1/8 x 3/32 x 1 1/16 LG	[illegible]	2	2		
176	COML	SOC HD CAP SCR/NYLOK #10-24UNC x 3/4 LG	H28	8	8		
177	4012287-676P01	BEARING HOUSING	H2[illegible]	2	2		
178	↓ -679G01	SWIVEL BLOCK	F2[illegible]	2	2		
179	COML	SOC HD CAP SCR 3/8-16UNC x 2" LG FULL THD	J30	4	4		
180	4012287-[illegible]	SHIM	G30	2	2		
181	COML	FL HD SCR/NYLOK #10-24 UNC x 1/2 LG	B18	6	6		
182	COML	SOC HD SCR/NYLOK 1/4-20 UNC x 3/4 LG	B18	12	12		
183	4013046-055P01	EXTENSION	E17	1			
183	4013046-056P01	EXTENSION	E17		1		
184	#CR-102	RETAINING RING	D18	1	1		
185	COML	FL HD (ALLEN) SCR/NYLOK #10-32 UNF x 9/16 LG	E17	4	4		
186	4013046-064G01	VANE ASSY	D17	1			
187	4013046-053P01	CASING	F18	1	1		
188	4013046-075G02	ASSY	A12		X		

[illegible]	[illegible]	[illegible]
79	4012287-648P01	BAFFLE
80	#2-13	O RING (C1)
81	EWB 0820-4-6	BOLT (H)
82	61170-428	LOCKNUT (H)
83	COML	FL. HD SOC CAP [illegible] #10-32UNF x 1/2 L[illegible]
84	COML	SOC HD CAP [illegible] #10-32UNF x [illegible]
85	4012287-752P01	RETAINER
86	#5-481	O RING (C2)
87	4012287-755G01	GEARSHAFT ASS[illegible]
88	5100-50	RETAINING RIN[illegible]
89	#RS	WAVE WASHER
90	4013017-982P01	NUT
91	4012297-680P01	PIVOT
92	4012287-86[illegible]	INLET TUBE
93	COML	SOC HD CAP SC[illegible] #10-32 UNF x 1/2 L[illegible]
94	4012287-892P01	GASKET
95	-[illegible]G01	OUTLET TUBE
96	-891P01	GASKET
97	-239P01	RING GEAR
98	-764P01	SHIM
99	-755G02	GEARSHAFT AS[illegible]
100	-240P01	RING GEAR
101	-[illegible]P01	RETAINING RING
102	-687G01	BRACKET
103	-[illegible]P01	STATOR VANE-[illegible]
104	↓ -[illegible]P01	STATOR VANE-[illegible]
105	80575-50	WASHER (N)
106	4012287-574P05	BLADE
107	8368-0	BASE (R)
108	LH8368-02	NUT (R)
109	4013042-365P01	SPACER
110	4012287-578P06	BLADE
111	210-M-95	WASHER (S)
112	4012287-751G01	CASING ASSY
113	4013046-059P01	LINER-SHROUD
114	4012287-846P01	RETAINING RING
115	4013017-985G01	CASING
116	COML	FL HD SOC CAP S[illegible] 1/4-20 UNC x 3/4 LG
117	4013046-074P01	RING-SEAL
118	4013017-984P01	SUPPORT
119	-987P01	INLET SCREEN
120	↓ -[illegible]P01	BRG HOUSING
121	5221835-[illegible]	NUT
122	#100KSFF	BEARING
123	#R26	WAVE WASHER
124	#CS-39	RETAINING RING
125	4013046-060P01	STATOR CASING-INLE[illegible]
126	4013046-057P01	CENTER BODY
127	EWB926-5-10	BOLT
128	C-6120-D	SLIP RING (A-3 [illegible])
129	COML	SOC HD SCR/NYLO[illegible] #8-32UNF x 1/2 LG
130	5003MS1P02	NUT
131	COML	SET SCR/NYLOK FL[illegible] #8-32 UNF x 5/16 LG
132	COML	SOC HD SCR/NYLO[illegible] #8-32 UNF x 3/4 LG
133	COML	SOC HD SCR/NYLOK #10-24 UNC x 5/8 LG
134	4013042-313P01	TUBE
135	4013017-993P01	RING
136	4013046-042G01	FRAME
137	COML	SOC HD CAP SCR/[illegible] #10-32UNF x 3/4 LG
138	COML	SOC HD CAP SCR/[illegible] 5/16-18UNC x 7/8 L[illegible]
139	4013017-983P01	BELLMOUTH
140	4013042-363P01	SLEEVE
141	361P01	STUB SHAFT
142	↓ 362P01	SHAFT
143	4013046-051P01	ROTATING SHROU[illegible]
144	4013046-049P01	DISK
145	4012287-671G01	BRACKET
146	-[illegible]G01	OIL JET
147	-879P01	GASKET
148	↓ -[illegible]	OIL JET
149	COML	DOWEL PIN 1/4 DIA x 7/8 LG
150	COML	DOWEL PIN 1/2 DIA x 1 1/4 LG
151	4012287-798G01	TORQUE ARM
152	-805P01	CLEVIS
153	↓ -806P01	SHOULDER SCREW
154	21FA-1028	LOCKNUT (H)
155	MD48-19	ROD END (V)
156	COML	JAM NUT 1/2-20UNF-2B
157	35-135-BK-100#	ALINCO LOAD CELL
158	4012287-801G01	BASE ASSY
159	COML	SOC HD CAP SCR/[illegible] 1/2-13UNC x 1 1/2 LG
160	COML	1/2" WASHER-MED
161	4012287-650G01	STAND
162	#391A156-600	GEARMOTOR TYPE C[illegible]

ASSY IDENT NO	
(1)	4013046-075G01
(188)	4013046-075G02

P

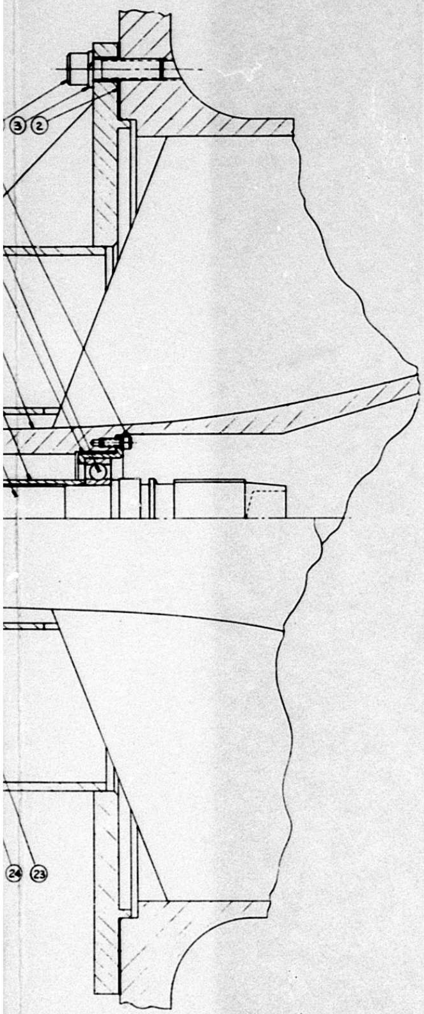

[illegible]	[illegible]	[illegible]	[illegible]	1	2	3	4
163	COML	DOWEL PIN 1/2 DIA x 1 1/2 LG	C25	2	2		
164	1/2 DIA x [illegible] LG	PULL DOWEL PIN (Y)	C25	8	8		
165	1/2 DIA x 1 LG	PULL DOWEL PIN (Y)	H27	4	4		
166	COML	SOC HD CAP SCR/NYLOK 1/2-13UNC x [illegible] LG	H27	8	8		
167	4012287-[illegible]	SHAFT	J27	2	2		
168	[illegible]	SEAL (Z)	H27	2	2		
169	4012287-[illegible]	RETAINER	J27	2	2		
170	COML	SOC HD CAP SCR/NYLOK #10-24UNC x 5/8 LG	J27	6	6		
171	SL58-N-05	LOCKNUT (M)	H28	2	2		
172	105 KRDU	BEARING (A)	J28	4	4		
173	4012287-678P01	SPACER	H28	2	2		
174	↓ -[illegible]P01	SPACER	H28	2	2		
175	COML	KEY 1/8 x 3/32 x 1 1/8 LG	H28	2	2		
176	COML	SOC HD CAP SCR/NYLOK #10-24UNC x 3/4 LG	H28	8	8		
177	4012287-674P01	BEARING HOUSING	H28	2	2		
178	↓ -679G01	SWIVEL BLOCK	F28	2	2		
179	COML	SOC HD CAP SCR 3/8-16UNC x 2" LG FULL THD	J30	4	4		
180	4012287-[illegible]P01	SHIM	B30	2	2		
181	COML	FL HD SCR/NYLOK #10-24 UNC x 1/2 LG	B18	6	6		
182	COML	SOC HD SCR/NYLOK 1/4-20 UNC x 3/4 LG	B18	12	12		
183	4013046-055P01	EXTENSION	E17	1			
183	4013046-056P01	EXTENSION	E17		1		
184	#CR-102	RETAINING RING	D18	1	1		
185	COML	FL HD (ALLEN) SCR/NYLOK #10-32 UNF x 9/16 LG	E17	4	4		
186	4013046-064G01	VANE ASSY	D17	1			
187	4013046-053P01	CASING	F18	1	1		
188	4013046-075G02	ASSY	A12		X		

[illegible]	[illegible]	[illegible]	[illegible]	1	2	3	4
79	4012287-648P01	BAFFLE	E16	1	1		
80	#2-13	O RING (C1)	E16	2	2		
81	EWB 0830-4-6	BOLT (H)	C16	10	10		
82	61170-428	LOCKNUT (H)	C16	10	10		
83	COML	FL. HD SOC CAP SCR/NYLOK #10-32UNF x 1/2 LG	B15	76	76		
84	COML	SOC HD CAP SCR/NYLOK #10-32UNF x 5/8 LG	B15	29	29		
85	4012287-752P01	RETAINER	B15	3	3		
86	#5-481	O RING (C2)	B15	1	1		
87	4012287-755G01	GEARSHAFT ASSY	B15	36	36		
88	5100-50	RETAINING RING (P)	B15	144	144		
89	#R5	WAVE WASHER (N)	A15	144	144		
90	4013017-982P01	NUT	E20	1	1		
91	4012297-680P01	PIVOT	A16	2	2		
92	4012287-865G01	INLET TUBE	A15	3	3		
93	COML	SOC HD CAP SCR/NYLOK #10-32 UNF x 1/2 LG	A15	18	18		
94	4012287-892P01	GASKET	A15	3	3		
95	-866G01	OUTLET TUBE	H15	3	3		
96	-891P01	GASKET	H15	3	3		
97	-239P01	RING GEAR	F16	2	2		
98	-764P01	SHIM	F16	1	1		
99	-755G05	GEARSHAFT ASSY	E16	[illegible]	[illegible]		
100	-240P01	RING GEAR	F16	2	2		
101	-686P01	RETAINING RING	H16	2	2		
102	-687G01	BRACKET	J16	1	1		
103	-698P01	STATOR VANE-SUPERSONIC	H16	36	36		
104	↓ -697P01	STATOR VANE-SUBSONIC	J16	36	36		
105	B0575-20	WASHER (N)	E17	[illegible]	[illegible]		
106	4012287-574P05	BLADE	E17	44	44		
107	8368-0	BASE (R)	E17	[illegible]	[illegible]		
108	L-48368-02	NUT (R)	E17	[illegible]	[illegible]		
109	4013042-365P01	SPACER	D18	AR	AR		
110	4012287-574P06	BLADE	C17	44	44		
111	210-M-35	WASHER (S)	E17	[illegible]	[illegible]		
112	4012287-731G01	CASING ASSY	H17	1	1		
113	4013046-059P01	LINER-SHROUD	F17	1	1		
114	4012287-846P01	RETAINING RING	F18	1	1		
115	4013017-985G01	CASING	C20	1	1		
116	COML	FL HD SOC CAP SCR/NYLOK 1/4-20 UNC x 3/4 LG	B20	12	12		
117	4013046-074P01	RING-SEAL	F18	1	1		
118	4013017-984P01	SUPPORT	C20	1	1		
119	-987P01	INLET SCREEN	F19	1	1		
120	↓ -988P01	BRG HOUSING	D15	1	1		
121	5221835-084	NUT	E19	2	2		
122	#100KSFF	BEARING	D18	3	3		
123	#R26	WAVE WASHER	F18	2	2		
124	#CS-39	RETAINING RING	C18	2	2		
125	4013046-060P01	STATOR CASING-INLET SIDE	F18	1	1		
126	4013046-057P01	CENTER BODY	D17	1	1		
127	EWB926-3-10	BOLT	D16	4	4		
128	C-6120-D	SLIP RING (A-3 5/32) (U)	D19	1	1		
129	COML	SOC HD SCR/NYLOK #8-32UNF x 1/2 LG	E20	6	6		
130	5003MS1P02	NUT	D16	4	4		
131	COML	SET SCR/NYLOK FL PT #8-32 UNF x 5/16 LG	E20	8	8		
132	COML	SOC HD SCR/NYLOK #8-32 UNF x 3/4 LG	E19	8	8		
133	COML	SOC HD SCR/NYLOK #10-24 UNC x 5/8 LG	B18	30	30		
134	4013042-313P01	TUBE	D21	1	1		
135	4013017-993P01	RING	B19	1	1		
136	4013046-042G01	FRAME	B18	1	1		
137	COML	SOC HD CAP SCR/NYLOK/D.H. #10-32UNF x 3/4 LG	C18	9	9		
138	COML	SOC HD CAP SCR/NYLOK 5/16-18UNC x 7/8 LG	B18	12	12		
139	4013017-983P01	BELLMOUTH	C18	1	1		
140	4013042-363P01	SLEEVE	D18	1	1		
141	361P01	STUB SHAFT	D18	1	1		
142	↓ 362P01	SHAFT	C18	1	1		
143	4013046-051P01	ROTATING SHROUD	B17	1	1		
144	4013046-049P01	DISK	A18	1	1		
145	4012287-671G01	BRACKET	A18	1	1		
146	-863G01	OIL JET	C20	1	1		
147	-879P01	GASKET	C20	2	2		
148	↓ -862G01	OIL JET	C19	1	1		
149	COML	DOWEL PIN 1/4 DIA x 7/8 LG	A28	4	4		
150	COML	DOWEL PIN 1/2 DIA x 1 1/4 LG	H21	2	2		
151	4012287-798G01	TORQUE ARM	E22	1	1		
152	-805P01	CLEVIS	D22	1	1		
153	↓ -808P01	SHOULDER SCREW	D21	2	2		
154	21FA-1026	LOCKNUT (H)	D21	2	2		
155	MD48-10	ROD END (V)	D22	2	2		
156	COML	JAM NUT 1/2-20UNF-2B	C22	2	2		
157	35-133-BK-100#	ALINCO LOAD CELL (W)	C21	1	1		
158	4012287-801G01	BASE ASSY	B22	1	1		
159	COML	SOC HD CAP SCR/NYLOK 1/2-13 UNC x 1 1/2 LG	B21	8	8		
160	COML	1/2" WASHER-MED	B21	4	4		
161	4012287-650G01	STAND	B30	1	1		
162	#351A136-600	GEARMOTOR TYPE CLC (X)	C25	2	2		

[illegible]	[illegible]	[illegible]	[illegible]	1	2	3	4
1	4013046-075G01	ASSY	A12	X			
2	4012270-952P01	GASKET	J10	1	1		
3	COML	5/8 MED. LOCKWASHER	J10	25	25		
4	COML	SOC HD CAP SCR 5/8-18UNF x 2 1/4 LG	J10	25	25		
5	COML	SOC HD CAP SCR/NYLOK 1/4-28UNF x 5/8 LG	J10	9	9		
6	2108	BEARING (A)	J10	1	1		
7	4012079-103P01	BRG HOUSING	J10	1	1		
8	4012270-904P01	FRONT FRAME	J10	1	1		
9	4012079-109P01	SPACER	J10	1	1		
10	↓ -108P01	SHAFT	J10	1	1		
11	#250	O RING (B)	J11	2	2		
12	COML	SOC HD CAP SCR/NYLOK 1/4-28UNF x 1" LG	J11	23	23		
13	4012287-436P01	HOUSING	J11	1	1		
14	-437P01	SPACER	J11	1	1		
15	↓ -434P01	COUPLING	J11	1	1		
16	#2-141	O RING (C1)	J11	1	1		
17	W-08	LOCKWASHER (A)	J11	1	1		
18	N-08	LOCKNUT (A)	J12	1	1		
19	4012287-438P01	COUPLING	J12	1	1		
20	4012270-985G01	SUPPORT FRAME	J12	1	1		
21	#125	O RING (B)	J12	2	2		
22	4408100	GEARBOX (D)	J12	1	1		
23	4012079-102P01	BRG HOUSING	B9	1	1		
24	R-210-C	BEARING (A)	B10	1	1		
25	S-98002CH-56	SEAL & RING (E)	B11	1	1		
26	RR 306	RETAINING RING (F)	B11	1	1		
27	#2-151	O RING (C1)	B11	1	1		
28	COML	KEY 1/4 x 1/4 x 2" LG	B11	2	2		
29	COML	SOC HD CAP SCR 5/16-18UNC x 1 1/2 LG	F13	16	16		
30	21FA-518	NUT (H)	F13	16	16		
31	COML	DOWEL PIN 1/8 DIA x 1/2 LG	F14	1	1		
32	H 2424 MOD.	GEAR (J) .500-.502 DIA BORE	F14	2	2		
33	4012287-[illegible]	BRACKET	F14	1	1		
34	3030HT8	MAGNETIC PICKUP (K)	E14	1	1		
35	COML	JAM NUT .625-18UNF	E14	1	1		
36	4012287-[illegible]	COUPLING	C13	1	1		
37	COML	DOWEL PIN 1/8 DIA x 1" LG	B14	1	1		
38	4012287-536P01	MOUNTING RING	B13	1	1		
39	↓ -[illegible]P01	GEAR	F14	2	2		
40	RR [illegible]	RETAINING RING (F)	C14	2	2		
41	#2-[illegible]	O RING (C1)	D14	1	1		
42	COML	SOC HD CAP SCR/NYLOK 1/4-20UNC x 5/8 LG	C14	12	12		
43	4012287-560P01	HOUSING	C14	1	1		
44	↓ -[illegible]P01	SHIM	C14	1	1		
45	COML	FL. HD SOC CAP SCR/NYLOK #10-32UNF x 5/8 LG	C14	30	30		
46	COML	SOC HD CAP SCR/NYLOK 1/4-20UNC x 1" LG	H14	40	40		
47	COML	1/4" MED WASHER	H14	4	4		
48	[illegible]	RATIOMOTOR (J)	H14	1	1		
49	4012287-[illegible]P01	SHIM	H15	1	1		
50	↓ -[illegible]P01	SHIM	H15	1	1		
51	[illegible]	BEARING (L)	F15	2	2		
52	4012287-[illegible]P01	RETAINER	F15	4	4		
53	↓ -[illegible]G01	JACKSHAFT ASSY	H15	1	1		
54	RS650	RETAINING RING (F)	E15	2	2		
55	4012287-[illegible]P01	RING	E15	2	2		
56	RR570	RETAINING RING (F)	E15	2	2		
57	UR 212	RETAINING RING (F)	E14	1	[illegible]		
58	#2-34	O RING (C1)	E14	1	1		
59	#5-284	O RING (C1)	E14	1	1		
60	RS412	RETAINING RING (F)	C14	3	3		
61	SL58-N-06	LOCKNUT (M)	C14	1	1		
62	4012287-562P01	SPACER	C14	1	1		
63	53-98008[illegible]	SEAL & RING (E)	C14	1	1		
64	4012287-755P02	RETAINER	C14	2	2		
65	1921S	BEARING (A)	C15	2	2		
66	4012287-570P01	SHAFT	C15	1	1		
67	WB #62	WAVE WASHER (N)	C15	2	2		
68	4012287-676P01	SLEEVE	C15	1	1		
69	2068	BEARING (A)	C15	1	1		
70	4013046-062P01	MAIN BRG HOUSING	C15	1	1		
71	4012287-467G01	HOUSING	B15	1	1		
72	4012287-929P01	LOCKNUT	D16	1	1		
73	#2-157	O RING (C1)	C16	1	1		
74	COML/MOD. HD. HGT-.140-.150	SOC HD CAP SCR/NYLOK #10-32UNF x 3/4 LG	C16	8	8		
75	4012287-654P01	SEAL-STATIONARY	D16	1	1		
76	4012287-558P01	SEAL-ROTATING	D16	1	1		
77	9109UK1	BEARING (A)	D16	1	1		
78		LOCKWIRE	C16	AR	AR		

E

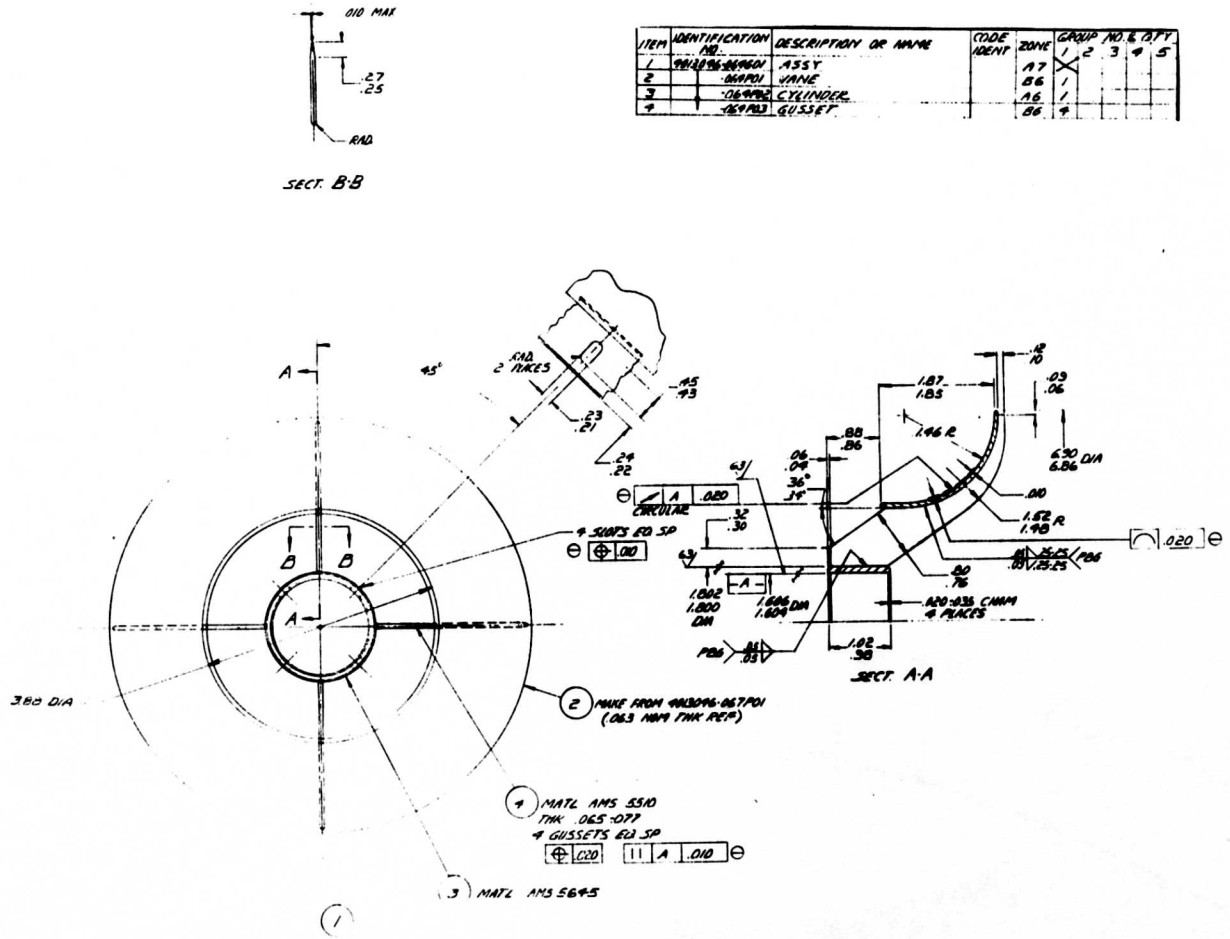

Figure 39. Circular Inlet Vane Used With Buildups B and C, Phase III Investigation.

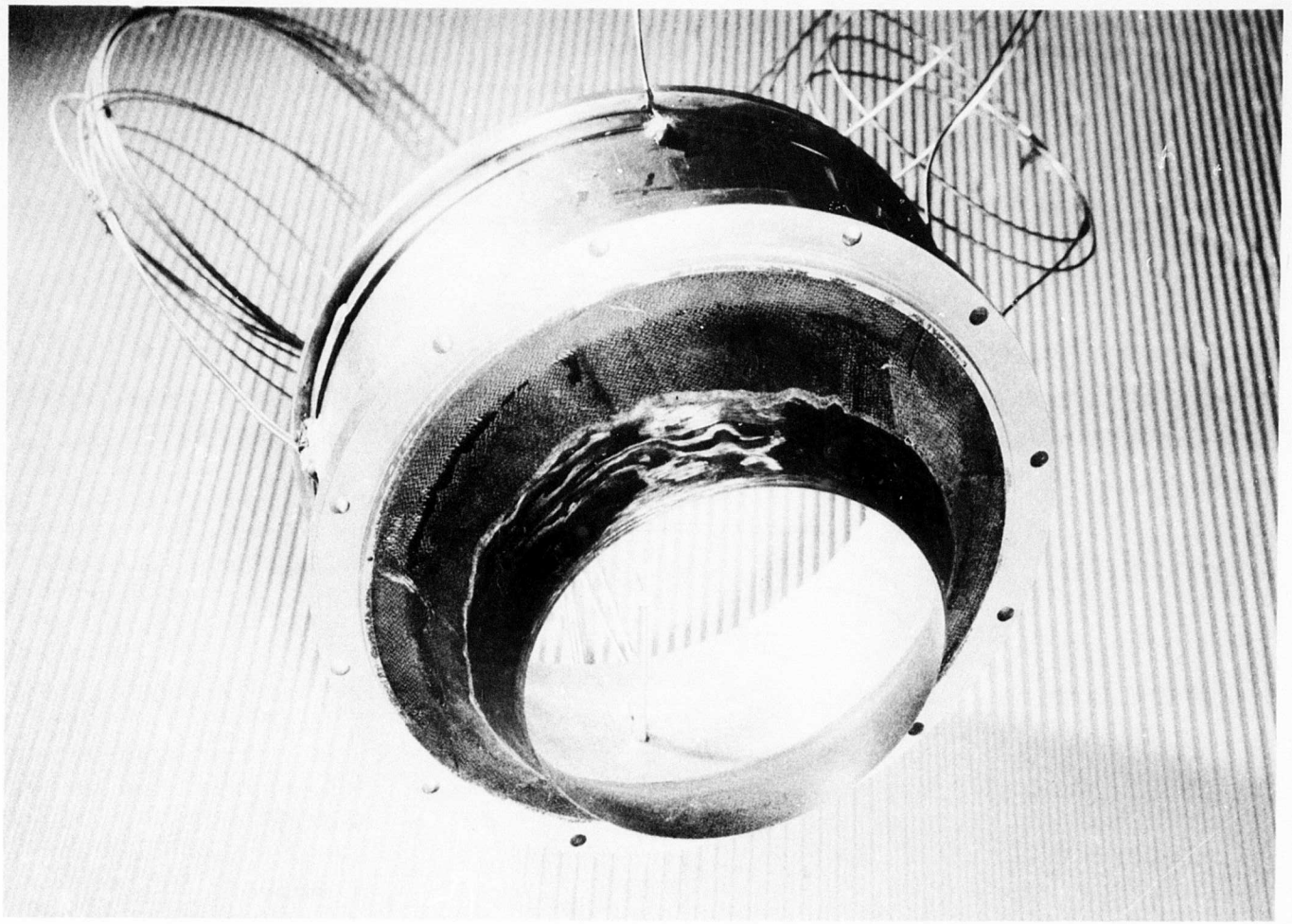

Figure 40. Graphite and Glass Fiber Modifications to Bellmouth Liner Used With Buildups B and C, Phase III Investigation.

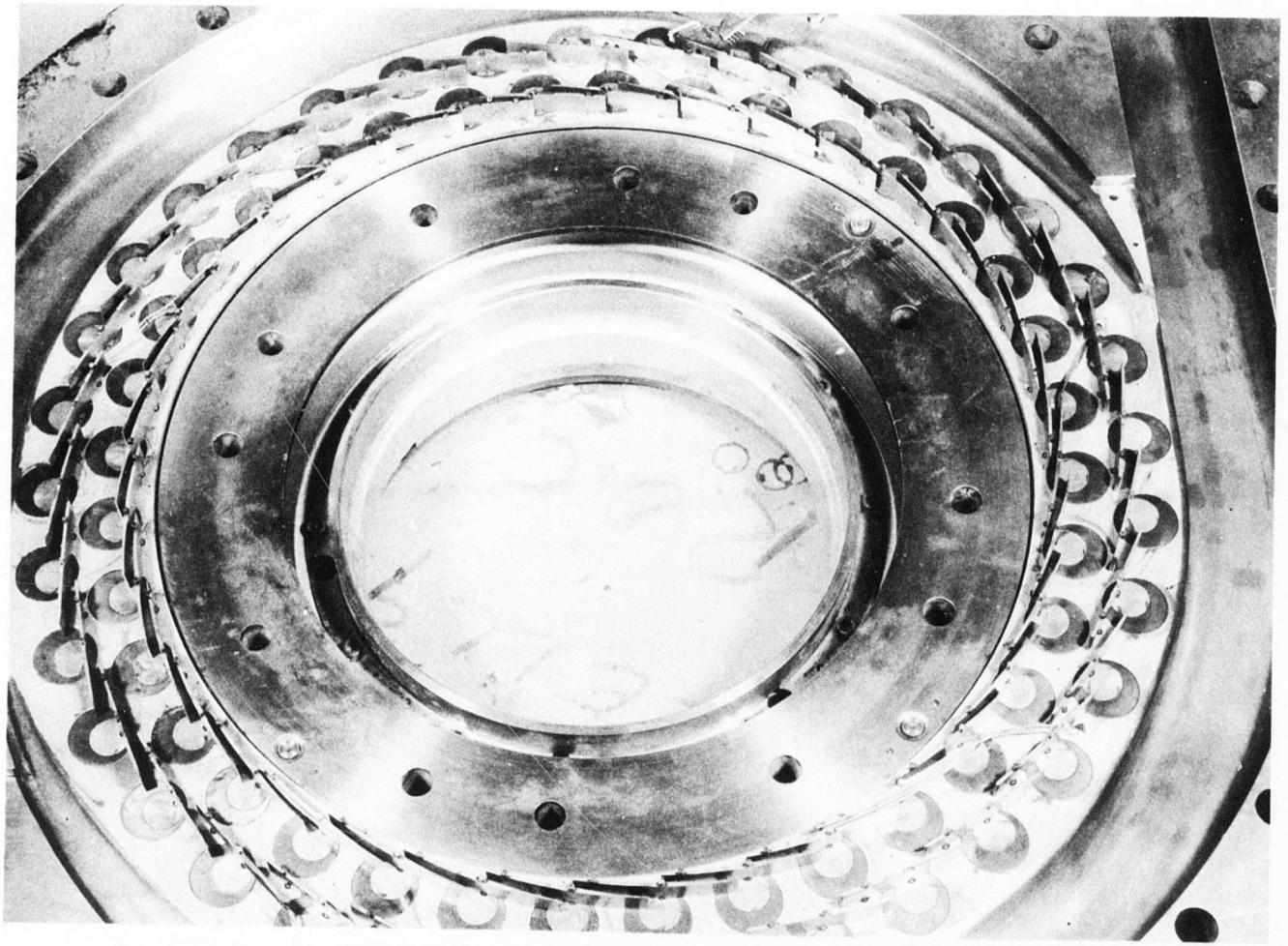

Figure 41. Assembly of Supersonic and Subsonic Stator Vanes in Stator Casing Used in Buildups B and C, Phase III Investigation.

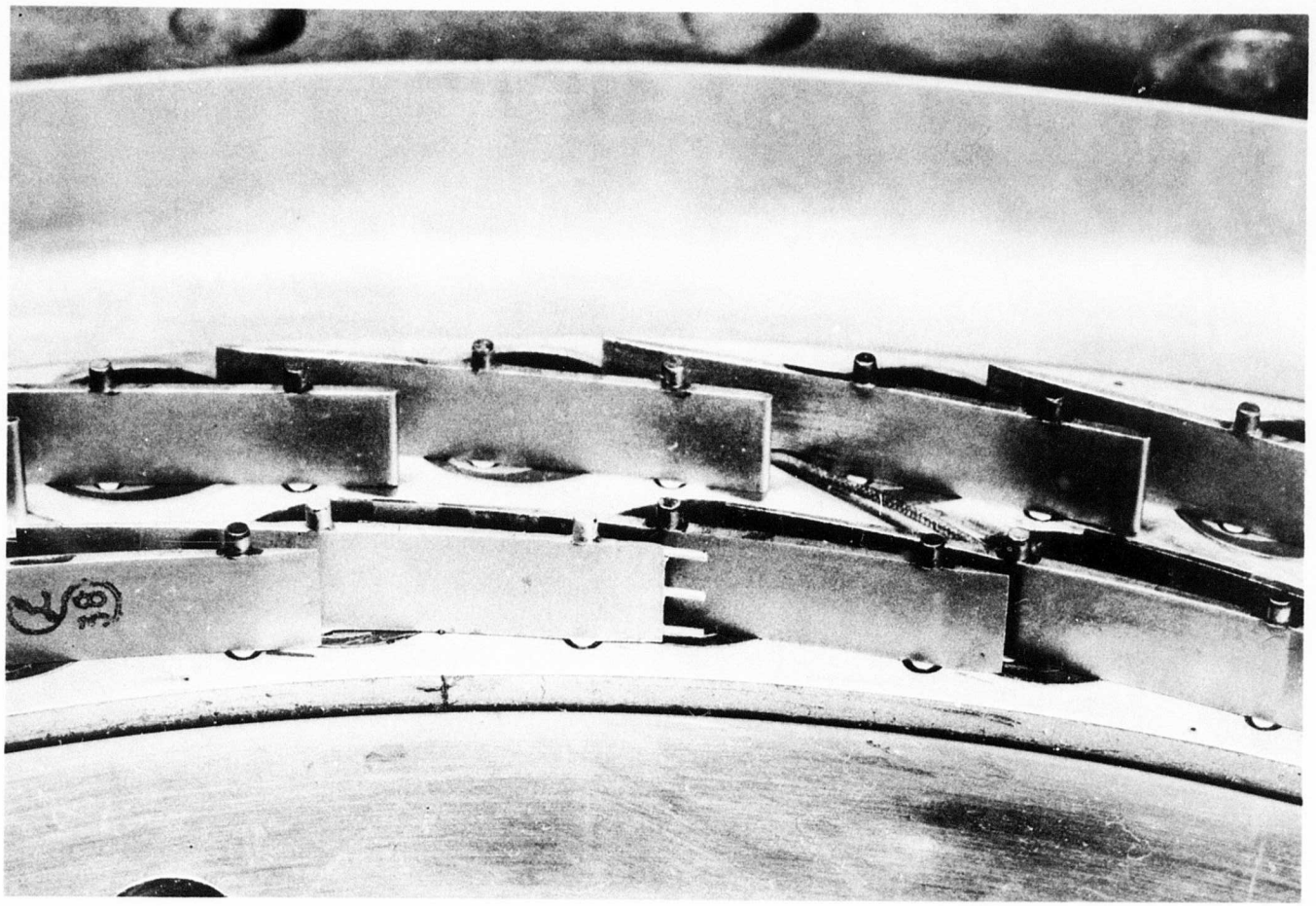

Figure 42. Total Pressure Tubes Installed at Leading Edge of Supersonic Stator Vanes.

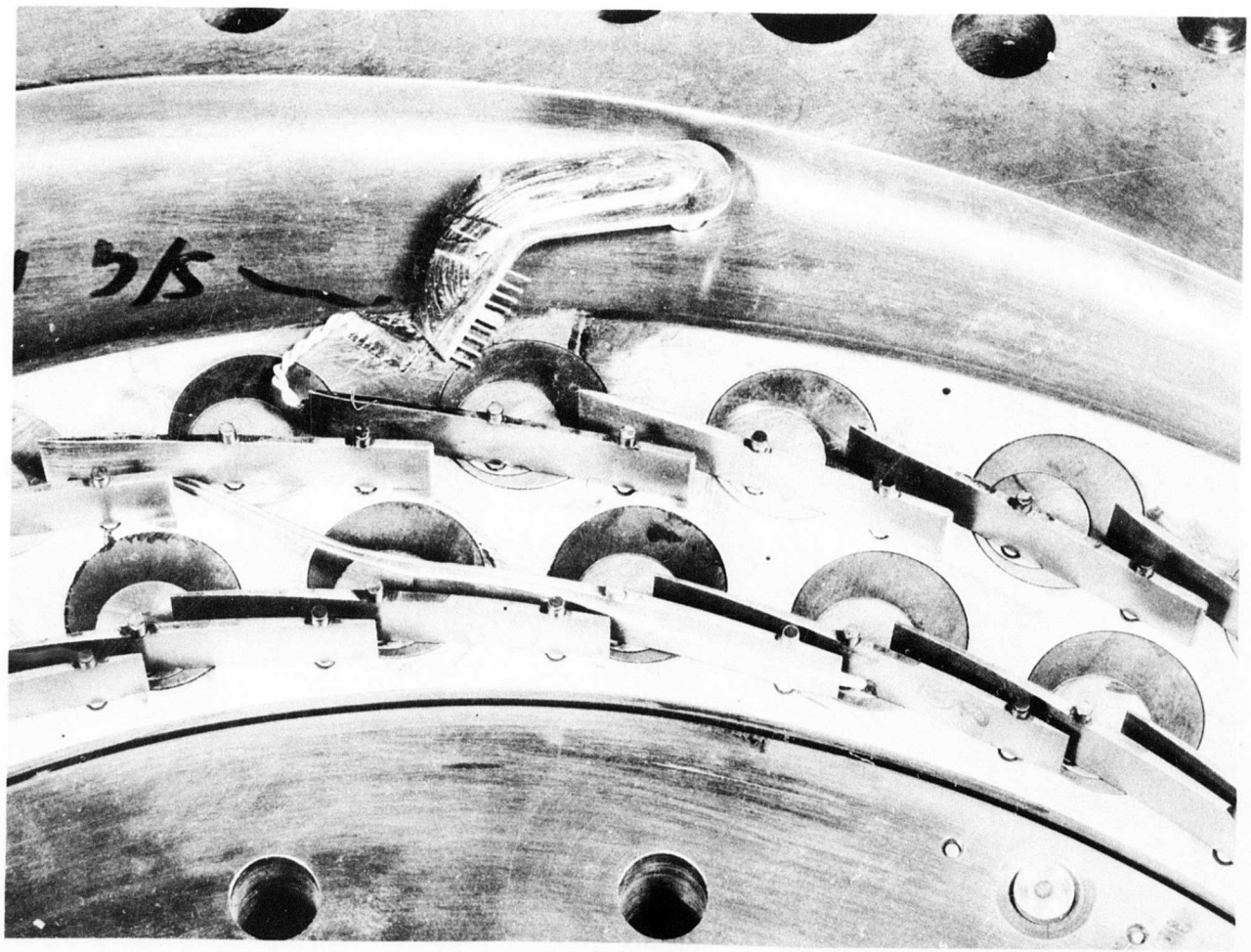

Figure 43. Flow Angle Measuring Tubes at Leading Edge of Supersonic Stator and Total Pressure Rake Downstream of Subsonic Stators.

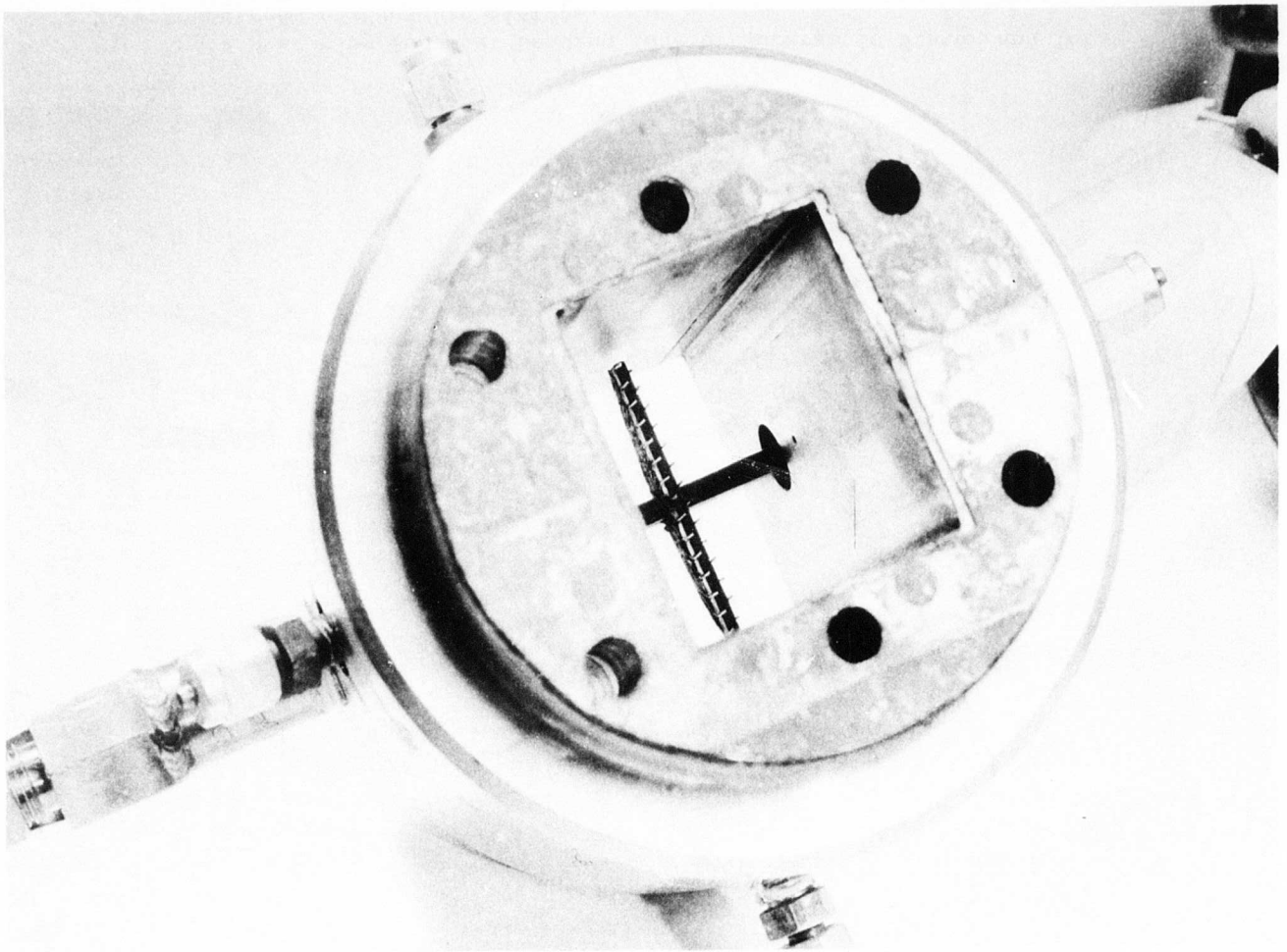

Figure 44. Rake Containing 15 Total Pressure and 14 Temperature Elements Used in Compressor Exit Arm (Plane 8) to Measure Overall Compressor Performance.

removed from the cell, Run Number 22 was fraught with a number of facility, test vehicle, and instrumentation problems. A new computer program for data reduction was also introduced, and difficulties in the use of this new program were encountered. Although test points were taken during the run at 33, 40, 50, and 60 percent speed, the primary information obtained was that the total pressure observed 0.05 inch from the shroud or from the disc was significantly lower than that observed on the passage centerline. A typical set of readings taken at 60 percent speed indicated a pressure of 30.77 psi near the shroud, 39.2 psi at the centerline, and 34.23 psi near the disc. Readings taken at the leading edge of the supersonic stator on the opposite side of the rotor at the same test point indicated very similar total pressures. Obviously, a very severe gradient total pressure existed which would make satisfactory stator performance very unlikely. A maximum speed of 70 percent was obtained during Run Number 22.

Run Number 23

The primary purpose of Run Number 23 was to obtain full speed operation of the compressor while rotor strain gages were still in service. A number of test points were taken at 40, 60, 70, 80, 95, and 100 percent speed. At 70 percent speed, a rotor total pressure ratio of 3.1 was obtained with an uncorrected rotor efficiency of 80.9 percent and an efficiency at subsonic stator exit of 75 percent with a Mach number of 0.426. The total pressure distribution at rotor exit was 38.6 psi near the shroud, 44.5 psi in the passage center, and 46.2 psi near the disc. An even greater difference between the minimum and maximum total pressures was observed at the opposite supersonic stator leading edge. At 100 percent speed, a variation of about 12 psi from the maximum of 50.4 psi at the centerline was observed. At speeds above 70 percent, it was not possible to move the subsonic vanes.

Run Number 24

During Run Number 23 a facility bearing temperature approaching 400°F was observed. This was well above the allowable limit for this bearing. For that reason, the speeds set during Run Number 24 were limited to a maximum of 70 percent. The pressure ratio-airflow characteristics of this compressor were measured at 5 airflow points at speeds of 40, 50, 60, and 70 percent. For all of these points, large differences of total pressure were observed between the readings near the shroud, on the centerline, and near the disc. A typical point at 70 percent speed showed a rotor pressure ratio of 3.0 and an uncorrected rotor efficiency of 76.2 percent, with a pressure ratio of 2.88, an efficiency of 73.1 percent, and a Mach number of 0.362 at subsonic stator exit. The distribution of total pressure at rotor exit was 39.65 psi near the shroud, 44.82 psi on the centerline, and 43.6 psi near the disc. For all of these points, the leakage through the forward seal was greater than the capacity to remove flow from the forward cavity. Because of this

inadequacy, hot air at low pressure was leaking into the compressor rotor through the gap between the bellmouth liner and the inner diameter of the rotating shroud.

Run Number 25

While it was not possible to increase the suction capacity from the forward cavity between runs (since the flow was limited by the area of the tubes which connect the cavity to the suction system), it was possible to change the axial location of the circular inlet vane. In an attempt to improve the flow conditions entering the rotor, the circular vane was moved 3/32 inch to the full forward position. Some improvements were made to the facility bearing to provide additional cooling. Run Number 25 was conducted to determine whether the circular vane movement was beneficial to compressor performance. The preliminary results of this run were very encouraging. For example, at 50 percent speed the total pressure was 26.62 near the shroud, 27.49 near the centerline, and 26.18 psi near the disc. On the opposite side of the compressor, the difference between the shroud and the centerline was only 0.75 psi. A pressure ratio of 1.84 with an efficiency of 81 percent at a Mach number of 0.32 was observed in the subsonic stator exit.

After acceleration to 70 percent speed during Run Number 25, both the supersonic and subsonic stator vanes were jammed in a closed position. As a result, it was not possible to obtain the proper airflow into the compressor. Nevertheless, test data were taken at 70, 78, and 85 percent speed. At 70 percent speed, the total pressure readings were 43.9 psi near the shroud, 45.3 psi at the centerline, and 43.1 psi near the disc. Similar small differences were observed on the opposite side of the rotor. At 78 percent speed, a maximum difference of about 3 psi from the maximum of 51.1 psi was observed. At 85 percent speed, a maximum difference of about 4.4 psi was observed with 65.4 psi in the center.

Since the seal leakage problem and the limited suction capacity problem had not been improved, a significant improvement in compressor performance had been obtained even though hot air at low pressure was still leaking into the rotor. Further improvements were made to the facility bearing to permit additional cooling, and a run was planned for April 22 with confidence that greatly improved compressor performance could be achieved with proper stator vane angles. Prior to the run, it was necessary to move the stators to a known position in order to calibrate the angular position meters. Erratic indications were obtained when the drive motors were actuated and, in fact, the large ring gear which drives the supersonic stators was found to be moving with no indication of such motion on the meters in the control room. Two of the gear teeth on the spindle to which the angle-indicating potentiometer was attached had been sheared. It seemed very likely that at least 1 pin of that particular supersonic stator vane had also been sheared although this could not be determined without disassembly of the compressor casing. The damaged spindle could not be replaced without disassembly of the casing.

The decision was made to remove the engine ROC from the test cell in order to make necessary modifications to the stator vane drive system, to provide increased suction capacity to the forward cavity, and to remove strain gage leads from the rotor disc and blades. Complete removal of the compressor permitted the necessary modifications to the ROC to be made. After disassembly of the compressor, it was found that 1 of the rotor blades had been damaged in the trailing edge region. The dust patterns observed suggest that this damage occurred during the assembly rather than during the disassembly and, therefore, existed during Runs Numbers 20 through 25. This rotor blade was replaced. The soot patterns on the rotor disc, the rotating shroud, and the rotor blades are shown in Figures 45, 46, and 47, respectively, following the Buildup B tests.

The silver foam seal used with the Phase III rotor performed satisfactorily although the evidence following disassembly was that the nominal clearance was greater than desired. Rub-in of the rotor seal teeth occurred only over about 120 degrees of the seal circumference. Maximum depth of the grooves was only 5 mils. Attempts were made to reduce the seal clearance and improve the concentricity of the seal before the next run of the ROC. Through improved sealing and increased suction capacity, it was anticipated that hot air leakage into the rotor could be prevented, thus providing further reason to expect significantly improved compressor performance.

TEST CONFIGURATION FOR BUILDUP C

The configuration of the ROC which was tested in the final buildup of the Phase III investigation was basically the same as Buildup B. The circular inlet vane, Phase III rotor blades, supersonic stator vanes, and subsonic stator vanes were all used. However, there were several significant minor differences in the final configuration, so it was decided to call the configuration used in the final rather extensive test sequences Buildup C. The forward seal was replaced and the reserve seal was employed with its diameter reduced by flame-spraying additional silver foam material. The forward seal was machined in place in the forward compressor casing to insure concentric alignment. The average clearance was approximately 0.012 inch with about 2 mils variation. Material was also removed from the smallest diameter of the forward casing to provide access to the clearance space on assembly. This was done to permit direct measurement of the actual seal clearance. Although concentric location of the seal was anticipated because of the method of final machining, a trial fitup to the rotor was made before installing stator vanes. This procedure made it possible to adjust the seal location before drilling for dowel pins, but this adjustment proved to be unnecessary.

The forward half of the compressor stator casing was drilled and tapped with 4 additional holes to improve the suction capacity for removing leakage air. This change should have more than doubled the ability to remove flow since only 3 holes were available previously.

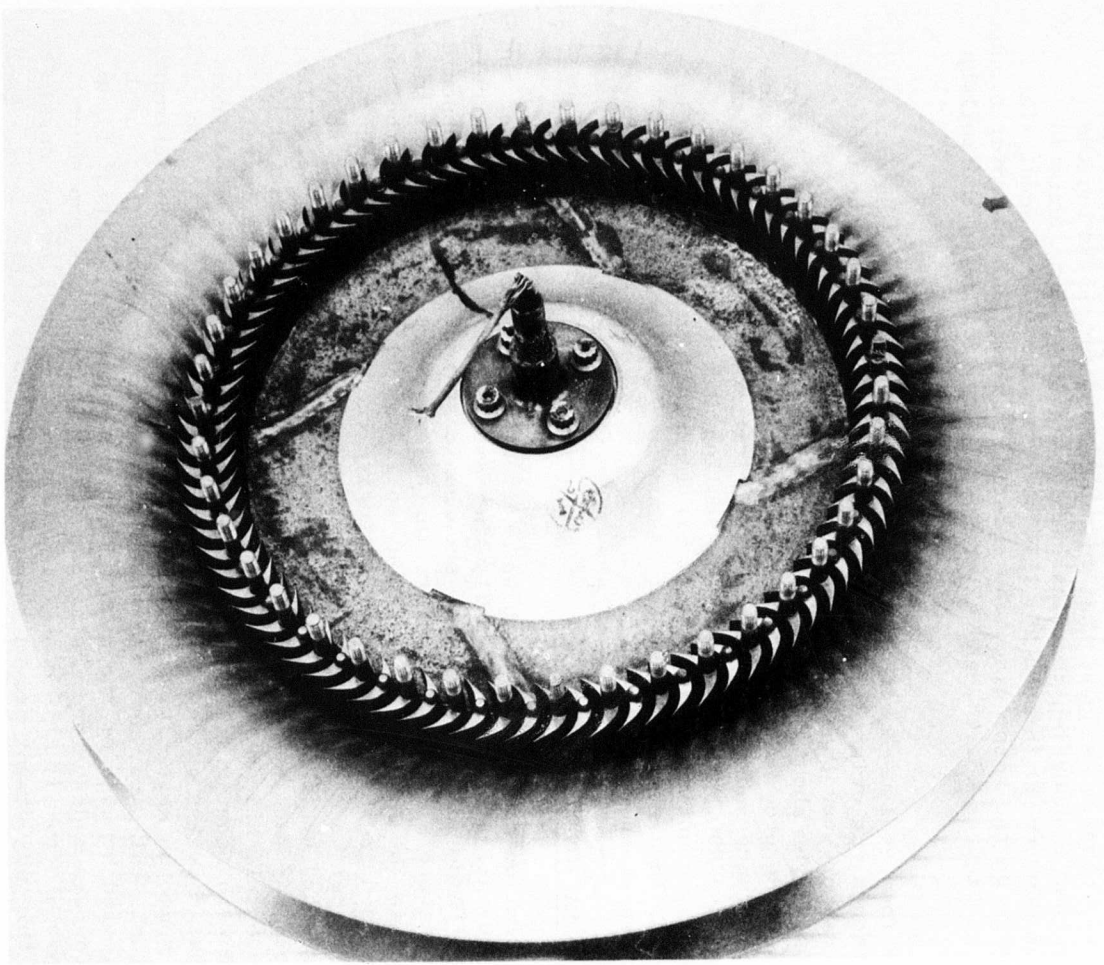

Figure 45. Rotor Blades and Disc Following Tests of Buildup B, Phase III Investigation.

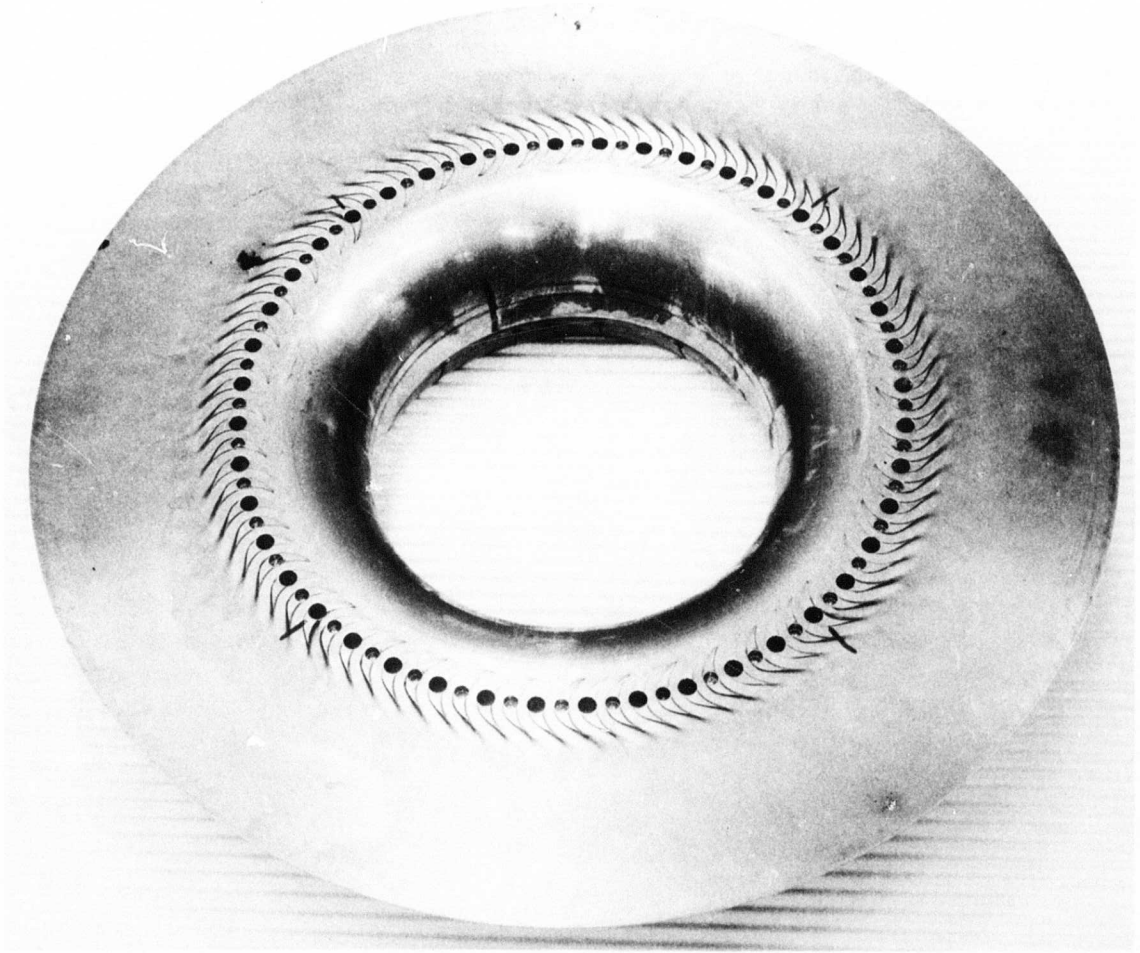

Figure 46. Rotating Shroud Following Tests of Buildup B, Phase III Investigation.

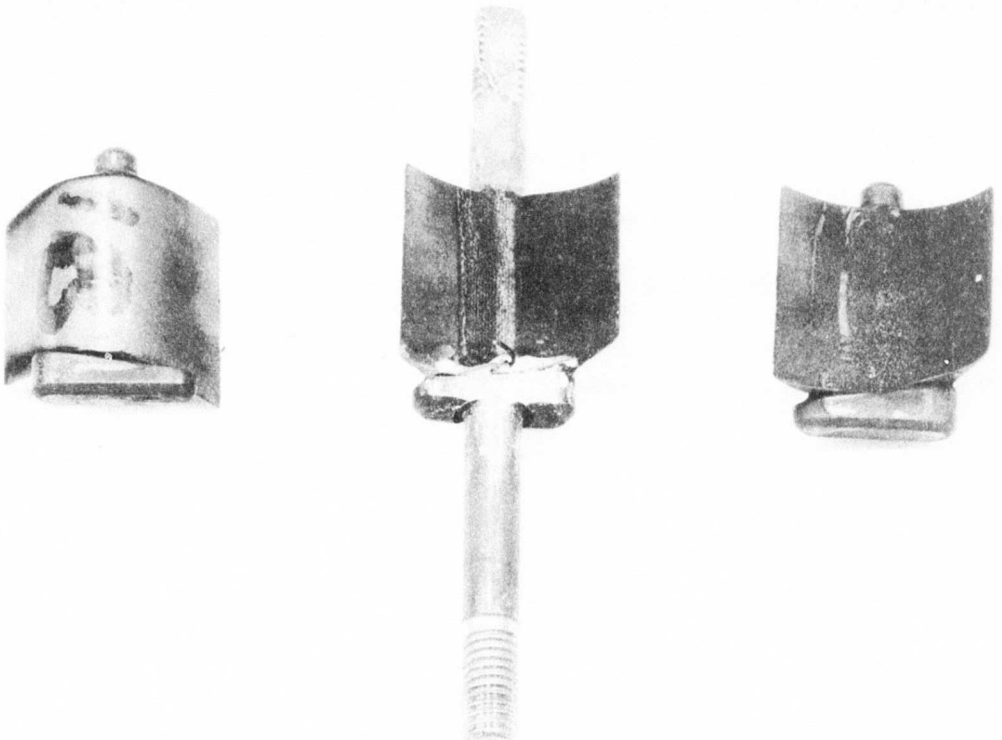

Figure 47. Rotor Blades Following Tests of Buildup B, Phase III Investigation (The Long Shank Blade (Center) was One of the Four on Which Strain Gage Leads Were Placed).

Strain gage leads were removed from the rotor disc, blades, and shroud. Careful measurement of the rotor blades in place on the disc was made to determine the cause of the shroud rim runout. One blade found to be long at the leading edge was eliminated from the assembly. A symmetrical distribution of the remaining longer blades was made. After installation, the shroud rim runout was found to be about 2 mils. This was a reduction from the 6-mil runout measured in Buildup A.

For previous assemblies of the Phase III rotor, additional washers had been added to achieve rotor balance. The blade shanks on which these balance washers had been used were found to be bent after 5 minutes of running at 100 percent speed. For the Buildup C assembly, balancing was achieved by grinding material from the spherical seat washers and from nonstressed sections of the disc and shroud. The torque used to tighten the nuts was increased to 32 inch-pounds. The previous values were 10 inch-pounds for the shroud and 15 inch-pounds for the disc. The calculations indicated that these modifications would reduce the stresses in the blade shanks so that bending would not occur during extended running at full speed.

A calculation of the rotor and stator casing temperature distribution was made to estimate the axial and radial growths of these parts at full speed. As a result of these calculations, the axial position of the rotor was changed from the 0.015-inch rotor disc protrusion cold to the 0.009-inch rotor disc protrusion cold. It is believed that improved rotor alignment and reduced leakage at high speeds were achieved by these changes.

The assembly and balance procedures used are presented in Appendix II. A special gage was made to insure accurate axial placement of the circular inlet vane at the nominal setting for Buildup C. By using the gage, it was found that the setting thought to be nominal during the test runs of Buildup B was about 0.30 inch farther aft than the nominal setting.

TEST PLAN FOR BUILDUP C

To avoid the stator actuation system problems, a different test plan was used. A series of fixed supersonic stator angles, 76, 79, and 82 degrees, was used. A series of fixed subsonic stator settings was also used. An angular difference between the 2 rows of 3, 6, and 9 degrees was set. This combination of 9 stator settings was tested over the range of speeds and airflows which could be established without incurring excessive test vehicle vibrations. Changes to the stator angles were only made with the compressor cool and at low speed--conditions such that binding of the actuation system had not been a problem. The stator angles referred to are measured between a tangent to the stator mounting pins and the radial direction at the stator leading edge. The bisector of the supersonic stator leading edge wedge angle (8 degrees) makes an angle of 1-1/2 degrees with the pin tangent in a direction nearer to radial; i.e., if

the supersonic stators were set at 76 degrees, the leading edge bisectors would make an angle of 74.5 degrees from radial. The subsonic stator leading edge makes an angle of 2 degrees with the pin tangent in a direction nearer to radial; i.e., if the subsonic stators were set at 70 degrees, the leading edge direction would be 68 degrees from radial. Thermocouples were added to the stator casings to help in assessing why the actuation system binds and to help in avoiding this problem. Strain gages were applied to actuation members to help prevent overdriving the gears and vanes and were monitored as described in Appendix III.

Although a relatively extensive series of test runs was required because of the systematic approach employed, the indications were that such a network of points would have to be run in order to find optimum supersonic and subsonic stator settings.

TESTS OF BUILDUP C

Testing of Buildup C began on May 29, 1968. This run used the first of 9 stator vane angle settings which were selected to form a systematic array hopefully covering the range of interest. The stator settings selected are illustrated in the following block diagram:

Supersonic	Subsonic		
76	73	70	67
79	76	73	70
82	79	76	73

Approximately 200 data points were taken in the process of determining the compressor performance for the selected settings. Not all speeds and not all of the predetermined airflows were tested because of either test vehicle vibrations or inability to operate the compressor without stall.

EFFECT OF STATOR VANE ANGLE ON ROTOR PERFORMANCE

General

A systematic series of tests was conducted in which the supersonic stators were set at 76, 79, and 82 degrees from radial. For each of the supersonic stator settings, 3 values of subsonic stator angle were tested. The values of the subsonic stator angles set were 3, 6, and 9 degrees open from the supersonic stator angle. In addition to the systematic tests, 1 series of points was taken with the supersonic stators set at 84.4 degrees and the subsonic stators set at 76.3 degrees. The final test runs were made with the supersonic stators 1 degree more open, 83.4 degrees from radial, without changing the subsonic stator angle from

the previous value of 76.3 degrees. For ease of comparison, all of the results pertaining to rotor performance and the appropriate predicted curves are presented in Figures 48 through 91. For various reasons, not all of these stator vane combinations were tested at all speeds intended nor over the full range of airflows intended. The primary reason for not completing all of the planned tests was poor performance of the compressor at high speeds with the stators open. The other major reason for not covering the full range of conditions was the occurrence of test vehicle vibrations at many combinations of compressor speed and throttle setting. Destruction of the main high-speed bearing eventually occurred, and the experimental program was concluded.

EFFECT OF STATOR VANE ANGLE ON ROTOR TOTAL PRESSURE AND EFFICIENCY CHARACTERISTICS

Supersonic Stators Set at 76 Degrees

Rotor performance for particular stator settings is compared with the summary total pressure and efficiency versus airflow characteristics that have been prepared from the 350 or more data points which were accumulated during Phase III testing. The total pressure ratio produced at 33 and 40 percent speed (Figure 48) agrees well with the generalized characteristics. At 50 and 60 percent speed, however, total pressure ratios and the efficiencies (Figure 59) observed are lower than the respective values shown on the summary curves. This is evidence that the supersonic vanes were too open when set at 76 degrees to permit efficient rotor operation at intermediate and high speeds.

Little change in rotor performance was observed when the subsonic stators were opened to 70 degrees and the supersonic stators were held at 76 degrees (Figures 49 and 60). Although the total pressure ratios observed at 60 percent speed compare well with the summary values, the static pressure ratio (Figure 69) was significantly lower than the value obtained with more closed stator settings, and the rotor efficiency was quite low (Figure 60). As discussed in greater detail in the section describing the effects of stator vane angle on rotor static pressure ratio, steady flow was not possible in the compressor at high speeds with the supersonic vanes set at 76 degrees. Closing the subsonic stators from 70 to 73 degrees did not appreciably affect the rotor performance. At low speeds, the rotor total pressure ratios (Figure 50) agreed with the summary values with a peak efficiency of about 88 percent (Figure 61). System instabilities were observed at speeds of 50 percent and higher, and inefficient performance resulted.

Supersonic Stators Set at 79 Degrees

Significant improvement in rotor performance was obtained at low and intermediate speeds when supersonic stators were closed from 76 to 79 degrees. At 40 and 50 percent speeds, rotor efficiencies in the 87 to

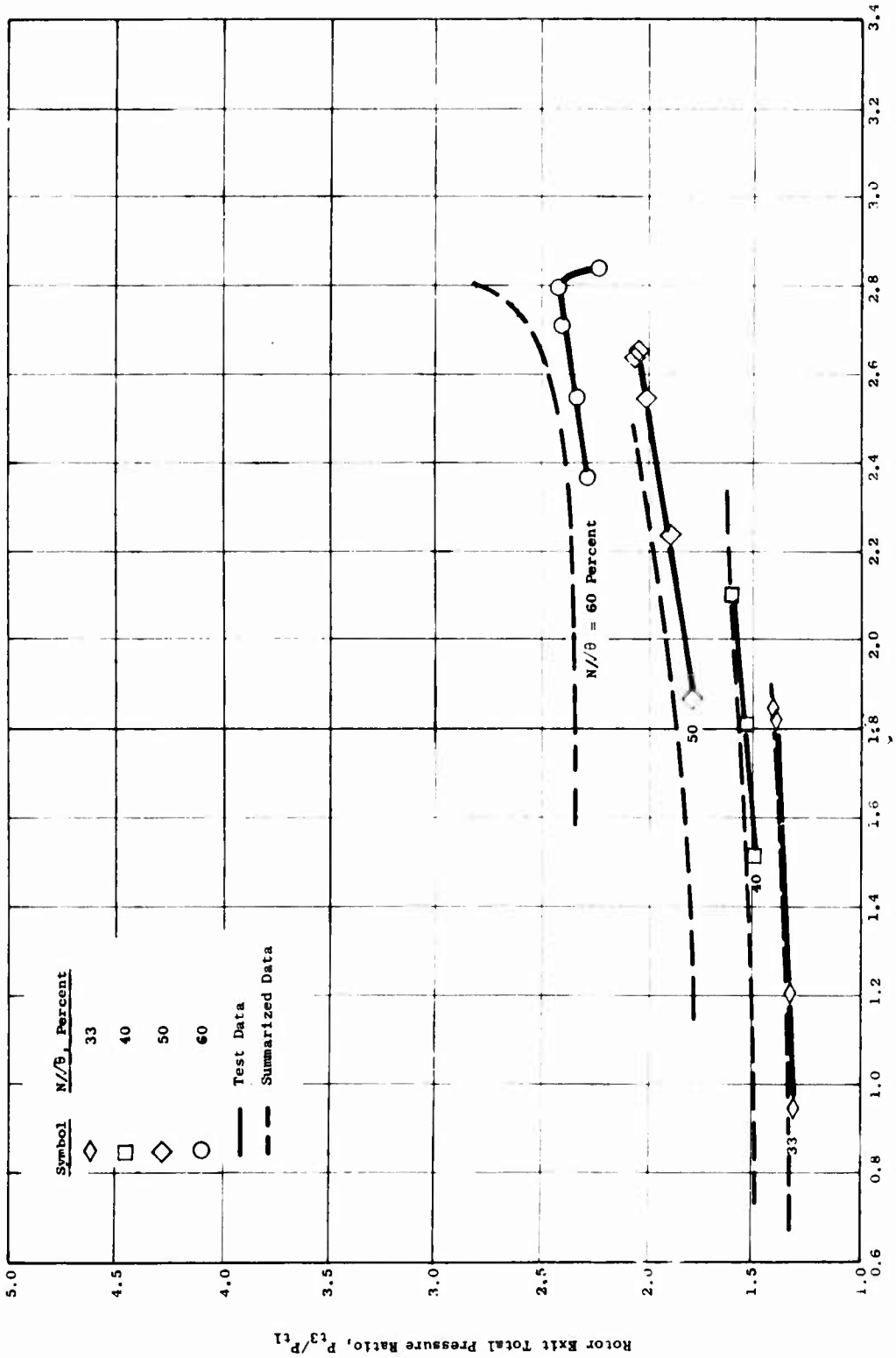

Figure 48. Total Pressure Ratio Versus Mass Flow With Supersonic Stators Set at 76 Degrees and Subsonic Stators Set at 67 Degrees.

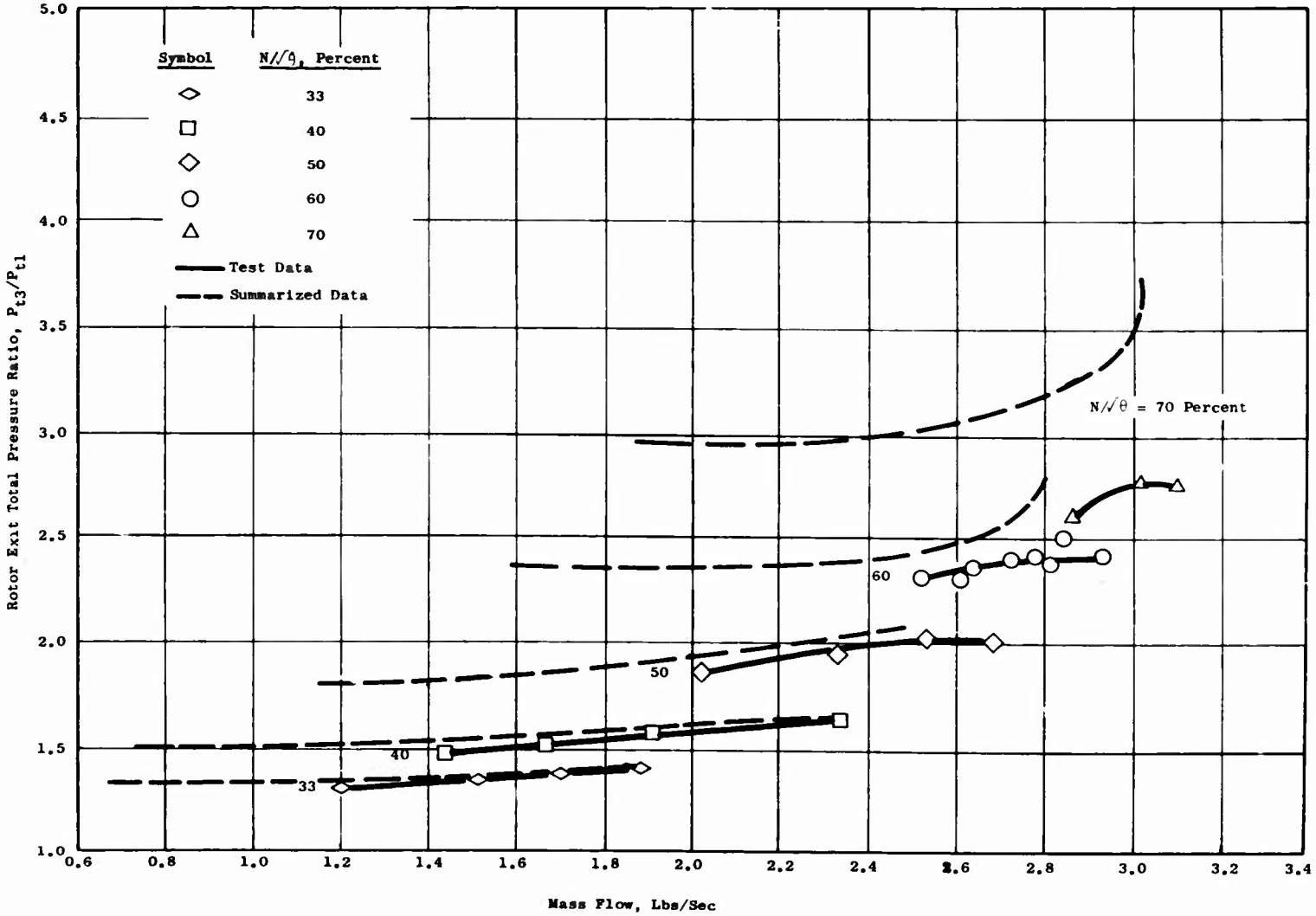

Figure 49. Total Pressure Ratio Versus Mass Flow With Supersonic Stators Set at 76 Degrees and Subsonic Stators Set at 70 Degrees.

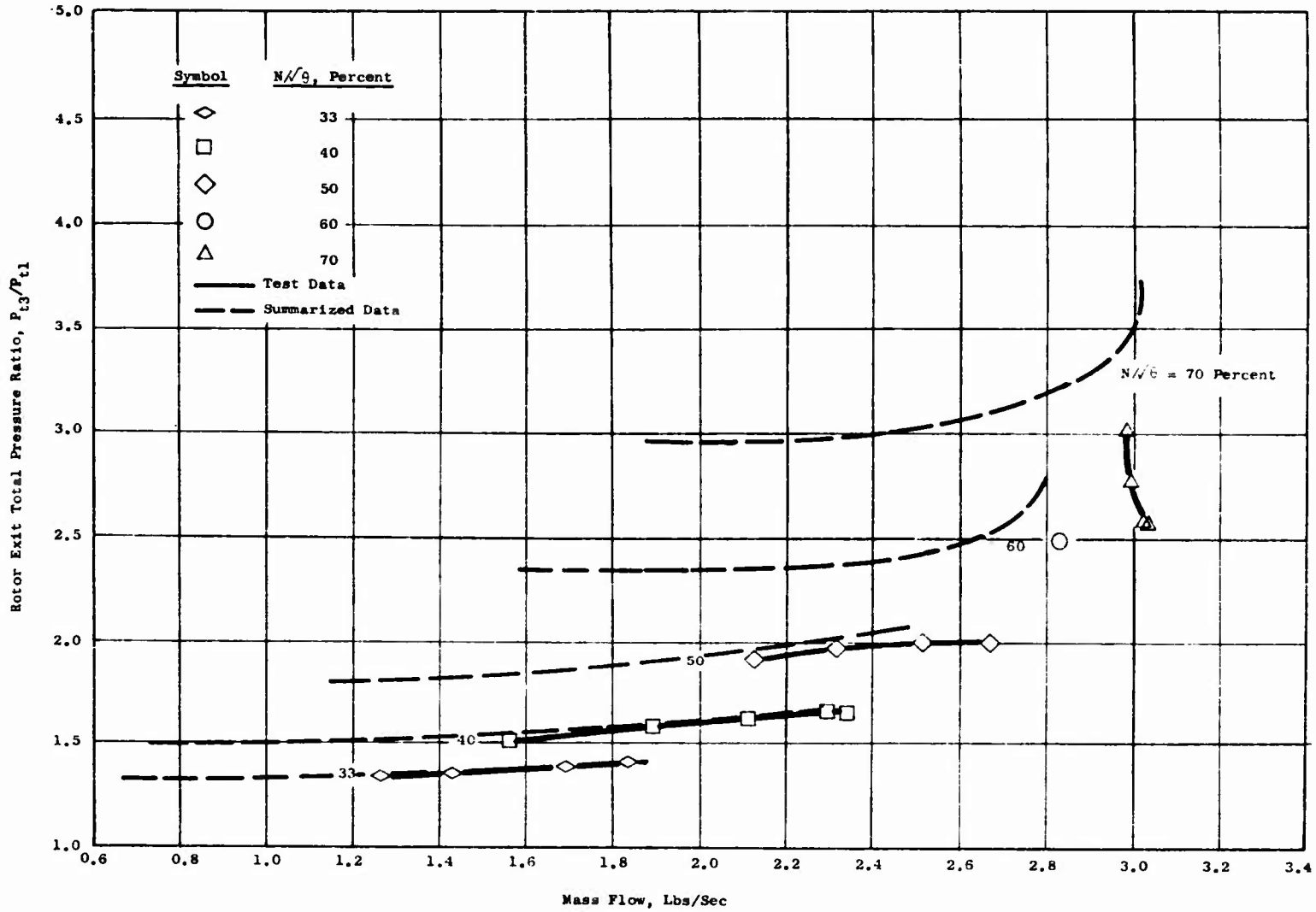

Figure 50. Total Pressure Ratio Versus Mass Flow With Supersonic Stators Set at 76 Degrees and Subsonic Stators Set at 73 Degrees.

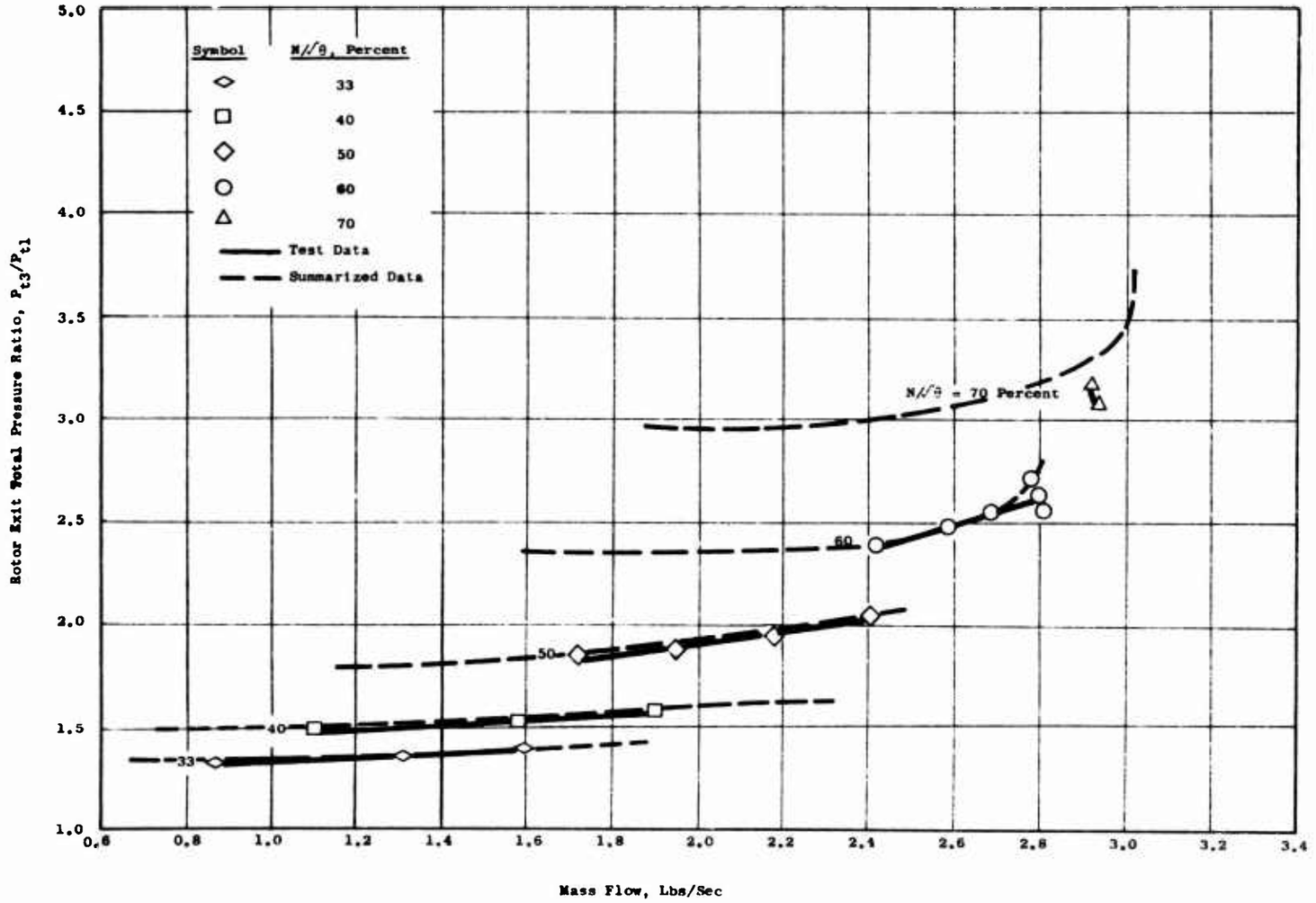

Figure 51. Total Pressure Ratio Versus Mass Flow With Supersonic Stators Set at 79 Degrees and Subsonic Stators Set at 70 Degrees.

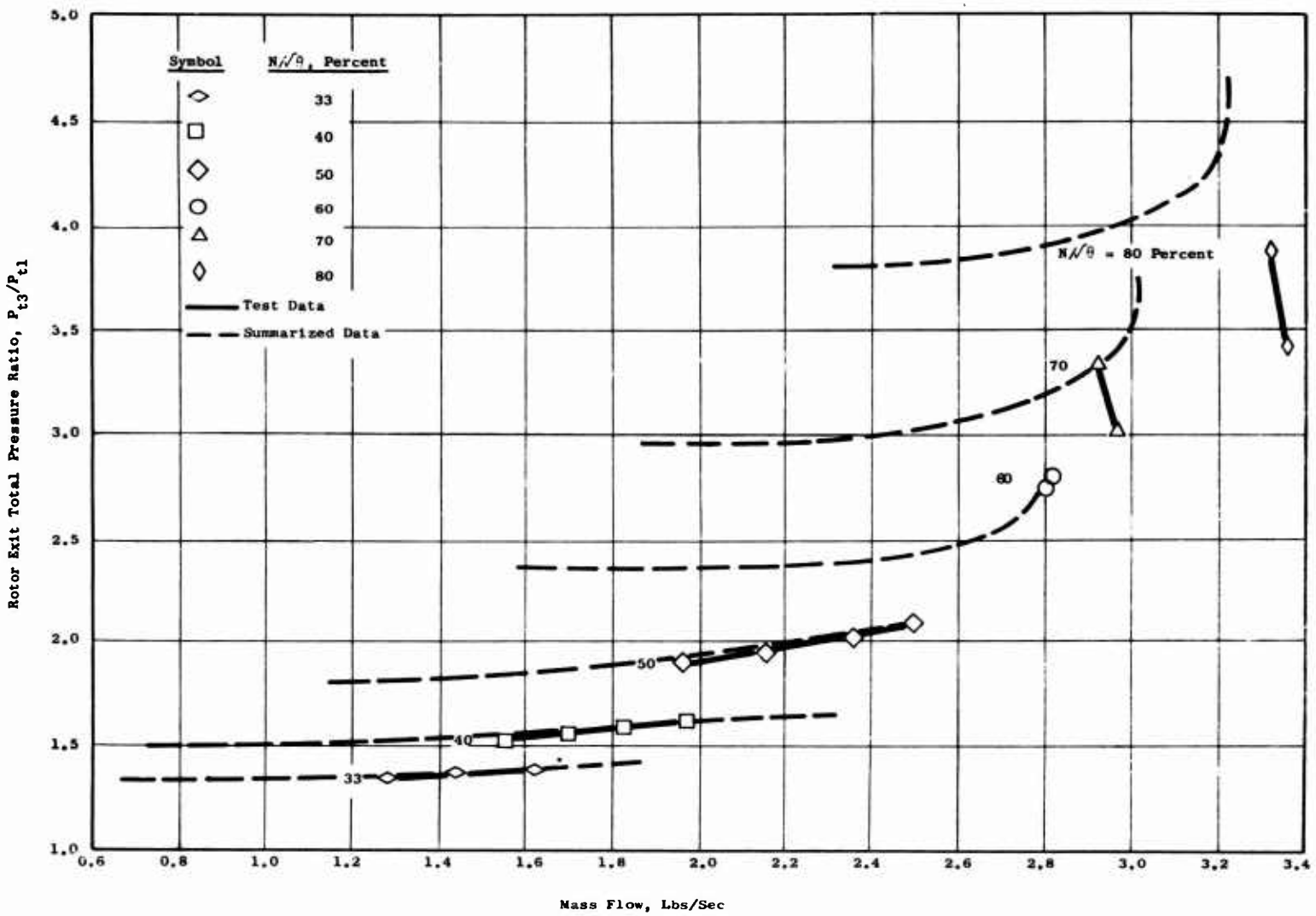

Figure 52. Total Pressure Ratio Versus Mass Flow With Supersonic Stators Set at 79 Degrees and Subsonic Stators Set at 73 Degrees.

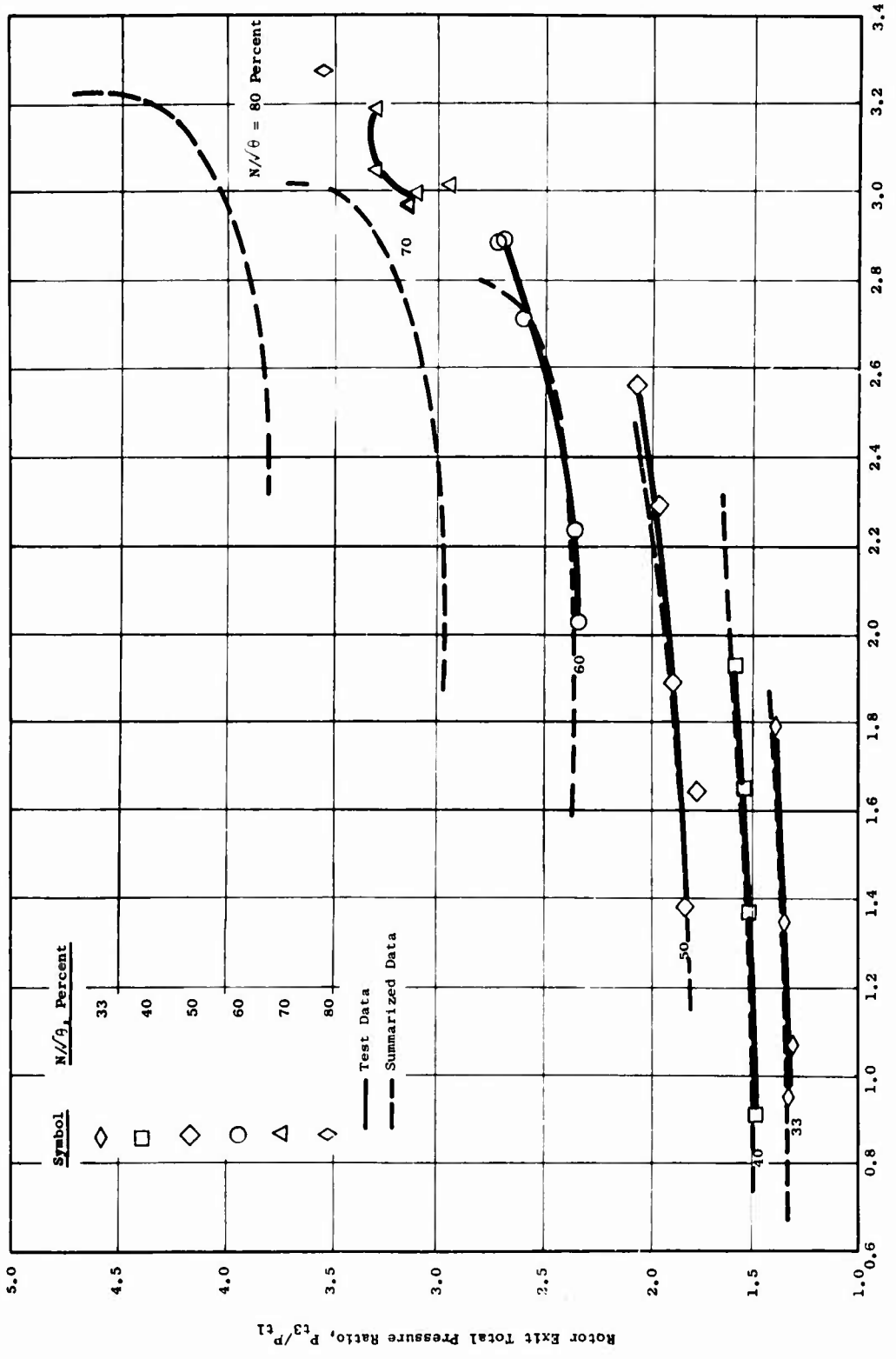

Figure 53. Total Pressure Ratio Versus Mass Flow With Supersonic Stators Set at 79 Degrees and Subsonic Stators Set at 76 Degrees.

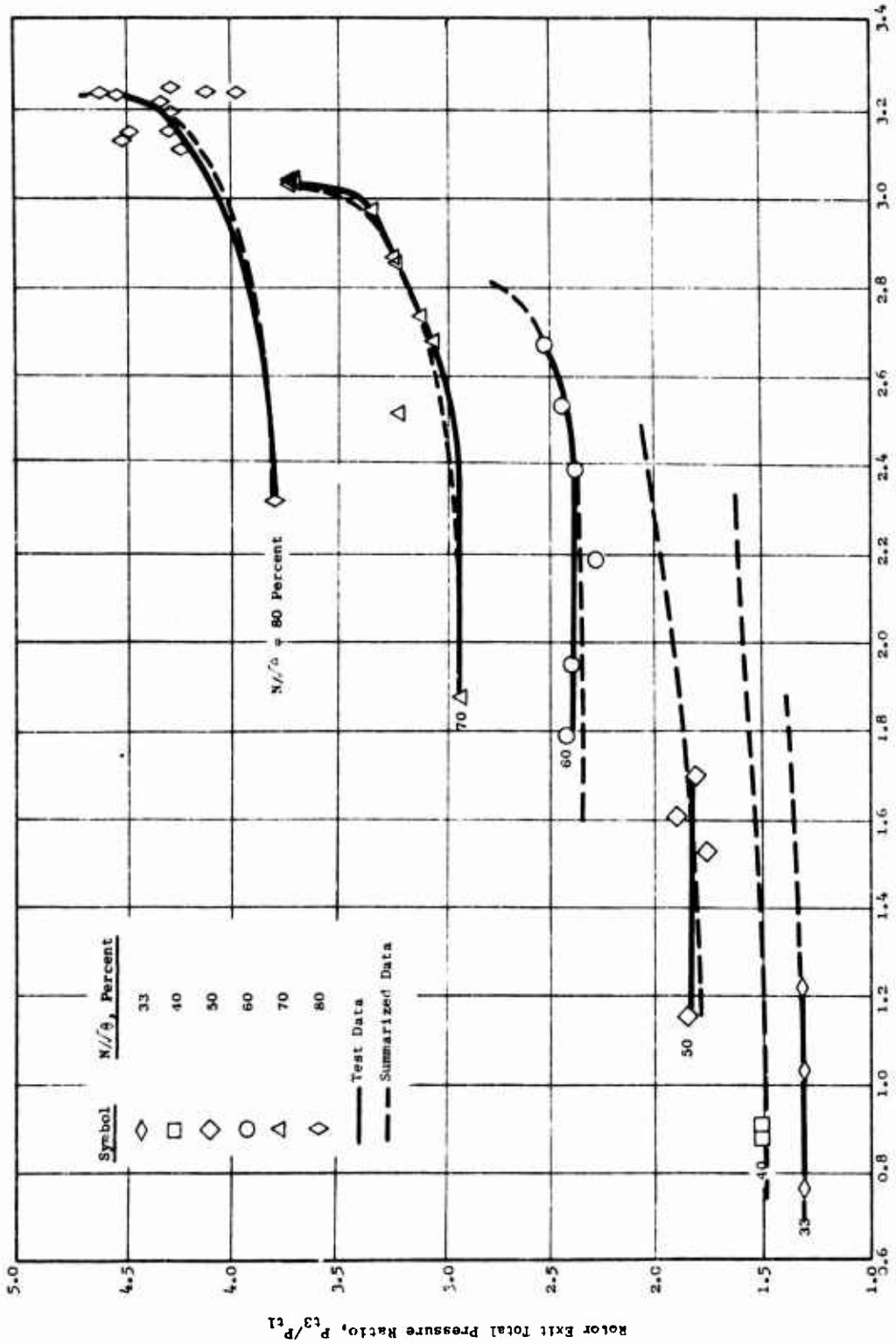

Figure 54. Total Pressure Ratio Versus Mass Flow With Supersonic Stators Set at 82 Degrees and Subsonic Stators Set at 73 Degrees.

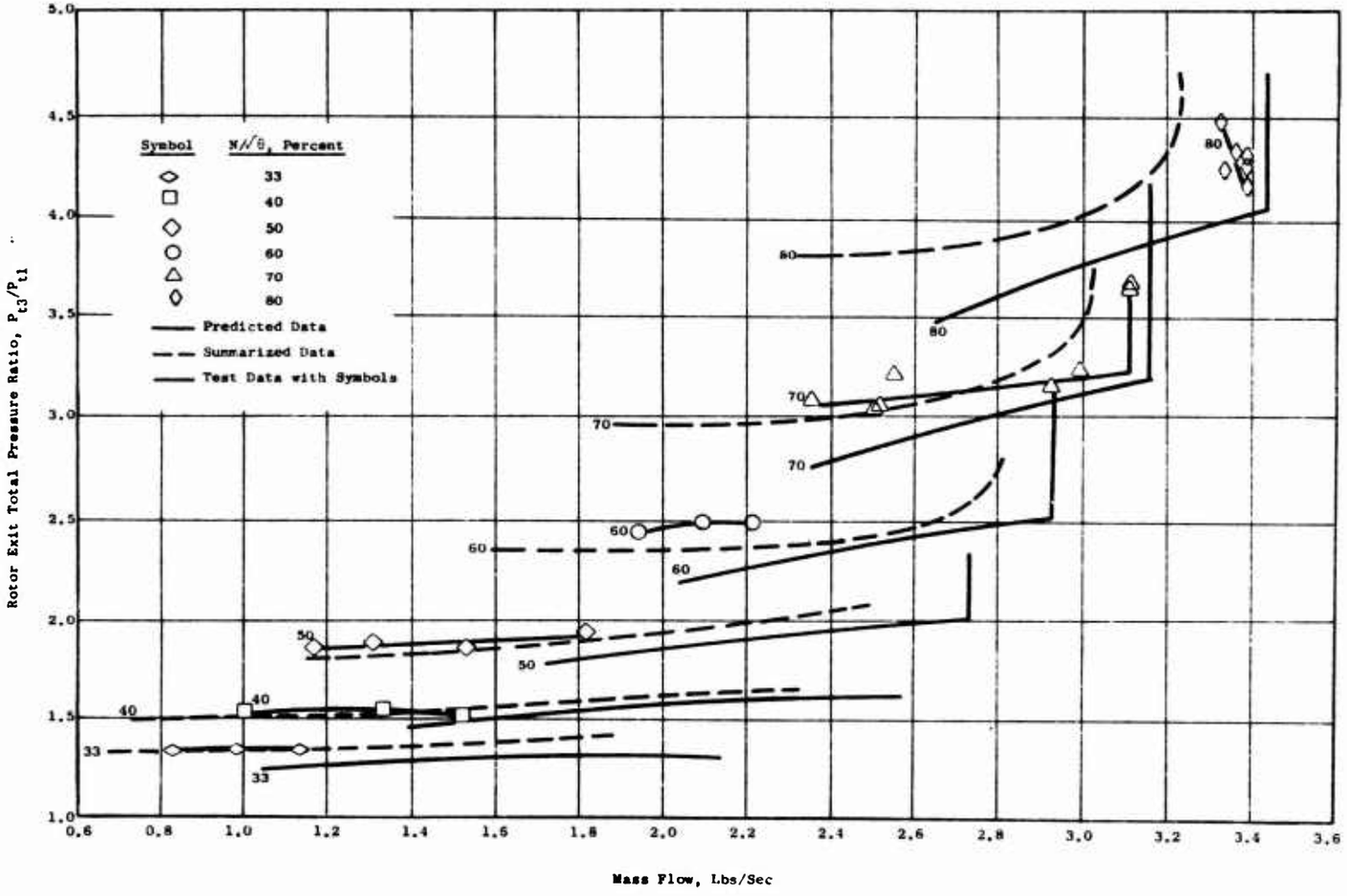

Figure 55. Total Pressure Ratio Versus Mass Flow With Supersonic Stators Set at 82 Degrees and Subsonic Stators Set at 76 Degrees.

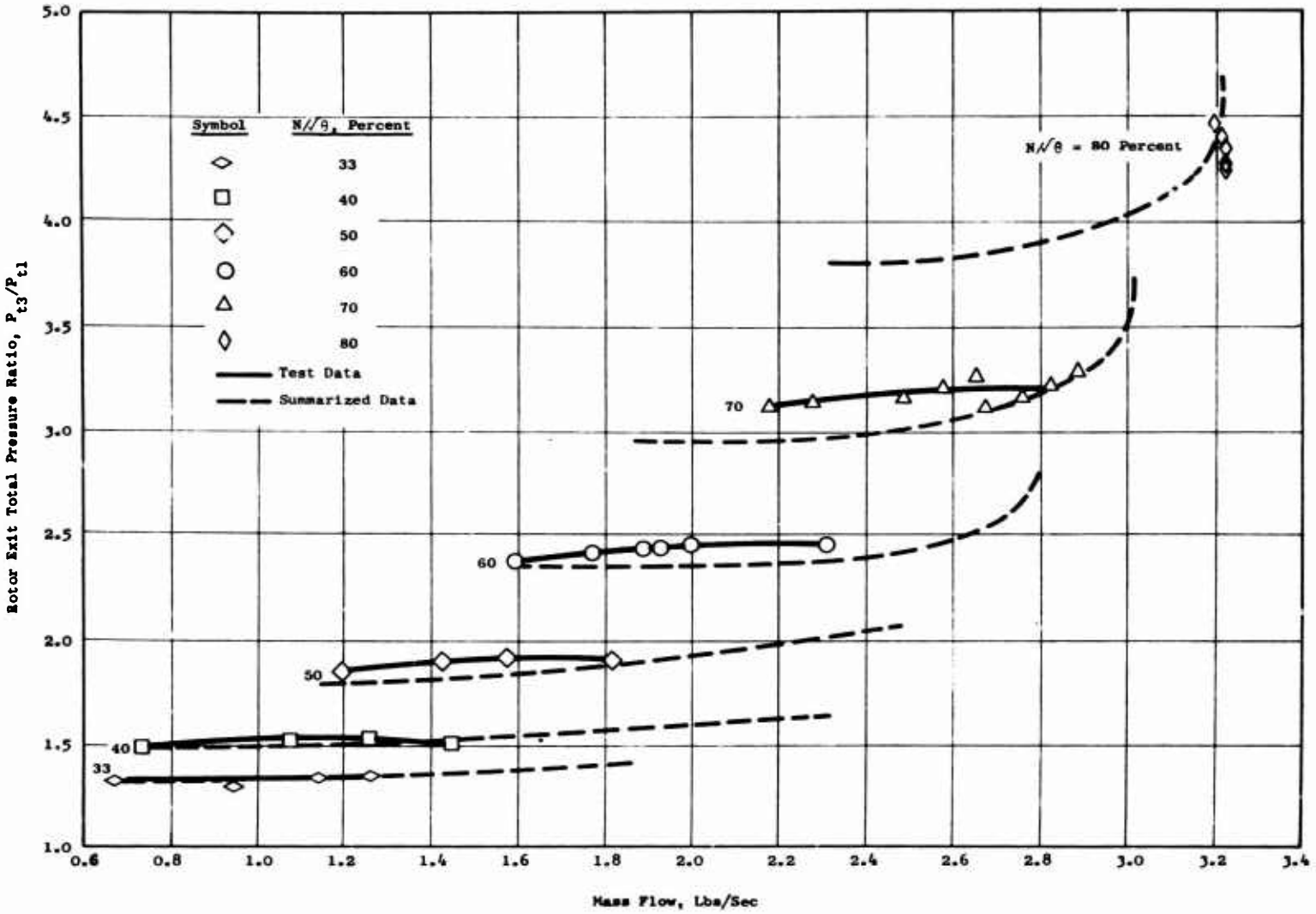

Figure 56. Total Pressure Ratio Versus Mass Flow With Supersonic Stators Set at 82 Degrees and Subsonic Stators Set at 79 Degrees.

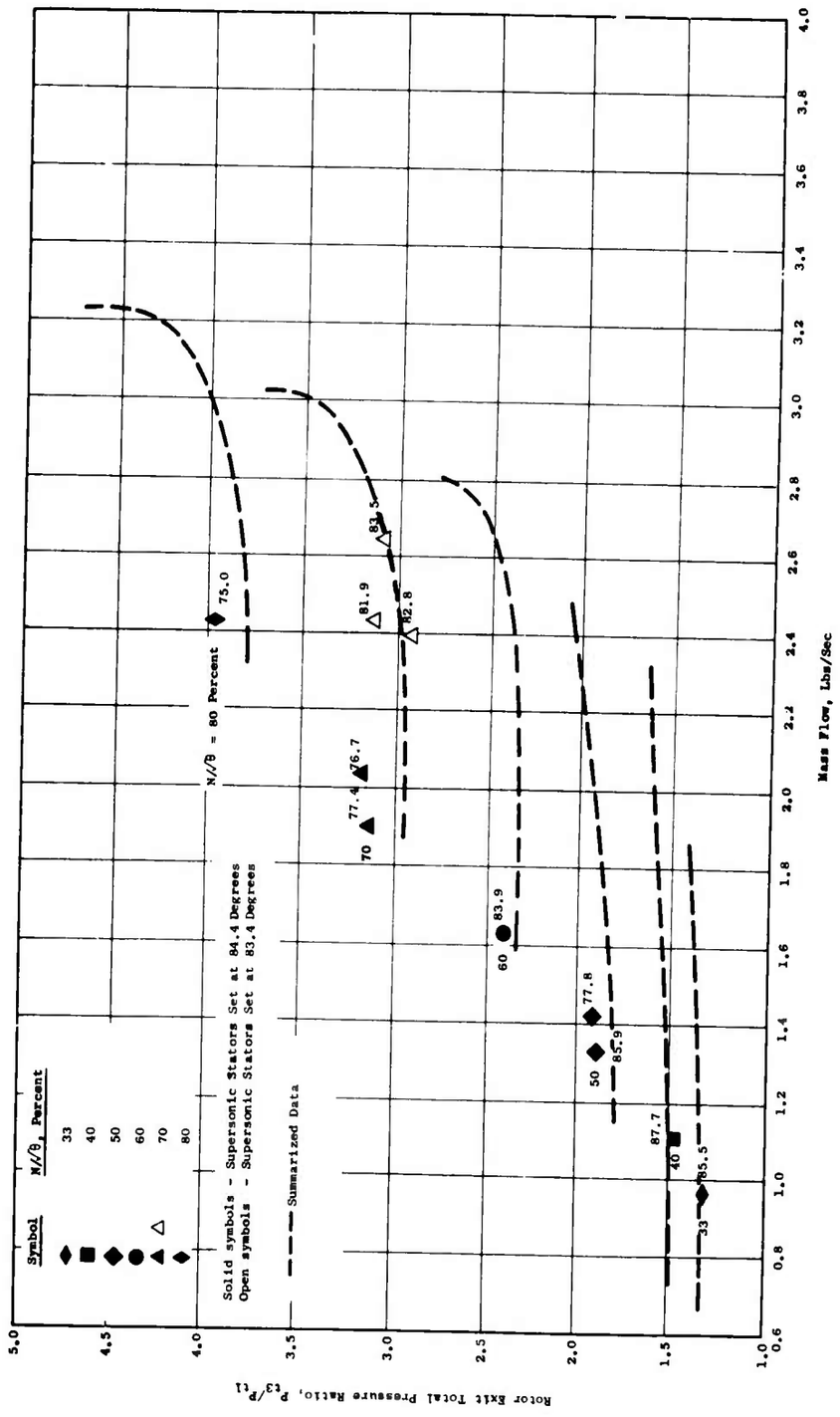

Figure 57. Total Pressure Ratio Versus Mass Flow With Supersonic Stators Set at 84.4 and 83.4 Degrees and Subsonic Stators Set at 76.3 Degrees for Low and Intermediate Speeds.

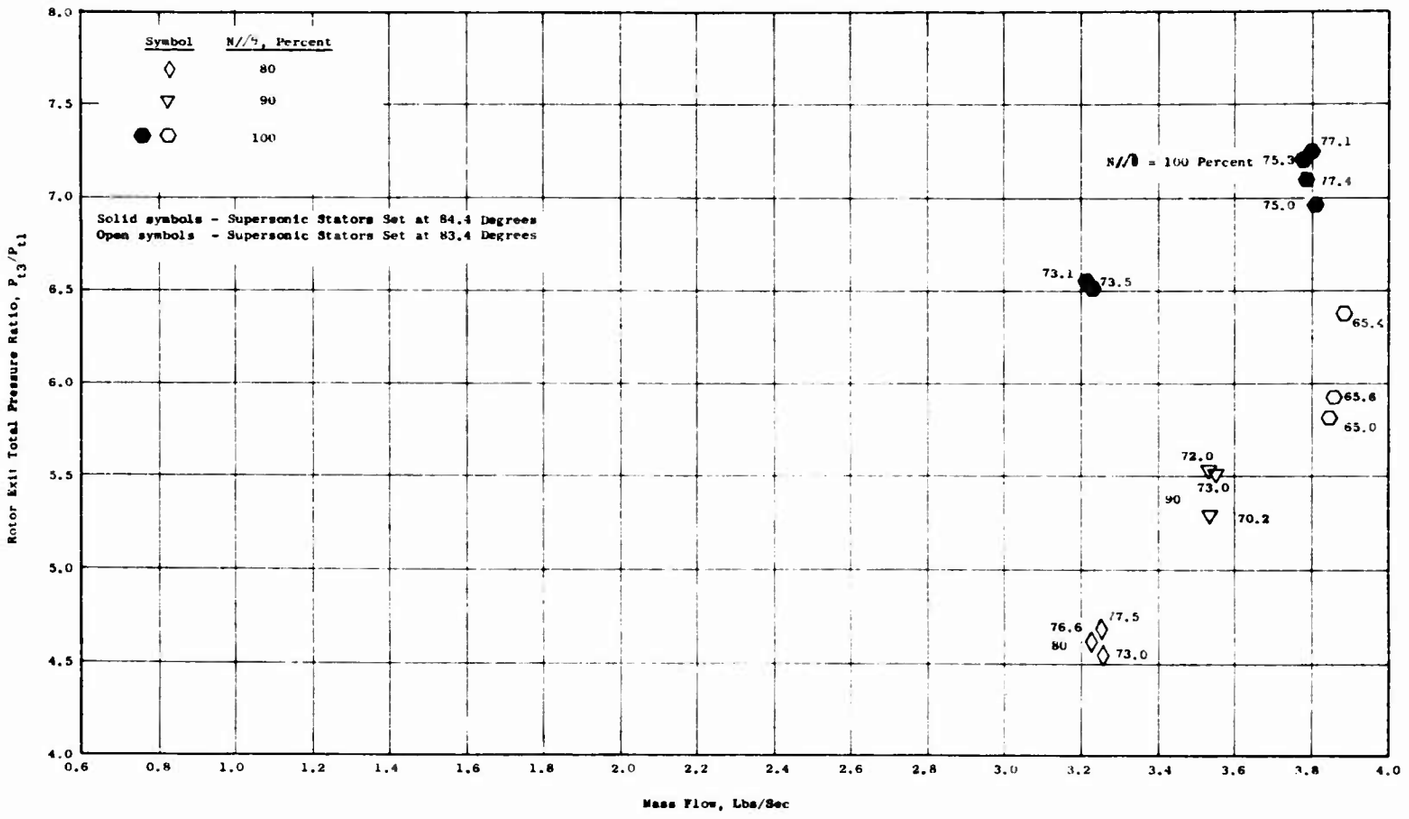

Figure 58. Total Pressure Ratio Versus Mass Flow With Supersonic Stators Set at 84.4 and 83.4 Degrees and Subsonic Stators Set at 76.3 Degrees for High Speeds.

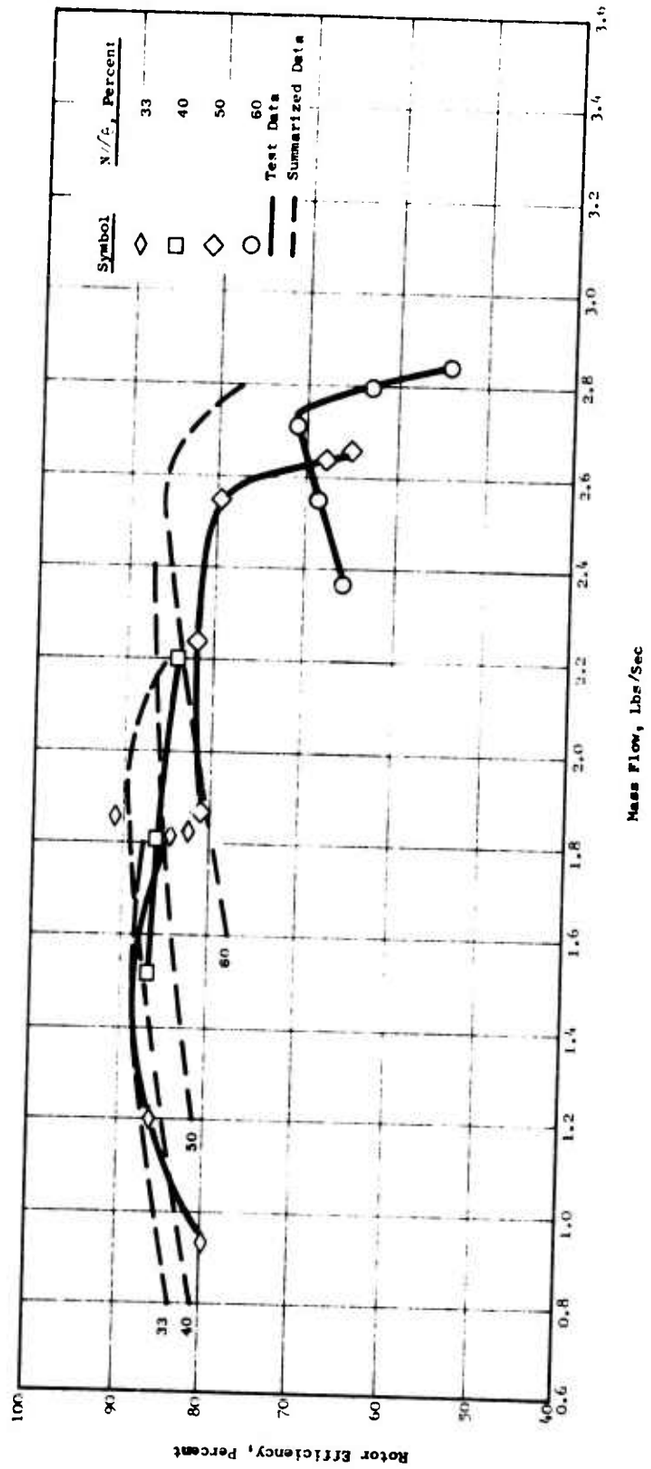

Figure 59. Rotor Efficiency Versus Mass Flow With Supersonic Stators Set at 76 Degrees and Subsonic Stators Set at 67 Degrees.

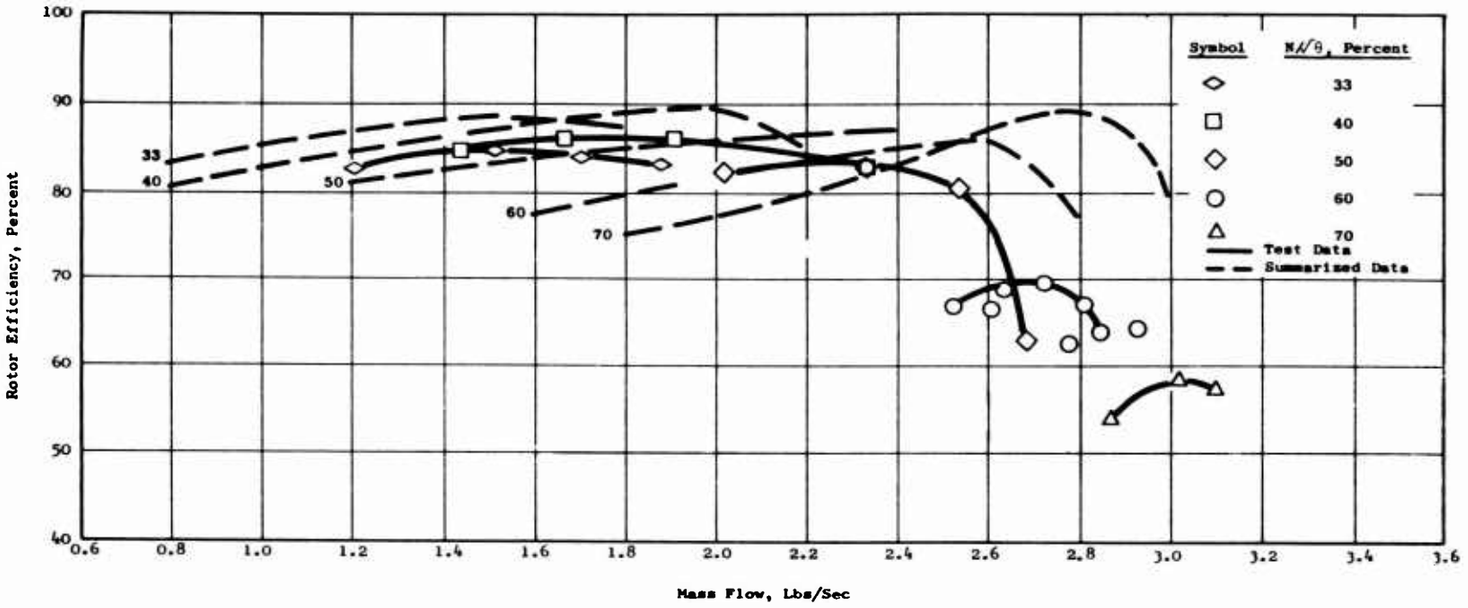

Figure 60. Rotor Efficiency Versus Mass Flow With Supersonic Stators Set at 76 Degrees and Subsonic Stators Set at 70 Degrees.

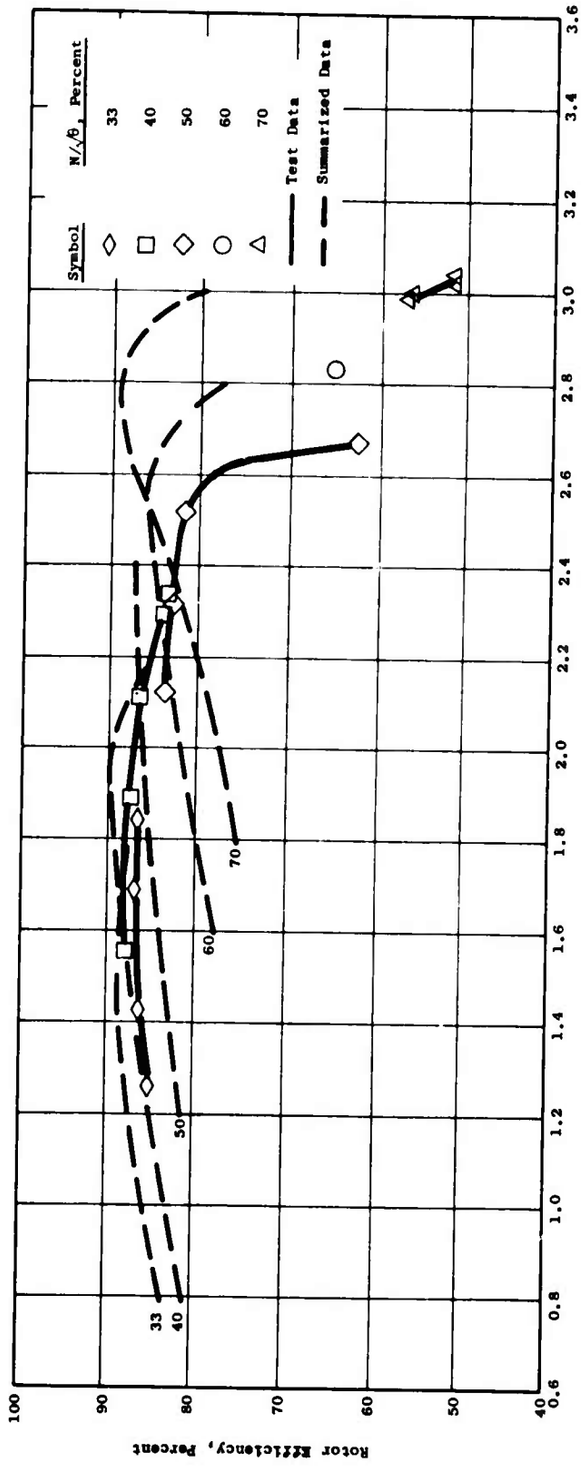

Figure 61. Rotor Efficiency Versus Mass Flow With Supersonic Stators Set at 76 Degrees and Subsonic Stators Set at 73 Degrees.

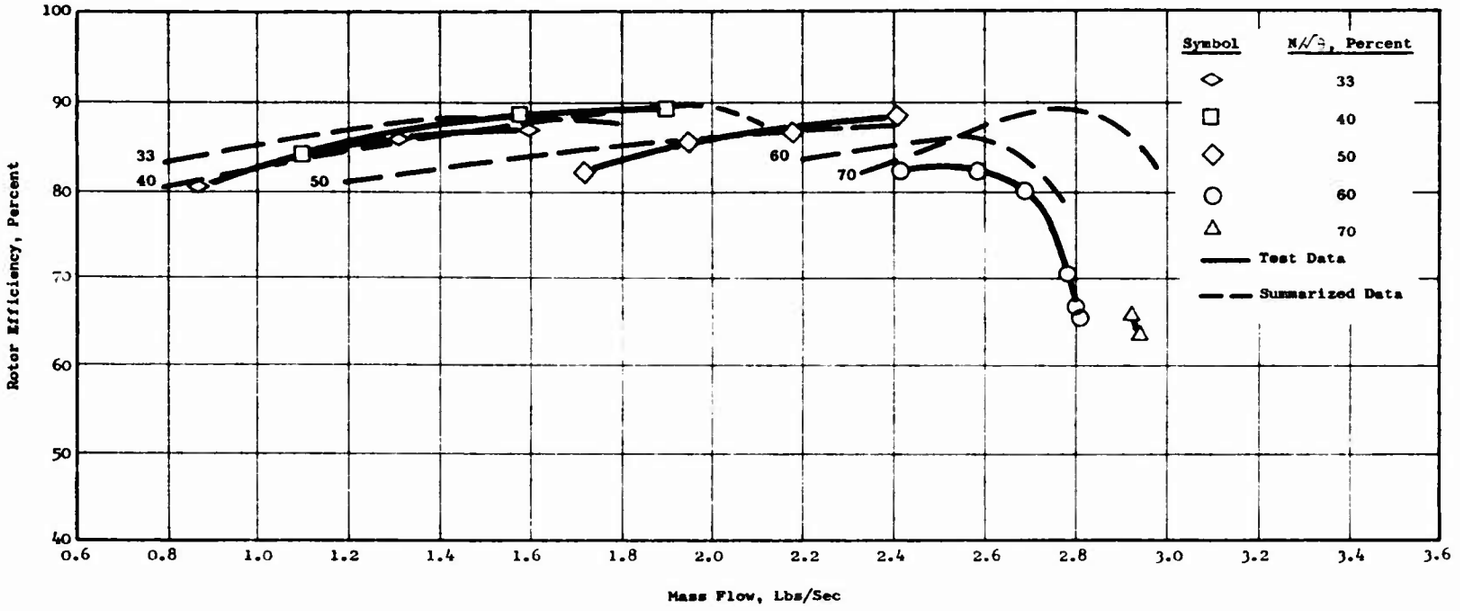

Figure 62. Rotor Efficiency Versus Mass Flow With Supersonic Stators Set at 79 Degrees and Subsonic Stators Set at 70 Degrees.

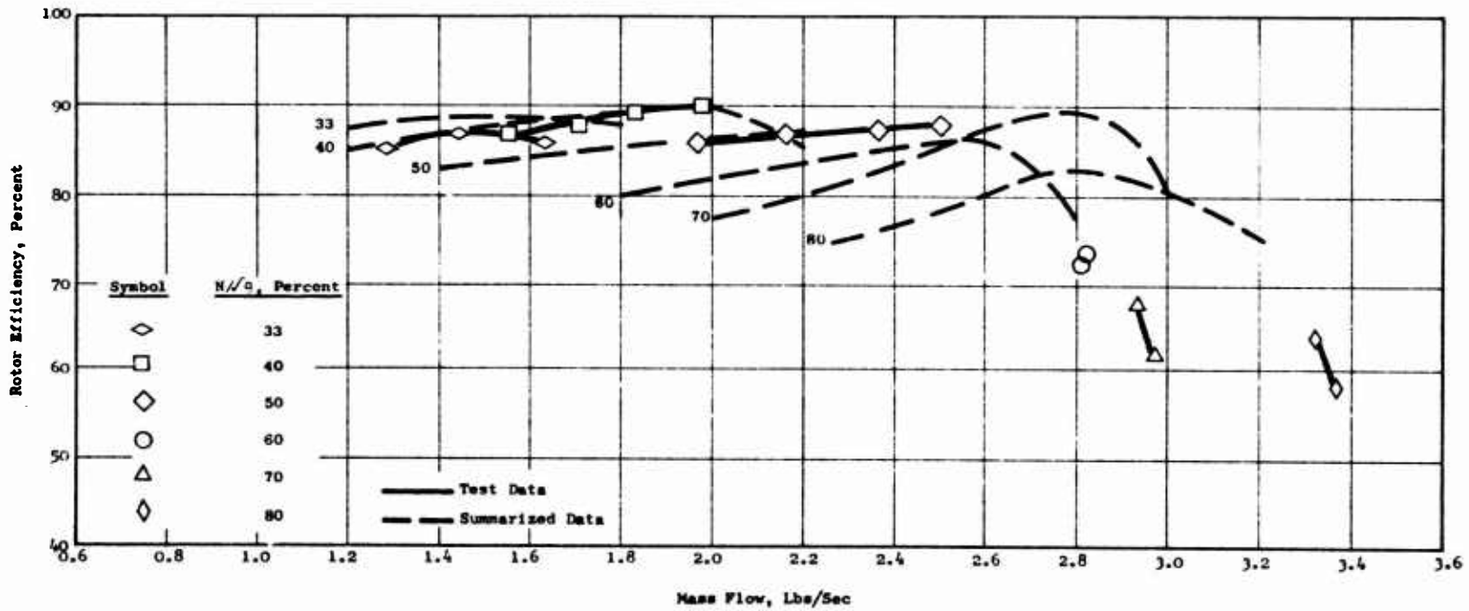

Figure 63. Rotor Efficiency Versus Mass Flow With Supersonic Stators Set at 79 Degrees and Subsonic Stators Set at 73 Degrees.

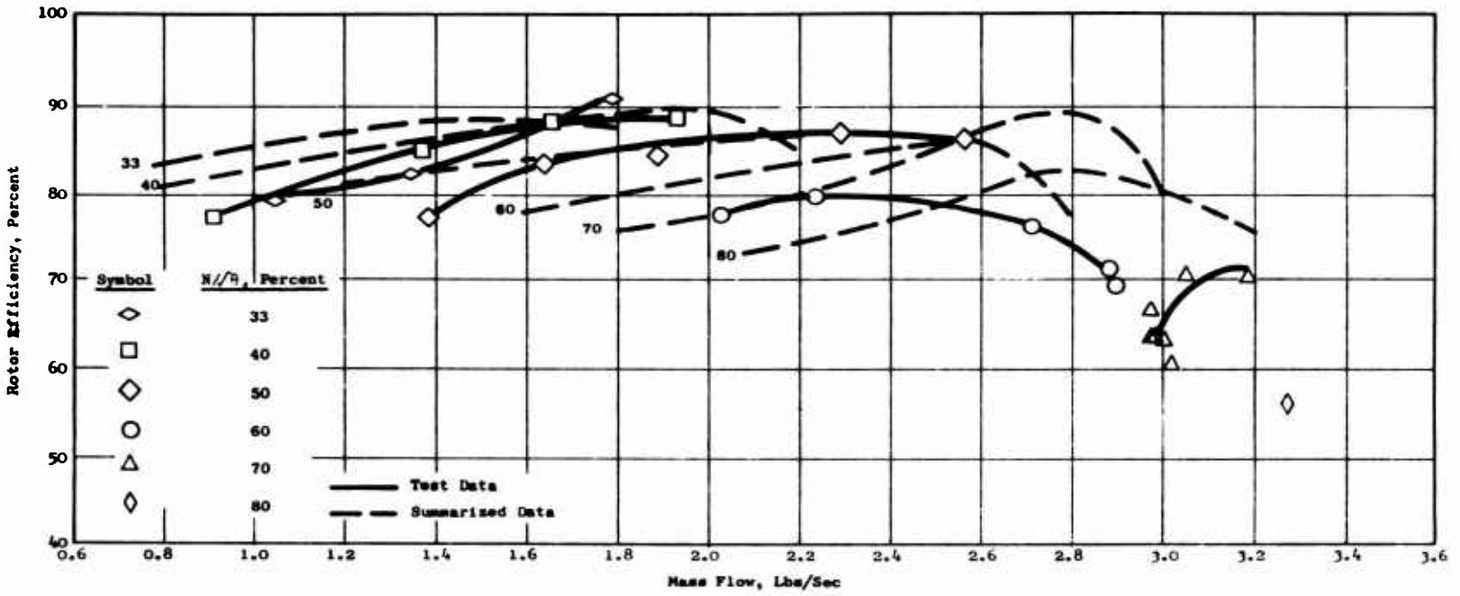

Figure 64. Rotor Efficiency Versus Mass Flow With Supersonic Stators Set at 79 Degrees and Subsonic Stators Set at 76 Degrees.

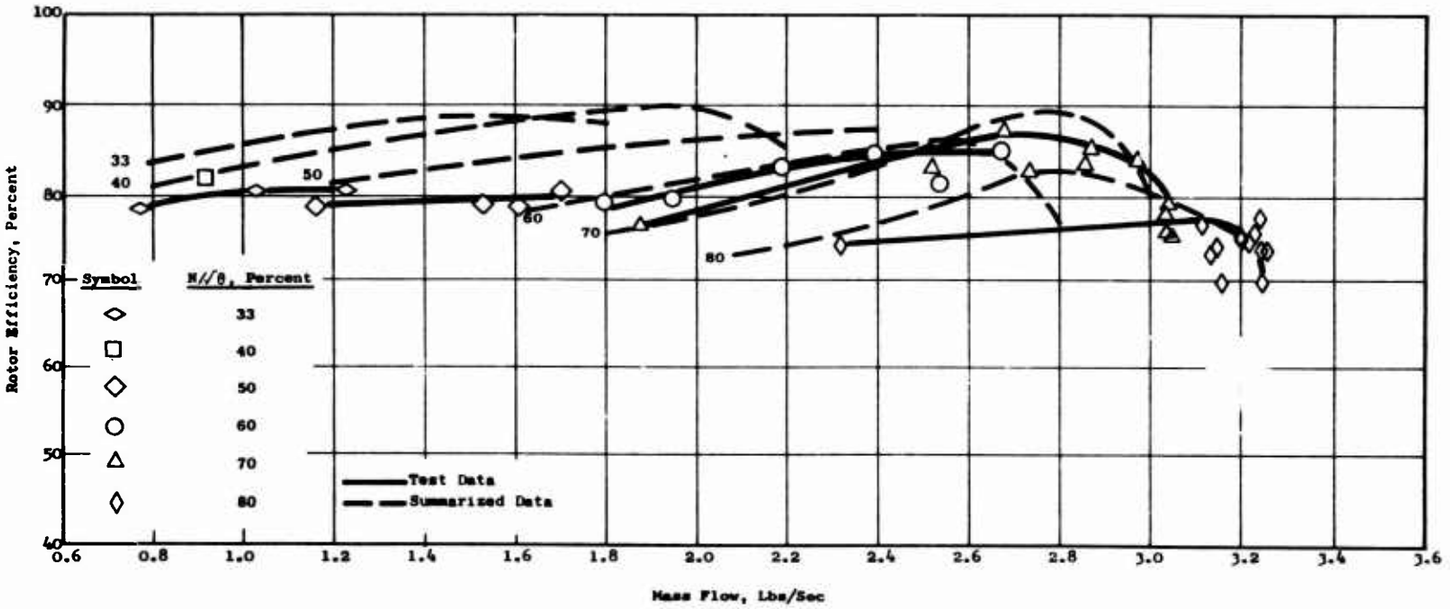

Figure 65. Rotor Efficiency Versus Mass Flow With Supersonic Stators Set at 82 Degrees and Subsonic Stators Set at 73 Degrees.

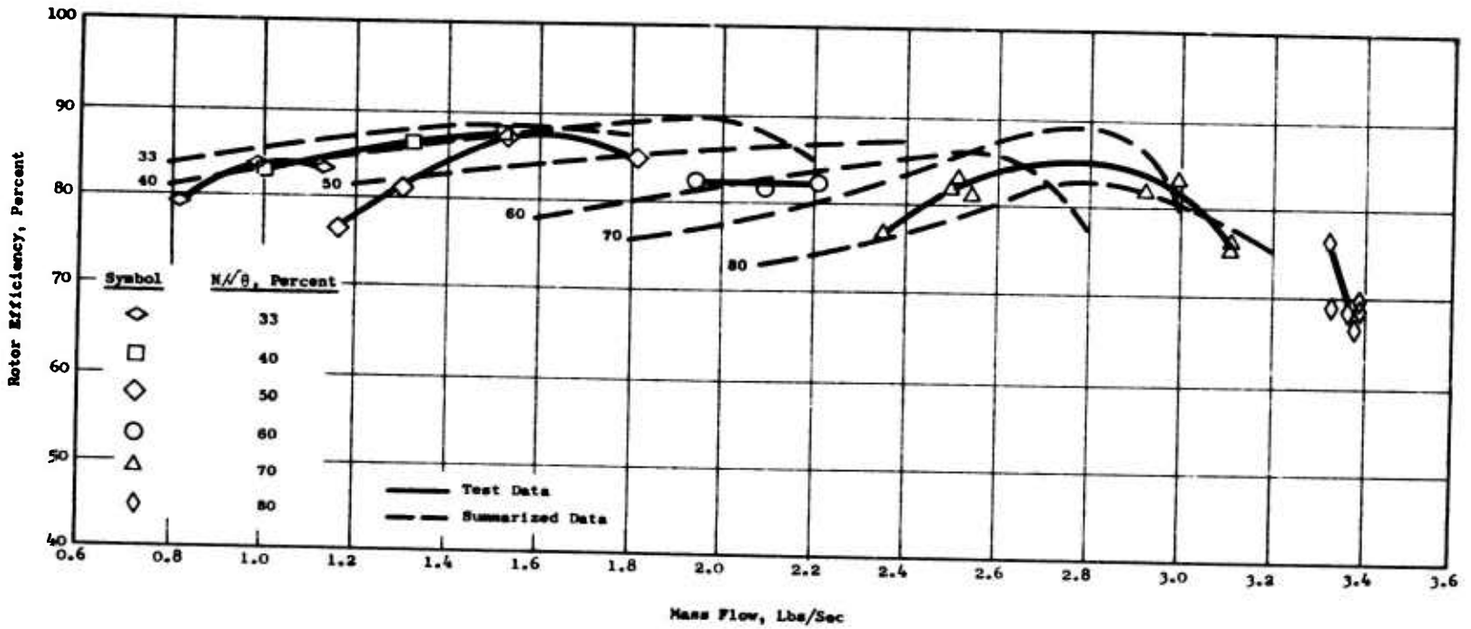

Figure 66. Rotor Efficiency Versus Mass Flow With Supersonic Stators Set at 82 Degrees and Subsonic Stators Set at 76 Degrees.

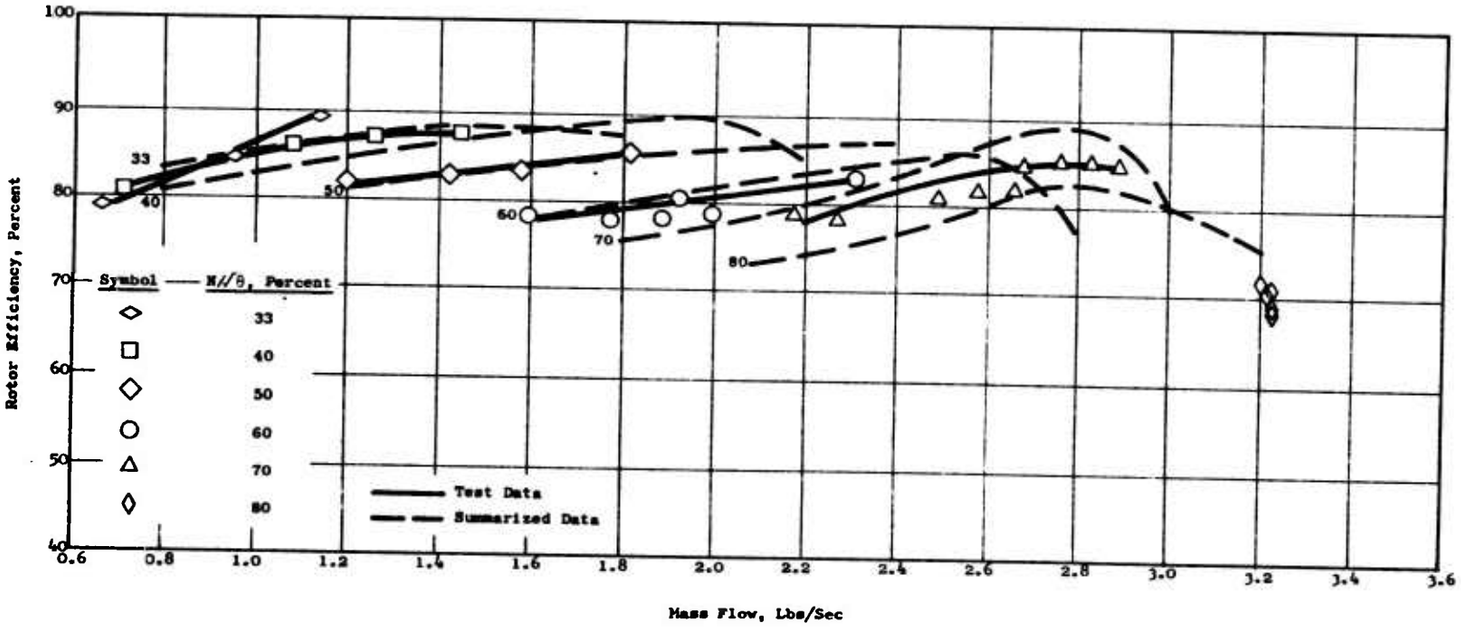

Figure 67. Rotor Efficiency Versus Mass Flow With Supersonic Stators Set at 82 Degrees and Subsonic Stators Set at 79 Degrees.

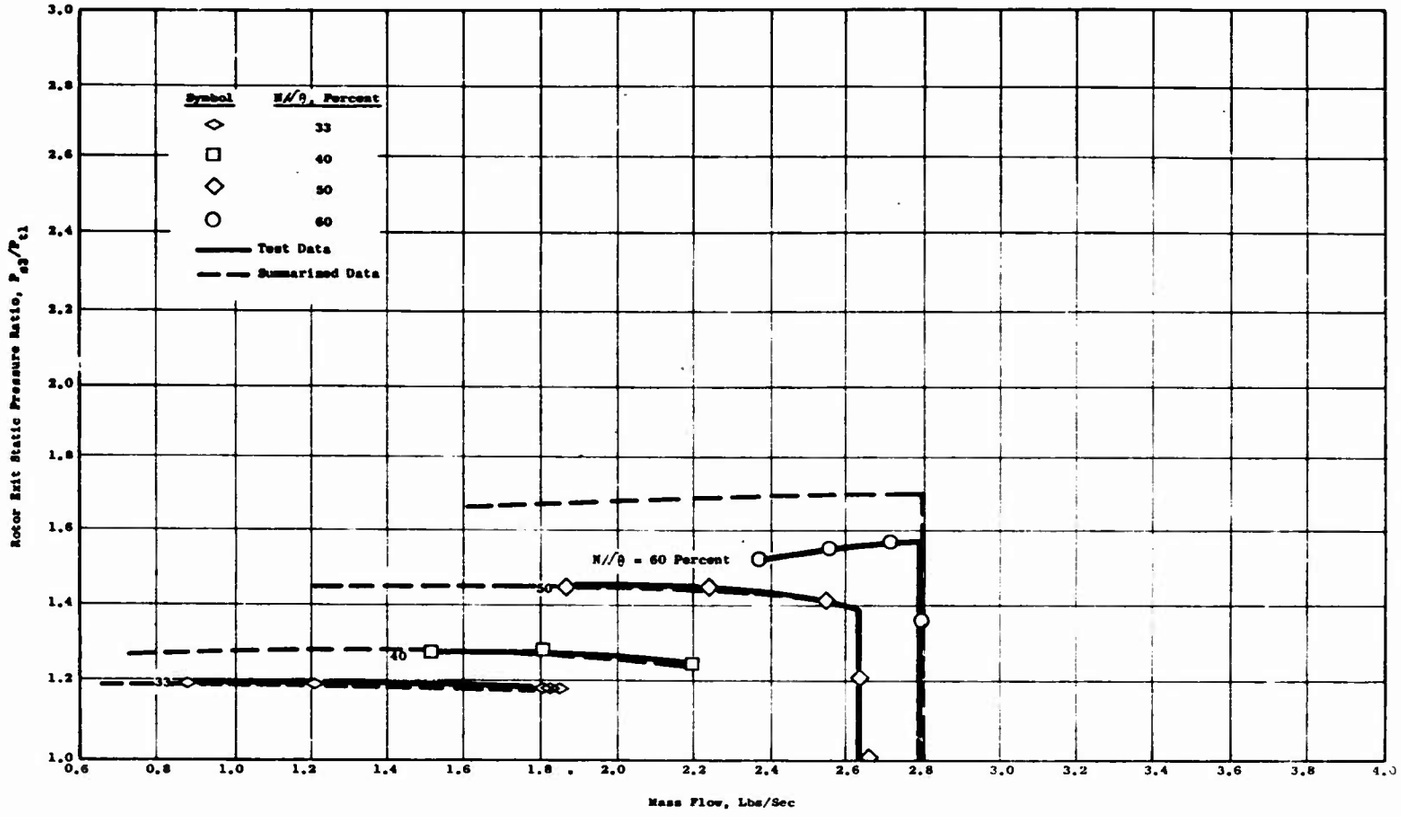

Figure 68. Static Pressure Ratio Versus Mass Flow With Supersonic Stators Set at 76 Degrees and Subsonic Stators Set at 67 Degrees.

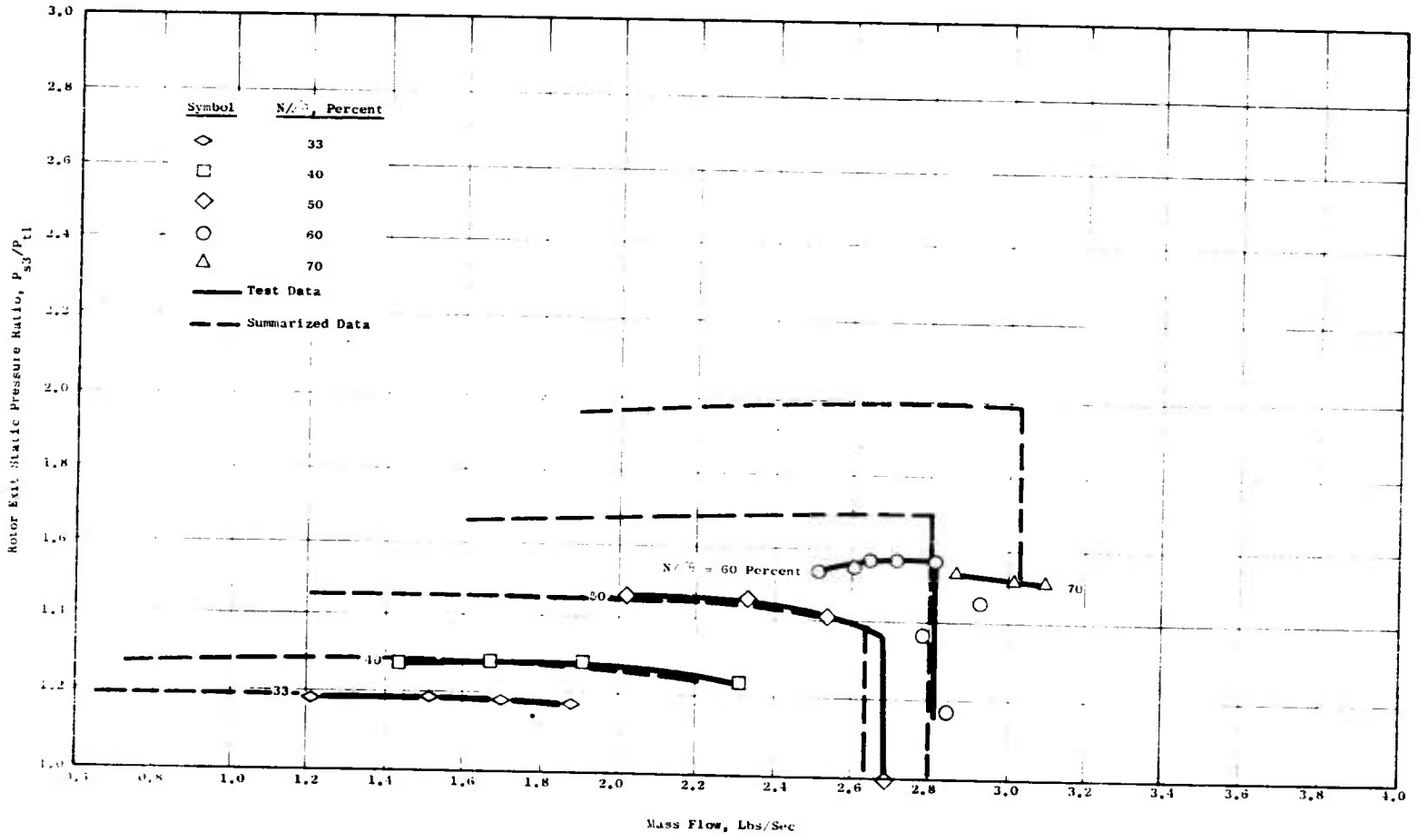

Figure 69. Static Pressure Ratio Versus Mass Flow With Supersonic Stators Set at 76 Degrees and Subsonic Stators Set at 70 Degrees.

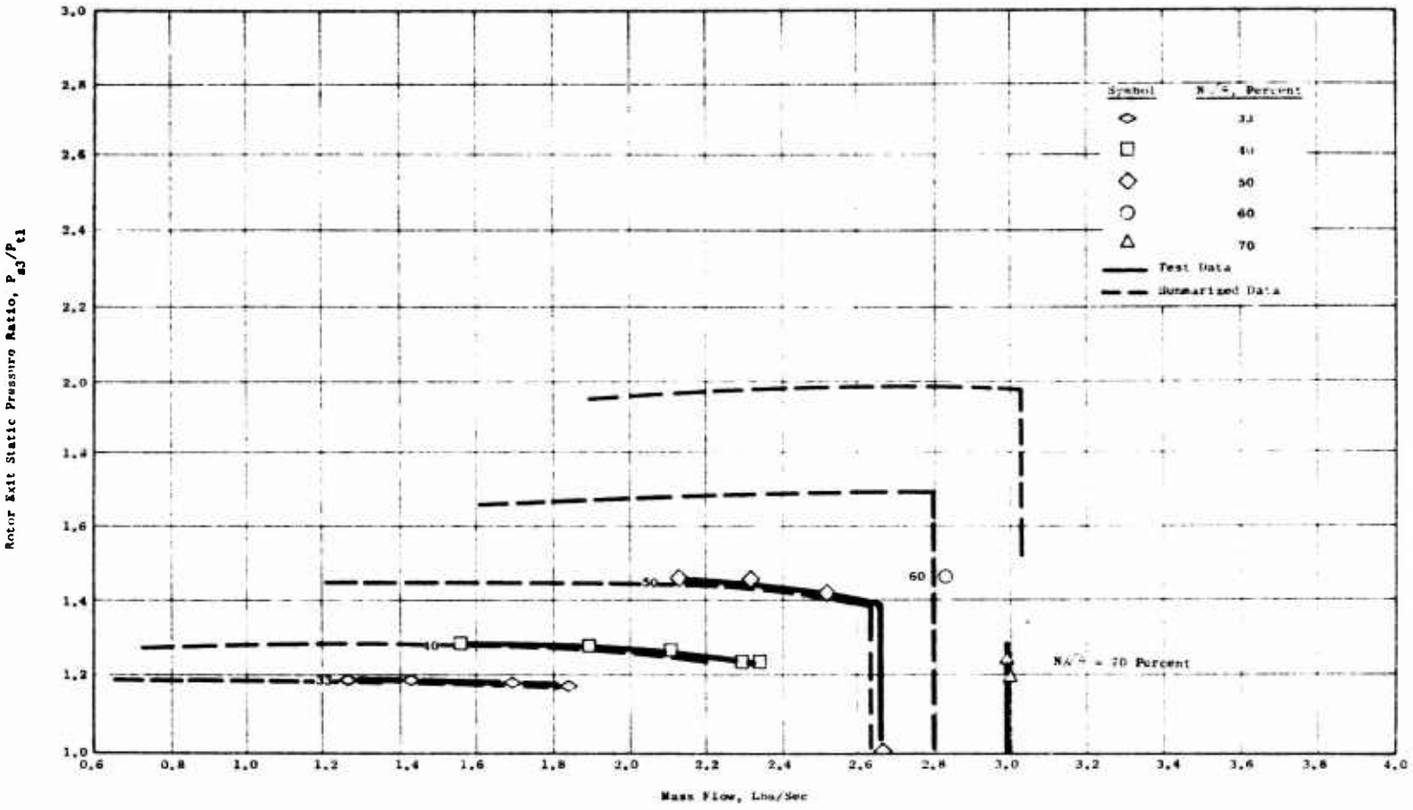

Figure 70. Static Pressure Ratio Versus Mass Flow With Supersonic Stators Set at 76 Degrees and Subsonic Stators Set at 73 Degrees.

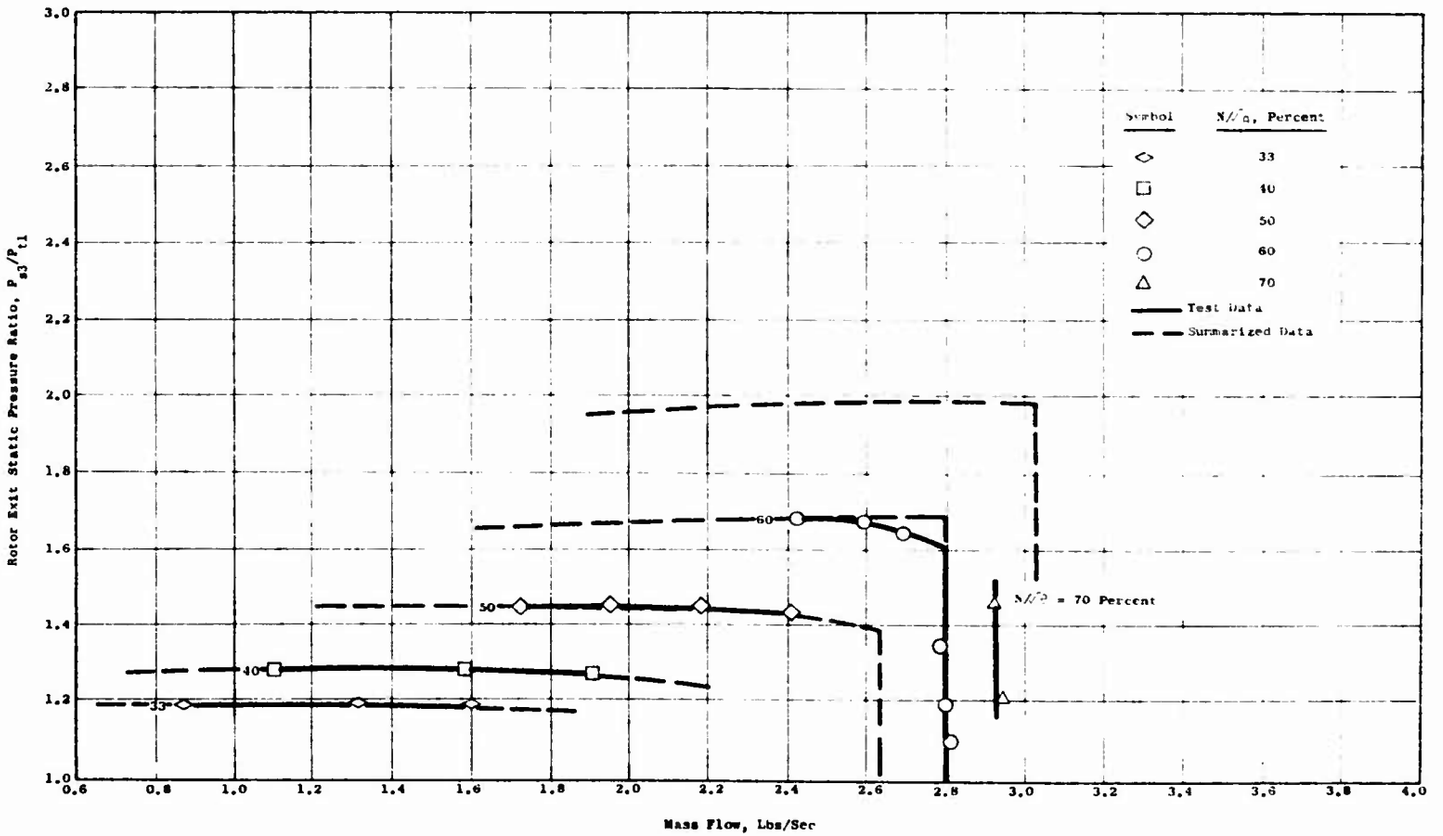

Figure 71. Static Pressure Ratio Versus Mass Flow With Supersonic Stators Set at 79 Degrees and Subsonic Stators Set at 70 Degrees.

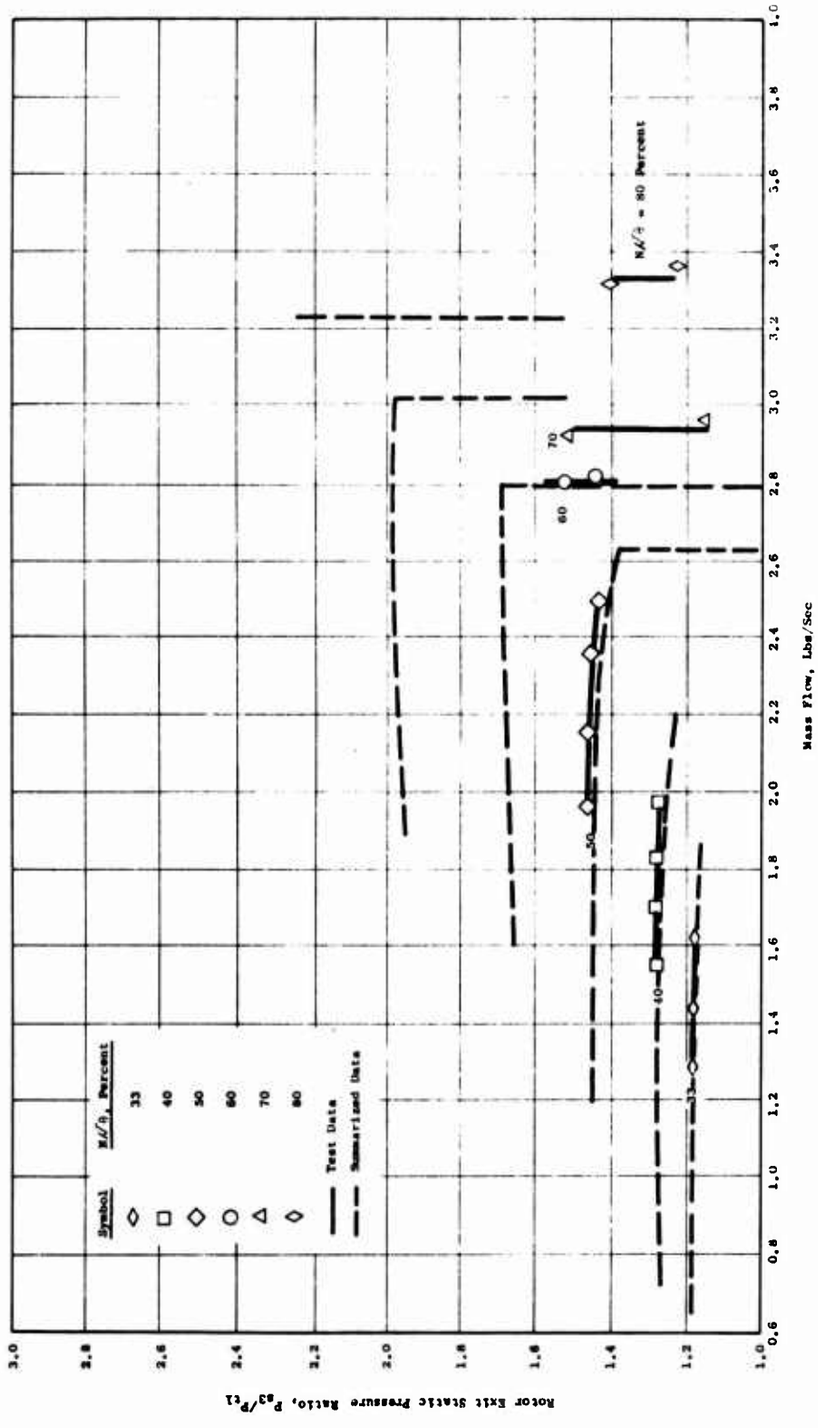

Figure 72. Static Pressure Ratio Versus Mass Flow with Supersonic Stators Set at 79 Degrees and Subsonic Stators Set at 73 Degrees.

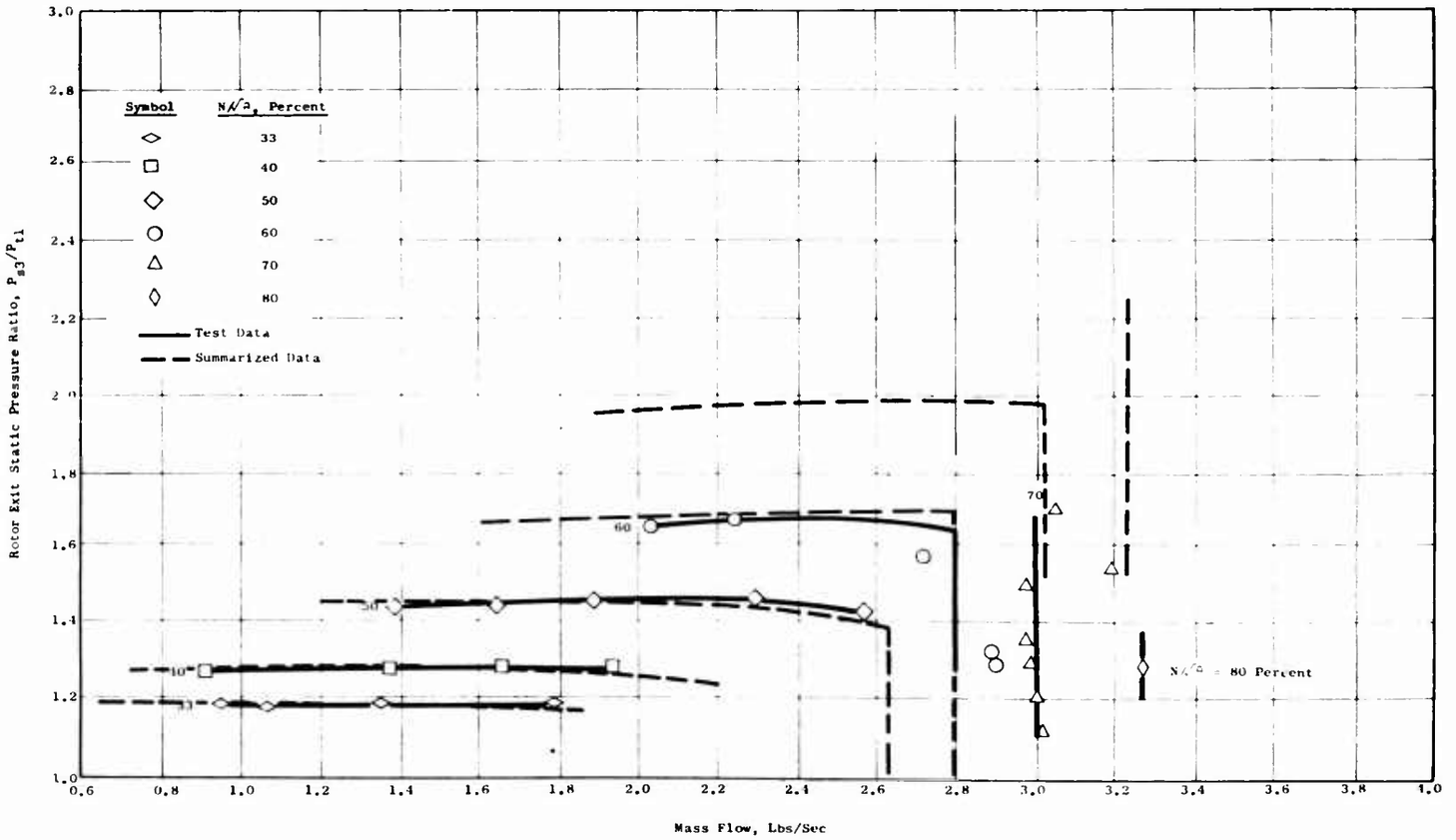

Figure 73. Static Pressure Ratio Versus Mass Flow With Supersonic Stators Set at 79 Degrees and Subsonic Stators Set at 76 Degrees.

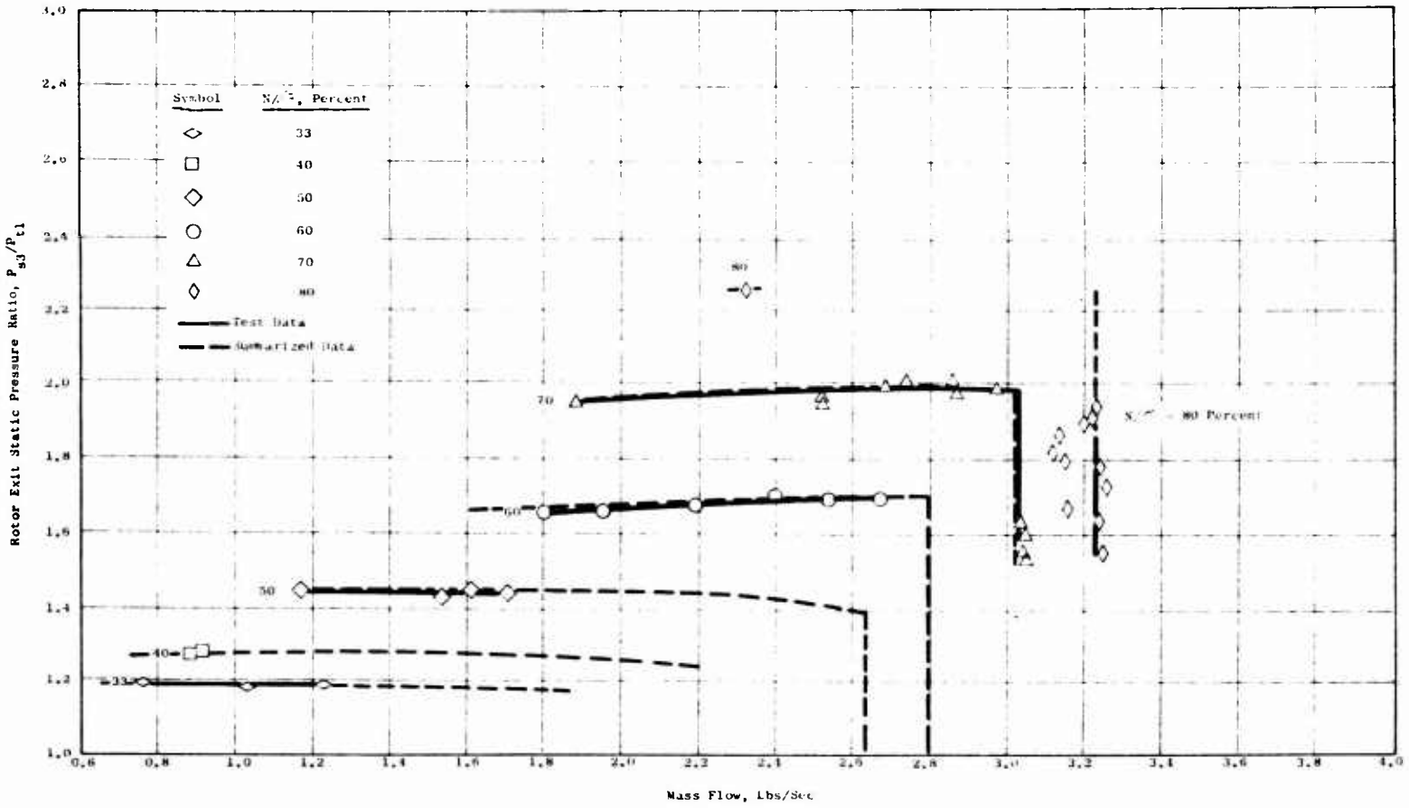

Figure 74. Static Pressure Ratio Versus Mass Flow With Supersonic Stators Set at 82 Degrees and Subsonic Stators Set at 73 Degrees.

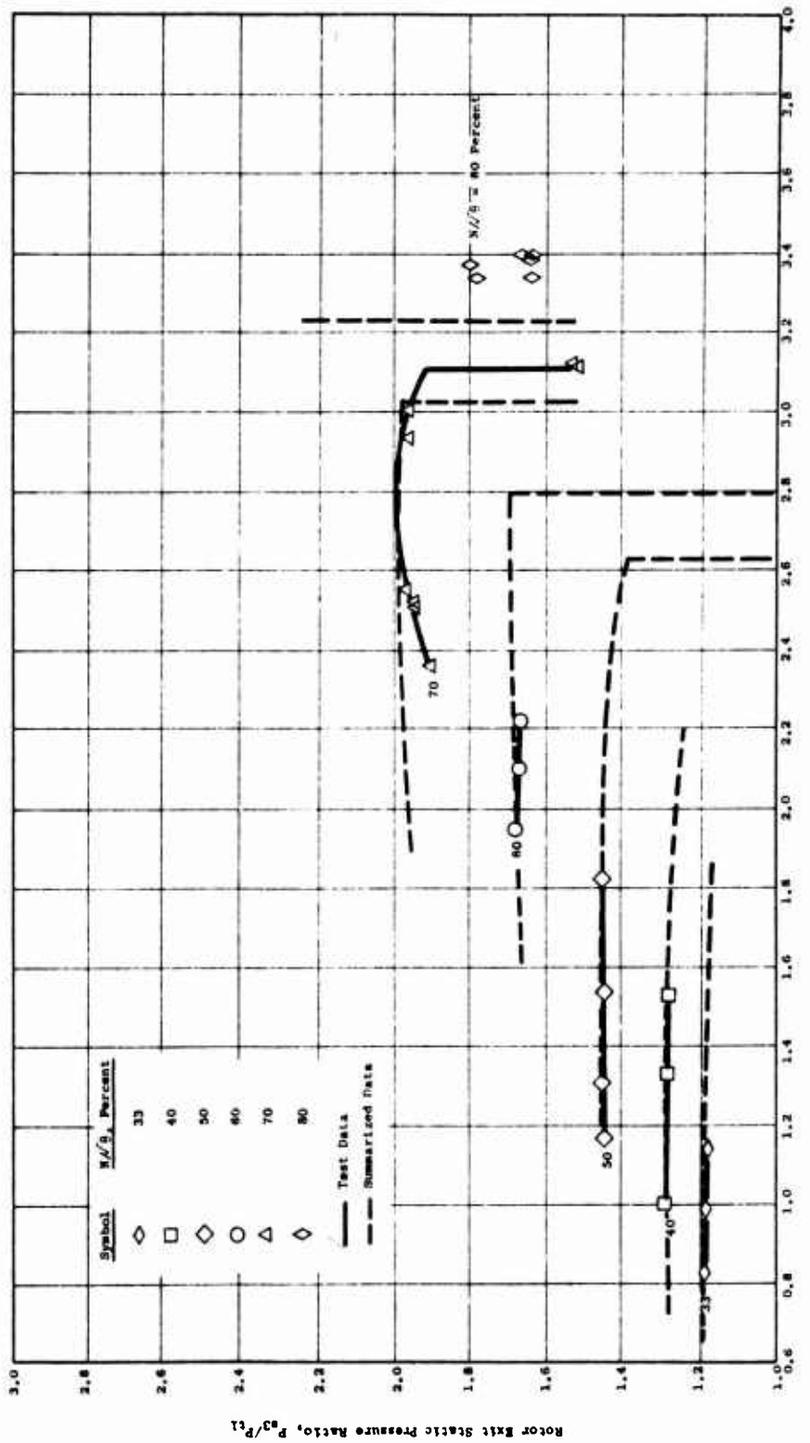

Figure 75. Static Pressure Ratio Versus Mass Flow With Supersonic Stators Set at 82 Degrees and Subsonic Stators Set at 76 Degrees.

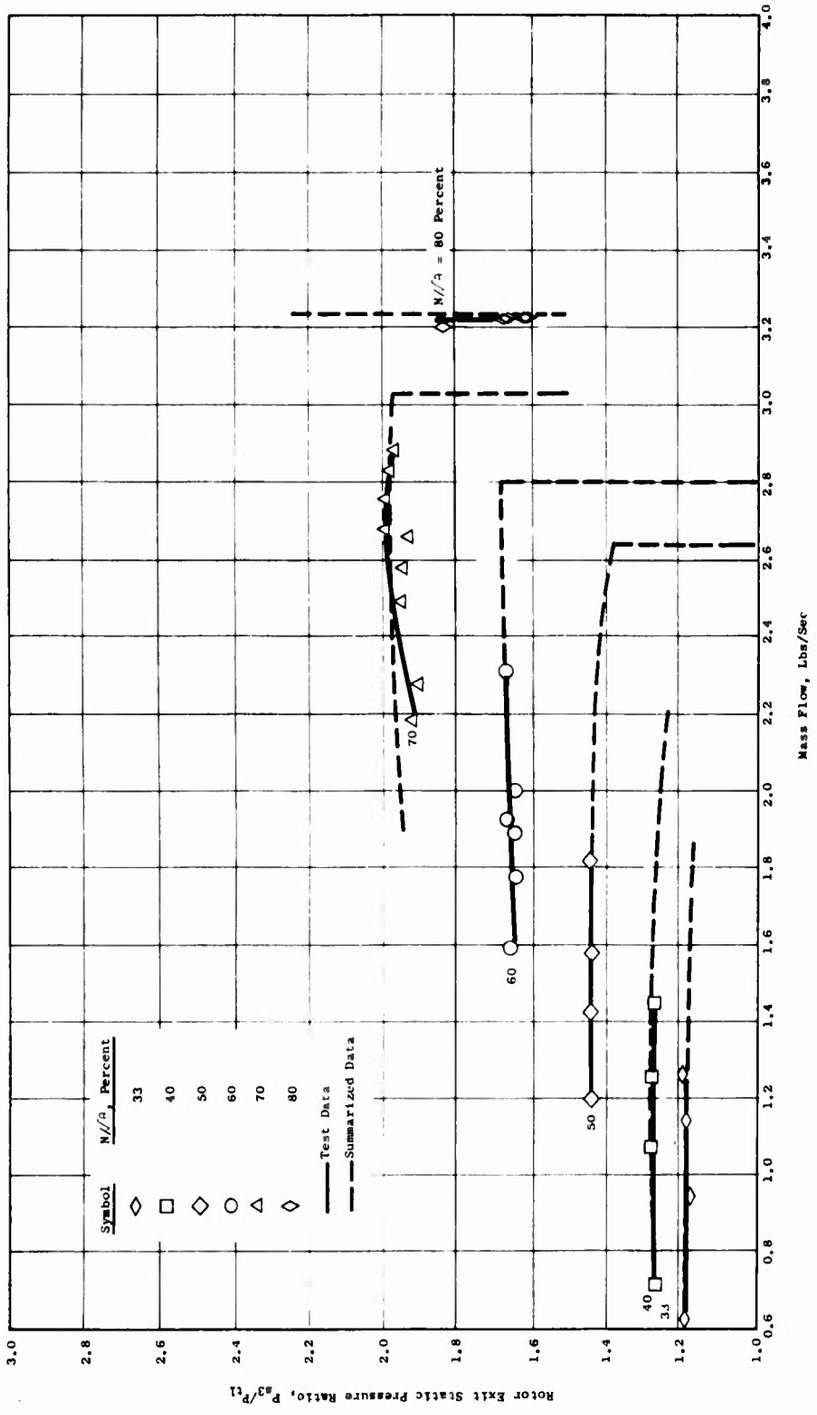

Figure 76. Static Pressure Ratio Versus Mass Flow With Supersonic Stators Set at 82 Degrees and Subsonic Stators Set at 79 Degrees.

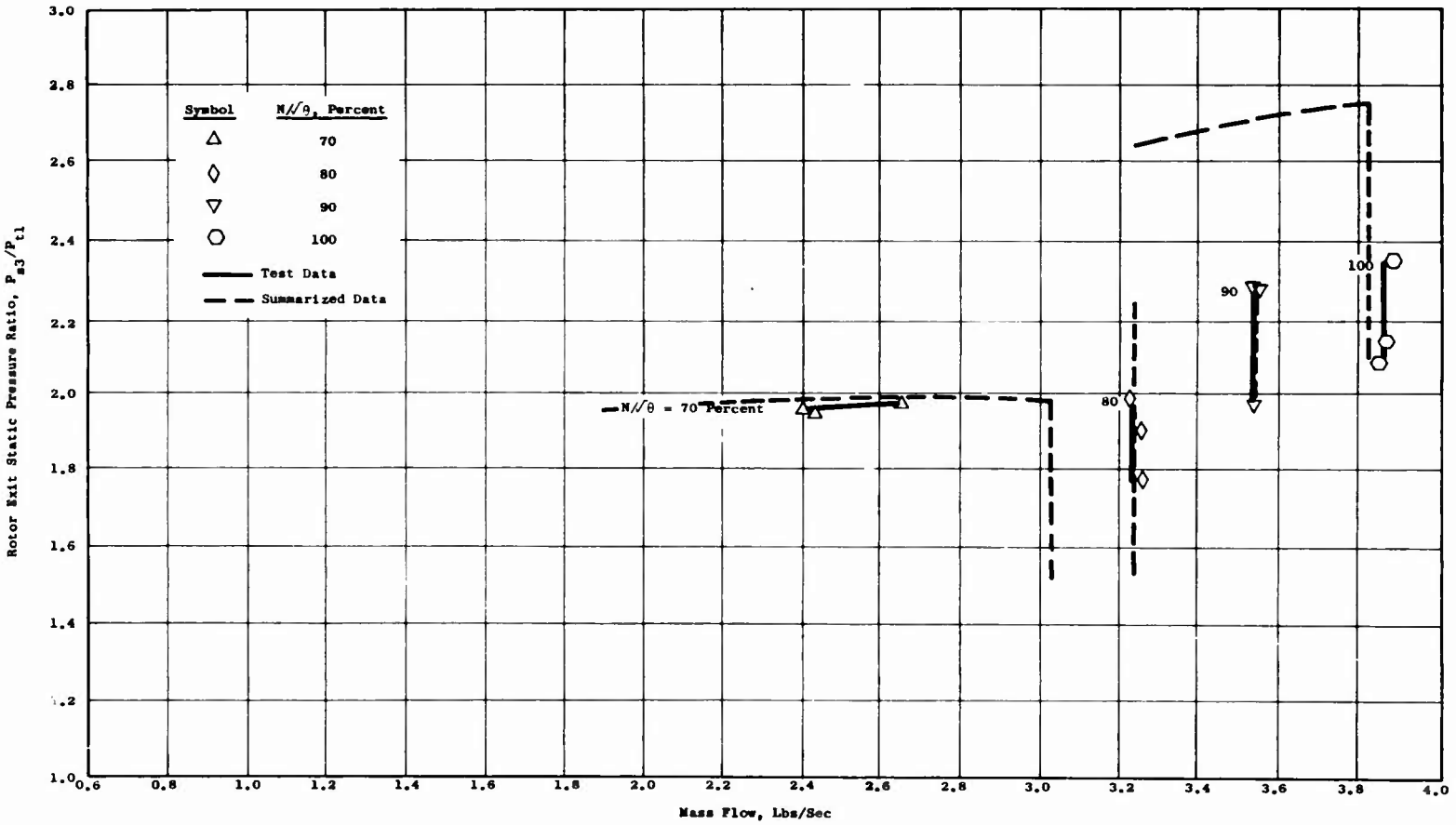

Figure 77. Static Pressure Ratio Versus Mass Flow With Supersonic Stators Set at 83.4 Degrees and Subsonic Stators Set at 76.3 Degrees.

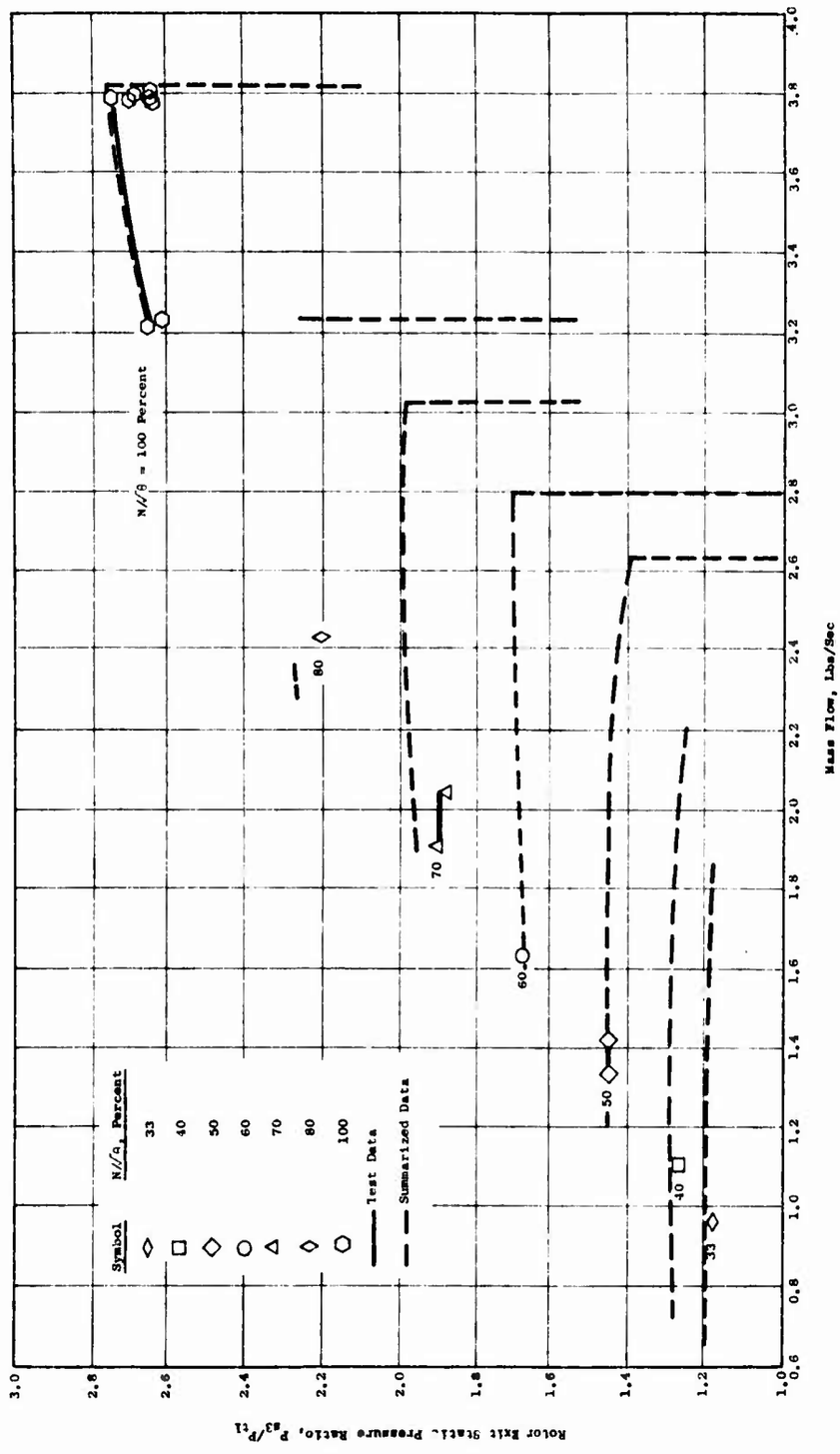

Figure 78. Static Pressure Ratio Versus Mass Flow With Supersonic Stators Set at 84.4 Degrees and Subsonic Stators Set at 76.3 Degrees.

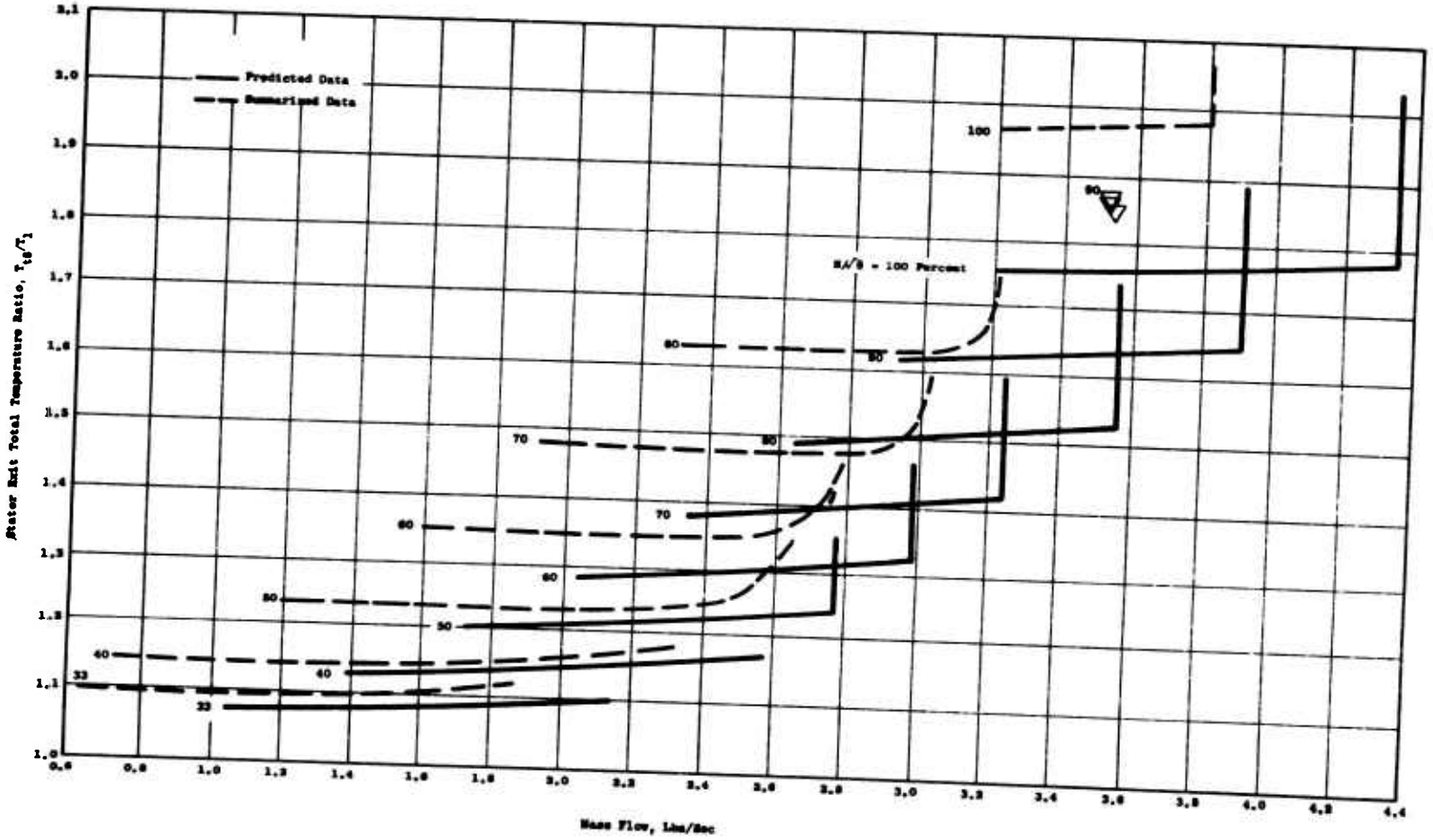

Figure 79. Predicted Total Temperature Ratio Versus Mass Flow.

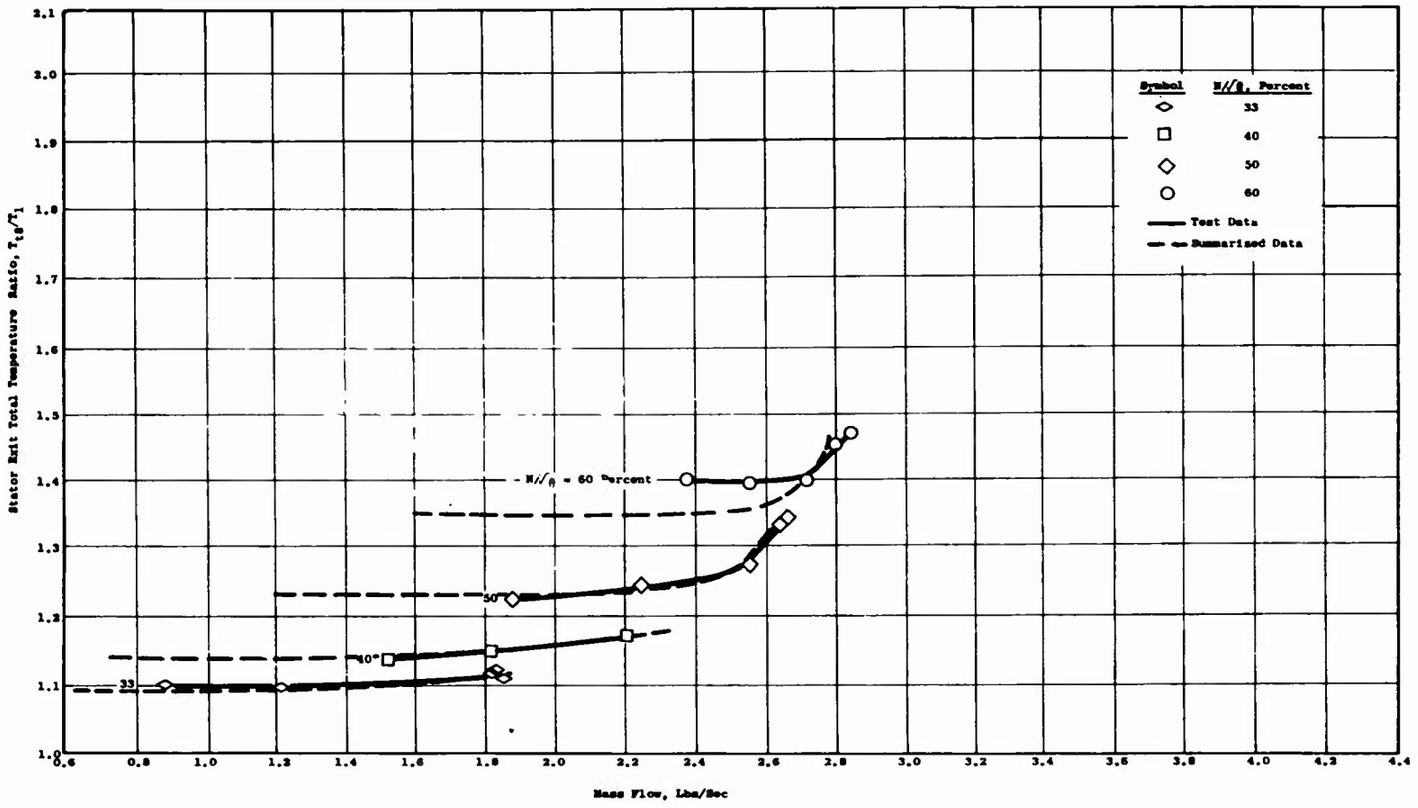

Figure 80. Total Temperature Ratio Versus Mass Flow With Supersonic Stators Set at 76 Degrees and Subsonic Stators Set at 67 Degrees.

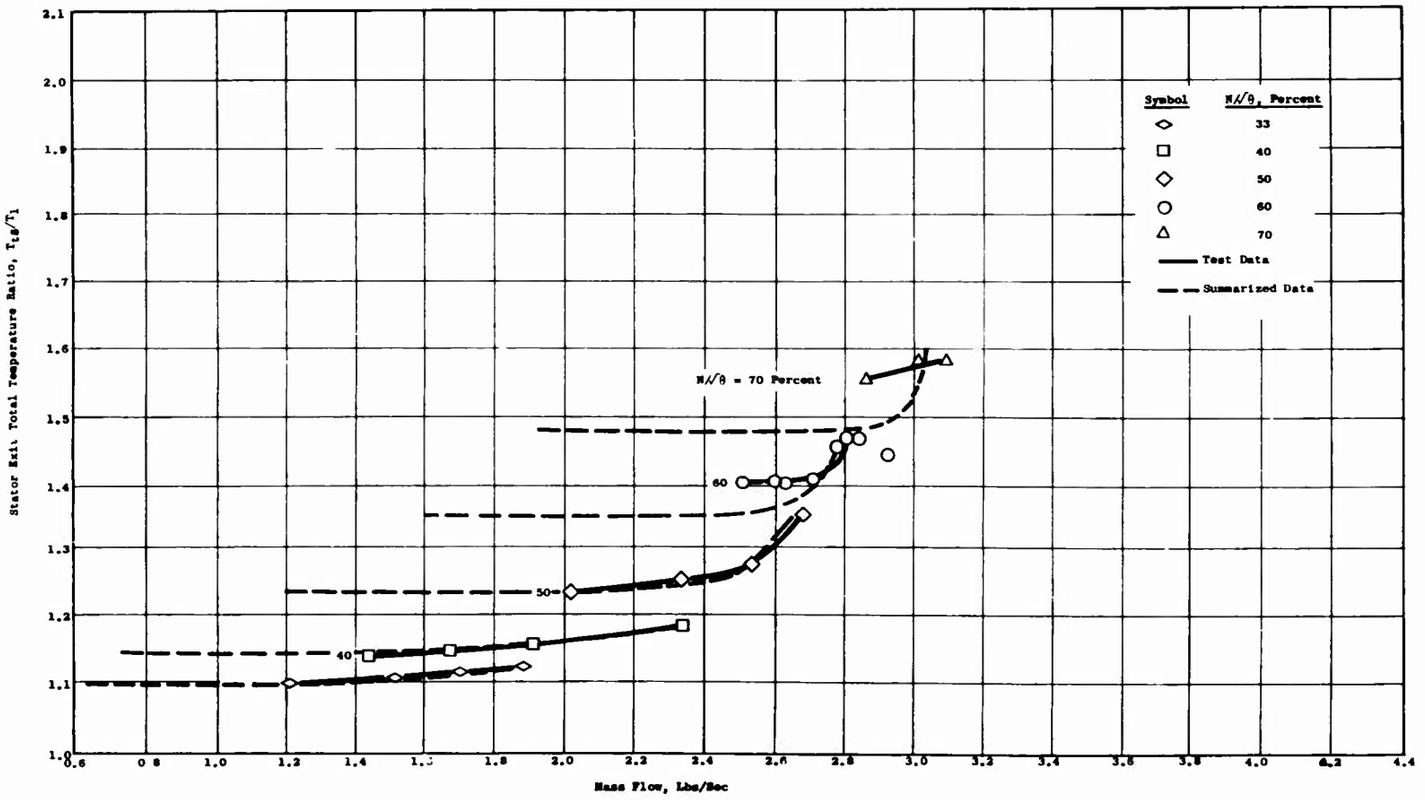

Figure 81. Total Temperature Ratio Versus Mass Flow With Supersonic Stators Set at 76 Degrees and Subsonic Stators Set at 70 Degrees.

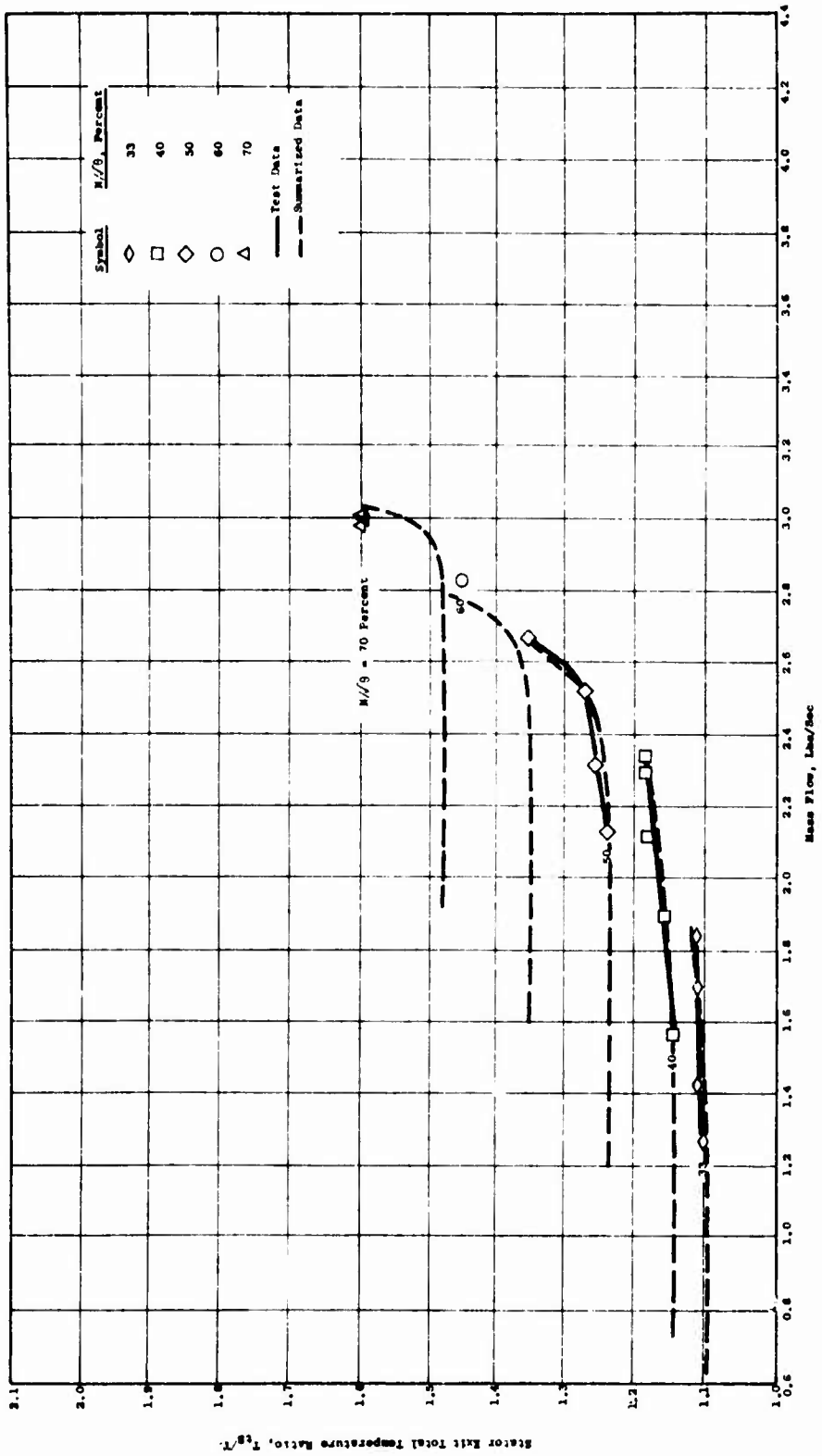

Figure 82. Total Temperature Ratio Versus Mass Flow With Supersonic Stators Set at 76 Degrees and Subsonic Stators Set at 73 Degrees.

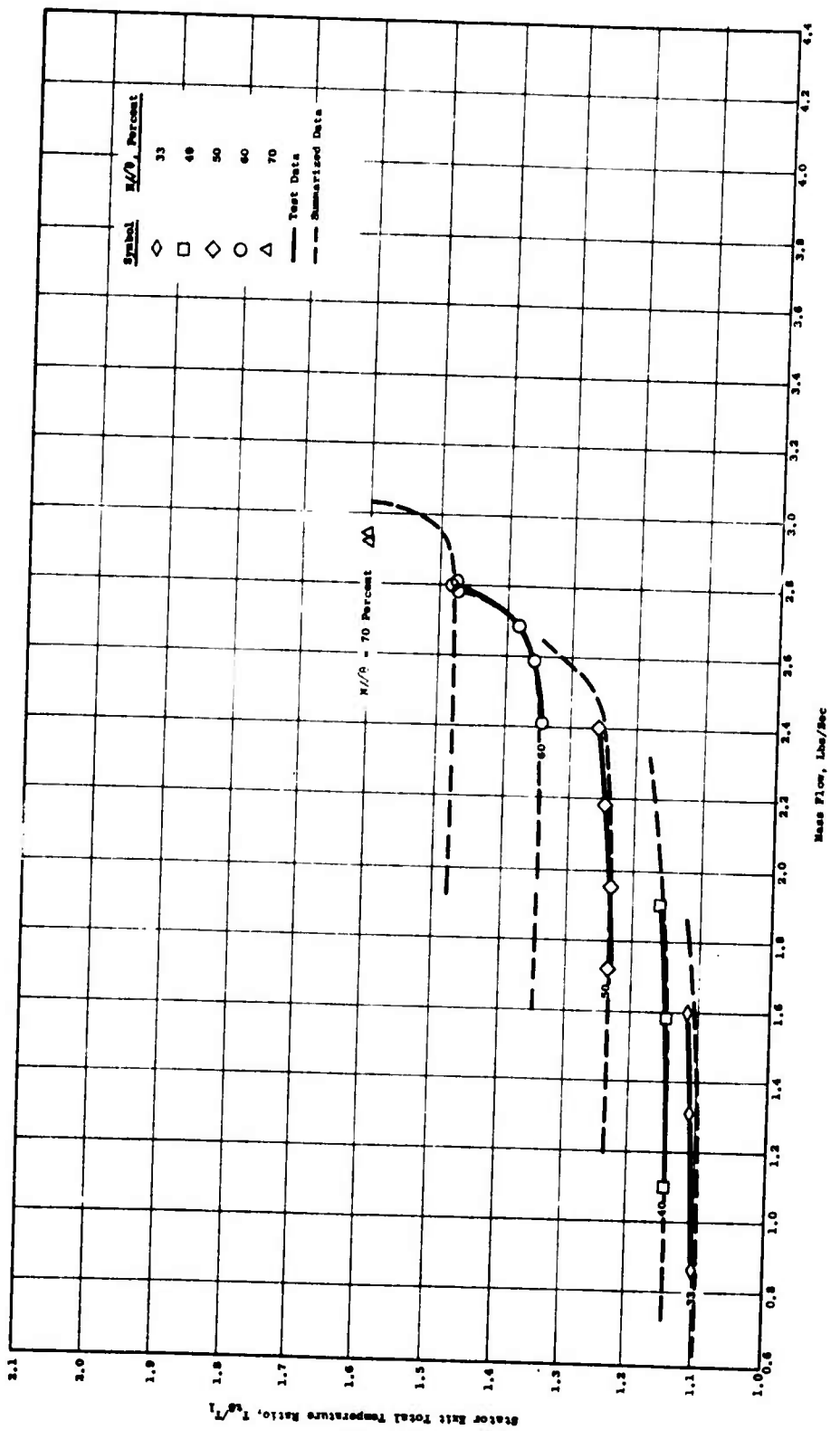

Figure 83. Total Temperature Ratio Versus Mass Flow With Supersonic Stators Set at 79 Degrees and Subsonic Stators Set at 70 Degrees.

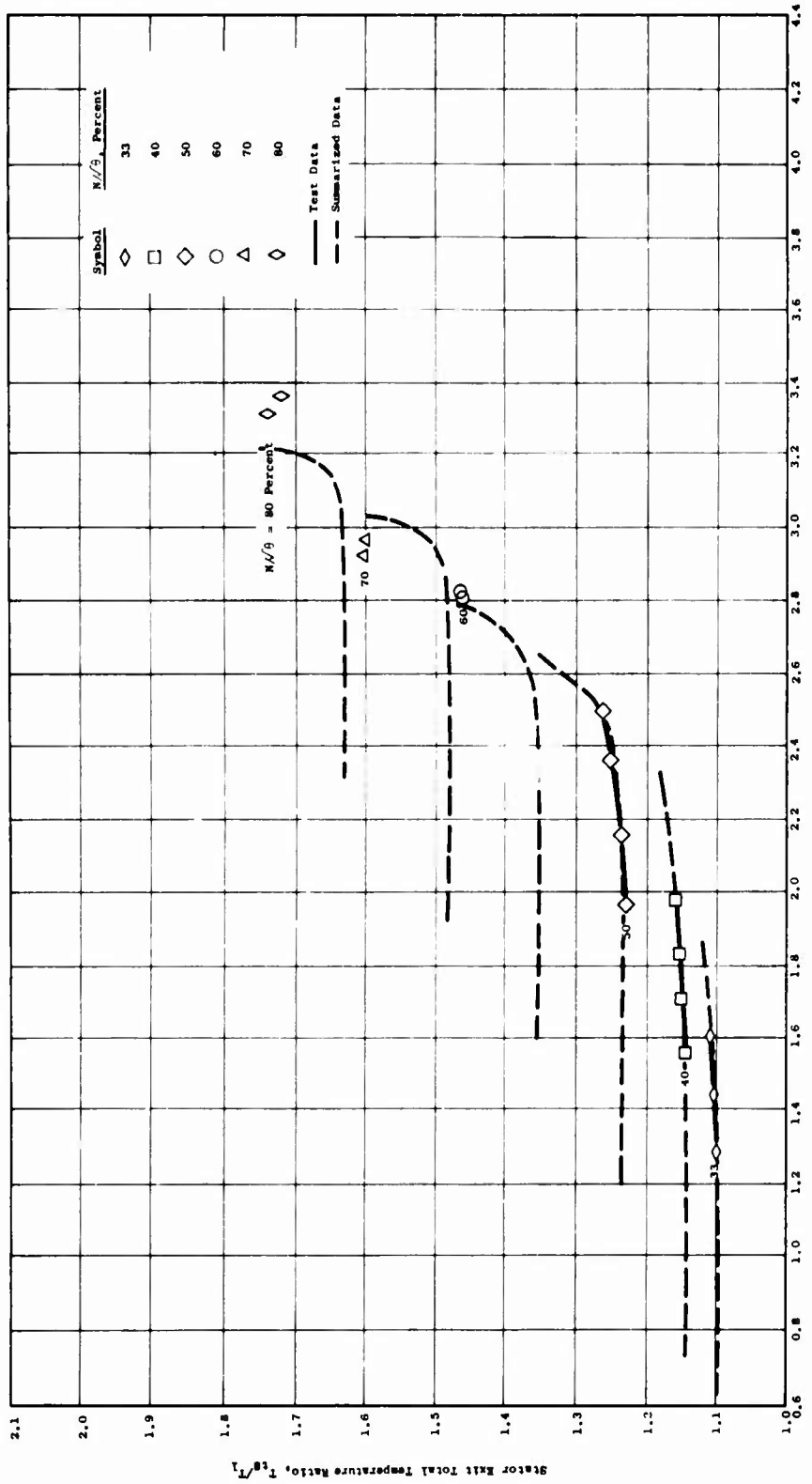

Figure 84. Total Temperature Ratio Versus Mass Flow With Supersonic Stators Set at 79 Degrees and Subsonic Stators Set at 73 Degrees.

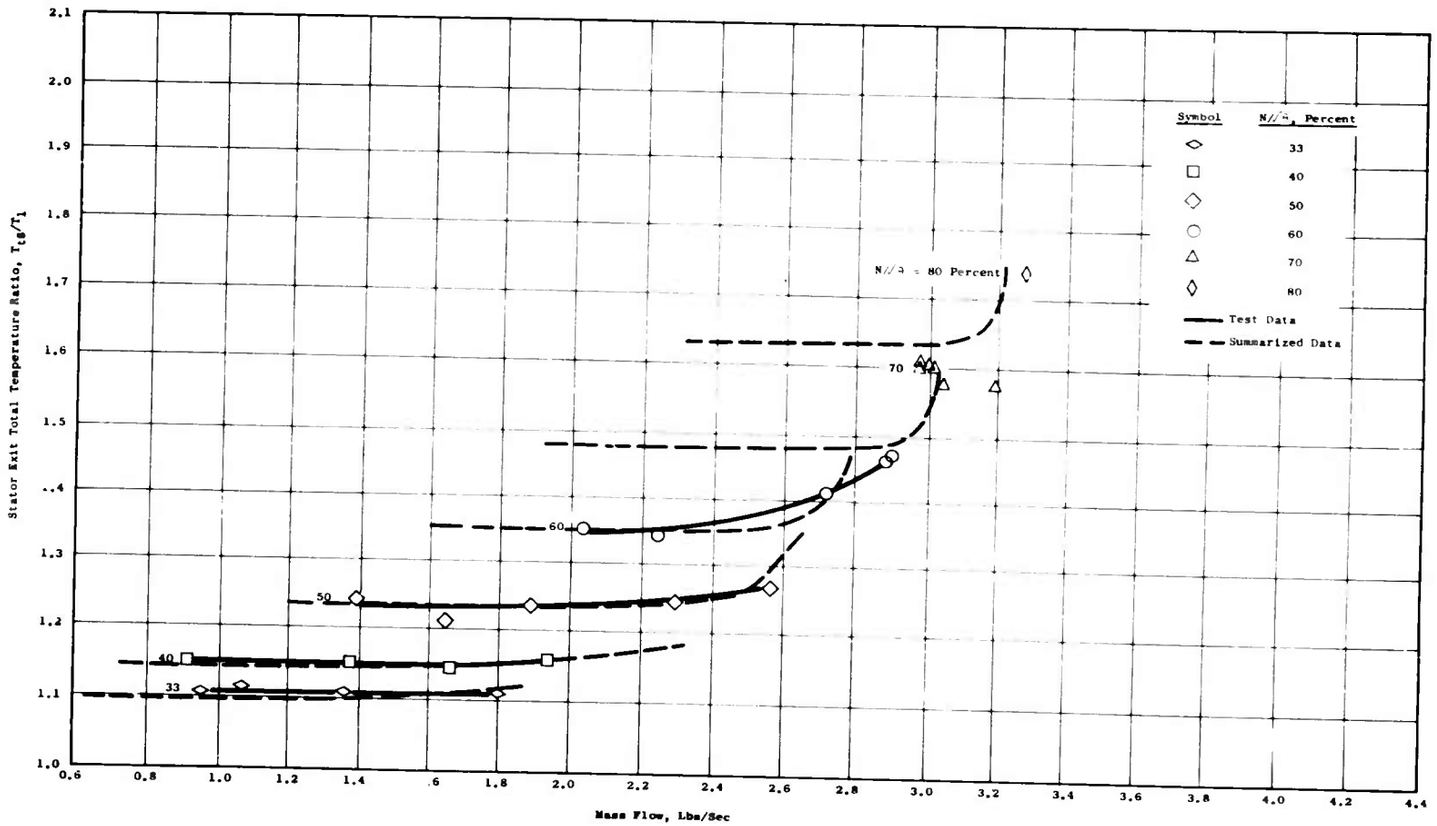

Figure 85. Total Temperature Ratio Versus Mass Flow With Supersonic Stators Set at 79 Degrees and Subsonic Stators Set at 76 Degrees.

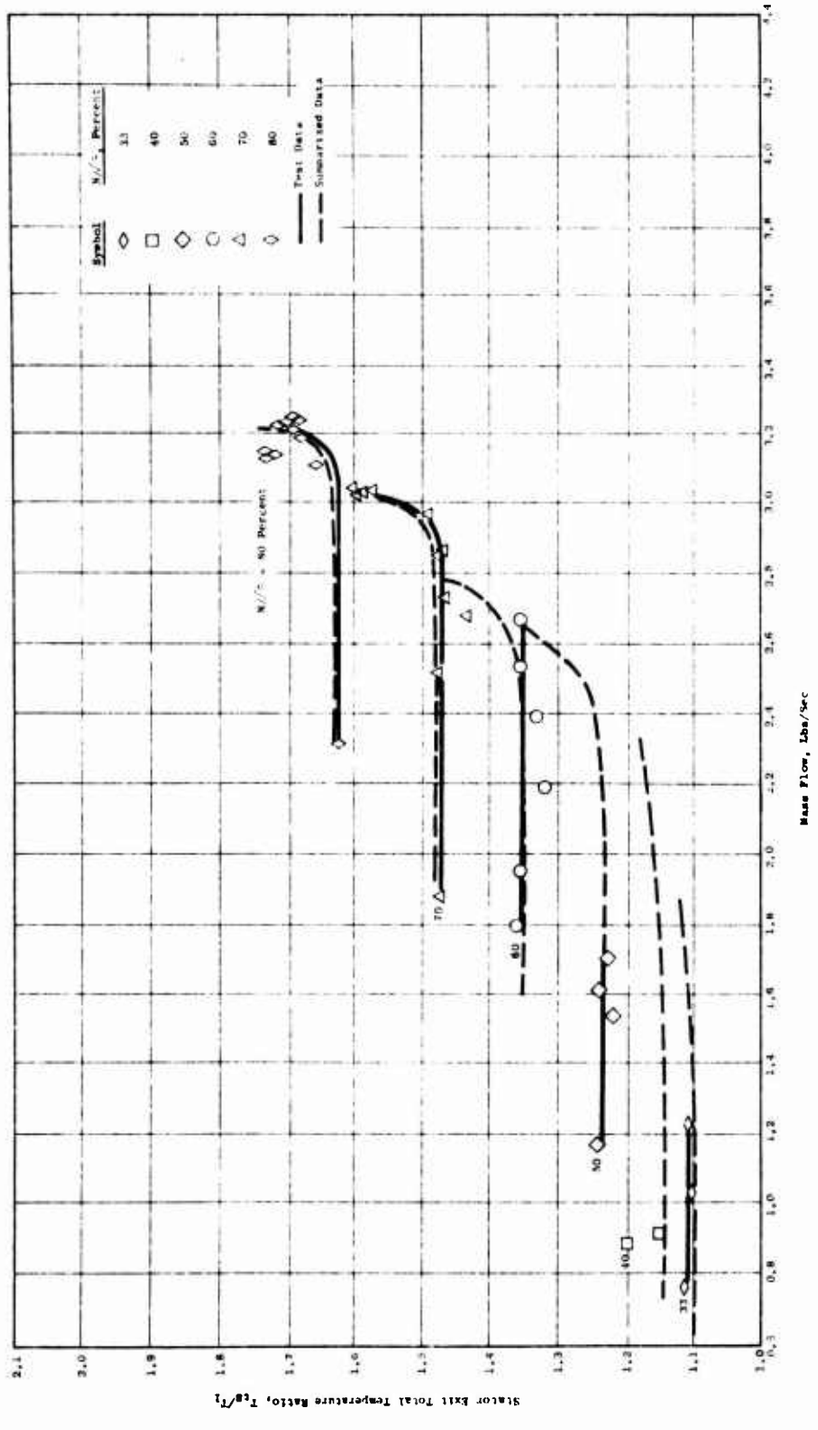

Figure 86. Total Temperature Ratio Versus Mass Flow With Supersonic Stators Set at 82 Degrees and Subsonic Stators Set at 73 Degrees.

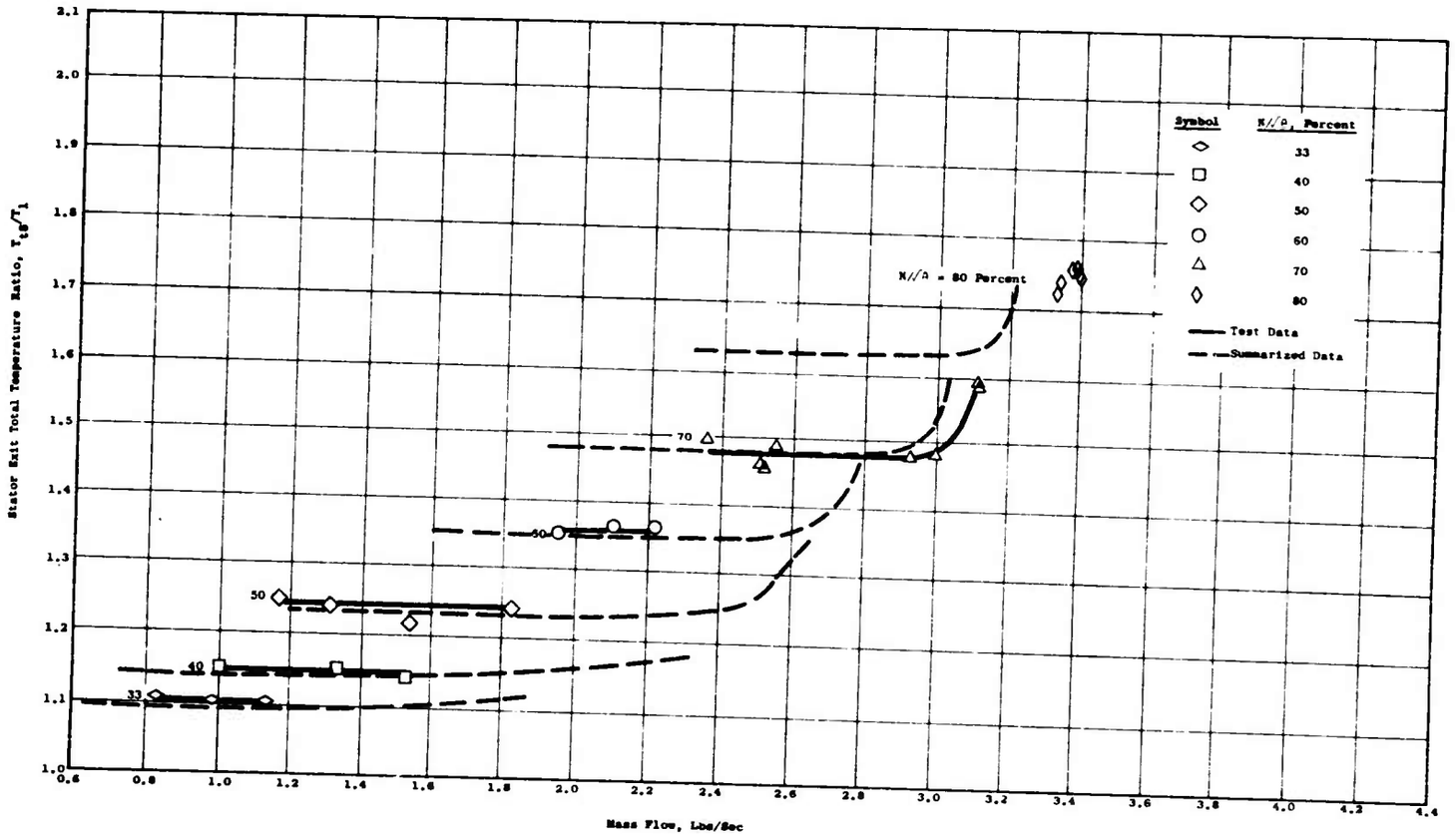

Figure 87. Total Temperature Ratio Versus Mass Flow With Supersonic Stators Set at 82 Degrees and Subsonic Stators Set at 76 Degrees.

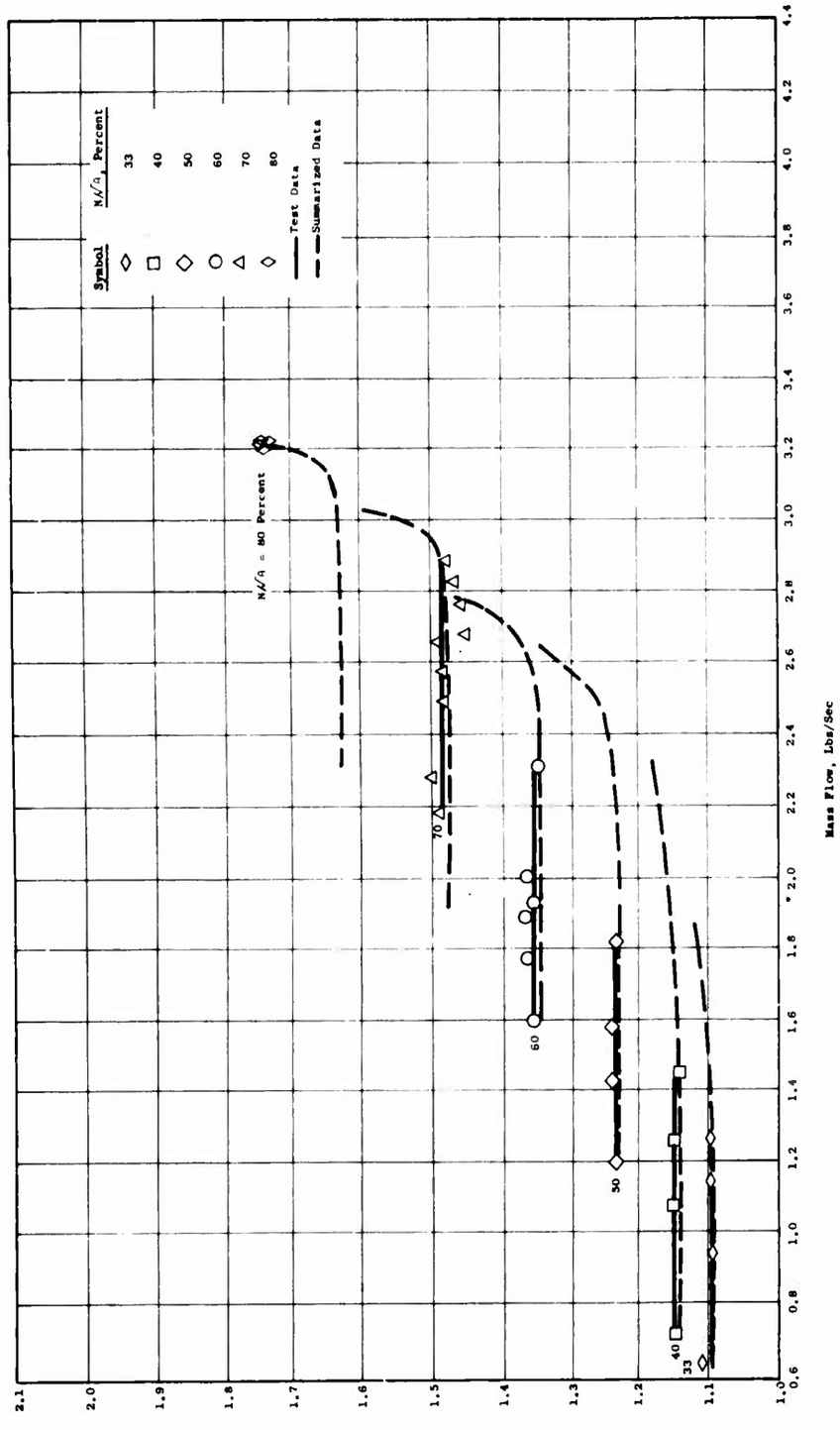

Figure 88. Total Temperature Ratio Versus Mass Flow With Supersonic Stators Set at 82 Degrees and Subsonic Stators Set at 79 Degrees.

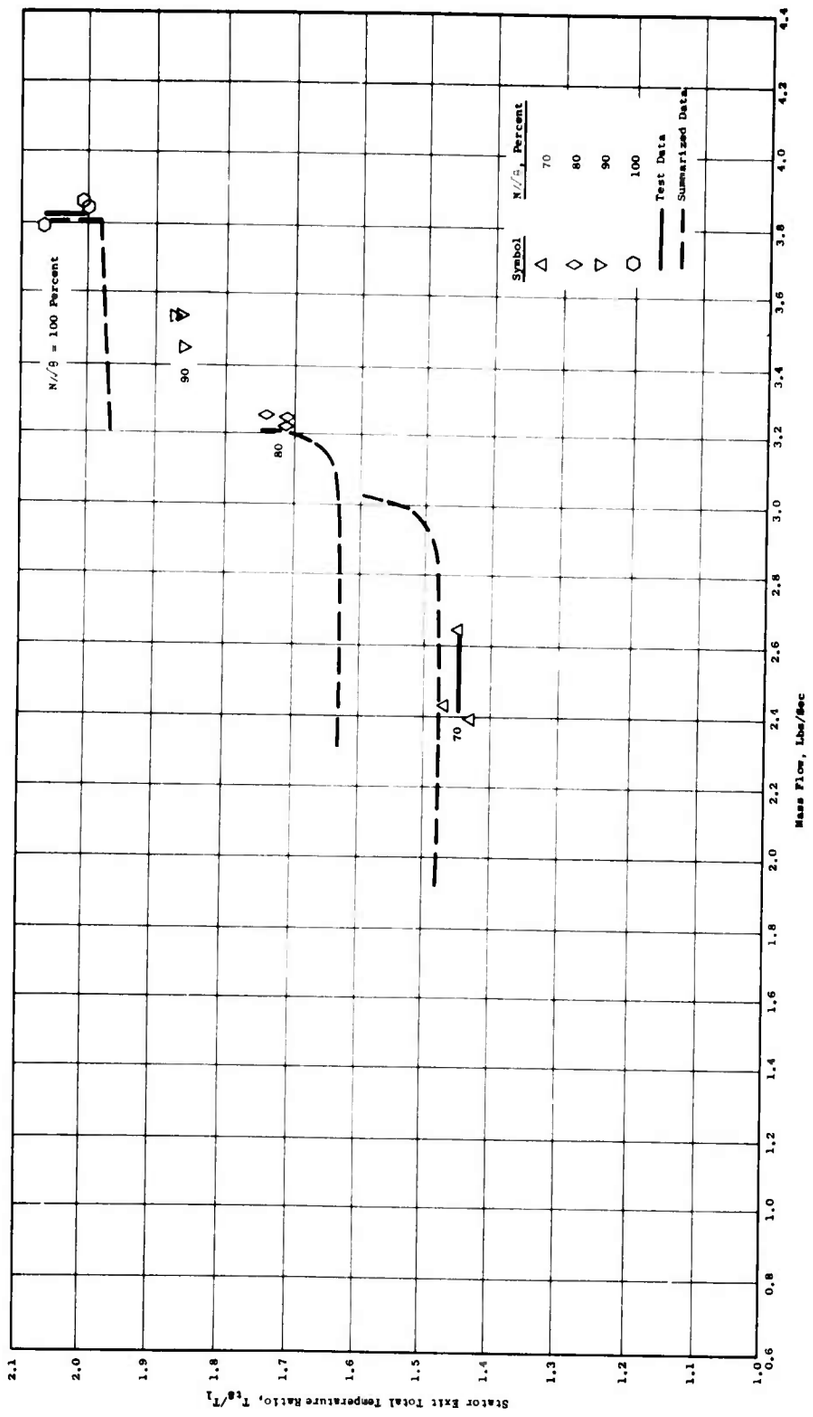

Figure 89. Total Temperature Ratio Versus Mass Flow With Supersonic Stators Set at 83.4 Degrees and Subsonic Stators Set at 76.3 Degrees.

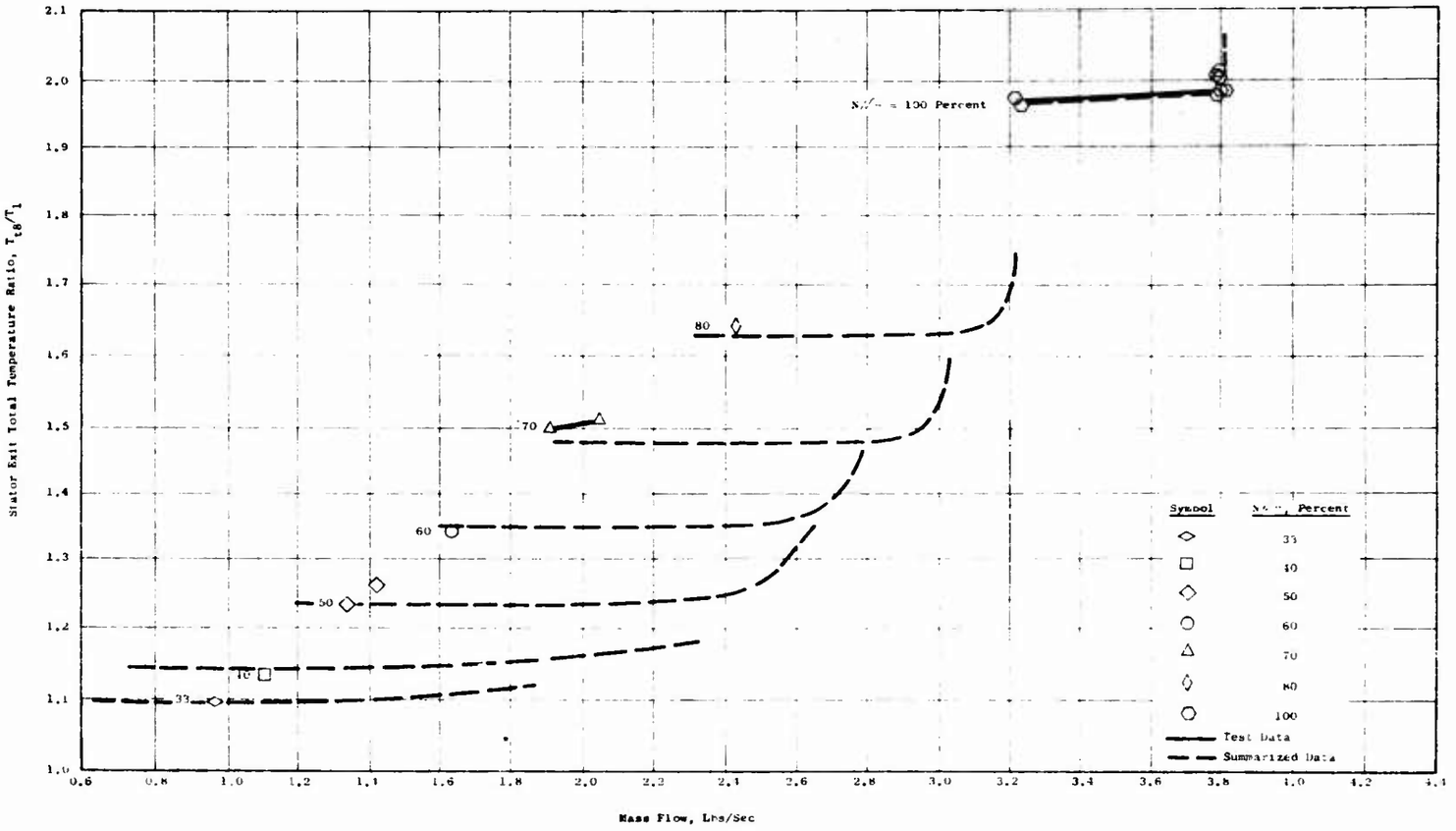

Figure 90. Total Temperature Ratio Versus Mass Flow With Supersonic Stators Set at 84.4 Degrees and Subsonic Stators Set at 76.3 Degrees.

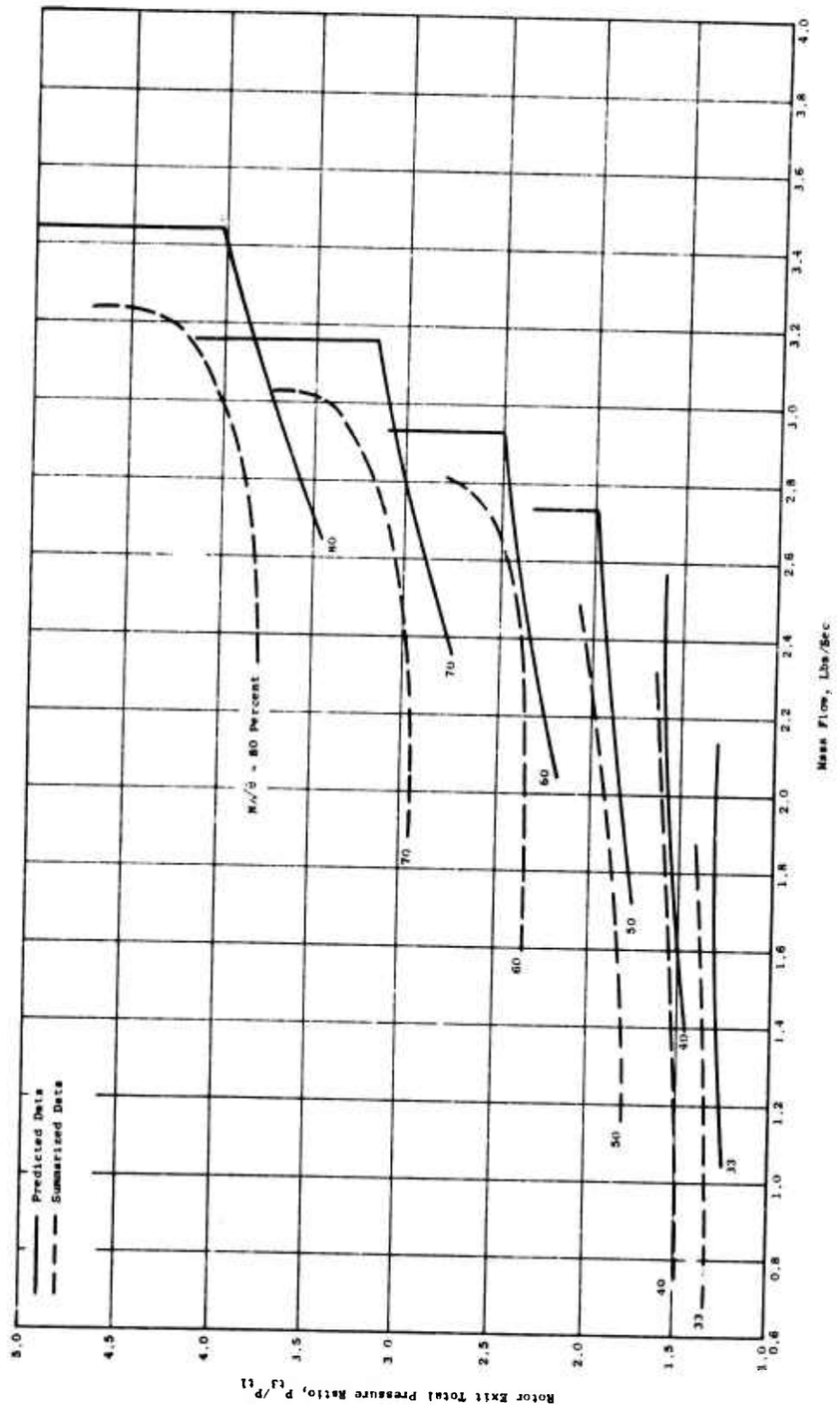

Figure 91. Total Pressure Ratio Versus Mass Flow for Predicted and Summarized Data.

89 percent range were observed (Figure 62) with subsonic stators at 70 degrees. The rotor total pressure ratio agreed well with the summary values at speeds in the 33 to 60 percent range (Figure 51), but the rotor efficiencies (Figure 62) were lower than values obtained with more closed supersonic stators. Very similar trends were observed with the subsonic stators closed to 73 and 76 degrees (Figures 52 and 53). Rotor efficiencies in the 87 to 90 percent range were measured at 40 and 50 percent speeds, but at 60 percent and higher speeds, rotor efficiencies of less than 80 percent were obtained (Figures 63 and 64). From these results, the powerful effect of supersonic stator setting on rotor performance can be seen clearly.

Supersonic Stators Set at 82 Degrees

Subsonic Stators Set at 73 Degrees

When supersonic stators were closed to 82 degrees, efficient performance of the rotor was obtained in the intermediate range of 60 and 70 percent speed. With the subsonic vanes set at 73 degrees, the rotor total pressure ratios (Figure 54) agreed well with the summary values over the full speed range tested from 33 to 80 percent. A test vehicle condition that contributed to the operating problems was the requirement to maintain an axial load on the main bearings. The projected area of the rotating shroud was less than that of the disc. When the rotor was producing a high static pressure rise, a significant axial load (as much as 800 pounds) was calculated to occur in the upstream direction. This load exceeded the rated axial force which the bearings could sustain for prolonged periods. To counteract this aerodynamic loading, the downstream bearing was preloaded by a spring washer to provide about 100 pounds force in the downstream direction. At high speeds, when the compressor was throttled from low to intermediate back pressures, a condition of zero net axial load on the bearings occurred. The angular contact bearings used are not positively positioned without axial load, and rotor vibrations are excited. Because of test vehicle vibrations, the most efficient rotor conditions were not established at 80 percent speed. The maximum efficiency obtained (Figure 65) was about 77 percent at 80 percent speed. The trend of the summarized efficiency contours suggests that values much closer to 85 percent should be obtainable at this speed. An attempt was made to establish 90 percent speed operation, but a comparessor tripout occurred before any data were taken.

Subsonic Stators Set at 76 Degrees

With the supersonic stators set at 82 degrees and the subsonic stators set at 76 degrees, the compressor airflow was so limited throughout the 33 to 60 percent speed range (Figure 55) that the rotor operated with rotating stall. In spite of that, rotor efficiencies in the range of 87 percent were obtained at 40 and 50

percent speeds (Figure 66). The total pressure ratios measured were in agreement with or slightly higher than the summary characteristic data for speeds up to 60 percent.

At 70 percent speed, rotating stall was observed at airflows less than about 2.6 lbs/sec. For airflows above 2.9 lbs/sec, rotating stall was not observed, but the rotor efficiencies were not appreciably higher than when rotating stall occurred. Unfortunately, test data were not taken with airflows in the intermediate range. Therefore, the peak efficiencies which should have occurred at airflows of about 2.8 lbs/sec were not obtained. Mechanical vibrations limited the range for which the compressor could be operated at 80 percent speed and prevented operation at 90 percent speed. Airflows higher than the summary values were measured at 70 and 80 percent speeds, suggesting that the supersonic stators may have opened to a value different from the 82 degrees which was set at the beginning of the test. As can be seen in Figure 55, the airflows observed were in good agreement with the predicted data.

Subsonic Stators Set at 79 Degrees

With the stator vane combination of 82/79 degrees, rotating stall apparently did not occur at airflows of 0.94 lbs/sec or higher at 33 percent speed judging from the high frequency response transducer records. That significant hysteresis occurs in this rotor is evident from the fact that rotating stall has been observed at airflows as high as 1.2 lbs/sec at this speed. In spite of the considerable closure of both sets of stator vanes, efficiencies in the 87 to 90 percent range were obtained at 33 and 40 percent speeds (Figure 67).

At 50 and 60 percent speeds, the maximum airflow obtainable was not sufficiently large to prevent the occurrence of rotating stall. It is probably for this reason that the maximum efficiencies observed at these speeds lie in the 83 to 85 percent range. When the compressor was throttled to airflows below 2.66 lbs/sec at 70 percent speed, rotating stall was encountered. The occurrence of rotating stall apparently coincides with an increase in rotor discharge total temperature and total pressure (Figure 56) and a decrease in rotor efficiency (Figure 67). Such behavior is not unreasonable for a rotor with forward turning blades operating with subsonic discharge flow. At 80 percent speed, compressor vibrations again prevented throttling the compressor to permit operation in the high static pressure ratio and high efficiency range.

Supersonic Stators Set at 84.4 Degrees and 83.4 Degrees

From the results of the systematic series of stator vane settings, it was evident that even with the supersonic vanes closed to 82 degrees, these vanes were still too open for best performance at speeds above 70 percent.

It might be noted here that at the end of the systematic runs described above, the supersonic stators were found to be set at 82.4 degrees. This change in the supersonic stator angle was probably caused by a combination of mechanical stackup and differential thermal growth effects in the supersonic stator system. Even though this did occur, it is felt that this was not a critical matter because the stator settings were only used as references and it was not required that an absolute angle setting be held.

Consequently it was decided to close the supersonic stators 2 degrees to 84.4 degrees. The subsonic stators, however, were left unchanged at 76.3 degrees.

Rather surprisingly, with the supersonic vanes closed to 84.4 degrees the compressor did not exhibit rotating stall at either 33 or 40 percent speed, and acceptable rotor efficiencies in the 85 to 88 percent range were observed at these speeds (Figure 57). As the compressor was accelerated above 40 percent speed, rotating stall commenced in the rotor and continued to exist as test points were taken up to 80 percent speed. Low efficiencies were observed, but the total pressure ratios measured (Figure 57) were about the same as the values shown on the summary curve. Rotating stall persisted at 90 percent speed, and there was some doubt that steady flow would be achieved at 100 percent speed. Fortunately, at about 96 percent speed, the rotating stall vanished and smooth operation of the compressor from both the aerodynamic and mechanical standpoints was achieved at 100 percent speed. Although the compressor could be operated at high speed for only a few minutes because of rapid rise in the high-speed bearing temperature, several test points at 100 percent speed were obtained by rapid acceleration from 50 percent speed or less. A maximum pressure ratio of 7.35 with a peak rotor efficiency of about 78 percent was obtained (Figure 58). Considering the various mechanical limitations which existed, this operating procedure was necessary to make high-speed testing possible and produced sufficient information to confirm that the rotor would run smoothly at full speed.

Because rotating stall was not eliminated from the rotor until 96 percent speed was achieved with the 84.4-degree supersonic vane setting, it was felt that a 1-degree opening of the supersonic stator might permit good performance to be obtained at 80 and 90 percent speeds as well as at 100 percent speed. The subsonic stator setting was not changed. During acceleration, rotating stall was eliminated from the rotor at about 83 percent speed, although later it was found possible to decelerate to 80 percent speed without inciting rotating stall. Only

a few test points were taken in the 70 to 100 percent speed range (Figures 57 and 58) with the 83.4/76.3 vane configuration before the main high-speed bearing failed. Although throttling of the compressor to highest static pressure ratios and hence, highest rotor efficiencies, was not accomplished in this speed range, smooth aerodynamic and mechanical operation of the compressor was established and improved efficiencies at 70 and 80 percent speeds were obtained.

EFFECT OF STATOR SETTINGS ON ROTOR STATIC PRESSURE AND EFFICIENCY CHARACTERISTICS

Supersonic Stators Set at 76 Degrees

From the large number of data points which were accumulated during Phase III testing, a summary plot of rotor static pressure versus airflow was prepared. This summary plot is used as a basis of comparison to illustrate the effects of stator setting on rotor performance. For the most open supersonic stator setting, 76 degrees, and for a 67-degree subsonic stator setting, the rotor performance at 33 and 40 percent speeds shows a static pressure-airflow characteristic (Figure 68) which is essentially identical to the summary curves. The efficiencies are generally about 2 points lower than the best values obtained during Phase III tests. At 50 percent speed, the static pressure-airflow characteristic is identical with the summary curve, but again the efficiencies are low (Figure 59). At 60 percent speed, however, the static pressure ratio produced is significantly less than the summary curve at airflows in the range of 2.3 to 2.7 lbs/sec. The reason for the low static pressure is evident from the high frequency response (static pressure) transducer records. At 33 percent speed for airflows greater than 1.2 lbs/sec, the transducer record is very smooth, showing only rotor blade wake fluctuations (Figure 96). At airflows less than 0.9 lbs/sec, a rotating stall was observed (Figure 96). Only minor static pressure fluctuations were observed at 40 and 50 percent speeds although rotating stalls were seen at the lowest flows. At 60 percent speed and with an airflow of 2.828 lbs/sec (Figure 96), only high frequency pressure variations were observed. When attempts were made to increase the rotor back pressure by closing the throttle, relatively low frequency pressure oscillations were observed (Figure 96). The pressure fluctuations occurred at a rate of about 1 per 10 rotor revolutions and are thought to be the result of stator vane stalling. When rotating stall in the rotor occurs, the rate of pressure fluctuations appears to be about 1 per 2 rotor revolutions. Further throttling of the compressor produced even more violent pressure fluctuations with amplitudes of about 1 atmosphere. When the airflow was throttled below 2.6 lbs/sec, the pressure fluctuations were observed at the inlet to the rotor as well as at all downstream transducer locations.

From these comparisons, it appears obvious that a supersonic stator setting angle of 76 degrees is too open for satisfactory performance of this rotor even at low speeds.

Tne results of tests with supersonic stators set at 76 degrees and subsonic stators set at 70 degrees (Figure 69) show very similar trends to the results with subsonic vanes at 67 degrees. Although reasonably satisfactory performance was observed at 33 and 40 percent speeds, the maximum efficiencies observed were lower by several points than the summary map for the same speeds and airflows (Figure 60). At 60 and 70 percent speeds, the static pressure ratios observed were significantly less, and the reason was again believed to be stator vane stalling.

When the subsonic vanes were closed to 73 degrees, and the supersonic vane angle was still held at 76 degrees, a measurable increase in rotor efficiency occurred at 33 and 40 percent speeds (Figure 61) although the overall static pressure-airflow performance (Figure 70) was unchanged. From these results with the supersonic stators set at 76 degrees, it is clear that the supersonic vanes are more open than desirable, particularly for operation of speeds of 50 percent and above. Changing the subsonic stators from 67 to 73 degrees resulted in an improvement in rotor efficiency at low speed. The supersonic stators are obviously predominant with regard to influencing rotor performance, and changes to the subsonic stators produced observable but only minor effects.

Supersonic Stators Set at 79 Degrees

Closing the supersonic stators from 76 degrees to 79 degrees permits the attainment of more efficient rotor performance in the range of speeds from 33 to 60 percent. Maximum efficiencies in the range of 88 to 89 percent were obtained in the 40 to 50 percent speed range. In contrast to the inability of the rotor to produce the nominal 60 percent speed static pressure ratio shown on the summary map at a supersonic stator setting of 76 degrees, a close approach to the summary value of static pressure ratio was achieved at a 79-degree setting (Figure 71). In the airflow range of 2.4 to 2.7 lbs/sec, the efficiency at 60 percent speed increased by 10 to 14 points. The transducer signals obtained with airflows in the range from 2.4 to 2.7 lbs/sec showed only rotor wake signatures with a magnitude of about 1 psi.

At 70 percent speed, the supersonic stators were too open to permit efficient flow. The transducer traces at 2.94 lbs of airflow per second show pressure fluctuations of 5 to 6 psi at a rate of slightly less than 1 per rotor revolution. Since the summary map choke airflow is about 3.03 lbs/sec, it is clear that a 79-degree supersonic stator angle is not satisfactory for rotor speeds above 60 percent.

When the subsonic stators were closed from 70 to 73 degrees, the general behavior of the compressor changed very little. Peak efficiencies in the 88 to 90 percent range were observed at speeds of 40 and 50 percent, and the operating characteristics (Figure 72) agreed with the summary data at lower speeds. Judging from the results obtained at the 79/70 and 79/76 degree stator settings (Figures 71 and 73), it should have been possible to obtain steady-state operating conditions in the airflow range from 2.0 to 2.7 lbs/sec at 60 percent speed. Attempts were made to establish airflows within this range with the 76/73 configuration, but compressor vibrations caused the automatic safety system to trip out. This operating problem was present for many of the test points. This compressor exhibits significant hysteresis when stall or surge is encountered through changes in throttle setting, rotational speed, or stator vane angle. Therefore, several methods of approaching a particular operating point exist. When an operating region is approached for the first time and no information exists concerning the stability of operation, the required time to try all approaches is not necessarily used in all instances. For the open throttle settings at 70 and 80 percent speeds, static pressure fluctuations of 8 to 10 psi appeared at a rate faster than 1 per revolution. As the compressor was throttled at these speeds, the large pressure fluctuations disappeared, but throttling to the efficient high back pressure range could not be obtained without vibrations which tripped out the system.

During the course of a particular run, small changes in stator vane angle occurred occasionally. This may account for the higher airflow observed at 80 percent speed with stators set nominally at 79/73 degrees. The changes were less than 0.5 degree, but even this amount is significant at nominal values near 80 degrees from radial.

Supersonic Stators Set at 82 Degrees

A rather surprising result observed with the supersonic stators set at 82 degrees was the high efficiencies obtained at low and intermediate speeds (Figures 66 and 67). This was particularly true at the combination 82/79 degrees, since peak efficiencies in the range from 87 to 89 percent were obtained at 33 and 40 percent speeds. At the 82/73-degree settings, the low-speed peak efficiencies were closer to 80 percent. At the latter setting, reasonably good efficiencies in the range of 85 to 87 percent were obtained at 60 and 70 percent speeds. A surprisingly broad range of operation (Figure 74) was also obtained at 60 and 70 percent speeds with the vane angle combination 82/73 degrees. Stable operating performance in the high static pressure ratio range could not be achieved at speeds higher than 70 percent. This result led to the use of more closed vane settings in the runs subsequent to the systematic series of the Phase III test.

Improved performance in the low-speed range was obtained with the subsonic stators closed to 76 degrees, suggesting that the 6-degree difference which occurs at this near-nominal condition of supersonic and subsonic stator setting (on the basis of the transonic cascade tunnel results) was not far from optimum. At 60 percent speed, Figures 66 and 75 illustrate that the full range of airflows was not established. This was also true at 50 percent speed and to a lesser extent at 70 percent speed for the nominal 82/76-degree combination.

At 33 percent speed, the transducer records indicate that rotating stall existed for all airflows tested. This includes the highest airflow which could be obtained with the throttle wide open. In spite of the unsteady flow, rotor efficiencies in the 83 percent range were obtained. At 40 percent speed, rotating stall occurred at airflows less than 1.4 lbs/sec, and again rather remarkable efficiencies in the 83 to 86 percent range were observed (Figure 66). At an airflow of 1.521 lbs/sec, the rotating stall was not present and a rotor efficiency of 87.7 percent was obtained at 40 percent speed. At 50 percent speed, all of the test points exhibited rotating stall. Nevertheless, rotor efficiencies in the range from 85 to 87 percent were obtained. This was also true at 60 percent speed for the airflow values which were set during the test series, but the peak efficiencies observed were in the 82 percent range. At 70 percent speed, operating points with and without rotating stall were obtained but little difference in maximum efficiency, about 82 percent, or static pressure ratio (Figure 75) was measured. Airflows higher than the summary value were obtained with open throttle at 70 and at 80 percent speeds, suggesting that slight opening of the supersonic stators may have occurred during the run.

With the stator vanes set at the 82/79-degree configuration, very efficient rotor performance, about 90 percent, was obtained at 33 percent speed (Figure 67). The rotating stall did not occur at an airflow of 0.94 lbs/sec, which was significantly lower than the airflow for which rotating stall occurred for many other stator vane settings at this speed. This is further evidence that appreciable hysteresis occurs in this compressor when entering or leaving regions of stalled operation. At 40 percent speed, rotating stall occurred at airflows less than 1.4 lbs/sec, but only a small drop in rotor efficiency from the peak value of 87.7 percent or in static pressure ratio (Figure 76) occurred when rotating stall was present. Although the compressor was operated with open throttle at both 50 and 60 percent speeds, it was not possible to obtain airflows sufficiently large to avoid rotating stall. In spite of the presence of rotating stall, efficiencies of 85.6 and 83.3 percent respectively were obtained at these rotational speeds. At 70 percent speed, smooth operation without rotating stall was obtained and efficiencies in the 85 percent range were obtained. High static pressure ratio and therefore efficient operation could not be obtained at 80 percent speeds because of mechanical limitations.

Summary of Systematic Stator Settings

In spite of quite satisfactory results during the Phase II testing at low and intermediate speeds with the stator vanes set relatively far open, evidence from this systematic series of runs is that the 76-degree supersonic setting is too open for best performance even at low speed. At 50 percent speed and above, this supersonic stator setting imposes a serious restriction on the rotor, and only poor performance was observed. Varying the subsonic stator setting while holding the supersonic vanes at 76 degrees had little or no effect on rotor performance.

Closing the supersonic stators to 79 degrees improved the performance at low and intermediate speeds, with maximum efficiencies in the 88 to 90 percent range being obtained at the 33 to 50 percent speeds. Again the influence of the subsonic stator angle was small with respect to rotor performance. Closing the supersonic stators to 82 degrees restricted the airflow at low and intermediate speeds such that rotating stall was generally present in the rotor. Surprisingly, the highest efficiencies at 33 percent speed were obtained with the 82/79-degree vane combination. Rotor efficiencies in the 85 percent range were obtained at 50 and 70 percent speeds. Once again no clear distinction as to the best subsonic stator vane setting could be drawn on the basis of the experimental data obtained.

Difficulties were encountered from both the mechanical and to a lesser extent from the aerodynamic operation of the test compressor in setting test points of high back pressure which seem to be directly related to efficient operation at high speeds. This situation seemed to be improved as the stators were closed. For this reason, it was decided to investigate the compressor performance with supersonic stators closed to 84.4 degrees while maintaining the nominal subsonic stator angle of about 76 degrees.

Supersonic Stators Set at 84.4 Degrees

From the evidence obtained during the systematic series of stator variations described in the preceding paragraphs, it was expected that rotating stall would exist in the compressor throughout the low and intermediate speed ranges. It was somewhat surprising then that very smooth flow with efficiencies in the 85 to 88 percent range were obtained at 33 and 40 percent speeds (Figure 78) at airflows significantly lower than those for which rotating stall had been previously observed. On accelerating to 50 percent speed, however, rotating stall was encountered and, in fact, persisted as the compressor was accelerated to 96 percent speed. Several test points were taken as the compressor was accelerated and, although rotating stall occurred, efficiencies in the 76 to 86 percent range were obtained. Smooth aerodynamic and mechanical operation of the compressor was observed at 100 percent speed. Efficiencies in the range of 76 to 78 percent with static pressure ratios ranging from 2.64 to 2.76 were measured. When the compressor was throttled at 100 percent speed from the maximum airflow observed of about 3.82 to 3.22 lbs/sec,

rotating stall was observed, but the operation was sufficiently steady to permit data to be taken. Rotor efficiencies of about 73.7 percent were obtained.

Supersonic Stators Set at 83.4 Degrees

Because the compressor remained in rotating stall over most of the speed range with the supersonic stators set at 84.4 degrees, it was believed that improved performance in the 70 to 90 percent speed range could be obtained if the stators were opened 1 degree. With the supersonic stators set at 83.4 degrees, a rapid acceleration to 90 percent speed was accomplished. Rotating stall persisted from about 50 percent to about 85 percent speed. Several test points were taken at 90 percent speed (Figure 77) under conditions of smooth aerodynamic and mechanical operation. Comparing these results with the summary data, it appears that sufficient throttling was not accomplished to achieve maximum static pressure ratio or efficiency. This rotational speed has been difficult to establish, and many tripouts have occurred at 90 percent for reasons which are not entirely clear. It is suspected that a compressor shaft critical speed was responsible for this high sensitivity at 90 percent speed. Rapid overheating of the main high-speed bearing occurred during these runs, and frequent "cool-down" periods of running at low speed were required between high-speed test points.

Two points were taken at 70 percent speed, 1 at an airflow of 2.394 lbs/sec with a rotor efficiency of 82.8 percent and the next at an airflow of 2.43 lbs/sec and with a rotor efficiency of 81.9 percent. Several attempts were made to obtain high static pressure ratio performance at 80 and 100 percent speeds, but compressor vibrations and bearing overtemperature seriously limited these attempts. On the final run being conducted at 100 percent speed, a very rapid bearing temperature indication was observed followed by a tripout. During the deceleration, high vibrations were observed on all meters. Bearing damage was suspected and later confirmed. The test point with slightly higher airflow and lower rotor efficiency exhibited rotating stall with static pressure fluctuations of 7 to 8 psia. Both of these points were taken at lower airflows than the value of about 2.7 lbs/sec at which rotating stall occurred during earlier runs. This behavior again illustrates the significant hysteresis which occurs with this compressor. The operating procedure used in approaching a particular test point markedly affects the manner in which the compressor will operate if the desired point is near the rotating stall range. Now that this range has been defined, it should be possible to establish operating points of improved performance with much greater certainty.

SUMMARIZED ROTOR PERFORMANCE

Summary curves of rotor total pressure ratio versus airflow characteristic have been prepared by using data taken from the systematic series of stator vane settings and from the 2 final runs with supersonic vanes set at 83.4 and 84.4 degrees. When compared with the predicted total

pressure ratio characteristics, it is seen that for all speeds the total pressure ratio produced with subsonic flow leaving the rotor blades is higher than the predicted value (Figure 91). This is true even though the total pressure values used were taken from a 3-tube rake located at the leading edge of the supersonic stators. Since 2 of the tubes in each rake were very close to the passage walls, the arithmetic average so obtained is probably lower than a mass-flow-averaged value would be. The explanation for the occurrence of higher total pressure ratios than predicted is that the subsonic Mach number leaving the rotor blades was higher than the predicted value. This result can easily occur if greater blockage exists at the exit of the rotor blades than exists in the two-dimensional transonic cascade tunnel tests of these blade sections. This hypothesis is supported by the fact that the total pressure ratio observed with supersonic flow leaving the rotor blades is less than predicted. This result would also be expected if the blockage were greater than predicted at the rotor blade exit. A similar conclusion is obtained when the summarized total temperature ratio obtained from the systematic series and the 2 additional test runs with supersonic vanes closed to 83.4 and 84.4 degrees is compared with predicted values (Figure 79) for the case of subsonic flow leaving the rotor blades. This hypothesis is not supported for the case of supersonic flow leaving the rotor blades (Figures 80 through 90) because the total temperature ratio is essentially the same as the predicted value. These apparently conflicting observations can be brought into a consistent picture if it is assumed that excessive blockage occurs only when a high static pressure rise is enforced on the rotor and high subsonic exit Mach numbers occur. If reduced blockage occurs when low exit pressures are impressed on the rotor, predicted supersonic rotor blade exit Mach numbers occur. In order to satisfy both total temperature and total pressure observations, it can be assumed that high losses occur in the rotating diffuser when supersonic relative flow enters the rotating diffuser.

The Mach number leaving the rotor blades tends to be higher than predicted for the subsonic regime. This suggests separation and higher losses in the rotor blades, although the rotor efficiency tends to be highest when the rotor back pressure is the highest. The rotor efficiencies are low when the rotor exit pressure is low and supersonic exit flow from the rotor blades exists. These observations strongly suggest that the optimum design for a Radial Outflow Compressor rotor might incorporate the use of sonic exit Mach number from the rotor blades and that significantly improved rotor performance might be achieved through application of this design philosophy.

EFFECT OF STATOR VANE ANGLE ON STATOR PERFORMANCE

General

The results obtained from the tests of a systematic series of supersonic and subsonic stator vane angle settings are presented in Figures 92 through 95. Comparative results obtained from supersonic cascade tests

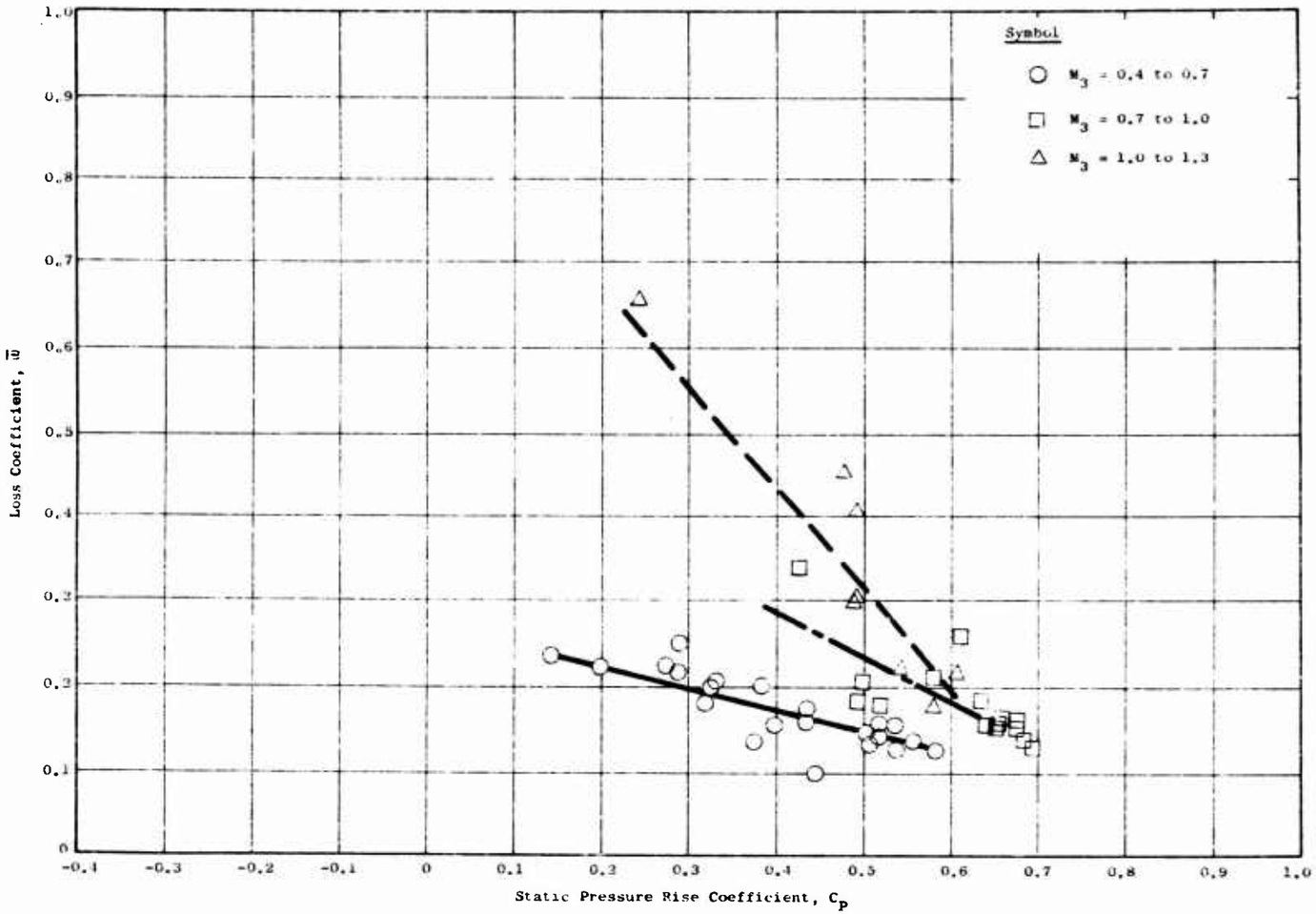

Figure 92. Stator System Loss Coefficient Versus Static Pressure Rise Coefficient for Supersonic Stator Vane Setting of 76 Degrees.

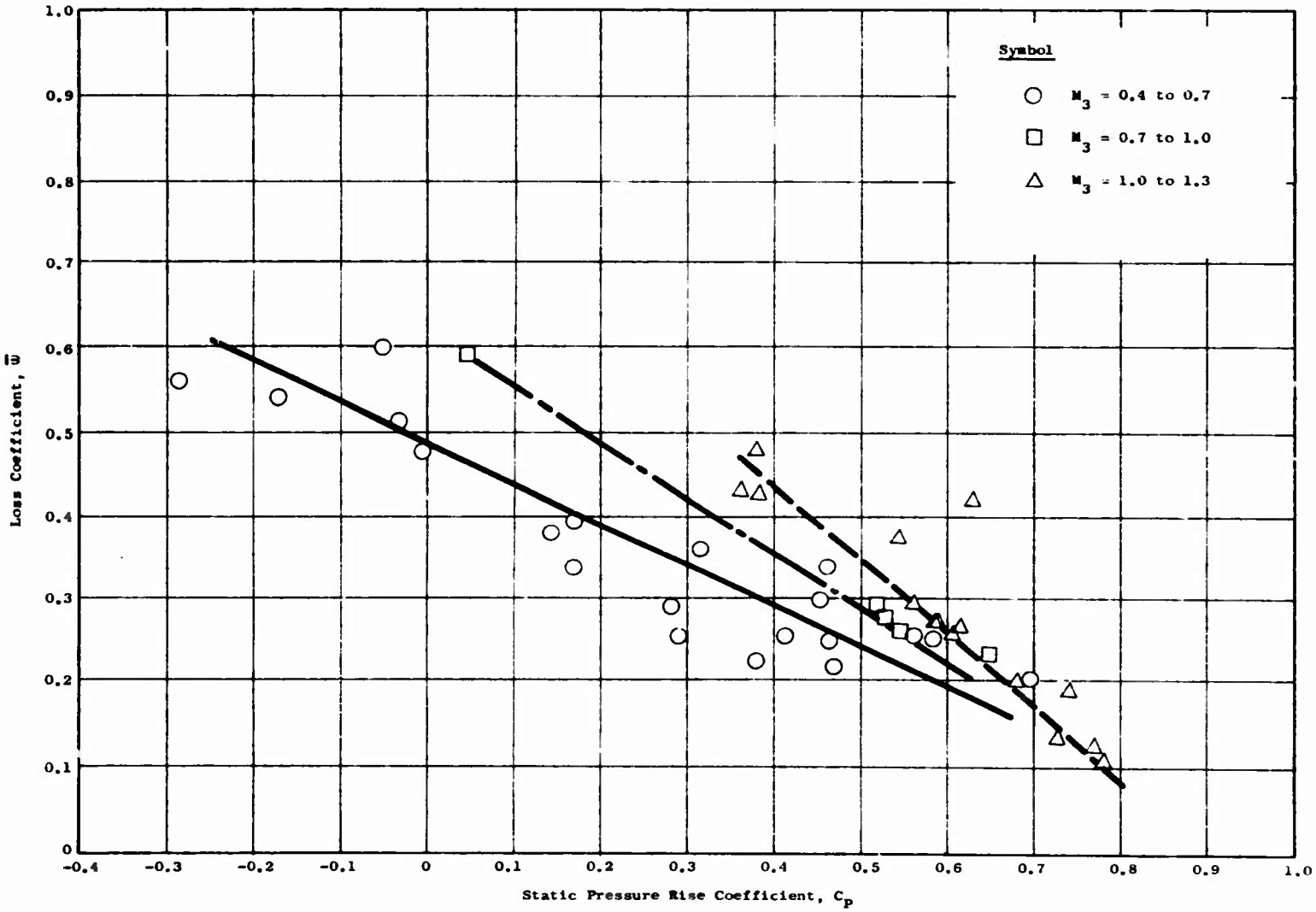

Figure 93. Stator System Loss Coefficient Versus Static Pressure Rise Coefficient for Supersonic Stator Vane Setting of 79 Degrees.

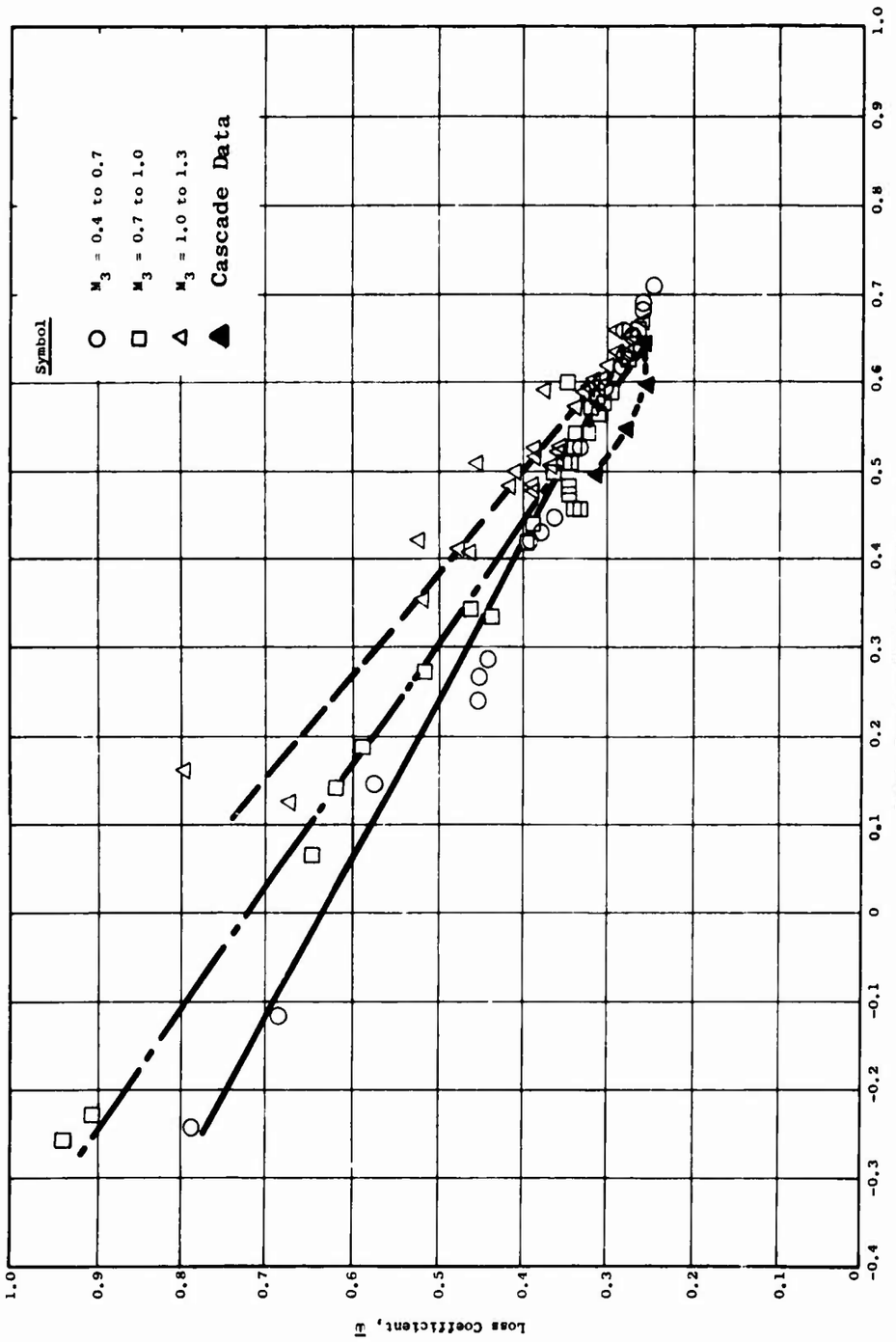

Figure 94. Stator System Loss Coefficient Versus Static Pressure Rise Coefficient for Supersonic Stator Vane Setting of 82 Degrees.

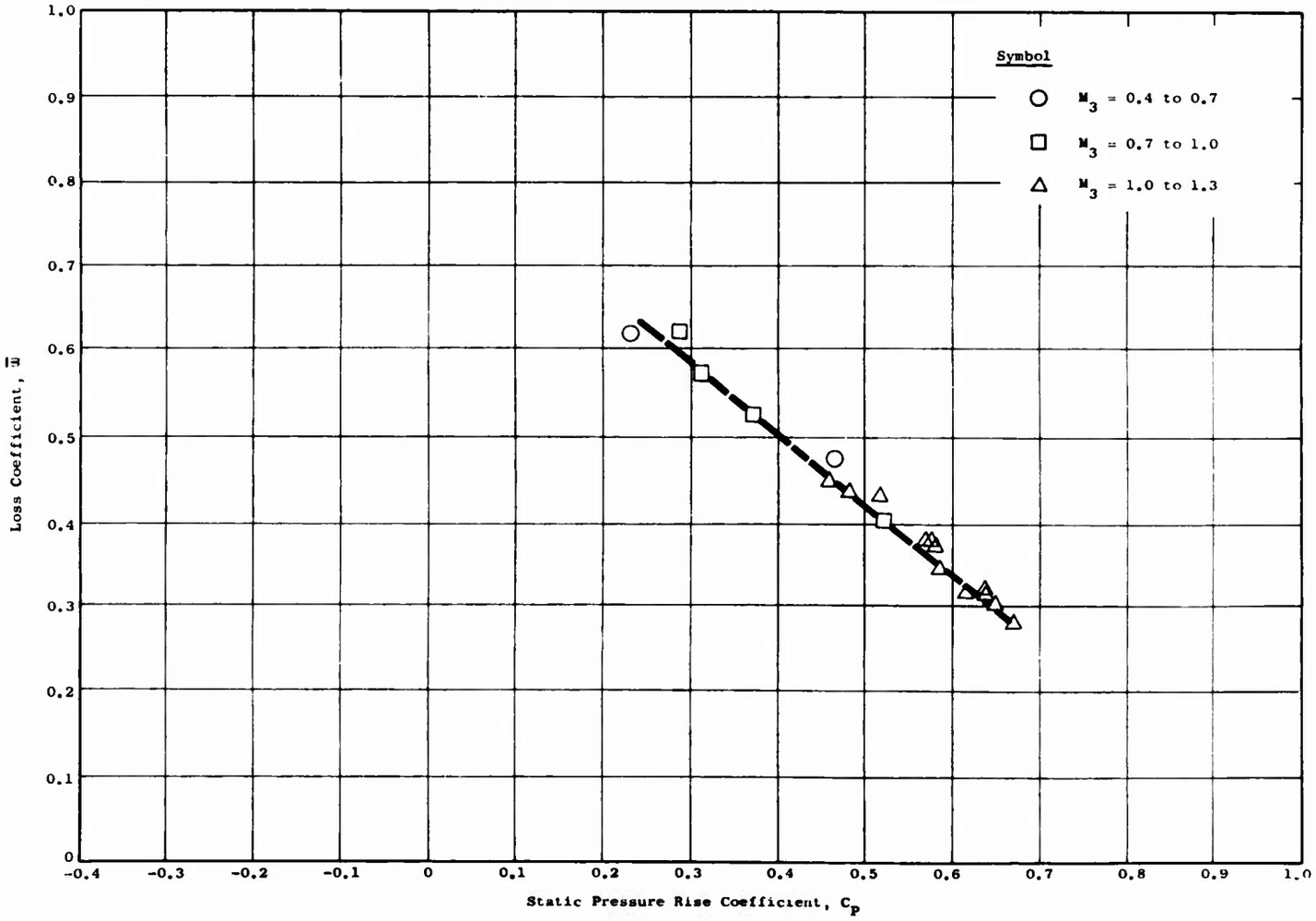

Figure 95. Stator System Loss Coefficient Versus Static Pressure Rise Coefficient for Supersonic Stator Vane Settings of 83.4 and 84.4 Degrees.

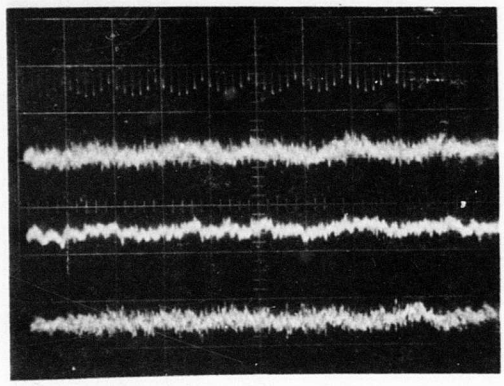

33 Percent Speed
Test Point - 33P3 Reading 290
Airflow 1.204
0.5 psi for Vertical Division
10 Rotor Revolutions are Shown

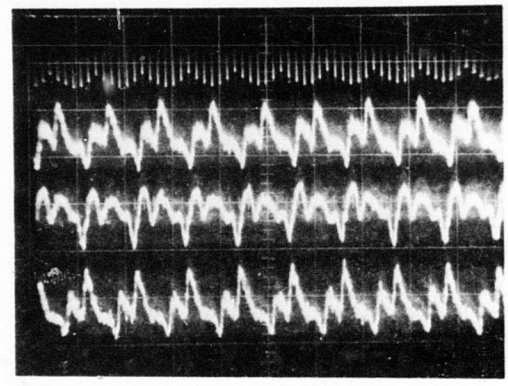

33 Percent Speed
Test Point - 33P4 Reading 291
Airflow 0.873
1.0 psi per Vertical Division
10 Rotor Revolutions are Shown

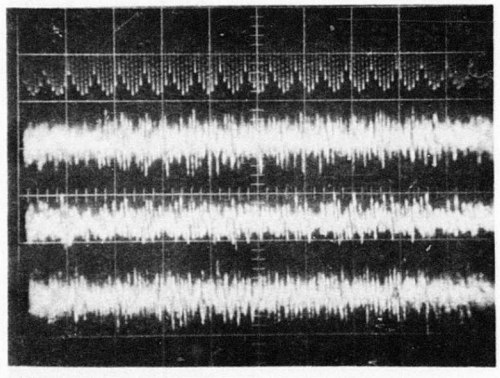

60 Percent Speed
Test Point - 60P3 Reading 304
Airflow 2.710
5.0 psi for Vertical Division
19 Rotor Revolutions are Shown

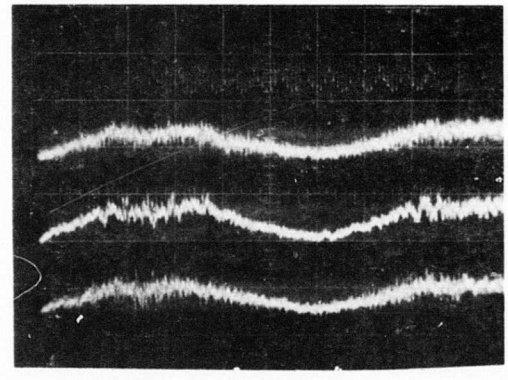

60 Percent Speed
Test Point - 60P1 Reading 302
Airflow 2.838
5.0 psi for Vertical Division
19 Rotor Revolutions are Shown

Figure 96. Oscilloscope Traces Obtained From High Frequency Response Static Pressure Crystals With Timing Trace Shown on Top.

at a Mach number of 1.3 are presented on Figure 94 because the supersonic vane setting of 86 degrees with a subsonic vane setting of 76 degrees represents the closest approach to the nominal conditions selected from supersonic cascade tests. The cascade test points were presented in Figure 161 of Volume I (Reference 2).

The test data used in calculating loss coefficients and static pressure rise coefficients presented in Figures 92 through 95 use an average of the 2 centerline total pressure readings taken at the leading edge of the supersonic stators. Total pressure at the subsonic stator exit was obtained by an arithmetic average of the readings from the total pressure rake located on the passage centerline. The supersonic stator inlet total pressure was taken from the centerline readings because when an arithmetic average of all 6 stator leading edge readings was used, excessively high values of static pressure coefficient and excessively low values of loss coefficient were obtained. Corrections for the total pressure loss due to normal shocks were made for $M_3 > 1$. This use of the data available is believed to provide the best comparison with the supersonic cascade data presented in Figure 94.

Working plots were made of loss coefficient and static pressure rise coefficient as a function of Mach number, but only a very poor correlation was evident. Similarly, the working plots of Figures 92 through 95 identified the subsonic stator vane angle settings, but no effect of subsonic vane angle on the loss coefficient versus static pressure rise coefficient correlation was evident.

Supersonic Stators Set at 76 Degrees

As noted in the section discussing the effect of stator vane setting on rotor performance, a supersonic stator angle of 76 degrees was too open to permit efficient rotor performance at intermediate and high speeds. The low values of loss coefficient, in the range from 0.13 for Mach numbers in the range from 0.4 to 0.7, and in a range of 0.14 for Mach numbers of 0.7 to 1.0, is very encouraging, particularly since static pressure rise coefficients in the range from 0.55 to 0.68 were obtained (Figure 92). Even for supersonic flow entering the stators, loss coefficients of about 0.20 were obtained with static pressure rise coefficient of about 0.60. These values indicate that this tandem stator system can operate efficiently in the required range of Mach number and static pressure rise coefficient. Since the rotor did not perform efficiently at higher speed with this stator configuration, the possibility of a mismatch between the rotor and the exit system of the compressor is suggested.

Supersonic Stators Set at 79 Degrees

A consistent trend of the effect of Mach number on stator performance is evident in the data taken with the stators set at 79 degrees (Figure 93). Somewhat higher loss coefficients are observed at low and intermediate

Mach numbers, but very satisfactory stator performance was obtained at supersonic speeds when the compressor was throttled to produce high static pressure rise coefficients. The values of loss coefficient observed, in the range of 0.125, are very encouraging since they are lower than the objective values set for the tandem blade row and less than the values observed in the supersonic cascade tests.

Supersonic Stators Set at 82 Degrees

A consistent although minor effect of Mach number was observed with the supersonic stators set at 82 degrees (Figure 94). The predominant effect on loss coefficient is the throttling of the compressor which appears as the value of the static pressure rise coefficient. Relatively good comparison is obtained between the stator performance observed in the compressor and that from the supersonic cascade tests presented on this figure. Although satisfactory rotor performance at low and intermediate speeds was obtained using this stator configuration, stator performance deteriorated significantly from more open settings; therefore, the overall compressor performance deteriorated.

Supersonic Stators Set at 83.4 and 84.4 Degrees

Due to the conclusion of the experimental program because of high-speed bearing failure, only a relatively small amount of data was obtained with the 83.4- and 84.4-degree supersonic stator settings (Figure 95). No effect of Mach number is apparent in these results. Most of the results were obtained with supersonic flow entering the stators, so the line code for supersonic Mach numbers was used in plotting this figure. Although good rotor performance was obtained at high speeds, stator loss coefficients observed were quite high, showing a minimum value of about 0.28. These results support the hypothesis that a mismatch of the ROC rotor and the stator system existed during these runs.

EFFECT OF STATOR VANES ON COMPRESSOR STAGE PERFORMANCE

The stage performance of the Radial Outflow Compressor is determined by the combined performance of the rotor, the stator system, the scroll collector, and the discharge diffuser. As was mentioned previously, the supersonic stator vanes exert a strong influence on the rotor performance. This influence is due to the limitations the supersonic stator imposes on the rotor mass flow, as well as the effect these vanes have on the stability of the flow in the rotor. In general, if the supersonic stators are set at a large angle the flow in the rotor is limited to values below design at low speed. As a consequence, rotor efficiency falls off and the rotor has a tendency to exhibit rotating stall. If the stators are set at too low an angle, the compressor flow tends to be unstable. This may be due to stator stall and its interaction with the rotor. Too low a stator angle at the higher speeds appears to cause a drastic reduction of rotor performance. The subsonic stators in general appear to exhibit a smaller effect on rotor performance. This

behavior is reasonable since, to a large extent, the rotor is isolated from the subsonic stators by the supersonic stators. In addition to affecting the performance of the rotor, the stator vane settings exert a strong influence on the performance of the stator system itself. Relative to the stator performance, it seems reasonable to anticipate that the supersonic stators have a strong influence on performance, and that the subsonic stators exert either a weak or a strong influence, depending on conditions at the supersonic stator discharge. The combined effect of supersonic and subsonic stator setting on stage performance is shown in Figures 97 through 102.

On the basis of analytical calculations of the discharge flow angle from the rotor it was felt that the following schedule of supersonic stator angle versus speed should result in acceptable stage performance.

Percent Speed	Supersonic Stator Angle
30	73.5
40	75.5
50	77.5
60	79.5
70	81.5
80	83.5
90	84.5
100	85.5

Examination of the efficiency curves in Figures 97 through 99 indicates that the best supersonic stator setting versus speed is as follows:

Percent Speed	Supersonic Stator Angle
33 - 50	76
60	79
70	82
100	84.5

The maximum stage efficiency varied from 80 percent at 40 percent speed to 70 percent at 100 percent speed. The maximum stage pressure ratio achieved was 6.23 at 100 percent speed (70 percent efficiency). On the basis of the relatively close agreement between the predicted optimum schedule and the measured optimum schedule, it is an open question as to whether improved performance can be obtained at 33 percent speed by a more open stator angle, or at 100 percent speed by a more closed stator angle.

The stage pressure ratio for the various supersonic stator angles tested is shown in Figures 100 through 102. The 100 percent speed points are not included in these figures. Comparison of the total pressure plots results in the same optimum stator schedule as was obtained by comparison of the efficiency plots. In general, the effect of the subsonic stator setting is shown more clearly in the efficiency plots than in the total pressure plots.

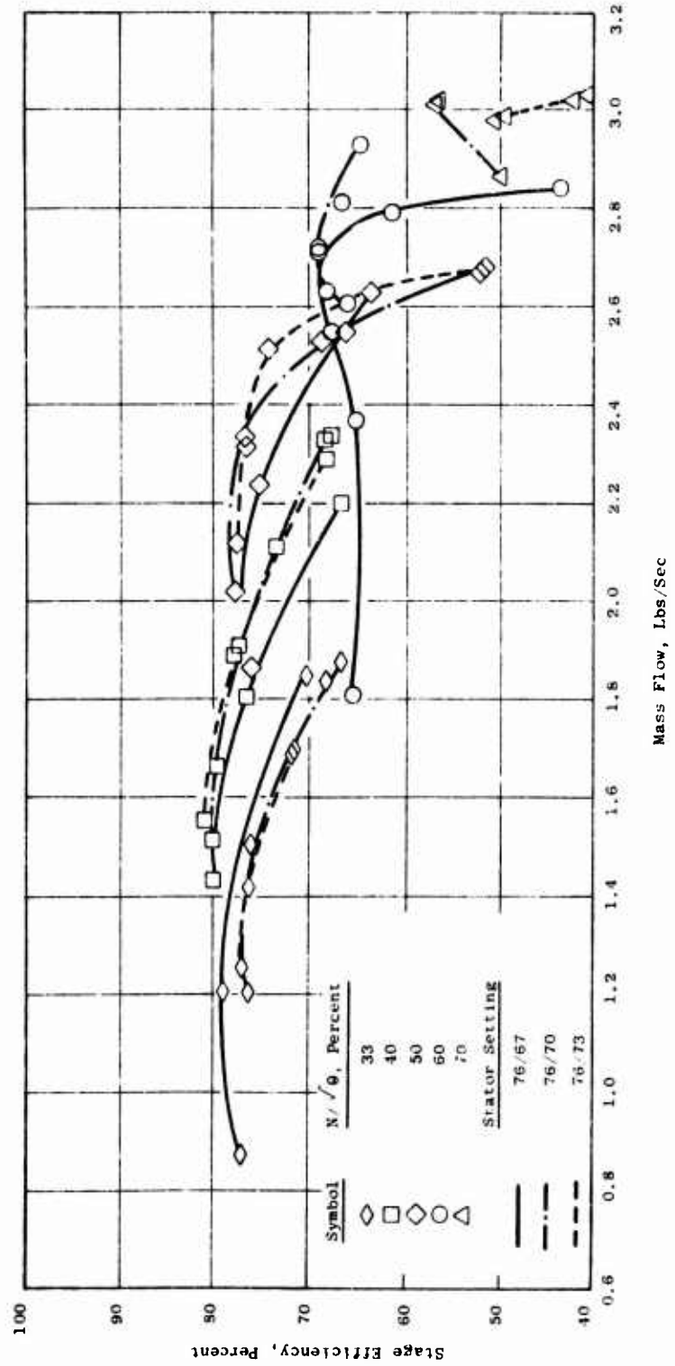

Figure 97. Stage Efficiency Versus Mass Flow With Supersonic Stators Set at 76 Degrees.

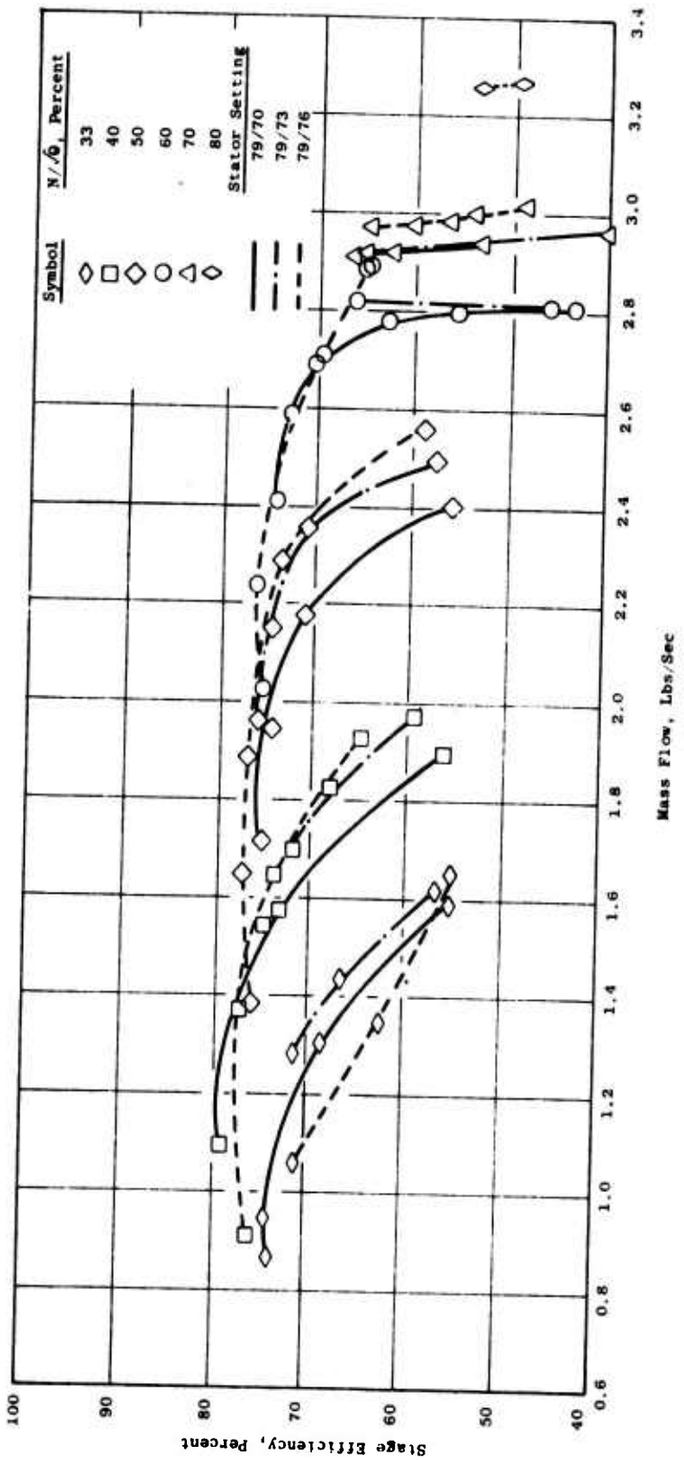

Figure 98. Stage Efficiency Versus Mass Flow With Supersonic Stators Set at 79 Degrees.

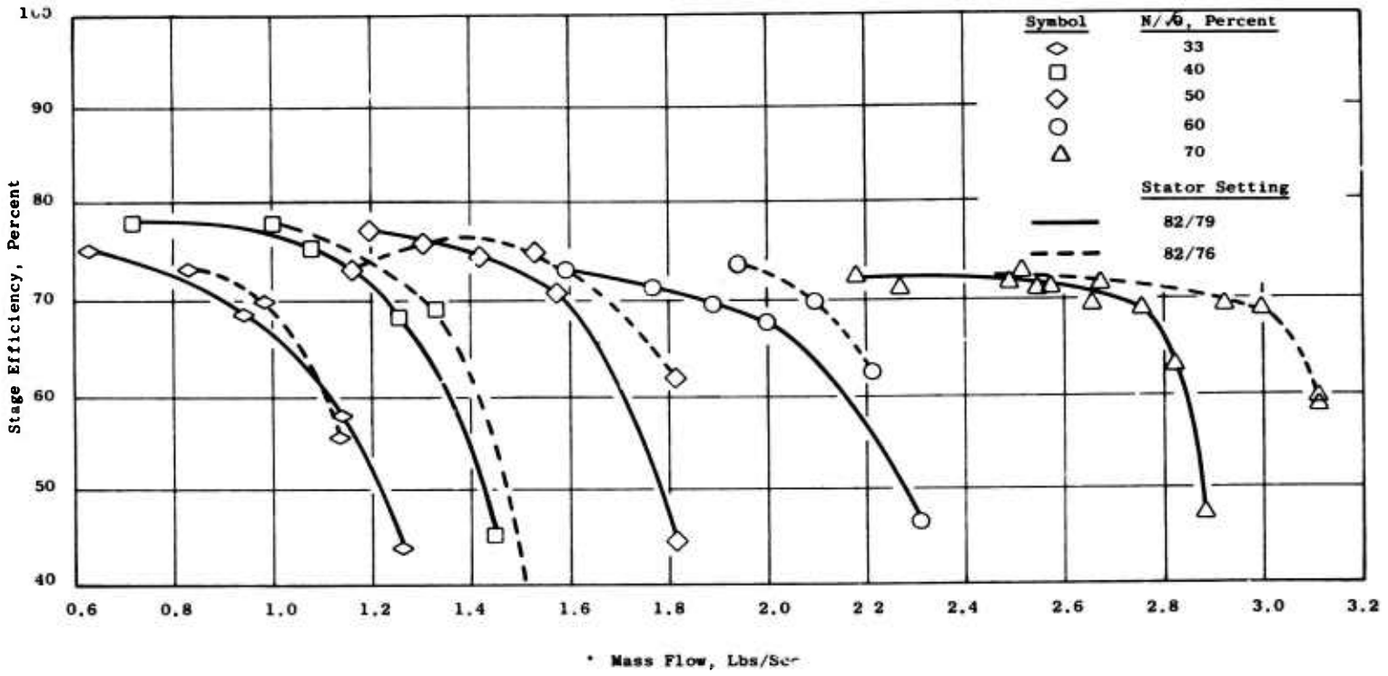

Figure 99. Stage Efficiency Versus Mass Flow With Supersonic Stators Set at 82 Degrees.

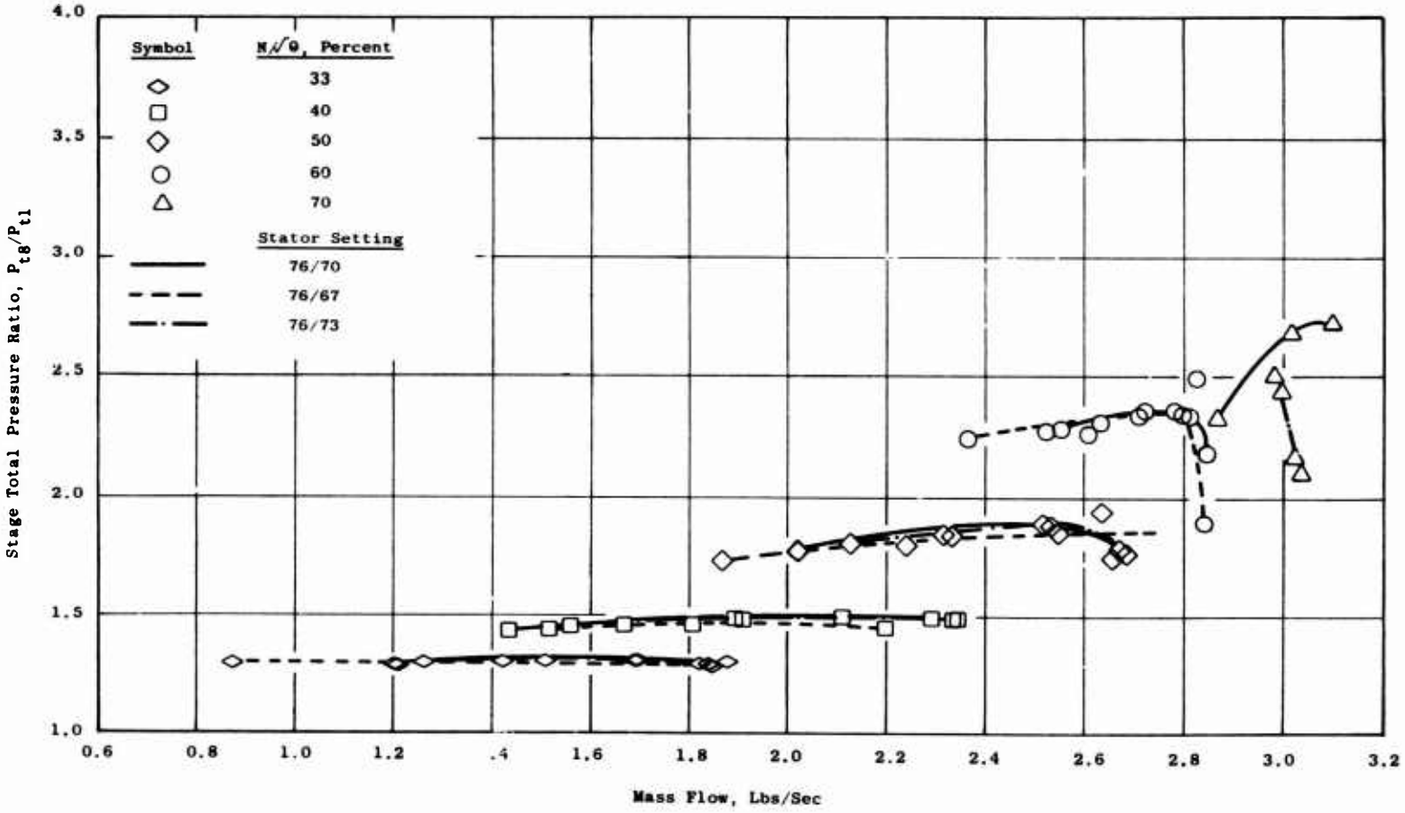

Figure 100. Stage Total Pressure Ratio Versus Mass Flow With Supersonic Stators Set at 76 Degrees.

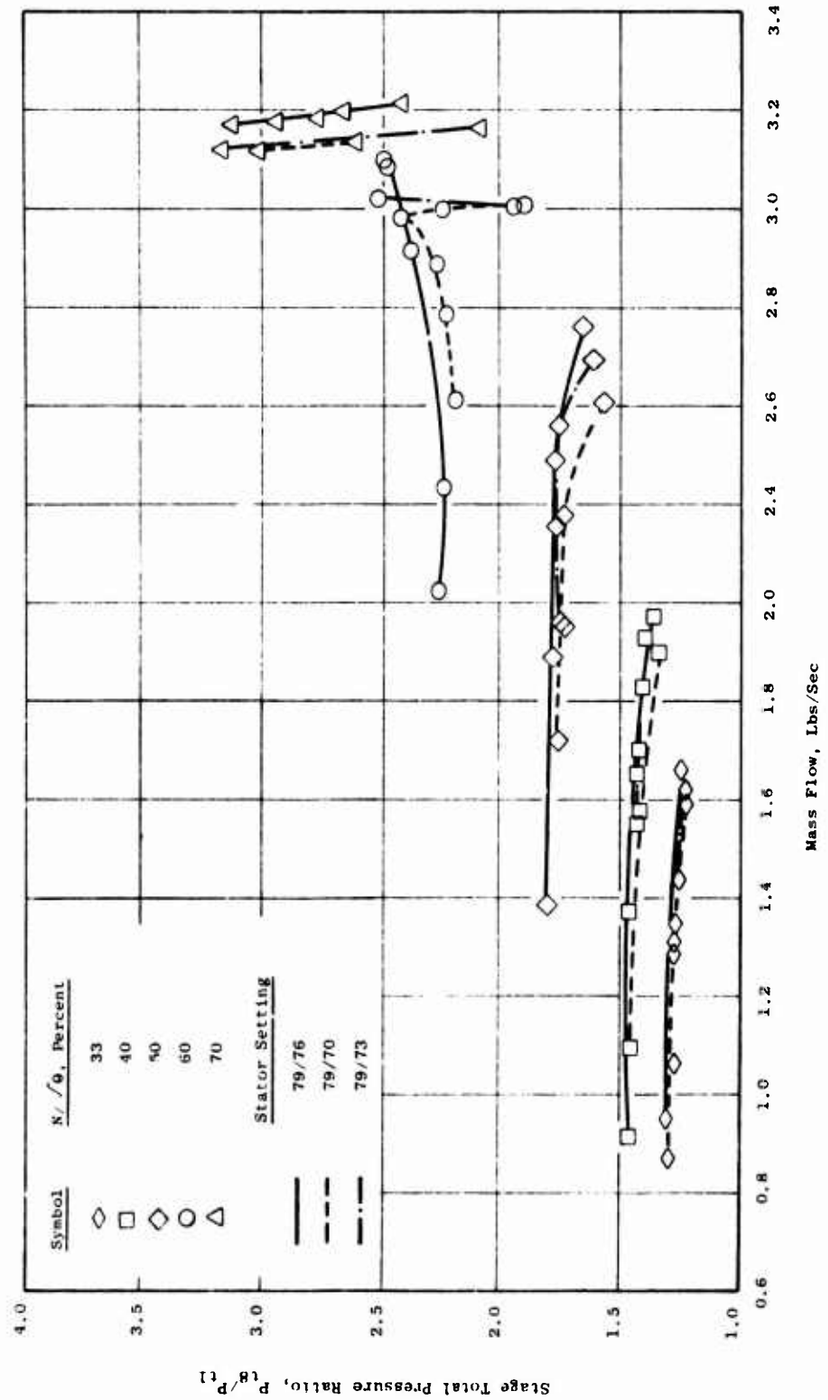

Figure 101. Stage Total Pressure Ratio Versus Mass Flow With Supersonic Stators Set at 79 Degrees.

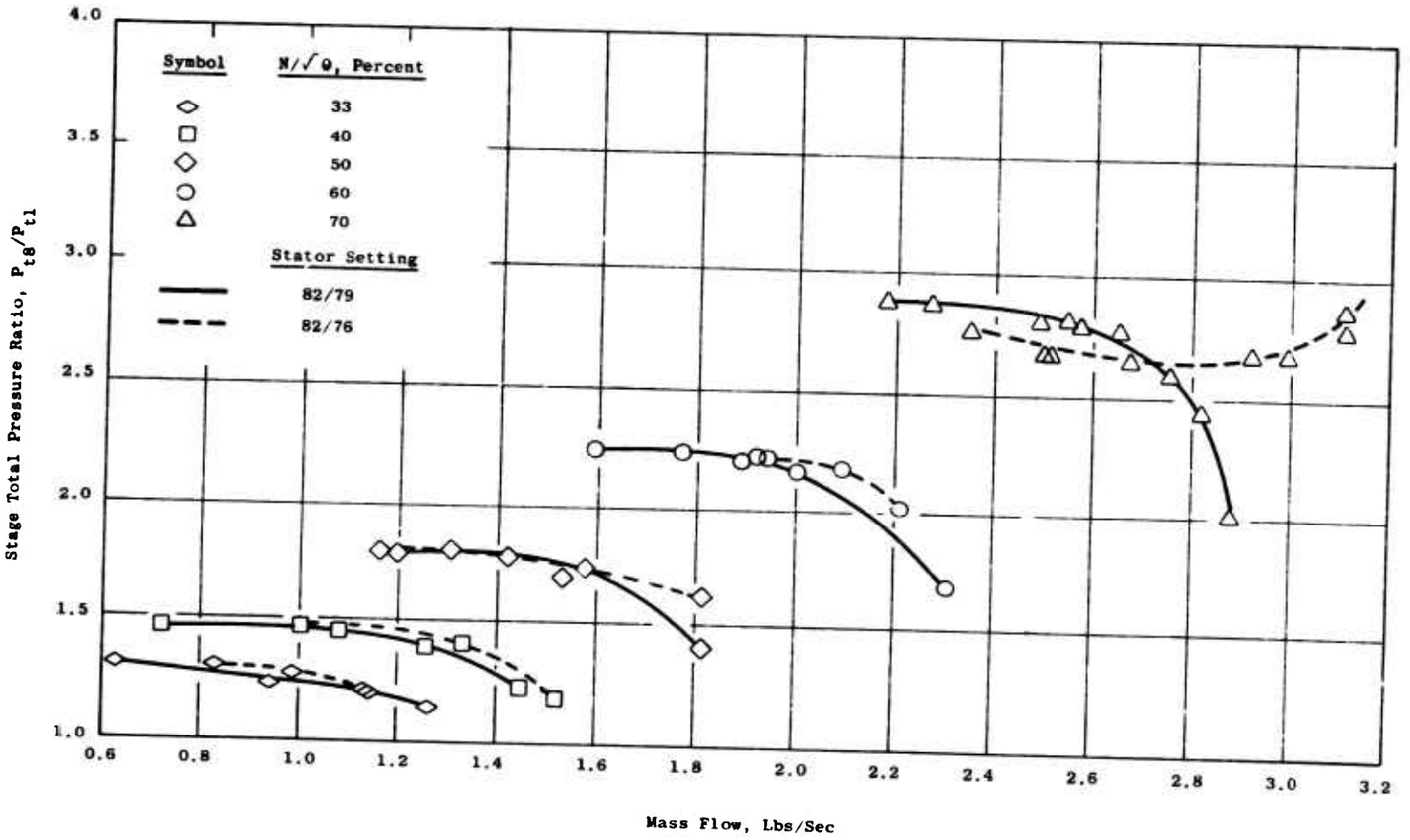

Figure 102. Stage Total Pressure Ratio Versus Mass Flow With Supersonic Stators Set at 82 Degrees.

MECHANICAL DESIGN AND PERFORMANCE

DESIGN REQUIREMENTS

The mechanical redesign of the Phase III rotor was based on and governed by the following requirements and restrictions:

1) The rotating diffuser contour (downstream of the blade trailing edge) was changed from the Phase II configuration. The flowpath width variation was defined, but there was flexibility to tilt the flowpath with respect to the radial direction.

2) To eliminate shroud vibration which restricted operation in Phase II, the rotating shroud leg adjacent to and forming part of the flowpath was to have a first critical frequency greater than the operating speed range by a safe margin. The goal was 15 percent over 100 percent physical speed.

3) The axial alignment at the transition between the rotating diffuser walls and the adjacent stator flowpath walls was not to change more than 0.005 inch from 50 to 100 percent physical speed.

4) The redesigned disc contour was to be such as to avoid the need for machining of the compressor housing, if at all possible. In general, changes in all existing parts were to be held to a minimum.

5) The same rotor blades and attachments were to be used.

DISC

The design of the Phase III disc was based primarily on the objectives of 1) the modified wall contour of the new rotating diffuser, 2) the requirement for limited axial deflection at the rim for maintaining flowpath alignment, and 3) minimum changes in other parts (stator, shaft, etc.). In addition, these requirements had to be satisfied for successful functioning of the mechanical system: 1) limited stress level in the disc, particularly at the bolt circle, and 2) radial growth compatibility between the disc and shroud bolt circles to prevent excessive bending and shear loading of the blades.

The predominant effect of the modified flowpath was the addition of a bulge on the side of the disc rim. This bulge produced a new load eccentric to the disc radial centerline which generated a moment that would bend the disc rim causing an undesirable axial deflection as well as added bending and radial stress. It was necessary to remove material

in some rim region to compensate for the added radial load, while adding material elsewhere to develop a compensating moment to oppose the tendency toward rotation of the rim. The sections being considered, then, generated radial forces approximately proportional to $A\bar{r}$, where A is the section area and $\bar{r}$ the radius of the section centroid, and moments about the disc radial centerline proportional to $A\bar{r}e$, where e is the axial distance from the disc centerline to the centroid. A groove was designed into the rim to compensate for the added weight of the flowpath bulge and was then shifted off center to balance the moment. The trade-off was such that a satisfactory combination could not be reached because of excessive thinning of the rim leg. This was aggravated by the fact that the disc web had to be shifted toward the drive end by the basic flowpath and shroud requirements, moving the disc centerline closer to the stator casing and reducing the clearance between the disc rim and the casing. It was first apparent that the casing liner would have to be eliminated, and it was finally decided that further analytical iterations were not worthwhile, considering the cost in time; so the disc rim was made symmetrical and the casing (Figure 103) was machined back to accommodate this. The Phase III disc is shown in Figures 2 and 3, and is sketched below:

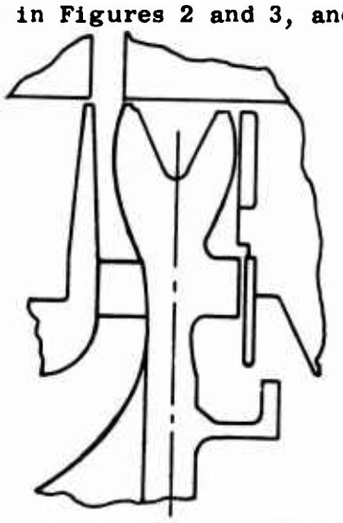

The shroud design that evolved for Phase III had somewhat higher radial growth at the blade bolt circle than the Phase II shroud, and so the disc rim load was made slightly higher to match the increased growth at the disc bolt circle while still limiting the stress to a safe level. The disc-shroud mismatch was limited to 0.003 inch radially by the blade deflection limit, and the disc was able to grow less than the shroud because of the effect of the web extending radially inward.

The drive hub on the disc was shortened, leaving the shaft the same, and this introduced a slightly greater radial restraint eccentric to the web centerline. The disc bending that resulted was not enough to exceed the rim axial deflection limits.

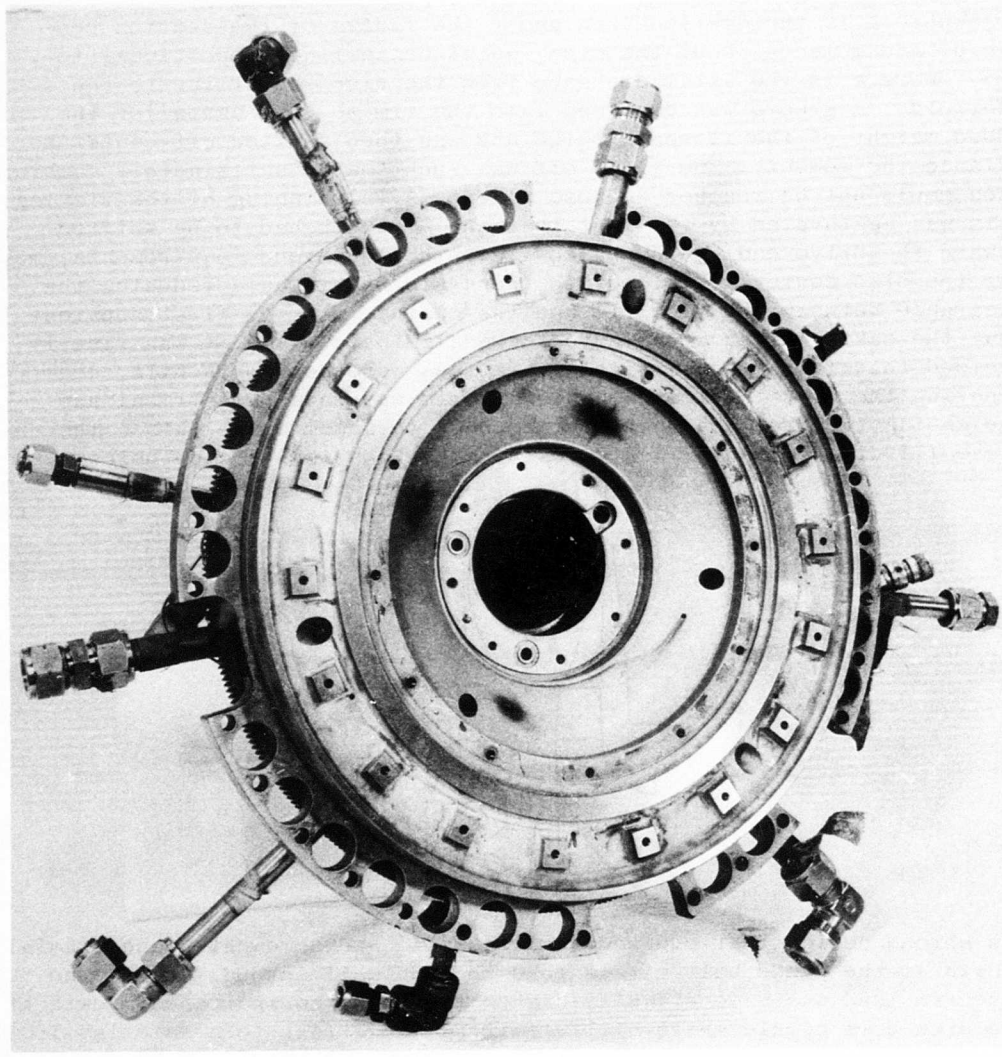

Figure 103. Bearing Housing With Face Machined Back.

Titanium 6Al-6V-25_n alloy remained the most favorable material for the disc because of its high strength-to-density ratio in an acceptable temperature range, and because of the availability of pancake forgings in this material.

SHROUD

General

The design of the shroud evolved through several stages to a configuration which would fulfill the mechanical requirements that 1) the first critical speed must fall outside the operating speed range, 2) there would be negligible shroud tip axial deflection, and 3) the design would need no development and would have high reliability.

Vibration Considerations

The first problem to be solved was that of shroud leg vibration, and other changes came about as a result of solving this vibration problem. Approaches were considered that would be light in weight to minimize stress growth. Facing the leg with a material such as filled honeycomb could provide very substantial damping, but the material behaviour could not be predicted with sufficient accuracy to guarantee success the first time; with the extremely high "g" field environment (over 240,000 "g" at the tip), it would be very difficult to assure successful attachment. A ribbed construction also had the disadvantage of not being amenable to sufficiently accurate analytical prediction of vibratory frequencies, as well as being high in fabrication and machining costs. The only method that met the requirements of time and cost as well as assurance of proper functioning was the use of a simple tapered leg with a taper ratio increased to the amount required to satisfy the vibration requirement. The increased weight of this leg required a proportionate increase in the weight required for balance against rotation. The compounded weight increase led to the need for a smaller inside diameter of the shroud to place more material in a lower "g" field region in order to be able to carry the increased load.

Axial Deflection

The effect of the heavier shroud leg in satisfying the vibration requirement was to introduce a higher overturning moment into the supporting ring section. This interaction caused rotation in the radial-axial plane and axial deflection at the rim as well as greater radial deflection at the blade bolt circle which increased the loading through the blades. A compromise had to be found between adequate counterweight to counteract the tendency of the entire shroud to rotate and small enough total radial load to keep radial growth within an acceptable limit.

Merely increasing the size of the leg on the other end of the shroud ring (within the space limits available), similar to the Phase II configuration, made too heavy a total radial load when the counterbalancing moment was satisfactory. This is shown below.

Phase II Configuration

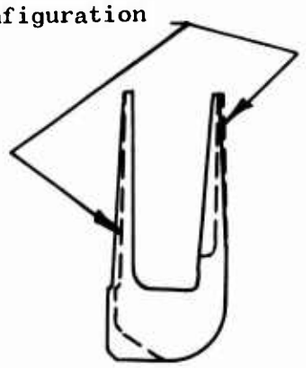

One approach investigated was to make the blade side leg very thin and then make it very short radially to keep its vibratory frequency high. This was to be accomplished by extending the shroud ring out to a deeper section with counterbored holes for access to the blade stems. The idea was to minimize the amount of leg that had to be balanced against rotation, while gaining a deeper and stiffer ring section to resist rotation. However, with larger outside diameter, along with the material lost because of the holes, the shroud reached the point of producing too high a hoop load without providing the stiffness that was desired.

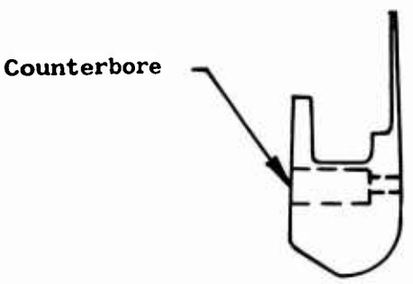

Another approach examined was the use of a high modulus-to-density ratio material such as beryllium as a restraining and support ring. When such a restraining ring was made large enough not to be overstressed, then the growth was not enough to maintain the radial growth compatibility with the disc to prevent blade loading. Furthermore, the prospect of using a relatively exotic material such as beryllium presented problems of procurement in a short time, and of quality assurance in an unfamiliar material where prime reliability would be absolutely essential.

Final Design

The final configuration (Figures 7 and 9) selected used an alternate clearance space available within the existing stator casing. In this concept, counterbalancing was done with "dead weight" lugs on the inlet end of the shroud ring. To form the counterweights, the ring was increased in length and then slotted axially to form multiple lugs. The slots interrupted the load path so that this end section could not carry hoop stress. The load of the entire mass produced a radial load at a maximum axial distance from the centroid of the ring. At the same time the centroid was kept as close as possible to the radial leg to minimize the moment arm of the load to be balanced. However, it was also necessary to reduce the inside diameter of the ring to provide material at a small enough radius to limit radial growth (to avoid shear loading of the rotor blades).

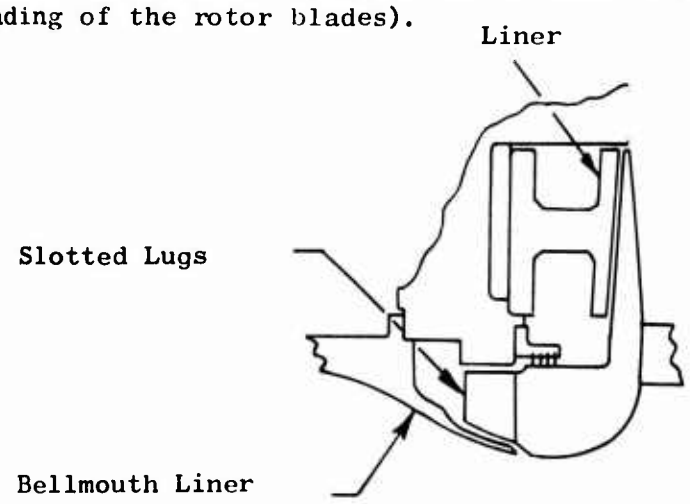

Comparison of Calculated and Measured Vibrations

The finished part was instrumented as shown in Figure 9 and vibrated to determine distribution and natural frequencies. The measured frequencies correlate moderately well with the calculated values, as shown in the tabulation below.

Vibratory Mode	Frequency Nonrotating (cps)	
	Calculated	Measured Assembled in Rotor
1 wave	-	2030
2 waves	1882	1560
3 waves	1947	2148
4 waves	2056	2190 (Mode is in question)

There was considerable difference between frequencies measured with the shroud bolted to a test fixture and those with the shroud standing free on Isomode pads and assembled in the rotor as shown in the following tabulation.

Vibratory Mode	Frequency Nonrotating (cps)			
	Bolted To Test Fixture	On Isomode Pads	Assembled In Rotor	
1 wave	2980	2094	2030	
2 waves	2666	1436	1560	
3 waves	2808	1878	2148	
4 waves	-	2152	2190	(Mode is in question)

The Campbell diagram in Figure 104 is based on the measured nonrotating frequencies in the assembled rotor and the calculated centrifugal stiffening effect, and shows the first critical speed to be about 12 percent over the design speed. The amplitude of vibration was too low to correlate it for stress-deflection calibration of the proximeters for scope limits in testing.

During high-speed compressor testing, no shroud vibration was detected with the proximeters, and only an indication of a minor resonance appeared from the strain gages.

Strain gage locations were established from the stress distribution data, and scope limits were based on these data.

Influence of Shroud Design of Adjacent Parts

With the single leg shroud configuration, the stator casing liner was changed to a member having an "H" cross section which retained the feature of keeping adjacent static and rotating surfaces at a 0.090-inch spacing. This clearance had been established as producing the least aerodynamic drag at the radius and surface speed of the shroud leg. The liner also provided a mounting for the proximeters next to the remaining shroud leg.

The use of a slotted ring section opened up a leakage path past the Phase II labyrinth seal location, and required relocation of the seal (see section on Labyrinth Seal, page 137). The slots were also undesirable aerodynamically if they opened into the flowpath wall, and so the inside diameter of the shroud lugs was increased to permit use of an inlet section adjacent to the shroud. The inlet (Figure 12) provided a smooth, continuous wall between the slots and the flowpath.

The first critical frequency of the final configuration was 12 percent over the compressor design speed. In reducing the shroud ring diameter, the inlet flowpath average Mach number and area variation were changed as shown in Figure 262 of Reference 2. With the inner contouring of the new shroud, the blending that was necessary for an aerodynamically

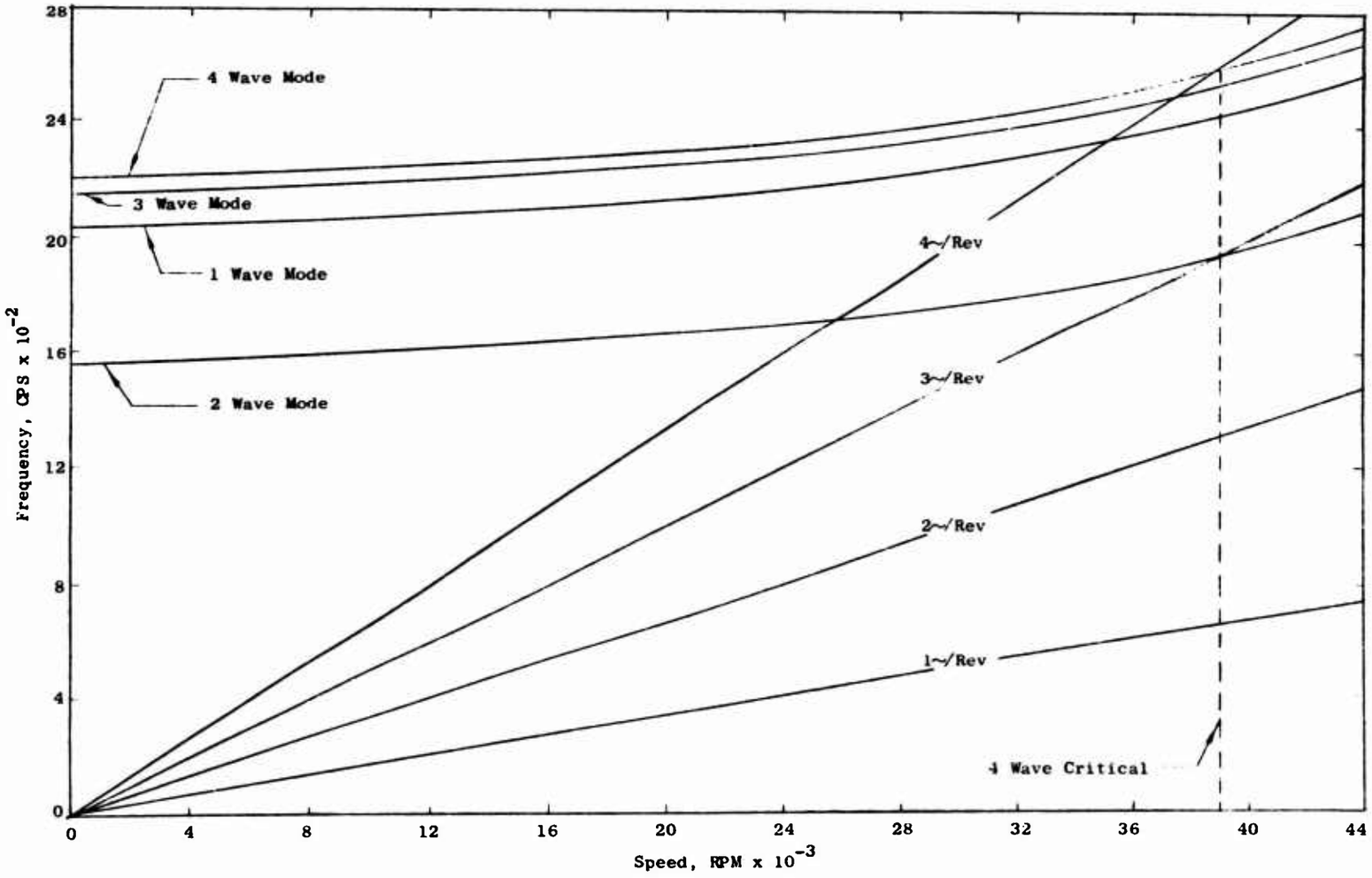

Figure 104. ROC Phase III, Buildup A Shroud Campbell Diagram.

acceptable rate of change of curvature continued to work in opposition to positioning of material in the ring section favorable to minimize the ring rotation. The result was to require the "dead weight" lugs to be as long as possible without becoming too slender in proportion to the height of the attachment section.

ROTOR BLADES

General

The Phase III rotor blades (Figure 105) were made with 6 Al-6V-2 Sn titanium alloy. This alloy has a tensile strength some 30 percent higher than the 6 Al-4V titanium used as an expedient for the Phase II blades procured for the first high-speed rig testing. The 6-6-2 titanium is a more recently available alloy than 6-4 titanium, and was needed to provide the properties required for operation at the design speed. These blades were first used in the Phase II testing.

Because of the problem of matching radial growth between the disc and shroud, the deflection limitations of the blade were reviewed. In addition, operation at 100 percent speed revealed that the nut and washer load on the blade threaded stems was marginally excessive, and this loading was reevaluated.

Airfoil Deflection

Considering the airfoil by itself, the stem mounting provides a restraint under which the airfoil will perform mechanically in a manner between the case of a simple cantilever free to rotate at one end and a double cantilever with both ends restrained against rotation. Between these extremes, the airfoil can accommodate a radial mismatch of .003 inch. The restraining moment preventing rotation at the ends, converted into coupled forces acting in the stem and near the airfoil edge, produces an axial load in the blade stem which, combined with the shear loading of the airfoil, constitutes a limiting stress. The deflection is limited to a fixed amount by the relative disc and shroud radial growths at the respective bolt circles.

Nuts and Washers

A review of stress in the threaded section of the blade stems revealed 1) that with the "g" load of the overhung threaded blade stem and hardware at 105%N, the threaded section cannot support the load in bending, as would be required, approximately, if the nut were perched on top of a partially compressed Belleville washer, and 2) the blade stem will bend until the nut is reacted at a point eccentric to the stem center. Figure 106 shows how the thread stress varies with eccentricity of the reaction point.

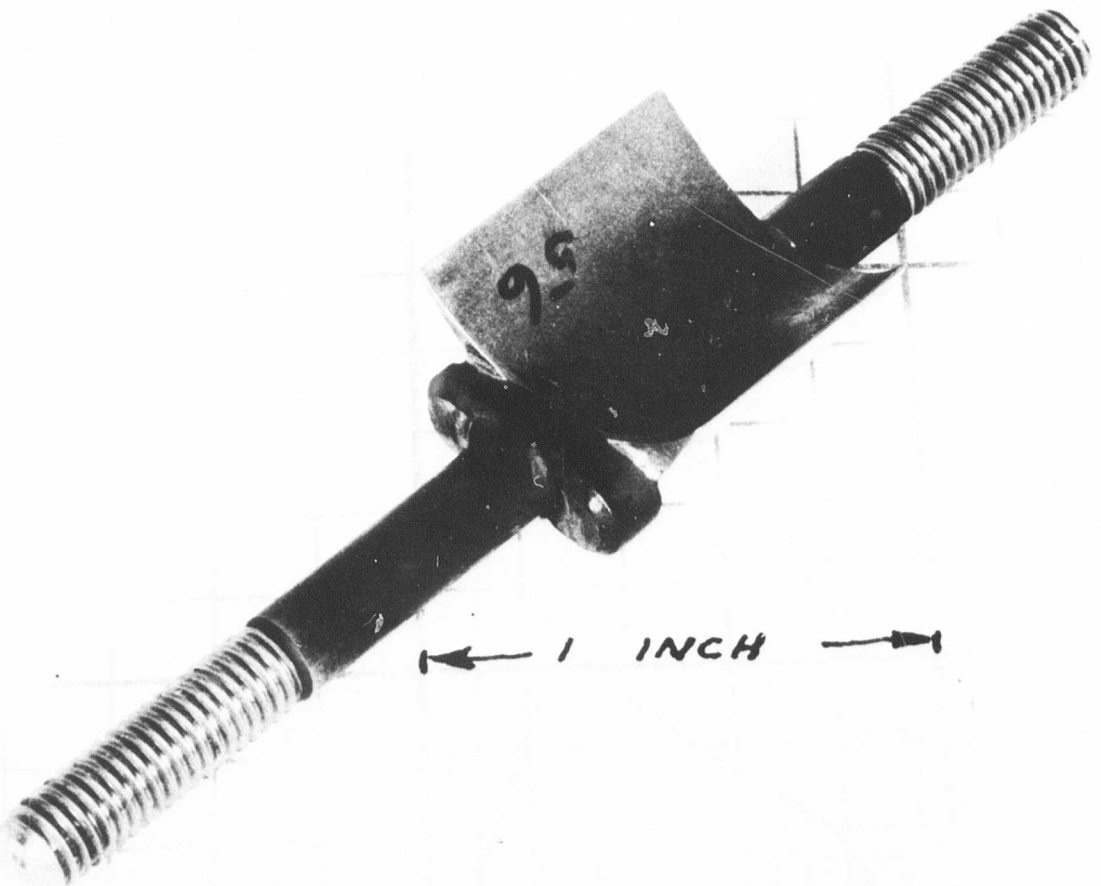

Figure 105. Phase III Rotor Blade.

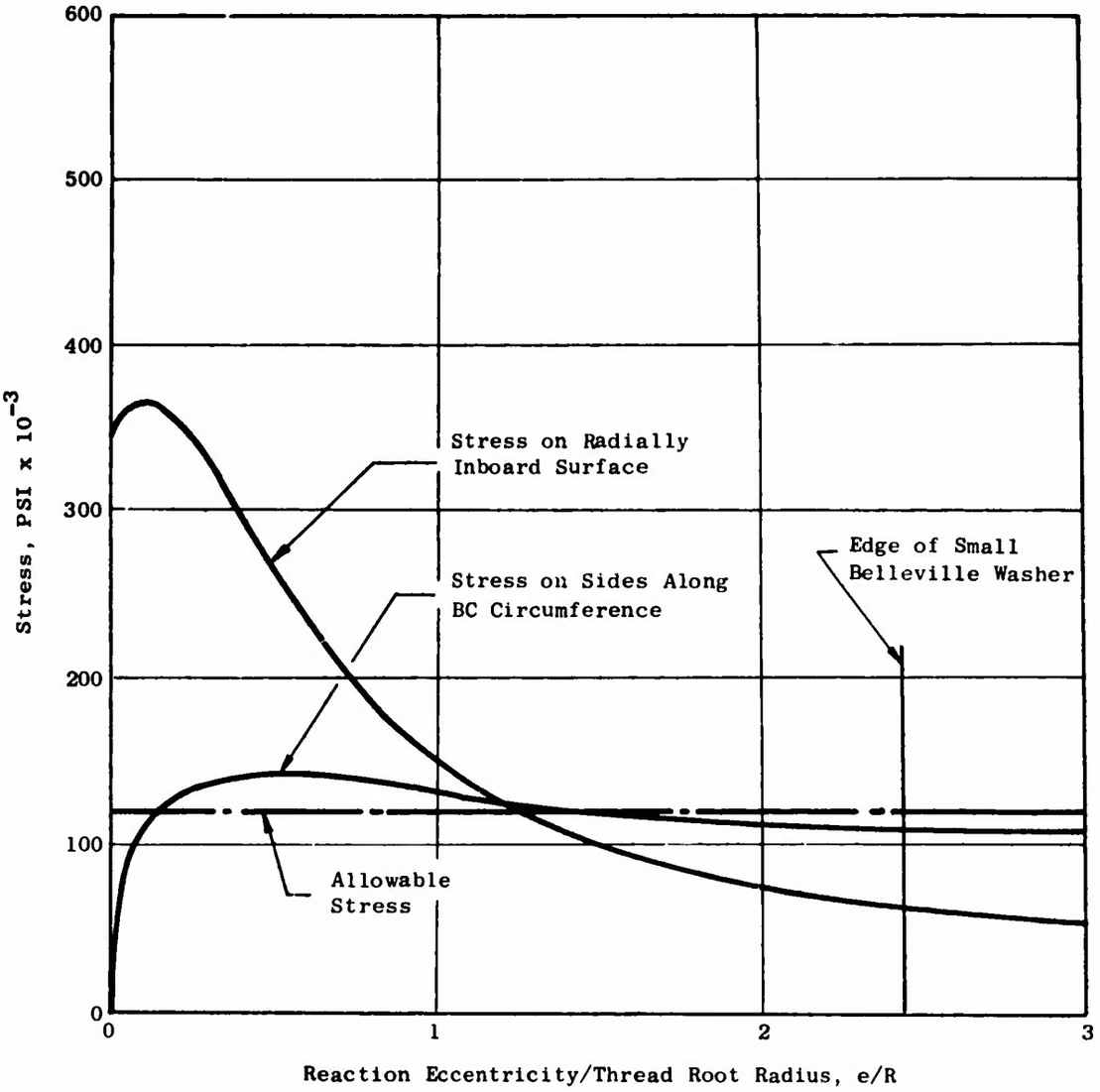

Figure 106. Blade Thread Root Stress Versus Reaction Eccentricity.

The stem prestress cannot be made high enough (because of combined stress limitations) for the stem elongation to accommodate all of the potential disc and shroud thinning at full speed, and so the Belleville washers must be used to prevent complete loosening. However, with higher prestress , the smaller Belleville washer provides an adequate deflection length for the relaxation that might occur, and will flatten without adding an excessive load to the stem. The flattening is necessary to insure minimum stem bending.

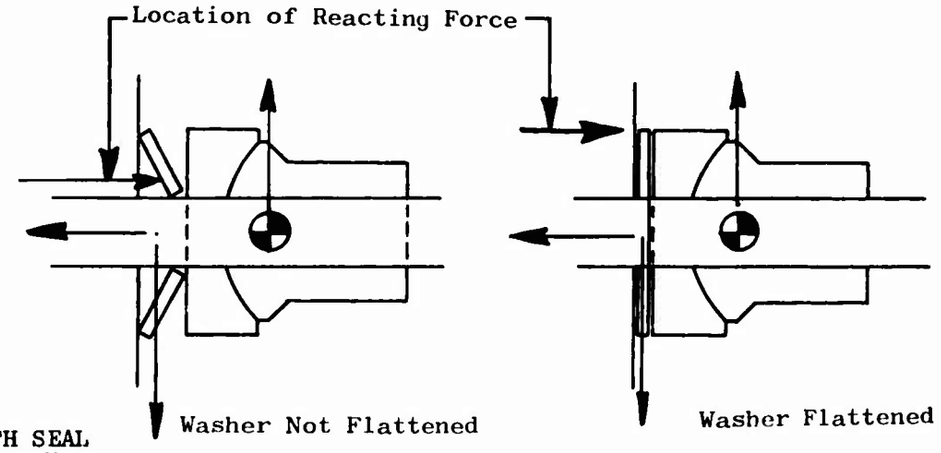

LABYRINTH SEAL

With the use of dead weight lugs on the shroud, the labyrinth seal for the inlet side of the rotor was relocated on the outer diameter of the shroud hub. The teeth were made integral with the shroud, as shown in Figure 9, and the seal race was initially made as a simple Teflon "L" section ring.

An existing shoulder in the stator casing was used as an external rabbet for centering the seal race.

In the initial running, gross overheating of the seal cavity occurred, apparently, as a result of turbulent heating and inadequate cooling airflow. The Teflon race expanded against the external rabbet and buckled; it was then destroyed by heavy rubbing against the shroud.

Because of the problem of assuring close control of temperature in the seal area (since this is also restricted by airflow management for rotor thrust control and for main stream leakage control), it was necessary to replace the Teflon seal race with a steel one in order to have a low thermal coefficient of expansion for better growth compatibility between the seal race and casing. Radial clearance was provided between the seal flange and the external rabbet to allow for the maximum expected temperature difference between seal and casing. This radial clearance (0.003 inch minimum) was small enough to prevent the possible radial shaft of the seal from allowing excessive leakage or preventing disassembly after seal tooth rub-in.

The seal race was faced with a .19-inch thickness of silver braze alloy which is an effective rubbing surface with titanium.

CIRCULAR INLET VANE

The circular inlet vane, used to minimize local high Mach number flow regions in the axial to radial turn and to help provide a flat velocity profile at the approach to the rotor, is essentially the same as the Phase II vane shown in Figure 107. A staggered weld was used at the strut-to-vane joint to eliminate weld distortion of the vane. The computed flux plot of the flow turning region indicated that a circular 90-degree arc would provide the desired function when the leading and trailing edges are located on a common stream line of the undisturbed flow stream.

Positioning by friction clamping was simple and successful in the Phase II configuration, and was used again in Phase III. The centerbody extension (slotted version shown in Figure 13) was a close fit over the turning vane hub, and clamped it to the centerbody with flat head screws running through both the extension and the vane hub.

The unslotted centerbody extension was for use if the turning vane was not used.

MECHANICAL INSTRUMENTATION

Mechanical diagnostic instrumentation used in conjunction with the Phase III rotor consisted of eight dynamic strain gages on the shroud leg and three proximeters mounted adjacent to the shroud leg.

The strain gage leads were cemented to the disc face as shown in Figure 17, and to blades having flats ground on the shroud side stems as shown in Figure 14. In the first buildup, the leads were run along the stem inside the nut and then over the outside of the nut back to the shroud surface, where the strain gages were attached. This region over the nut was especially susceptible to lead failures, and subsequently the leads were routed as shown on the trial specimen in Figures 108 and 16. Here both the Belleville washer (underneath) and the spherical seat washer were grooved to accommodate four leads each. Only the grooved Belleville washer was used, and this was quite successful in the 150,000 "g" field.

Aerodynamic heating in the cavities behind the shroud caused deterioration of the cement on the shroud strain gages and in the proximeters mounted

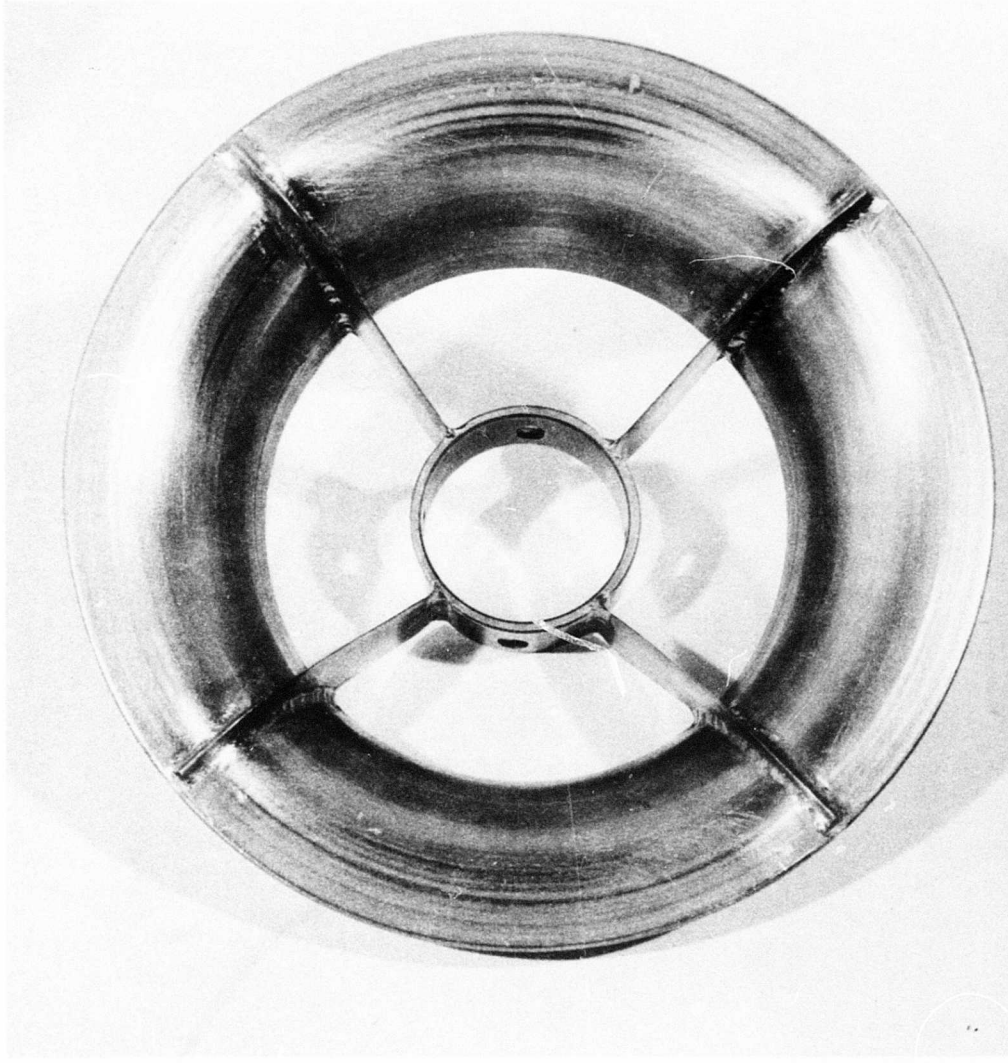

Figure 107. Phase II Circular Inlet Vane.

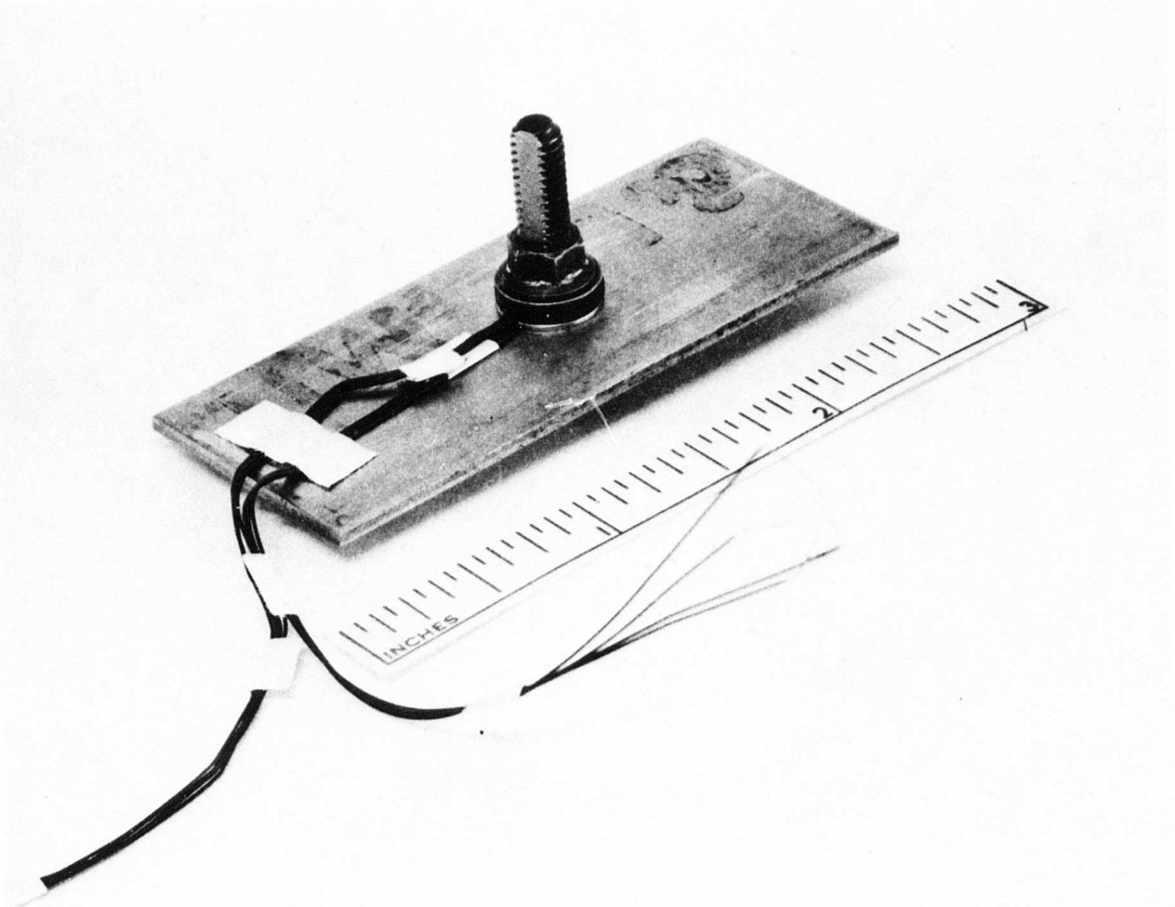

Figure 108. Trial Specimen for Rotor Blade Lead Routing.

on the casing liner during the initial running. All of this instrumentation was destroyed and had to be replaced. Heat discoloration of the liner gave a rough indication of a metal temperature of 900°F. After this occurrence, thermocouples were added to the casing wall in this region and monitored to avoid reoccurrence of such a temperature rise. All cavity temperatures were subsequently kept below about 450°F, but at the end of testing the proximeters showed deterioration again.

No shroud vibration was detected beyond a low level minor resonance, and so the final running was done with no shroud strain gages, because they had become inoperative and were removed.

The proximeters showed the shroud face runout, and indicated rotor shaft flexure, based on the phase relationship of the three proximeter readings. No shroud vibration was detected by the proximeters.

ROTOR ASSEMBLY AND BALANCE

In assembling the rotor, special attention was given to the fit-up of the disc, blades and shroud in order to minimize gaps at the ends of the airfoils and runout of the flowpath walls. Some blade stems were reduced slightly at the airfoil end to assure complete seating in the disc holes, and the blade positioning platforms were trimmed to provide 0.003 inch or less airfoil-to-disc clearance. Selective positioning of blades minimized the airfoil-to-shroud gap, and resulted in reduction of axial runout of the shroud leg to 0.003 inch.

The balance procedure was modified in the last buildup to prevent bending of the outer end of the blade stems at high speed. No balance washers were used, only the smaller size Belleville washers were used, spherical seat washers were ground shorter for use as negative balance washers, and the nut torque was increased to keep the Belleville washers flattened as much as possible.

After running the Phase III vehicle, rotor bearing play was checked in the assembled vehicle. Free travel at the shroud end in moving the rotor by hand was 0.002 inch in the radial direction and 0.006 inch in the axial direction.

RESULTS AND CONCLUSIONS

1) Performance of the Phase II rotor during Buildup F testing was very satisfactory and agreed with predictions up to and including 70 percent speed. The calculated value of the Radial Outflow Compressor efficiency at 70 percent speed using the Phase II, Buildup F rotor data and the Phase III stator loss coefficient (0.15) obtained with open stator vane settings is 85.6 percent, at a pressure ratio of 3.635 and an airflow of 2.94 lbs/sec. This calculated performance represents an improvement over existing compressors in this airflow and pressure ratio range.

2) The Radial Outflow Compressor operated at conditions cited in the previous paragraph is believed to be a useful device. This is particularly true when the Radial Outflow Compressor is supercharged by preceding compressor stages.

3) Although the Phase III rotor was more efficient than the Phase II rotor at low speeds, the high speed performance was not as good and fell below predictions.

4) The setting of the supersonic stator vanes has a very powerful effect on rotor performance. At high speeds, improved rotor performance was obtained by closing the supersonic stators 1.4 and 2.4 degrees beyond the nominal setting. Low speed performance was not detrimentally affected by this stator vane closure, although airflow was reduced.

5) Varying the setting of the subsonic stator vanes over the 6-degree range investigated did not sensibly affect compressor performance.

6) Efficient stator system performance was obtained at supersonic stator vane angles of 76 and 79 degrees. Stator system loss coefficient increased significantly at supersonic vane angles of 83.4 and 84.4 degrees (where improved rotor performance was obtained).

7) A significant mismatch occurred between the rotor operating characteristics and the stator system operating characteristics. An improvement of overall compressor efficiency of as much as 7 points should be obtained by proper matching of the rotor and stator.

8) The decrease in stator system performance for closed vane settings is believed to be due to two factors: 1) an increase in expansion area ratio between the minimum area or throat near the leading edge and the exit area near the trailing edge and 2) intersection of the wakes from the supersonic stator vanes with the subsonic stator vanes.

9) It is believed that the modification employed in the rotating vaneless diffuser of the Phase III rotor was too large. Improved high speed performance can probably be achieved by an intermediate configuration or by return to the original Phase II rotating vaneless diffuser.

10) Significant blockage of the flow occurred at the rotor blade exit when high back pressures were impressed on the rotor.

11) Supersonic Mach numbers near design values were obtained at the rotor blade trailing edge when low back pressure was impressed on the rotor. It is believed that high losses occurred in the rotating vaneless diffuser with supersonic velocities entering the rotating vaneless diffuser.

12) The design philosophy of the Radial Outflow Compressor has been firmly established at speeds up to and including 70 percent. Uniform flow conditions into the stator system were obtained at speeds up to and including 70 percent.

13) It is tentatively concluded that Radial Outflow Compressor rotor blades should be designed for sonic exit conditions to obtain improved high speed performance.

14) Improved high speed rotor performance can probably be obtained by increasing the rotor blade chord length and thereby increasing the rotational speed at the rotor blade trailing edge. With sonic rotor blade exit velocity, and with absolute and relative flow angles nearer to radial, the rotating wall vaneless diffuser performance should be improved.

15) The Radial Outflow Compressor rotor is sensitive to inlet flow conditions at the rotor blade leading edges. A circular inlet vane is helpful toward providing uniform flow entering the rotor blades.

16) Design of a suitable inlet guide vane system for a Radial Outflow Compressor is a difficult task because of the sensitivity of the rotor to nonuniform axially and possibly circumferential inlet flow conditions.

17) The Phase III Radial Outflow Compressor rotor is mechanically rugged and could be operated under conditions of rotating stall in either the rotor or the stator system without difficulty.

18) Although the variable stator system used with the Radial Outflow Compressor test vehicle was complex, expensive, and caused numerous operating problems, it is nevertheless believed to be highly desirable for research and development testing because the compressor performance is very sensitive to small changes in supersonic vane setting.

19) An independent thrust balancing system would eliminate test vehicle operating problems which were encountered at most conditions of high rotor static pressure rise.

RECOMMENDATIONS

1) Only a few hours of Radial Outflow Compressor running at speeds above 70 percent were obtained before bearing failure. Further testing of the Phase III vehicle should be conducted. Optimum circular inlet vane position should be determined.

2) The supersonic stator vanes should be modified to improve the matching between the rotor and stator systems.

3) The Phase III rotor should be modified in two stages to the Phase II, Buildup F rotating vaneless diffuser configuration. This will permit demonstration at full speed of the potential indicated during tests up to and including 70 percent speed.

4) An improved Radial Outflow Compressor using larger chord blades with a modified area distribution through the rotor blades to produce sonic exit flow should be designed, built, and tested to demonstrate the potential performance calculated for this compressor design.

5) Improved stator systems possibly employing sweep, circular passages, boundary layer control, and/or three-dimensional compression surfaces should be developed. The transonic cascade tunnel would be a useful device to employ in this development.

6) A better discharge system than the scroll collector should be developed for use with the Radial Outflow Compressor.

7) Improved instrumentation for measuring rotor exit total pressure variations at high rates of response should be developed for both Radial Outflow Compressor and conventional compressor investigations.

8) Improved methods of attaching rotor blades to the shroud and disc, such as diffusion bonding, should be developed.

9) The possibility of machining the Radial Outflow Compressor rotor from one forging or casting should be investigated.

REFERENCES

1. Erwin, J.R. and Vitale, N.G., RADIAL OUTFLOW COMPRESSOR COMPONENT DEVELOPMENT (U), Volume II, Phase II - Design, Fabrication, and Test of an Experimental Compressor (U), USAAVLABS Technical Report 68-38B, U.S. Army Aviation Materiel Laboratories, Fort Eustis, Virginia, March 1969.

2. Erwin, J.R. and Vitale, N.G., RADIAL OUTFLOW COMPRESSOR COMPONENT DEVELOPMENT PROGRAM, Volume I, Phase I - Aerodynamic and Mechanical Design Analysis and Diffuser Tests, USAAVLABS Technical Report 68-38A, U.S. Army Aviation Materiel Laboratories, Fort Eustis, Virginia, May 1969.

APPENDIX I

SUMMARY OF THE COMPRESSOR CONFIGURATIONS AND TEST POINTS WITH COMMENTARY

Date	Buildup	Run	Test Points	Speed Range (Percent)	IGV	Circular Vane	Supersonic Stators	Subsonic Stators	Comments
2-7-68	A	-	0	30	No	No	No	Yes	Subsonic stators - Open inlet - No circular inlet vane - Traverse Probes - Siezed and sheared off inlet fairing - Vehicle vibrations high at 10,000 rpm - No data taken.
2-9-68	A	19	14	90	No	No	No	Yes	Cut off inlet - 8 rotor strain gages switched - Facility bearing overheated - No rotor strain gages left - Teflon seal destroyed - Liner overheated (900°F) - Shroud strain gages burned off.
2-24-68	A	20	6	70	No	No	No	Yes	Cast aluminum inlet - Spliced strain gages (4) - Silver braze metal seal race (for labyrinth) - Excessive speed tripping due to vibrations - Data to 60 percent speed.
2-26-68	A	21	-	80	No	No	No	Yes	Lead shot added to bearing housing - Same as 2 24 - Inlet still okay.
2-27-68	A	-	-	90	No	No	No	Yes	Ran to 90+ percent speed - Vehicle vibrations high - Speed trips with no indication why - Bet facility bearing - Vane actuation broken off - Bellmouth No. 2 liner cracked 1 4 inch from edge around 60 degrees - Proximeter to 23 mils below 11,000 rpm.
4-15-68	B	22	7	70	No	Yes	Yes	Yes	Pyrolytic graphite bellmouth liner.
4-17-68	B	23	14	100	No	Yes	Yes	Yes	Subsonic vanes jammed at 77 degrees position - 100 percent speed (5 minutes) - Took 1 data point at 100 percent speed with stators at 78 degrees (supersonic) and 77 degrees (subsonic) - P P 4.8, efficiency 57 percent.
4-18-68	B	24	54	70	No	Yes	Yes	Yes	Took maps at 50, 60, and 70 percent speed - Took 30 data points at 70 percent speed at different stator and throttle settings - Best performance 81 percent efficiency - Speed limited to 70 percent by facility bearing temperature.
4-19-68	B	25	16	85	No	Yes	Yes	Yes	Circular inlet vane moved 0.10 inch to full forward position - Supersonic vanes jammed at 79.5 degrees and subsonic vanes jammed at 77 degrees - Damage sustained to 1 rotor blade, probably in assembly - Pinion gear on 1 supersonic stator spindle sheared.
5-29-68	C	26	51	80	No	Yes	Yes	Yes	Silver seal clearance reduced - Suction capacity from forward cavity (PV4) increased - Rotor reworked removing strain gage leads - Inlet turning vane set at nominal 0.362 inch from rotor shroud - Modified gearbox discharge to cool facility bearing - Stator casing to rotor offset reduced .006 inch - Obtained performance maps to 80 percent speed at 76 73, 79 73, and 82 73 degrees on stators.
6-3-68	C	27	55	80	No	Yes	Yes	Yes	Obtained performance maps to 80 percent speed at 82 73 and 82 76 degrees on stators.
6-4-68	C	28	62	80	No	Yes	Yes	Yes	Obtained performance maps to 80 percent speed at 82 79 and 79 76 degrees on stators.
6-5-68	C	29	28	70	No	Yes	Yes	Yes	Obtained performance maps up to 70 percent speed at 79 76 and 76 70 degrees on stators.
6-6-68	C	30	53	100	No	Yes	Yes	Yes	Obtained performance maps up to 80 percent speed at 76 67 and 79 70 degrees on stators - Set 84.4 76.3 for 100 percent speed point - Obtained 3 data points at 100 percent speed - Best performance was 7.32 pressure ratio and 76 percent efficiency.
6-7-68	C	31	12	100	No	Yes	Yes	Yes	Opened stators to 83.4 76.3 degrees - Took data at 70, 80, 90, and 100 percent speed - Performance at 100 percent speed dropped to 5.93 pressure ratio, and 66 percent efficiency - Changed stators to 83.4 74.8 degrees - Took 1 reading at 100 percent speed - Performance was 5.82 pressure ratio and 66 percent efficiency - Unable to control compressor No. 1 ball bearing with cooling air while at 80 percent speed - Decelerated to 0 speed - Had sudden increase in vibrations (up to 10 mils) on the decel from 10,500 rpm to 1,000 rpm - Post-test teardown revealed failed No. 1 ball bearing - The bearing labyrinth oil seal was worn - There was no other damage.

APPENDIX II

ROTOR ASSEMBLY AND BALANCE PROCEDURE FOR BUILDUP C

GENERAL

The ROC 1A3 (B/U B) rotor was returned to the service area for: 1) removal of all instrumentation, 2) removal of a damaged blade, 3) removal and replacement of the four reworked (for instrumentation) blades, and 4) verification of runouts.

DISASSEMBLY

1) Rotor runouts were taken before teardown and are designated by the letter B in Figure 109.

2) The shroud was removed and photographs were taken of the flowpath areas.

3) All parts were cleaned and replacements found for the damaged blade (no stem configuration) and the 4 instrumented blades (stem configuration).

4) Instrumentation was removed from the disc area, and the flamespray was cleaned and polished.

ASSEMBLY

1) All blade airfoils and leading edges were benched smooth and polished.

2) Selective fit of the stem-type blades was started (Figure 110). The objective was to insure that the blade was seated in its race track slot and had an airfoil clearance of 0.003 inch or less at the disc.

3) During the fit-up operation, it was discovered that some of the blade stems were bent on the short side. Some bent stems on the long side had been previously noted. Further investigation indicated blade stems bent on both the long and short sides and in a quantity approaching the number of balance washers installed during the 1A3 build. No reference marking between balance weights and blades had been made. It was concluded that the installation of the balance washers could have caused the observed bending.

4) Spare blades were located and reworked to allow proper fit-up.

5) The shroud was installed with all nuts torqued to prior specified torques. Runouts on the shroud then were measured and found to be prohibitive (0.0055 inch) for final build. The shroud was removed, and runout measured in a free state was in the order of 0.002 inch.

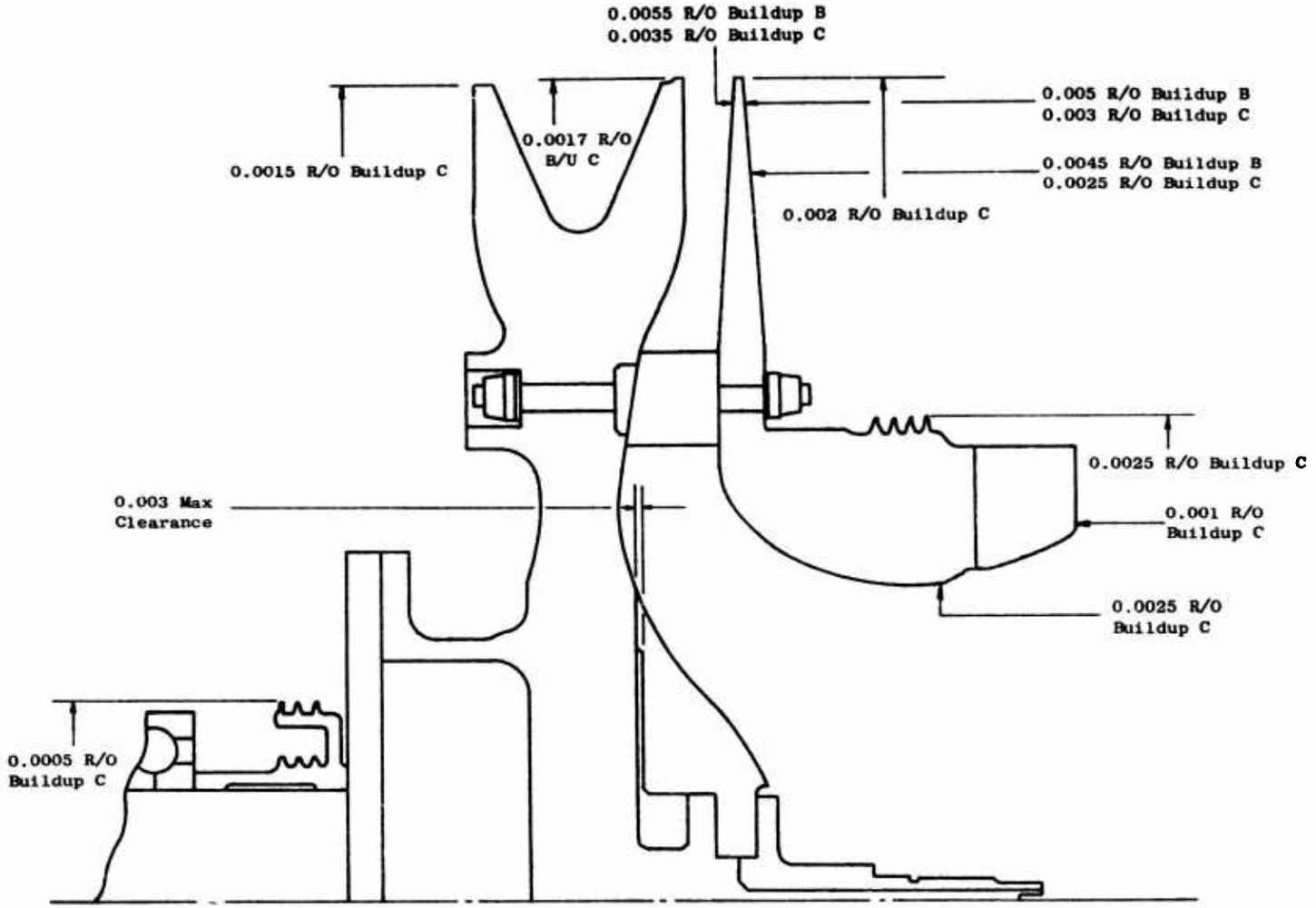

Figure 109. Values of Rotor Runout (R/O) Measured After Buildup B Testing and After Assembly for Buildup C Testing.

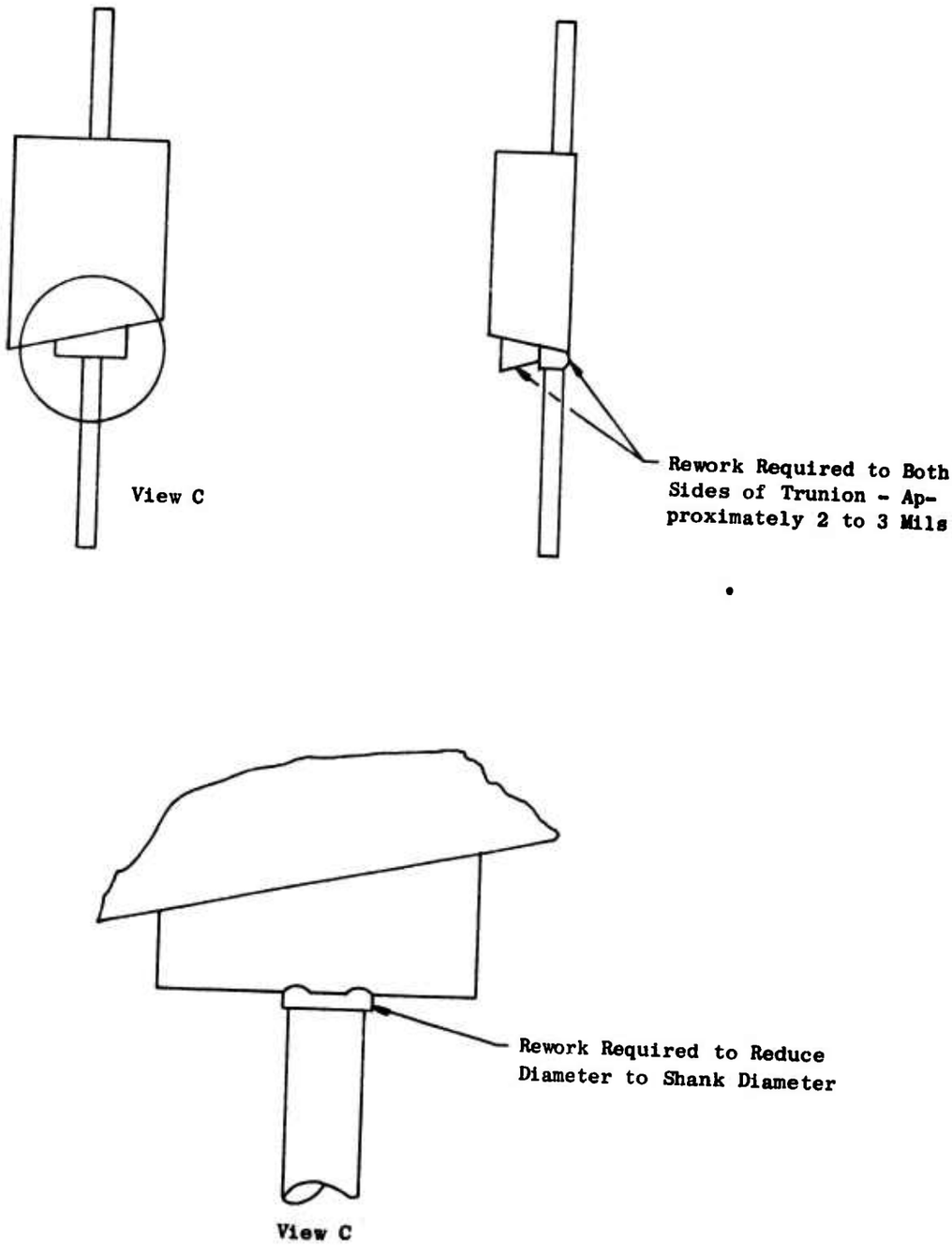

Figure 110. Blade Modifications Required to Fit Rotor Disc.

6) A setup was made to measure the relative height of the airfoil sections, and these heights were found to vary 0.007 inch. Selective interchange of high and low blades was accomplished to reduce this height variance to less than 0.004 inch.

7) The shroud was mounted and the nuts were torqued to 30 inch-lbs. Runout on the shroud was taken and recorded as 0.0025 inch.

8) The shroud was match marked and removed. All the stub blades were now installed. The shroud was again installed and the nuts were torqued to 30 inch-lbs. The shroud runout was again taken and was recorded as 0.003 inch.

9) The final build configuration was now delineated as having a final nut torque of 36 inch-lbs. In addition, the large Belleville washer on the disc side was to be replaced with the smaller Belleville washer. Also, the final balanced rotor was not to have any balance washers installed at either side of the blade stem. Using the reduced size spherical seat washers and/or grinding at the disc and shroud was designated for balance provisions.

10) The rotor was assembled to the shaft and returned to the service area.

11) The Belleville washers were replaced and all blade stem nuts torqued to 36 inch-lbs.

BALANCE

1) A total of 20 spherical seat washers was reworked to reduce the overall height to enable use as balance weights.

2) The completed rotor was sent to the microbalancer. Some problems were encountered in mounting the tooling to this machine. Considerable rework was accomplished to enable the tooling to be properly fitted. It was required to spring load the pedestal to counteract the overhanging rotor effect (Figure 111).

3) A setup was made for a force moment balance operation. Repeatability of angle and amount of unbalance were inconsistent with this setup. Part of the problem was attributed to the inability of the workpiece to maintain a constant speed because of its pumping action. A piece of masking tape was used to cover the airflow passage and reduce the pumping action. This fix enabled maintaining constant speed and calibration stability. A cross plane setup (Figure 111) was used for better plane separation and accurate calibration.

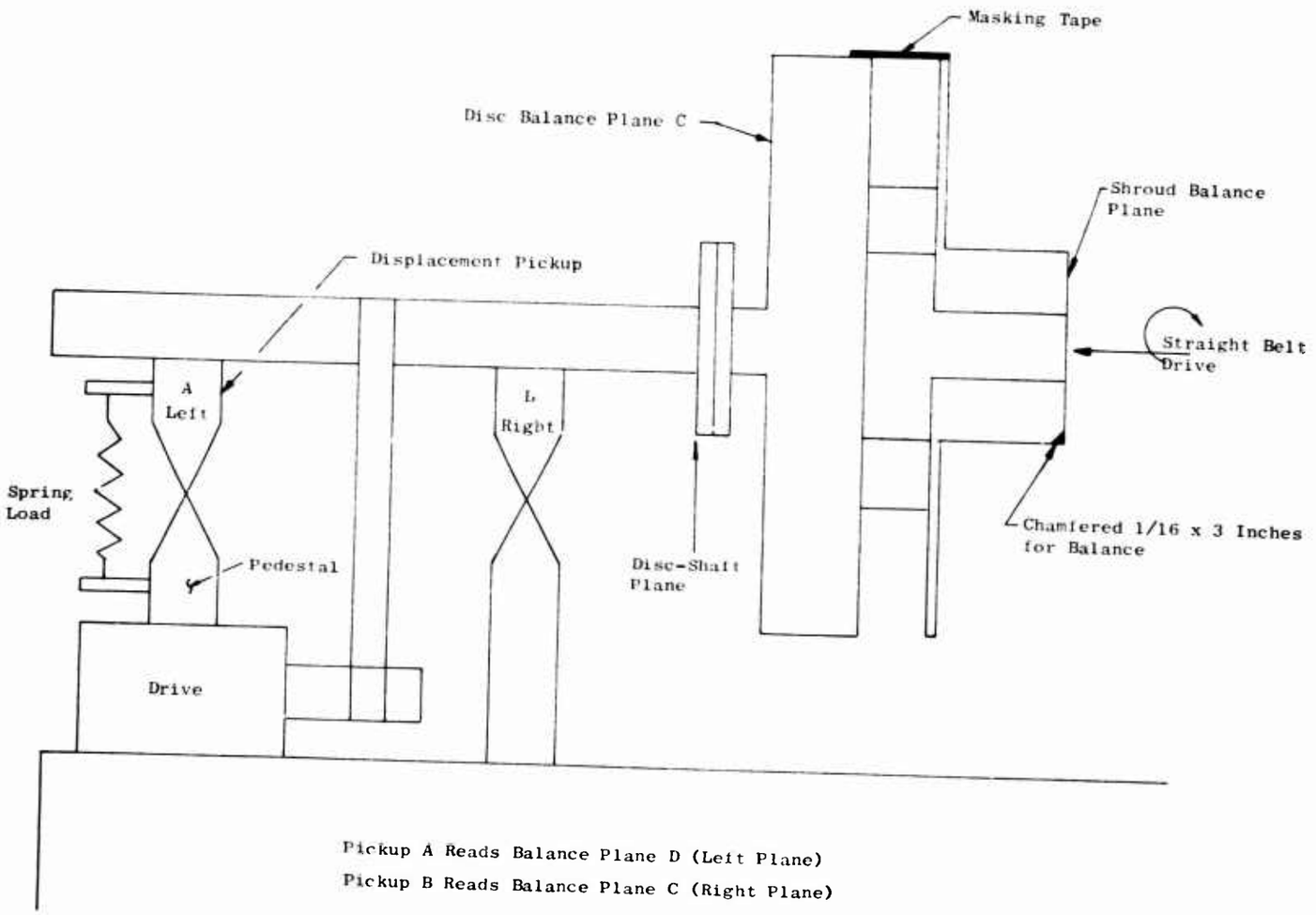

Figure 111. General Arrangement Used in Balancing Phase III Rotor.

4) The calibration was completed and checked out by introducing known unbalances at various planes and angles. The original unbalance reading was 6.0 grams in plane C (disc side) and 2.0 grams in plane D (shroud saw cut counterweight). Two of the original washers (approximately 3 grams each) at the disc-shaft plane were removed and the unbalance was recorded as 1.2 grams in plane C and 2.0 grams in plane D. Twelve reduced-height spherical washers were added to the shroud side and the unbalance was recorded as 0.35 gram in plane C and 0.04 gram in plane D. Two small (1/2 gram) washers were added at the disc-shaft bolt circle and the unbalance was recorded as 0.25 gram in plane C and 0.2 gram in plane D. Three more reduced height spherical washers were added to the shroud side and the unbalance was recorded as 0.1 gram in plane C and 0.2 gram in plane D. At this point, it was determined that addition of more washers would only produce cross effects that would not improve the balance. The remainder of the unbalance reduction was to be accomplished by grinding at the disc bolt circle and the saw cut counterweight.

5) Several academic investigations were conducted at this time. One was to twist the drive belt to enable rotation of the workpiece in the opposite direction to reduce pumping effects. Unbalance was recorded as 0.4 gram in plane C and 0.6 gram in plane D. By adjusting the calibration potentiometers, it would have been possible to balance in this manner. It was decided not to recalibrate if removal of the tape had no adverse effects to the unbalance. The tape was removed and the unbalance was recorded as 0.45 gram in plane C and 0.6 gram in plane D (twisted belt). Tape effects were considered negligible.

6) The tape was now reinstalled and the drive belt untwisted and unbalance recorded as 0.2 gram in plane C and 0.2 gram in plane D. Approximately a 1/16-inch chamfer was ground on the saw cut counterweight and reduced the unbalance to 0.04 gram in plane C and 0.05 gram in plane D. Grinding spanned a circumferential distance of 3 saw cuts (approximately 3 inches). The rotor was removed from the balance machine and installed into the dolly.

INSPECTION

The rotor was set up in "V" blocks in the service area and all runouts were taken. The amount of runout at several critical locations for Buildup C is noted by the letter C on Figure 109. This completed the build sequence.

APPENDIX III

INSTRUMENTATION AND CONTROL EQUIPMENT

The control panel used during test of the ROC is shown in Figure 112. Located on this panel are the monitoring devices and controls required for the safe operation of the test vehicle. The station used to indicate and control the pressures and temperatures in the cavities upstream and downstream of the compressor rotor is shown in Figure 113. The manometers at left are used to indicate small differences in pressure across the upstream and downstream seals.

The instrumentation used to monitor and analyze compressor and test vehicle strain gage signals and vibration pickups is presented in Figure 114. When high frequency response crystal pickups are used to measure rotor exit static pressure variations, additional oscilloscopes, cameras, and magnetic tape recording equipment are used.

The equipment used to print digital values of pressures, temperatures, flow angles, stator vane angles, and other test data is shown in Figure 115. The system also punches paper tape which can be used directly in the teleprinter connected with the GE shared time computer system. The system permits conversion of the digital printout to engineering units and calculation of area-averaged performance parameters within a few minutes after completion of data recording. The recording equipment used for plotting the total pressure and flow angle obtained by traverses of aerodynamic instrumentation across the compressor flowpath is presented on the left in Figure 116. At the right is the continuous recording equipment for monitoring test vehicle vibrations, oil temperatures, and other operating information useful in avoiding unsafe regions and in determining the reason for a particular system tripout.

In addition to the equipment shown on the preceding phtographs, aerial camera photographs of a 100-tube manometer board using water, tetrabromoethane or mercury, as appropriate, are taken for each test point. Barometric pressure and room temperature are observed and recorded manually.

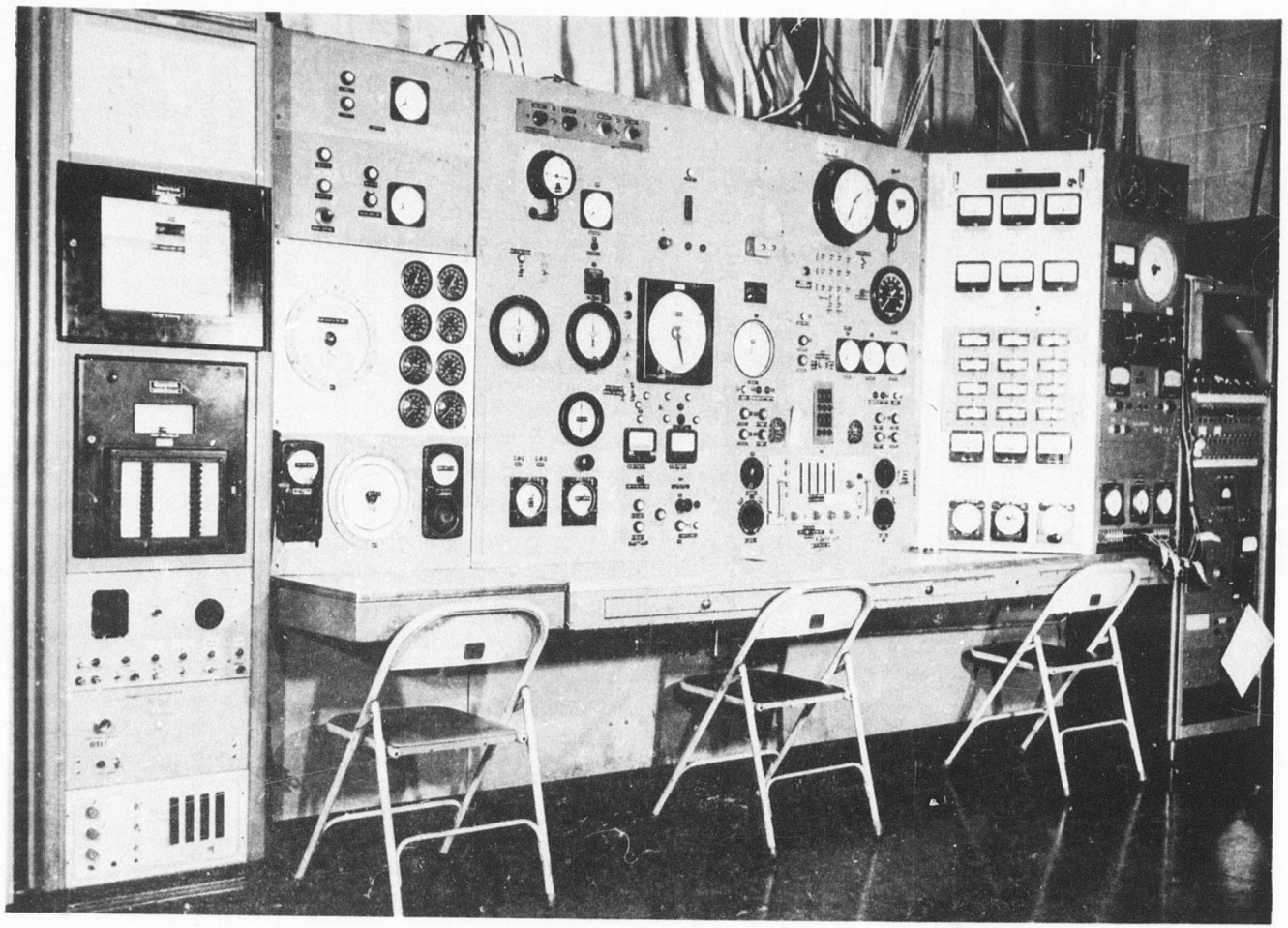

Figure 112. Central Control Panel Used for Control and Indication of ROC Speed, Throttle Setting, Stator Vane Angle, and Indication of Vehicle Vibrations and Bearing Temperatures.

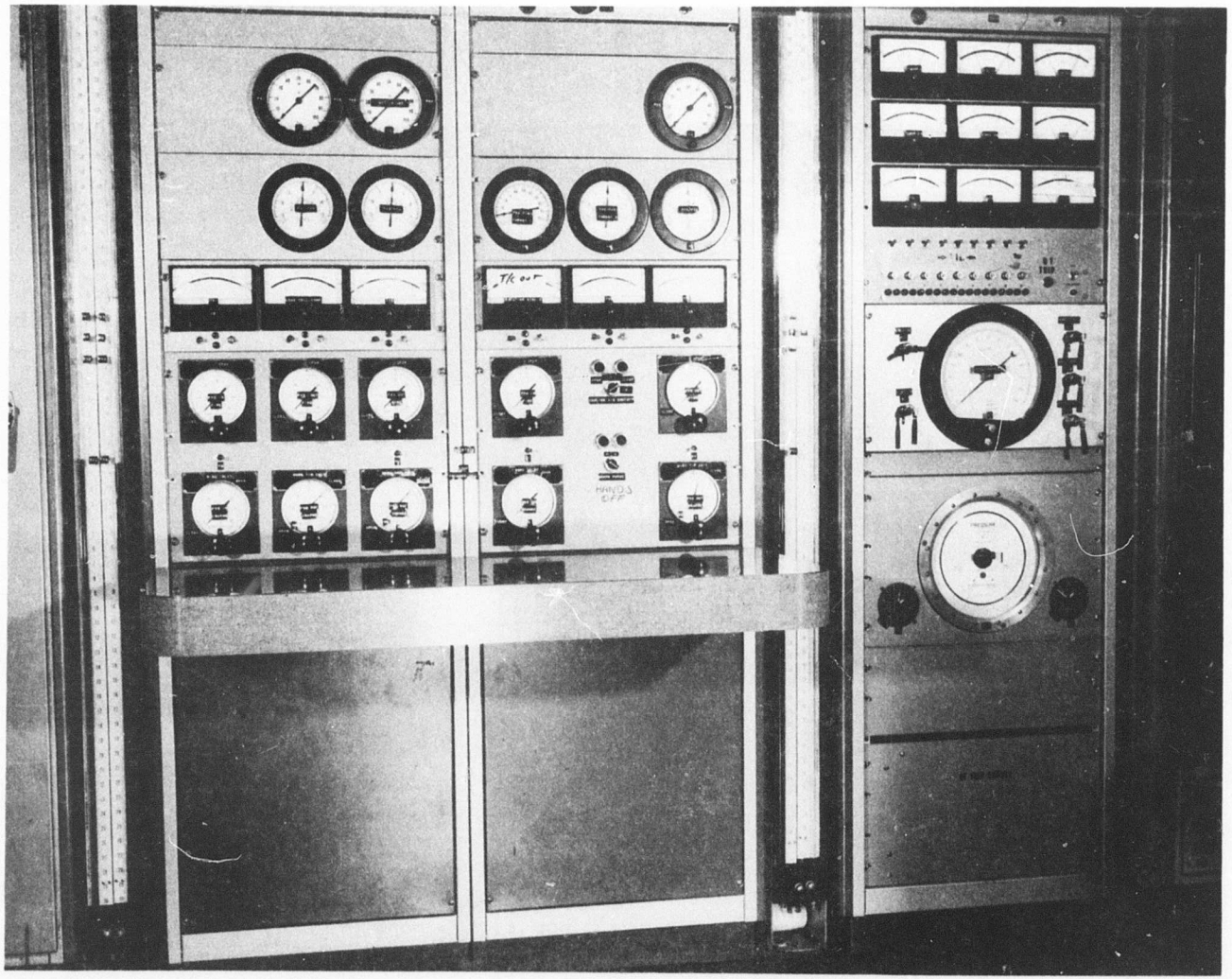

Figure 113. Panels Used for the Control and Indication of the Pressures and Temperatures in the Cavities Upstream and Downstream of the Compressor Rotor.

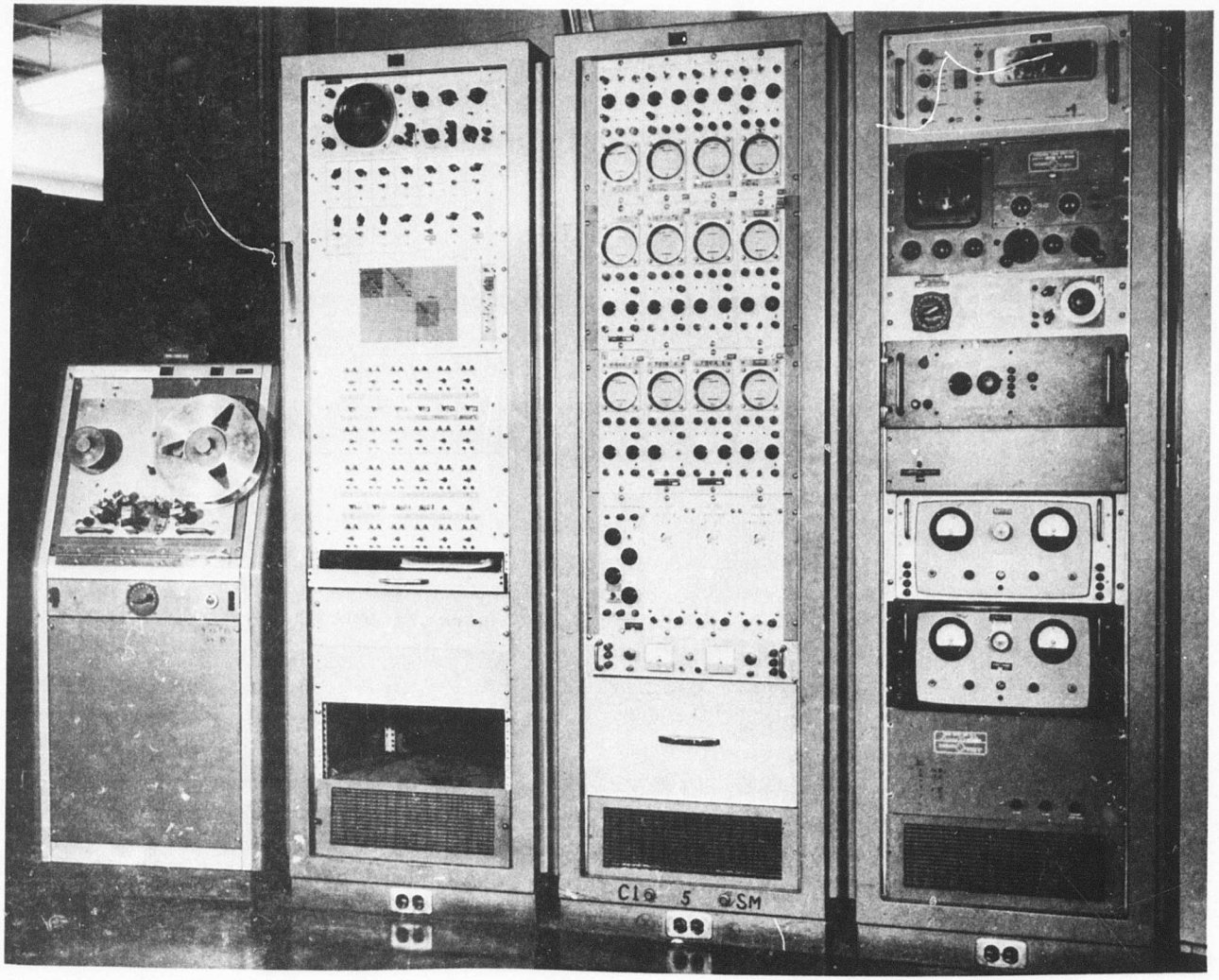

Figure 114. Instrumentation Used to Monitor and Analyze Compressor and Test Vehicle Strain Gage and Vibration Pickup Signals.

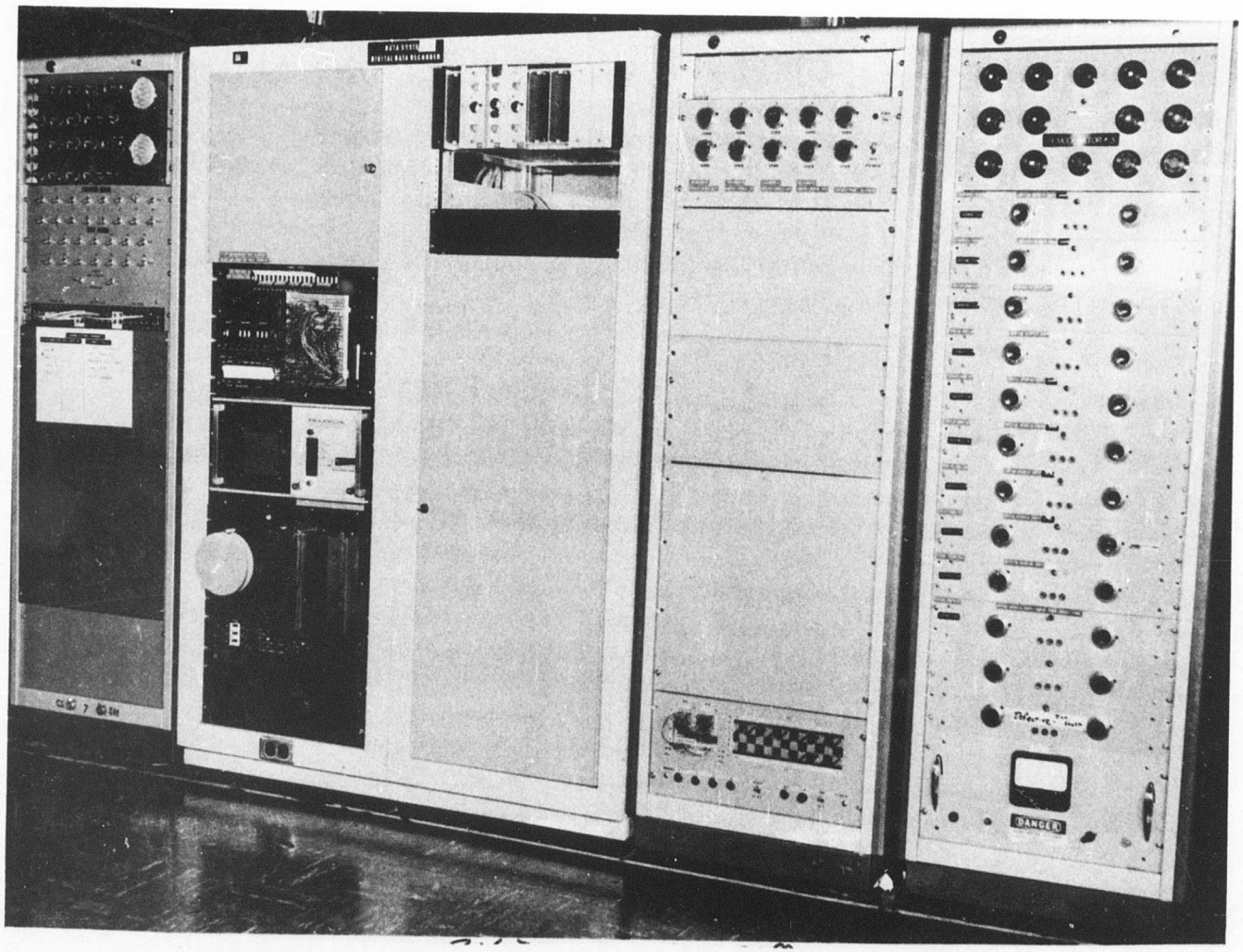

Figure 115. Equipment Used to Datatize, Print, and Punch Tape for Values of Test Pressures, Temperatures, Flow Angles, and Vane Angles.

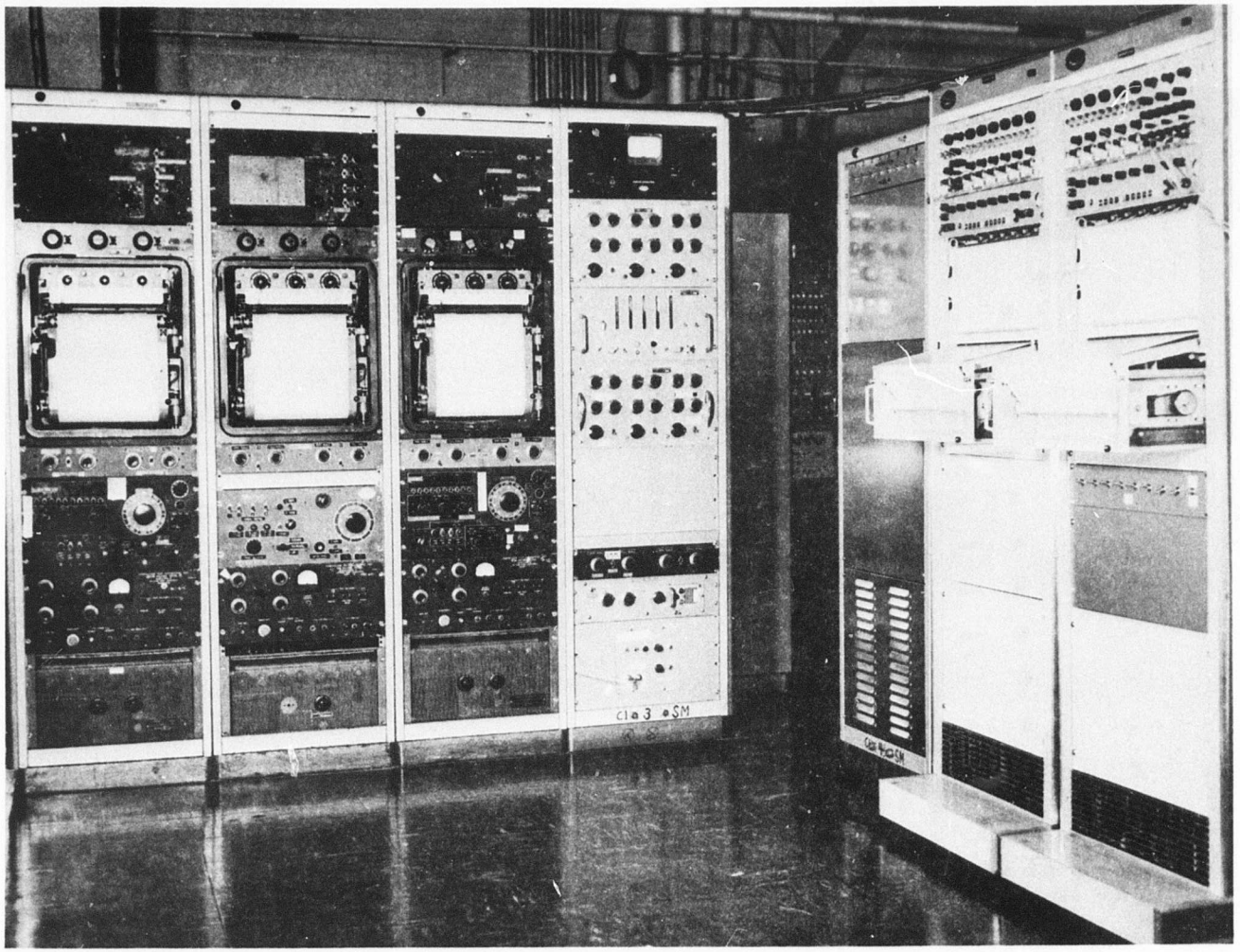

Figure 116. Recording Equipment Used for Plotting Total Pressure and Flow Angle Traverse Results.

Unclassified
Security Classification

DOCUMENT CONTROL DATA - R & D

(Security classification of title, body of abstract and indexing annotation must be entered when the overall report is classified)

1. ORIGINATING ACTIVITY (Corporate author)	2a. REPORT SECURITY CLASSIFICATION
Aircraft Engine Group General Electric Company Cincinnati, Ohio 45215	Unclassified 2b. GROUP

3. REPORT TITLE

Radial Outflow Compressor Component Development - Phase III - Mechanical Design and Experimental Investigation Using Modified Rotor

4. DESCRIPTIVE NOTES (Type of report and inclusive dates)

Final Report

5. AUTHOR(S) (First name, middle initial, last name)

John R. Erwin

6. REPORT DATE	7a. TOTAL NO. OF PAGES	7b. NO. OF REFS
August 1969	181	2

8a. CONTRACT OR GRANT NO.	9a. ORIGINATOR'S REPORT NUMBER(S)
DA 44-177-AMC-180(T) b. PROJECT NO. Task 1G121401D14413 c. d.	USAAVLABS Technical Report 68-38C 9b. OTHER REPORT NO(S) (Any other numbers that may be assigned this report)

10. DISTRIBUTION STATEMENT

This document is subject to special export controls and each transmittal to foreign governments or foreign nationals may be made only with prior approval of US Army Aviation Materiel Laboratories, Fort Eustis, Virginia 23604.

11. SUPPLEMENTARY NOTES	12. SPONSORING MILITARY ACTIVITY
Volume III of a three-volume report	US Army Aviation Materiel Laboratories Fort Eustis, Virginia

13. ABSTRACT

The purposes of the Phase III investigation were to apply the information obtained from the experimental and analytical investigations of the first two phases to the design of an improved ROC and to demonstrate this improvement by tests of a complete compressor over the full speed range. Because of delays in completing the earlier phases and due to the inevitable time expenditure occurring in the design and procurement phases of obtaining new rotating parts, the selection of the Phase III rotor design was made prior to the time that all of the Phase II test results were available. In particular, the excellent rotor performance observed at 70 percent speed during the last testing sequence of the Phase II investigation, Buildup F, was not obtained until after the Phase III rotor design was committed to manufacture. A summary of information concerning each test run is presented in Appendix I.

The evidence from tests of Buildup F and from the low-speed investigation of the vaneless diffuser having one stationary porous wall and one rotating wall is that more severe effective static pressure gradients can be sustained by a rotating wall than the earlier Phase II results had indicated (uniform inlet conditions to the rotor are evidently critical to efficient rotor performance). In retrospect, more contraction of the rotating vaneless diffuser was probably incorporated into the Phase III rotor design than was necessary for best high-speed performance.

DD FORM 1 NOV 68 1473 REPLACES DD FORM 1473, 1 JAN 64, WHICH IS OBSOLETE FOR ARMY USE.

Unclassified
Security Classification

14. KEY WORDS	LINK A		LINK B		LINK C	
	ROLE	WT	ROLE	WT	ROLE	WT
Compressor						
High-Pressure-Ratio Compressor						
Radial Outflow Compressor						
Variable Geometry Diffuser						
Rotating Diffuser						